Organotypic Basolateral Amygdala Slice Cultures: A Model for Stress-related Circuitry

by

Sheldon David Michaelson

A thesis submitted in partial fulfillment of the requirements for the degree of

Doctor of Philosophy

Department of Pharmacology
University of Alberta

ABSTRACT

Stress generates an adaptive behavioral and physiological response that prepares an organism for new environmental pressures. However, if stressors are perceived as uncontrollable, prolonged, or severe, they can produce exaggerated responses and result in neuropsychiatric syndromes such as anxiety and depression. Many brain regions respond to stress with the basolateral amygdala (BLA) regulating emotional processing. Glutamatergic principal cells are the major output neurons of the BLA and mediate behavioral stress responses. These cells respond to stress with dendritic hypertrophy and increased spine densities. Several endogenous neuromodulators alter BLA output cell activity, including the anxiolytic neuropeptide Y (NPY) and the anxiogenic corticotrophin releasing factor (CRF). Daily (5 x d) injections of NPY or urocortin (CRF-R1 and CRF-R2 agonist) induce a persistent state of stress resilience or vulnerability, respectively. While the mechanisms governing the acute actions of NPY and CRF on the stress response in the amygdala are well established, the signal transduction pathways mediating NPY- and CRF-induced stress resilience and vulnerability are unknown. We hypothesized that chronic CRF treatment would recapitulate the effects of stress observed on BLA principal cells and NPY treatment would result in the opposite effect, namely, dendritic hypotrophy. We tested this in male rats *in vivo* and using a novel organotypic slice culture preparation of BLA (BLA OTCs) we recently developed, optimized and validated. BLA OTCs (6 w postnatal equivalent age) were treated with varying concentrations of NPY, CRF, NPY prior to CRF, CRF prior to NPY, NPY-receptor-subtype-selective agonists, NPY + protein phosphatase inhibitors or CRF + kinase inhibitor for 5 days. Electrophysiological and morphological changes in neurobiotin-filled neurons were analyzed 7-14 days after peptide treatment.

In BLA OTCs, NPY, and the Y5-agonist, but not the Y1-agonist, decreased excitatory drive onto principal cell, while also reducing cell capacitance and culminated in dendritic hypotrophy as determined by Sholl analysis. CRF and the anxiogenic Y2-agonist produced opposite effects to those same neuronal properties observed with NPY and the Y5-agonist, and similar to that seen with stress. The BLA OTC preparation thus may predict structural changes that accompany stress resilience and vulnerability. NPY and CRF cause opposite effects on BLA dendrites correlating with behavioral changes seen with peptide treatment *in vivo*, which can be prevented when incubated with the opposing neuropeptide. Moreover, NPY- and CRF-induced structural plasticity is regulated by the opposing actions of the protein phosphatase calcineurin and the protein kinase Ca2+/calmodulin-dependent protein kinase II, respectively. To confirm our finding and further validate the BLA OTC model, NPY, Y1-agonist or a Y5-agonist were injected daily (5 x d) into the BLA of 7 week-old rats; social interaction (SI) was assessed and similar recordings were made in acute BLA slices 4 weeks after the first injection. NPY, and the Y5-agonist increased SI time at all experimental time points studied (up to 4 weeks). Intra-BLA injections of the Y1-agonist increased SI on days 1 and 5 after injection but did not affect SI long-term. BLA principal cell dendrites were retracted in NPY- and Y5-agonist-treated, but not Y1 agonist-treated rats. These studies indicate a novel structural correlate of stress resilience and vulnerability, while demonstrating the potency of the BLA OTC model for studying the underlying cellular and molecular mechanisms of stress/anxiety-related behavior.

PREFACE

The majority of work presented in this thesis was performed using an *in vitro* culture system, which was developed and optimized *de novo* by myself for the basolateral amygdala. The bulk of the validation of the model was achieved early during optimization. To push the limits of productivity in the lab, Ms. Ana Miranda and I consolidated our time, energy, and expertise. Thus, a number of the studies presented here involved combining data sets to meet the requirements for statistical analysis. We have split the data fairly, to be presented as our own data while providing acknowledgements as appropriate.

For the portions of work presented here that involved *in vivo* experiments, other members of the lab including Ms. Miranda and Dr. Heika Silveira were instrumental in preparing animals for study, as they performed nearly all surgeries, cannulations, drug injections, and behavioral analyses. In Chapter 2, the electrophysiological and morphological data from postnatal 14 day old rats, was acquired jointly by Ms. Miranda and myself. In Chapter 3, Ms. Miranda assisted with data acquisition/analysis not only in the cultured CRF , NPY treated group, but also for *ex vivo* slice studies from repeatedly NPY-injected animals. In Appendix I, results from all Y5-agonist and antagonist experiments from both organotypic cultures and *ex vivo* preparations, are the intellectual property of Ms. Miranda and will be incorporated as results into her thesis work; however, as I did have a hand in concept formation, acquiring/analyzing data, I present the data as part of Appendix I to explain my previous findings. In Chapter 5, all data was acquired by both Ms. Miranda and myself, however, as concept formation was strictly executed by Dr. Colmers and myself, I will incorporate the results as part of this thesis.

A version of Appendix II has been published as Michaelson SD, Paulsen IM, Kozuska JL, Martin IL, Dunn SM (2013) Importance of recognition loops B and D in the activation of human 5-HT(3) receptors by 5-HT and meta-chlorophenylbiguanide. Neuropharmacology 73: 398-403. JL Kozuska assisted in the design, data collection/analysis and contributed to manuscript edits. IM Paulsen assisted in a portion of the data acquisition/analysis. IL Maritin contributed to research design and assisted in manuscript edits. SMJ Dunn was the supervisory author and was involved with concept formation. I performed the bulk of the studies, analyzed data, wrote and assisted in editing the manuscript.

All animal procedures were approved by the University of Alberta Animal Care and Use Committee: Health Sciences, in accordance with the guidelines of the Canadian Council on Animal Care.

"The ultimate measure of a man is not where he stands in moments of comfort and convenience, but where he stands in times of challenge and controversy."

Martin Luther King, Jr.

“A thesis is never finished, only abandoned when in a passable form”

Unknown

ACKNOWLEDGMENTS

The past seven years have afforded me the opportunity to work and grow alongside some truly amazing individuals. As my time here comes to an end, I cannot help but reminisce on all the good, bad, and ugly times that have contributed to my evolution and arrival at this juncture. I would like to thank a number of individuals who have truly made an impact on my success.

To my original supervisor, the late Dr. Susan Dunn, I never had the chance to thank you for providing me the opportunity to explore the intricacies of neuroscience, so thank you. Although our time together was short-lived, I am forever grateful for your patience and generosity you showed me when I was a naïve, ignorant, young graduate student.

To my present academic supervisor and mentor, Dr. William F. Colmers, thank you for taking me under your wing and allowing me to continue on this scientific journey. You were the first person to reach out and offer a helping hand when my scientific career was in jeopardy, and I will never forget that. Your willingness to teach, share your acquired knowledge, and provide insight has been invaluable in my current and future successes. I have made a few (hundred) mistakes over the years, but you always afforded the opportunity to learn a number of important lessons, and have had my back on a number of occasions. I hope to make you proud, and reach a level of excellence that you set for yourself.

To Dr. Peter Light, the only surviving member of my original supervisory committee, thank you for enduring this process with me. I have learned so much from you, both in terms of scientific resourcefulness, and also how to conduct oneself in a professional manner. Those lessons will never be forgotten. To Dr. Janice Urban, a close collaborator of the Colmers lab

and a member of my supervisory committee, thank you for your kindness and compassion. Your encouragement and guidance during the early years of my current project kept me in positive spirits.

To my examining committee members, Drs. Matt Hill and Peter Smith, thank you for taking the time to critique this thesis. I hope you enjoy reading it exponentially more than I did writing it. And Dr. Smith, thank you for the wonderful reference letters you have written for me over the years. Your lies and deceit afforded me the opportunity to successfully obtain an AIHS studentship, and I am grateful.

To Dr. Andy Holt, the current graduate student coordinator in the Department of Pharmacology, thank you for your open door policy. There have been a number of situations that you managed to devise a constructive solution for all parties involved, and your service has not gone unnoticed.

To past and present members of the Dunn and Colmers laboratories, specifically: Dr. Janna Kozuska, Ms. Isabelle Paulsen, and Dr. Ian Martin, thank you for getting me through those first few years when I literally had no idea what I was doing; To Dr. Chris Carter, thank you for being an ear to vent to. You are the person who convinced me to pursue graduate school, and the reason I am still currently unemployed. Some of my fondest memories of this place are smoking darts with you and Judy in Susan's lab by the radioactive hood during the annual Christmas parties; Mr. Kevan Smith, Dr. Rebecca Mercer, Dr. Trevor Hamilton, Dr. Barbora Doslikova, Mr. James Mackay and Ms. Mandy McKinty, you have all made coming to work everyday a pleasure. Thank you for our scientific discussions and putting up with my shenanigans. James, I hope to one day read your blog entitled "Things I thought I'd never hear

while working in a lab". Every result in this thesis was accomplished with the help and support from all of you. To Ms. Ana Miranda, you have been incredibly influential in this work. Without your hard work, dedicated thirst for knowledge, and countless hours of patching what seems like thousands of cells, this story would not be complete. You have such a bright future ahead of you, and I wish you luck in your future endeavors.

To the following agencies, thank your for providing the financial resources and support throughout my studies: Department of Pharmacology, University of Alberta, Alberta Innovates- Health Solutions, Government of Alberta, Novartis Pharmaceutical Canada Inc., Campus Alberta Neuroscience, Canadian College of Neuropsychopharmacology.

To my wonderful family: Mom, Dad, and Teresa, thank you for your unwavering support and devotion to my success. You have been my rock through everything, and I would not be the man I am today with your love.

Last but certainly not least, my better half, and lovely wife Aisha. Thank you for choosing to stand by me, and always making sure my needs are met. You have been so incredibly strong throughout this entire process. You have dealt with so many lonely nights, cancelled plans, and have taken a back seat to my most recent addiction that is science. I would not have triumphed in this venture without you, so thank you and I love you and Sage.

TABLE OF CONTENTS

LIST OF TABLES

LIST OF FIGURES

LIST OF ABBREVIATIONS

5-HT	5-hydroxytryptamine
5-HT3AR,	5-hydroxytryptamine type 3A receptor
5-HT3ABR	5-hydroxytryptamine type 3AB receptor
ACTH	adrenocorticotropic hormone
AEA	anandamide
Ahx	[ahx$^{5-24}$]NPY
AIP	autocamtide-2-related inhibitory peptide
AMPA	α-amino-3-hydroxy-5-methyl-4-isoxazolepropionic acid
ANOVA	analysis of variance
AP	anteroposterior
BA	basal amygdala
BDNF	brain-derived neurotrophic factor
BLA	basolateral amygdala complex
BM	basomedial amygdala
BNST	bed nucleus of stria terminalis
BZD	benzodiazepine

$[Ca^{2+}]i$	intracellular calcium concentration
CamKII	calcium/calmodulin-dependent protein kinase II
cAMP	cyclic adenosine monophosphate
CaN	calcineurin
CCK	cholecystokinin
CeA	central amygdala
CeL	centrolateral amygdala
CeM	centromedial amygdala
CGP	CGP71683A
ChR2	channelrhodopsin 2
Cm	capacitance
CNS	central nervous system
cPP	[cPP1–7,NPY19–23,Ala31,Aib32,Gln34]hPP
CREB	cAMP response element-binding protein
CRF	corticotropin-releasing factor
CRF-R1	corticotropin-releasing factor type 1 receptor
CS	conditioned stimulus

CsA	cyclosporine A
CSF	cerebrospinal fluid
Ctrl	control
DIC	infrared-differential interference contrast
DL-AP5	(2R)-amino-5-phosphonovaleric acid
DV	dorsoventral
EC	external capsule
EP	equivalent postnatal
EPM	elevated plus maze
ERK	extracellular signal-regulated kinase
FAAH	fatty acid amide hydrolase
fMRI	functional magnetic resonance imaging
$GABA_A$	gamma aminobutyric acid type-A
GAS	general adaptation syndrome
GIRK	G-protein-coupled inwardly-rectifying potassium
HBSS	Hank's balanced salt solution
HCN	hyperpolarization-activated cyclic nucleotide-gated

HPA	hypothalamic-pituitary-adrenal
ICV	intracerebroventricular
IEI	inter-event interval
I_h	hyperpolarization-activated non-selective cation current
IIR	inwardly-rectifying current
IP_3	inositol 1,4,5-triphosphate
ITC	intercalated cell clusters
KN-62	CaMKII inhibitor
K-S	Kolmogorov–Smirnov
LA	lateral amygdala
LC	locus coeruleus
LTD	long-term depression
LTP	long-term potentiation
MAP	mitogen-activated protein
mCPBG	meta-chlorophenylbiguanide
mGluR	metabotropic glutamate receptor
ML	mediolateral

mTOR	mammalian target of rapamycin
NA	noradrenaline
NAc	nucleus accumbens
nAChR	nicotinic acetylcholine receptor
NBI	NBI 27914 hydrochloride
NGF	nerve growth factor
NMDA	N-methyl-D-aspartate
NPY	neuropeptide Y
NR2B	NMDA-receptor subunit 2B
ns	non-significant
NT-3	neurotrophin 3
NTS	nucleus tractus solitarii
OA	okadaic acid
OCD	obsessive-compulsive disorder
OFT	open field test
OTC	organotypic slice cultures
$P75^{NTR}$	p75 neurotrophin receptor

P	postnatal
PBS	phosphate buffered saline
PFC	prefrontal cortex
PI3K	phosphatidylinositol 3-kinase
PKA	protein kinase A
PLC	phospholipase C
PP1	protein phosphatase 1
PP2A	protein phosphatase 2A
PP2B	calcium/calmodulin-dependent phosphatase 2B (aka. Calcineurin)
PP	pancreatic polypeptide
PTSD	posttraumatic stress disorder
PVN	paraventricular nucleus of the hypothalamus
PYY	peptide YY
R_{in}	input resistance
RMP	resting membrane potential
SAD	social anxiety disorder
SEM	standard error of mean

sEPSC	spontaneous excitatory postsynaptic current
SI	social interaction
sIPSC	spontaneous inhibitory postsynaptic current
SLC6A4	solute carrier family 6 (neurotransmitter transporter), member 4
SOM	somatostatin
SNRI	serotonin-norepinephrine reuptake inhibitor
SSRI	selective serotonin reuptake inhibitors
tPA	tissue plasminogen activator
TrkB	tropomyosin-related kinase B
TRPC	transient receptor potential channels
UCN	urocortin
US	unconditioned stimulus
VGCC	voltage-gated calcium channels
Vh	holding potential
VIP	vasoactive peptide
WT	wild type

CHAPTER 1: General Introduction

Anxiety

Anxiety and its related disorders, including panic disorder, agoraphobia, social anxiety disorder (SAD), generalized anxiety, obsessive compulsive disorder (OCD), specific phobia and posttraumatic stress disorder (PTSD), are marked by excessive fear and avoidance, often in response to specific objects or situations in the absence of any true danger, and represent the most common of the neuropsychiatric disorders, with a lifetime prevalence estimated to be as high as 31% (Kessler et al., 2007). The annual cost to Canada for anxiety disorders, including both direct and indirect costs, was already estimated to be $65 billion USD in 1994 (Stein and Hollander, 2002). Despite most cases of anxiety being mild and often transient in nature, they can cause a significant burden on the quality of life for patients and substantially impair their functional status (Weisberg et al., 2007, Martin-Merino et al., 2010). Moreover, anxiety is frequently co-morbid with other neuropsychiatric conditions, such as major depression, mood, or substance abuse disorders, coupled with the lack of efficacy, undesirable side effects or drug interactions of current pharmacotherapies, making prolonged psychiatric symptoms and debilitation a familiar occurrence (Hirschfeld, 2001, Bandelow et al., 2008, Bandelow et al., 2015).

For years, conventional pharmacological treatment of anxiety disorders relied on benzodiazepines (BZD), which act as positive allosteric modulators of the gamma aminobutyric acid type-A ($GABA_A$) receptor, a ligand-gated ion channel mediating most fast inhibition in the central nervous system (CNS). BZD treatment results in an increase in the frequency of $GABA_A$ receptor channel opening, thereby increasing neuronal inhibition (Cascade and Kalali, 2008). Although BZDs seem to work well for treating anxiety-related disorders, their inhibitory properties and lack of subtype-specificity, coupled with the

widespread distribution of $GABA_A$ receptors in the CNS, result in undesirable side effects such as sedation, fatigue, muscle relaxation and amnesia, adverse effects that limit their long-term effectiveness (Griffin et al., 2013). Furthermore, their tendency to induce tolerance and dependence, coupled with age-related physiological changes that can lead to altered pharmacokinetics, and for drug-drug interactions has forced clinicians to re-evaluate the safety of long-term BZD use. Recently, several classes of antidepressants such as selective serotonin reuptake inhibitors (SSRIs), serotonin-norepinephrine reuptake inhibitors (SNRIs) and tricyclic antidepressants have been prescribed as first-line anxiolytic treatments, as their mechanism of action is more refined, primarily focusing on increasing neurotransmitter availability at the synapse, which has the potential for reduced adverse effects (Dinan, 2006). However, common side effects such as insomnia or sleepiness, sexual dysfunction, stomach upset, headache, orthostatic hypotension and weight gain produce high rates of patient non-adherence. Additionally, a large percentage of subjects do not respond to mono-therapy, and therefore require other treatment options (Saveanu et al., 2015). Recently, the pharmaceutical industry has encountered many hurdles in developing novel treatment options and has all but abandoned drug development in psychiatry (Schatzberg, 2015a, b). The main reason stems from the lack of knowledge of the neurocircuitry and biological systems that govern those mechanisms that allow for desired therapeutic effects, as well as those underlying the undesirable adverse actions. Therefore, there is a clear need to develop our understanding of the neurological processes that are involved to aid with the improvement of newer and more specialized pharmaceuticals.

Animal Models of Stress, Anxiety and Fear

The assessment of anxiety in humans is fairly straightforward, usually occurring either in a clinical setting or by self-assessment through questionnaires and interviews (Rose and Devine, 2014). Because this is not feasible in animals, especially rodents, a number of methods have been developed to evaluate anxiety-like behavior in experimental models. Most of these behavioral tests are based on the observation that rodents tend to avoid open spaces and bright lights, presumably due to their fear of vulnerability to predators. Avoidance of open space is classically studied in the elevated plus maze (EPM) and the open field test (OFT), in which increased time spent and entries into the open arms of the EPM or more time spent in the middle of the arena and away from the high walls of the open field, respectively, is correlated with less anxiety (Crawley, 1985, Pellow et al., 1985). In the light-dark test, rodents are able to freely move between light and dark areas of the enclosure; the more time spent in lit areas is indicative of a less anxious phenotype (Costall et al., 1989). While these are the most common anxiety testing paradigms, others include the forced swim test and Vogel conflict drinking test (modified) that are used as alternatives in certain studies (Porsolt et al., 1977, Engel et al., 1984). The issue with the above tests discussed is the propensity for the animals to become habituated to the paradigm if performed repeatedly. In essence, repetition skewed responses as animals learn that time spent in the open arms, in the center of the field, or in the light area has no negative consequences. The social interaction (SI) test is a useful alternative for experiments that must be repeated, in which an experimental animal in placed in an open field with a novel counterpart and the time spent in, and number of, interactions is quantified as an index of the experimental animal's anxiety level; increased interactions and time spent interacting is negatively correlated with anxiety level (File and Hyde, 1978).

Much of our understanding of learned fear stems from studies using Pavlovian fear conditioning. In its most basic form, an initially neutral conditioned stimulus (CS, for example a tone) is repeatedly presented paired with an aversive unconditional stimulus (US, e.g., an unpleasant electrical shock). After repeated pairings, the CS alone will elicit a conditioned fear response, observed as increased freezing behavior, fear-potentiated startle or skin conductance responses. Extinction is an active form of inhibitory learning that occurs when a CS that previously predicted a US no longer does so over time (Brown et al., 1951). This simplistic model of acquiring fear, followed by extinction has relevance to certain phobias, and reports have indicated impaired extinction in animal models of, and human patients suffering from, PTSD (Blechert et al., 2007, Wessa and Flor, 2007, Milad et al., 2008). There are many variations of this paradigm that are distinguishable based on whether aversive events are administered or anticipated but will not be discussed any further [for review see, Davis et al. (2010)].

Fight or Flight

Our brains react to potentially dangerous situations by preparing our bodies for action. A classic example is the reflex reaction of withdrawing our hand from a hot stovetop, which requires no conscious thought. These instincts have been engraved into our biology since prehistoric times, as a mechanism to survive potentially fatal encounters. Building on Claude Bernard's work on homeostasis and the maintaining constant of the "milieu interieur", Walter Cannon coined the term "fight or flight" in 1915, to describe the physiological reaction of an animal in response to a perceived harmful event, attack, or threat to survival (Bernard, 1878, Cannon, 1915). The fight or flight response, also known as the acute stress response, involves a coordinated effort of the autonomic nervous system to regulate and fine-tune the activity of

the sympathetic and parasympathetic nervous systems (Jansen et al., 1995). This ultimately triggers neural responses and the release of stress-related hormones and neurotransmitters such as adrenaline, noradrenaline and cortisol (corticosterone in rodents) that stimulate the body and prepare it for action. The activities of these mediators typically include the following: accelerated heart rate and respiration, constriction of most peripheral blood vessels with enhanced blood flow to muscle, dilation of the pupils, tunnel vision, disinhibition of spinal reflexes, shaking, mobilization of the immune system and liberation of metabolic energy stores (McEwen and Lasley, 2002). The physiological changes that occur are activated to divert energy to vital biological systems within the body that allows the organism to flee or fight the anticipated danger.

Stress

Acknowledged as the "father" of the stress field, Hans Selye first described stress in 1936 as, "acute nonspecific nocuous agents that affect the body (Selye, 1998)"; however, a stressor is now better defined as an adverse condition that disturbs the homeostasis of the body and activates an adaptive response (Reichmann and Holzer, 2015). In Selye's early work, he noticed the body has an uncanny ability to adapt to external stressors so that internal homeostasis can be maintained. Furthermore, the capacity of the body to control or limit the stress does have an upper limit and continuous periods of stress tend to dampen the body's ability to cope. His work ultimately led to the "General Adaptation Syndrome (GAS)", a model comprising three elements which describe the body's response to stress (Selye, 1946). In the initial "Alarm Stage", the body labels the stress as a threat or danger and activates the flight or fight system to counteract the stress and restore balance. In the second "Resistance Stage" the body's defenses become weaker as the stress is eradicated or lessened. Although it

remains alert to fight off additional stressors, its capability is diminished as energy has been allocated to repair damaged tissue and reduce production of stress hormones. Finally, in the "Exhaustion Stage", the body loses its ability to combat a persistent stress, and stress overload can lead to pathophysiological conditions. Together, this work suggests a paradox, which stress in the short-term, is a normal, adaptive response, which can increase health and performance when kept within an optimal range. However, when these same physiological responses are persistent, as occurs during chronic stress or extreme bouts of stress, performance can deteriorate and lead to abnormal stress-responses. This spectrum of effects follows an inverted-U-shaped dose-dependent relationship, as represented in Figure 1.1.

Allostasis, Allostatic Load and, Overload

First introduced by Sterling and Eyer in 1988 and later popularized by Bruce McEwen, the GAS has been refined and can be described in terms of allostasis, allostatic load and overload. Allostasis generally refers to an active process that achieves stability through change (Fisher and Reason, 1988, McEwen, 2006). The body responds to internal and external stressors through non-linear interactions of mediators such as cortisol, the hypothalamic-pituitary-adrenal (HPA) axis, the autonomic, metabolic and immune systems to reach an adaptive state of allostasis. Upon perception of stressful stimuli, the brain triggers allostasis, to adapt to the changing environment and which is then rapidly shut off once the threat is past. However, chronic stress, coupled with dysregulation of the allostatic pathway can put pressure on this homeostatic mechanism. Over time this response can accumulate as allostatic load, specifically the wear and tear that results from chronic over- or underactivity of allostatic mechanisms (McEwen, 1998). Allostatic overload is the cumulative pathophysiology that can result from this dysregulation and excessive stress, which not only manifests itself as

neuropsychiatric disorders, but can play a role in the etiology of obesity and diabetes or neurodegenerative and cardiovascular disorders (McEwen et al., 2015c).

An individual's perception and, ultimately, its response to stress are dictated by numerous factors including genetics, previous experiences, the environment and behavior. By far the most frequently studied gene in regards to anxiety-related personality traits is the serotonin transporter gene (*SLC6A4*), in which the short (s) allele polymorphism was shown to be strongly associated with a vast number of anxiety-related vulnerability traits, although other genes do seem to be involved (Sen et al., 2004). Major negative life events such as traumatic car crashes, wartime combat experience or neglect and abuse can also play a role in shaping an individual's ability to perceive and manage stress, while behaviors such as smoking, lack of exercise or substance abuse can exacerbate the effects of stress (McEwen, 1998). These types of factors contribute to the magnitude of the allostatic load an individual can sustain before overload occurs. Individuals who can accumulate larger degrees of allostatic load before negative consequences occur, are deemed stress resilient, conversely, individuals whose capacity for allostatic load is lessened, are considered stress vulnerable/susceptible. This concept is illustrated in Figure 1.2, as the effects of stress on allostasis/allostatic load and overload follow a dose-dependent inverted U-curve.

Hypothalamic-Pituitary-Adrenal Axis

The principal effectors of the stress response are located in a collection of brain structures commonly referred to as the HPA axis [for review see Smith and Vale (2006)]. Neurons located in the medial parvocellular subdivision of the paraventricular nucleus (PVN) of the hypothalamus synthesize and secrete the peptide corticotropin-releasing factor (CRF),

which is transported from its release site at the median eminence to the anterior pituitary via the hypophysial portal vessels. There it binds to CRF type 1 receptors (CRF-R1) on pituitary corticotropes (Rivier and Vale, 1983), which results in the release of adrenocorticotropic hormone (ACTH) into the systemic circulation. ACTH's principal target is the adrenal cortex, where it triggers glucocorticoid synthesis and secretion. The downstream effectors of the HPA axis are the glucocorticoids, which act both via glucocorticoid and mineralcorticoid receptors, and have numerous roles in both central and peripheral tissues to regulate physiological activity. However, they also provide eventual feedback inhibition at the levels of the hypothalamus and pituitary to inhibit the release of CRF and ACTH, which triggers cessation of HPA activity, and in other central brain structures to arrest stress-related activity (Keller-Wood and Dallman, 1984, Munck et al., 1984). Although this response is generally adaptive in nature, deficient or excessive activation of the HPA axis may develop into pathologies (McEwen and Stellar, 1993).

Neurocircuitry of Fear, Stress, and Anxiety Disorder

To better develop future treatments for anxiety and its related disorders, we must first understand the neurocircuitry involved in mediating normal physiological responses to stress, and how the dysregulation of these pathways involved leads to increased vulnerability to stress. An important aspect of the circuitries involved in regulating fear, stress and anxiety responses is its overlap and interaction with one another. They are not mutually exclusive from each other, either in terms of the brain regions involved or their ability to influence one another. On the one hand, this enables research in the field of stress or fear to be translated to studies of anxiety and vice versa, but this intertwined circuitry also creates problems in interpreting results and caution must be taken in drawing conclusions from certain studies.

Although glucocorticoids are the main effector molecules of the HPA axis that act mainly downstream to mediate the stress response, there are numerous mediators and neural circuits in many brain regions that fine-tune the HPA axis. A growing body of literature, mainly in rodents, but in humans as well, has examined the neurocircuitry associated with fear/stress responses and their ability to modulate anxiety-related behavior. Key components include the amygdala, bed nucleus of stria terminalis (BNST), hippocampus, periaqueductal gray, thalamic nuclei, insular cortex and the prefrontal cortex (PFC, Figure1.2A, for reviews see, Shin and Liberzon (2010), Calhoon and Tye (2015), McEwen et al. (2015a)). Although all of these brain regions play critical roles in the etiology of stress and anxiety, we have focused our attention to a particular brain region within the limbic system, the amygdala, which will be the emphasis of the physiology and circuitry to be discussed.

Amygdala

The amygdalae, located deep in the medial temporal lobes, are two almond shaped structures comprising multiple interconnected nuclei including the basolateral complex [BLA; consisting of the lateral (LA), basal (BA) and basomedial (BM) groups], central nucleus (CeA; consisting of the lateral (CeL) and medial (CeM) subdivisions), cortical nucleus, medial nucleus and the intercalated cell clusters (ITCs, Figure 1.2B) (Krettek and Price, 1978, Janak and Tye, 2015). Although the amygdala is found in most vertebrates, suggesting the circuitry and function of the amygdala is evolutionary conserved, some species differences in cytoarchitecture and neurocircuitry do exist (Janak and Tye, 2015). Simplistically, neurotransmission through the amygdala can be considered to originate in the LA, which receives an array of sensory information about the external environment from the thalamus and cortical regions (McDonald, 1998). This information is passed forward via projections to

the BA, BM and CeA. There are bi-directional connections from the BLA to many cortical regions, including the PFC, BNST and hippocampus, while unidirectional connections are made from the BLA to the dorsomedial striatum and nucleus accumbens (NAc) (Figure 1.2C). For an extensive review see (Calhoon and Tye, 2015). It is generally thought that the striatum, BNST and CeA transmit integrated BLA signals to behavioral outputs, with the CeA playing a major role in governing the expression of fear responses and projections to the BNST influencing motivated behaviors and anticipatory anxiety (Walker et al., 2003, Corbit et al., 2013, Stamatakis et al., 2014). Other connections also play a role in conveying sensory information to intra- and inter-amygdala regions of the CNS [for review, see Janak and Tye (2015)].

The BLA is morphologically and cytoarchitecturally similar to the cortex, consisting of mainly glutamatergic, spiny projection cells (~80-90 %) and spine-sparse, local circuit GABAergic interneurons (~10-20 %), while the CeA largely comprises GABAergic neurons resembling striatal medium-sized spiny neurons while the ITC contains small, densely packed, spiny, ovoid GABAergic neurons (Hall, 1972, McDonald, 1982, Rainnie et al., 1993, Sun and Cassell, 1993).

The amygdala has long been known to regulate emotion and motivation, in part by processing fearful and rewarding environmental sensory, information. The first clues as to the role of the amygdala in regulating emotional behaviors stemmed from early lesion studies in the rhesus monkey (Brown and Sharpey-Schäfer, 1888). Following bilateral ablation of the temporal lobe, it was evident the subjects still retained senses of sound and sight, however, they clearly no longer understood the meaning of them and certain behaviors such as aggression, fear and defensiveness were reduced. Although these crude early studies did not

specifically distinguish the role of the amygdala in these behavioral outcomes, they were the first to define a region of the brain responsible for connecting sensory information to their emotional meaning. Later, direct lesions of the amygdala induced experimentally in rodents and primates and observed in humans reinforced these early ideas and revealed the amygdala to be crucial for reinforcing positive and negative stimuli, and especially a type of learning called fear conditioning (Weiskrantz, 1956, Blanchard and Blanchard, 1972, LeDoux et al., 1990, Adolphs et al., 1994, Anderson and Phelps, 2001).

The Amygdala in Fear Conditioning/Extinction

Unlike anxiety, which can be evoked by potential, circumstantial or anticipated threats, fear is generally more adaptive and transient in nature, being prompted by actual sensory inputs from imminent threats. Numerous studies in both humans (using functional magnetic resonance imaging (fMRI)) and animals have used Pavlovian fear conditioning to highlight the importance of the amygdala in the acquisition and extinction of fear (LeDoux et al., 1990, Quirk et al., 1995, Lang et al., 2000, Quirk et al., 2003, Pare et al., 2004, Phelps et al., 2004, Barrett and Armony, 2009). Synaptic plasticity seems to be required for fear learning, as retrieval of fear memories requires reconsolidation and protein synthesis, and plasticity in the LA develops before the conditioned fear behavior does, suggesting plasticity is key in driving the behavioral outcome (Quirk et al., 1997, Rogan et al., 1997, Nader et al., 2000, Repa et al., 2001).

In recent years, there has been a surge in amygdala research examining the neurocircuitry and emotional behavior regulated by the amygdala in several experimental animal species, driven mainly by recent advances in technology that have allowed the precise

identification and specific targeting of individual cell types based on their molecular profile and connectivity (Tye and Deisseroth, 2012, Jennings and Stuber, 2014, Sternson and Roth, 2014, Namburi et al., 2015, Tovote et al., 2015). These technological approaches, especially optogenetics, have led to recent advances in the stress/fear field. For example, with channelrhodopsin 2 (ChR2, a light activated excitatory opsin) expressed only in LA principal neurons, it was demonstrated that LA projection neurons are crucial in fear conditioning, as photoactivation of LA neurons substituted effectively for a footshock as an US, resulting in conditioned freezing when paired with an auditory CS (Johansen et al., 2010). Another study determined that photoactivation of ChR2-expressing glutamatergic terminals arising from the auditory cortex in the LA can replace the CS when paired with a conventional US, resulting in freezing behavior and long-term potentiation (LTP) (Nabavi et al., 2014). Other studies using optogenetics have shown that inactivation of the CeL or activation of the CeM induces unconditioned freezing, indicating that the CeM is under tonic inhibitory control by the CeL and the CeL is required for acquisition, while the CeM is required for the expression of the fear response (Ciocchi et al., 2010). Furthermore, using extracellular *in vivo* recordings, it was shown the CeL contains two distinct populations of inhibitory cells that have opposing functions in fear conditioning. One population is termed CeL^{ON} and is excited by the CS, whereas the other (CeL^{OFF}) is inhibited. Although both populations inhibit one another and both project to the CeM, CeL^{ON} neurons respond more quickly to the CS, indicating they act to inhibit CeL^{OFF} neurons projecting to the CeM, and the resulting disinhibition of the CeM promotes the conditioned fear response (Ciocchi et al., 2010, Haubensak et al., 2010).

The Amygdala in Anxiety

Anxiety is far less understood than fear and much remains to be elucidated to properly understand this more complex emotional response. In contrast to fear, anxiety is elicited by less specific and less predictable threats, or by those that are physically and psychologically more distant. Although there is substantial overlap in the neural substrates and circuitry involved in anxiety and fear, the precise circuits involved are only beginning to emerge. Regardless, in humans, an abundance of data implicates the amygdala's role in mediating anxiety-related behavior. For example, amygdala enlargement is associated with higher levels of anxiety, and levels of anxiety can be reliably predicted by morphometry and intrinsic functional connectivity of specific amygdala nuclei in both children and adults (De Bellis et al., 2000, Etkin and Wager, 2007, Schienle et al., 2011, Baur et al., 2012, Qin et al., 2014). Furthermore, amygdala activity is elevated during fear conditioning and anticipatory anxiety in patients with social anxiety relative to healthy subjects (Boehme et al., 2014). With the conserved nature of the amygdala across species, neural circuits underlying anxiety have predominantly been examined in rodent models, making these findings most likely translational to our understanding in humans. In rodent models, expression of the immediate early gene *c-fos* is seen in the amygdala following exposure to the anxiogenic context of the EPM (Silveira et al., 1993, Butler et al., 2012). Moreover, pharmacological inactivation of the amygdala with a direct injection of the $GABA_A$ receptor agonist muscimol is anxiolytic in the EPM, while injection of the $GABA_A$ receptor antagonists bicuculline or picrotoxin produced anxiogenic-like effects in SI tests (Sanders and Shekhar, 1995, Moreira et al., 2007).

Great emphasis has been placed on identifying the roles of specific nuclei and the neuronal phenotypes within them that orchestrate emotionally-relevant behavior through their

intricate neurocircuitry and the coordinated activation of their downstream projections. Within the amygdala, two nuclei that have received the most attention are the CeA and BLA. The CeA appears to be the primary site for eliciting conditioned fear responses, although it does play a role in mediating anxiety-like behavior, while the BLA is proposed to be an integrator and relay center in the acquisition of fear and the expression of emotion (Shekhar et al., 2005). For the purposes of this thesis, focus will be placed on the BLA, however, for more detailed reviews on other regions of the amygdala, see (Shin and Liberzon, 2010, Adhikari, 2014, Janak and Tye, 2015, Tovote et al., 2015).

The Basolateral Amygdala

The BLA is the chief regulator of emotional responses, as it receives robust, highly processed multimodal sensory inputs from various cortical regions, then integrates and processes these inputs to allocate salience, and valence. Salience refers to any aspect of a stimulus that, for any of many reasons, stands out from the rest and valence, the intrinsic attractiveness (positive valence) or aversiveness (negative valence) of an event, object, or situation. The BLA then choreographes the expression of behavioral responses through an intricate network of downstream projections (LeDoux, 1992). The efferent target sites mediating stress-related behavior include the CeA and BNST, while the NAc is important for positive reward cues, the hippocampus for memory consolidation and the frontal cortex for stimulus coding and top-down control of output (McDonald, 1998, Pitkanen et al., 2000, Roozendaal et al., 2002, Schoenbaum et al., 2003). The activity of the BLA is regulated by a coordinated balance of glutamatergic-excitatory and GABAergic-inhibitory neurotransmission, that can be modulated by various mediators including cortisol, 5-HT, NA, neuropeptide Y (NPY) and CRF. This activity maintains an overall inhibitory tone over this

nucleus, and consequently any disruption of this basal level can have profound effects on emotional behavior (Rainnie et al., 1991a, b, Sajdyk and Shekhar, 1997b, a, Giesbrecht et al., 2010).

As previously mentioned, there are two main types of neurons found within the BLA; Glutamatergic projection neurons (making up ~85 % of the neuronal population) containing Ca^{2+}/calmodulin-dependent protein kinase II (CaMKII, also used as a neuronal marker) and calcineurin (CaN, a protein phosphatase), and GABAergic interneurons (making up ~15 % of the neuronal population) that are immuno-positive for GABA and a number of other neuropeptides such as somatostatin (SOM), NPY, vasoactive intestinal peptide (VIP), cholecystokinin (CCK), and/or calcium binding proteins including parvalbumin, calbindin and calretinin (McDonald, 1982, McDonald and Pearson, 1989, McDonald, 1992, McDonald and Mascagni, 2001, Sah et al., 2003). The glutamatergic projection neurons can be classified into two groups based on their morphologies and electrophysiological characteristics, however for future use, we will make no distinction between these groups and label all glutamatergic projection neurons as "principal neurons" (Rainnie et al., 1993). Class I pyramidal neurons have a pyramidal perikaryon with spine-laden apical and basal dendrites. Their electrophysiological properties include the highest input resistances, long membrane time constants and long action potential duration with regular firing pattern showing accommodation. Class I stellate neurons have somewhat larger cell body with a stellate appearance and spine-laden dendrites. Electrophysiologically, they have lower input resistance than Class I pyramidal neurons, a shorter membrane time constant, shorter action potential duration, and a delay in firing after injection of depolarizing current, but can also support burst firing. GABAergic interneurons were initially described as Class II neurons that were smaller

in size than Class I cells and are multipolar with spine-sparse dendrites. Electrophysiological characteristics relative to Class I cells include intermediate values for input resistance, membrane time constant, action potential duration, and burst firing, with little or no accommodation of action potential trains. GABAergic interneurons have since been further classified based on their detailed electrophysiolgical characteristics coupled with morphology and the expression of suites of neuropeptides plus calcium binding protein as noted above, specifically: 1) parvalbumin+/calbindin+ (~50 % of all interneurons), 2) SOM+/NPY+/calbindin+, 3) large multipolar CCK+, often with calbindin+, and 4) small bipolar and bitufted that are VIP+, calretinin+ and CCK+ (McDonald and Pearson, 1989, Washburn and Moises, 1992, Rainnie et al., 1993, Kemppainen and Pitkanen, 2000, Martina et al., 2001, McDonald and Mascagni, 2001, 2002, Mascagni and McDonald, 2003, Spampanato et al., 2011). Although comprising only ~15% of the total neuronal population, local GABAergic interneurons have profound effects on determining excitability of BLA principal neurons, as well as the ability to provide feedback inhibition, through their immense network of synaptic connections acting both via fast ($GABA_A$-mediated) and slow (metabotropic $GABA_BR$-mediated) inhibitory synaptic transmission, and thus maintain BLA principal neurons at low spike frequencies (Pare and Gaudreau, 1996, Woodruff and Sah, 2007). Based on this, it has been postulated that modulation of local inhibition is a critical component in the regulation of emotional behaviors [for review see Spampanato et al. (2011)].

Stress-induced Synaptic and Structural Plasticity in the BLA

From the studies presented above, it is clear the BLA plays a major role in generating and regulating stress/fear-related responses, however, during allostasis and as allostatic load becomes too great and overload occurs, there are changes that occur within the BLA that can

have adaptive or maladaptive consequences. One such example is the effects of stress on memory consolidation, memory retrieval and working memory. Emotionally arousing events, such as threatening encounters, engage a number of endocrine and neurotransmitter systems that ultimately activate the BLA, which is also pivotal in modulating memory consolidation (McGaugh, 2000). Enhanced memory for stressful or emotionally relevant events is highly adaptive as it helps individuals remember important information and serves to prepare them for future encounters, however, exposure to extremely aversive experiences can lead to highly emotional, traumatic and fearful memories, which contribute to the etiology of anxiety-related disorders such as PTSD (Baratta et al., 2015). Conversely, stress impairs memory retrieval and working memory, which is thought to prevent memory distortion thereby enhancing accuracy of the memory (Wolf et al., 2004). The stress-induced effects on memory in the BLA are mediated in part due to alterations in synaptic and structural plasticity.

As mentioned above, under basal conditions, principal neurons in the BLA receive tonic $GABA_A$-mediated inhibition. Stress-induced excitation of the nuclei caused by glutamate-mediated N-methyl-D-aspartate (NMDA) receptor activation can overcome this inhibitory tone, leading to calcium influx, greater net activation of the cell and also long-term changes in synaptic plasticity (Rainnie et al., 1991a). Synaptic plasticity such as long-term potentiation (LTP) and long-term depression (LTD), which are believed to be cellular substrates for memory formation during learning are evident in BLA (Chapman et al., 1990, Clugnet and LeDoux, 1990, Collingridge and Bliss, 1995). Both LTP and LTD are active learning processes that enhance or diminish, respectively, the efficacy of a synapse, typically through altered postsynaptic receptor expression/insertion or in some cases altered neurotransmitter release, and generally take place at glutamatergic synapses (Rumpel et al.,

2005, Shekhar et al., 2005, Makino and Malinow, 2009, Nedelescu et al., 2010). While the exact intra-cellular mechanisms involved in synaptic plasticity in the BLA are still being resolved, kinases such as CaMKII, mitogen-activated protein (MAP) kinase, protein kinase A (PKA) and extracellular signal-regulated kinase (ERK) are widely involved in the development and maintenance of LTP, while phosphatases such as calcineurin have also been shown to mediate LTD in several brain regions (Schafe et al., 2000, Lin et al., 2003a, Sweatt, 2004, Lin et al., 2005). In addition to the rapid changes underlying synaptic plasticity, these intracellular signaling cascades can also induce specific changes in gene expression, ultimately leading to altered protein expression and synaptic and structural plasticity (Josselyn et al., 2001, Maren et al., 2003, Rattiner et al., 2005).

In addition to its effects on functional synaptic plasticity, stress can also result in the remodeling of neurons and structural plasticity. In the hippocampus and prefrontal cortex, acute and chronic stress induces dendritic retraction and spine loss, which is transient in nature (Conrad et al., 1999, Sandi et al., 2003, Cook and Wellman, 2004, Hill et al., 2011, McEwen et al., 2015d). It has been postulated that this could be an adaptive response that limits the excitotoxic effects of enhanced glutamate release in these regions, thereby preventing permanent damage (McEwen, 2001). However, if there is no reversal of the stress-induced architectural changes, cognitive impairment or anxiety-related disorders may develop (McEwen et al., 2015b, McEwen et al., 2015d). In contrast, the BLA responds to acute stress by increasing spine density, while chronic stress induces increased spine density and dendritic hypertrophy in principal neurons, which are both coupled to elevated anxiety-like behavior (Vyas et al., 2002, Vyas et al., 2004, Mitra et al., 2005, Vyas et al., 2006, Adamec et al., 2012, Hill et al., 2013, Padival et al., 2013b). Furthermore, compounds that reduce excitability of

BLA neurons, such as the SK channel activator 1-EBIO, reduce anxiety-like behavior, while transgenic overexpression of the type-2 SK channel causes dendritic retraction in the BLA, and reductions in anxiety-like behavior (Mitra et al., 2009, Rosenkranz et al., 2010). Interestingly, unlike in the hippocampus and PFC, these stress-mediated effects on dendritic hypertrophy in the BLA are long lasting, which suggests they may not be adaptive, and instead represent a structural correlate in the etiology of anxiety-like behavior. To date, a number of studies have investigated potential signaling pathways that are involved in mediating stress-induced morphological changes. Brain-derived neurotrophic factor (BDNF), a neurotrophin which facilitates plasticity and growth, appears to be a prime signaling candidate. In the BLA overexpression of BDNF occludes the morphological effects of chronic stress, while BDNF haploinsufficiency prevents stress-induced morphological changes (Govindarajan et al., 2006, Lakshminarasimhan and Chattarji, 2012). Other potential signaling modulators include tissue plasminogen activator (tPA, although this effect was only observed in the medial amygdala), CRF, lipocalin-2 and endocannabinoids (Matys et al., 2004, Bennur et al., 2007, Hill et al., 2013, Skrzypiec et al., 2013). Therefore, developing means to prevent dendritic expansion of BLA principal neurons or triggering hypotrophy following stress may therefore provide an opportunity to treat patients with anxiety-related disorders.

Neuropeptide Regulation of the stress response

A perplexing aspect of the stress response is its complexity, not only with respect to the neurocircuitry involved in various brain regions, but also with respect to the multiplicity and diversity of modulators that play a role. However, there are many factors that influence the pattern and magnitude of our response to stress, including its duration (acute vs. chronic), type (physical threat vs. anticipatory), context in which it appears (familiar place vs.

unfamiliar), and genetics, sex or age. Therefore, evolution has apparently provided a multitude of mechanisms that may influence the stress response at different sites along the stress pathway and for each unique type of stress. In addition to glutamate and GABA, the classical CNS neurotransmitters that mediate fast excitatory and inhibitory synaptic transmission, respectively, the BLA is subject to regulation by a number of other factors, including but not limited to, serotonin (5-HT), noradrenaline (NA), endocannabinoids and BDNF. Relevant to this specific work, there is a large body of accumulating evidence that suggests two neuropeptide systems: NPY and CRF orchestrate opposing regulation of responsiveness to stressful stimuli in the BLA, and ultimately result in anxiolysis and anxiogenesis, respectively. In addition to the findings that these neuropeptides can reciprocally modulate anxiety- and stress-related behaviors independently of each other, evidence suggests CRF and NPY interact directly to maintain emotional balance, and that disruption of this homeostatic mechanism could contribute to maladaptive stress responses and anxiety (for review see (Heilig et al., 1994, Sajdyk et al., 2004). Targeting a neuropeptide system to treat anxiety-related disorders might help improve clinical outcomes, as these systems are not as widely distributed as are the classical neurotransmitters, they have low levels of tonic activity but also have a long duration of action due at least in part to low mobility caused by their relatively large size and the lack of specific removal from synaptic space by reuptake systems.

Neuropeptide Y

NPY is a 36-amino acid peptide belonging to a family of structurally similar biologically active peptides, including the enteric peptide YY (PYY) and pancreatic polypeptide (PP) (Tatemoto et al., 1982). NPY is derived by specific proteolytic processing from a precursor (pre-pro-NPY), and C-terminal amidation. NPY is one of the most abundant

neuropeptides found in the human brain, with high expression levels in the neocortex, the limbic system including the hypothalamus, hippocampus, and amygdala, the basal ganglia and the brainstem locus coeruleus (LC), the nucleus tractus solitarii (NTS) and the spinal cord (Adrian et al., 1983, Brakch et al., 1997, Caberlotto et al., 2000, Kask et al., 2002). Within the BLA, NPY is localized to a subset of GABAergic interneurons that typically co-express SOM (McDonald, 1985). A number of peripheral tissues also express NPY, including sympathetic nerves innervating virtually all organs and blood vessels except for those directly innervating the skin including the adrenals, lungs, urinary tract, spleen, and the reproductive organs (Sah and Geracioti, 2013). With such a wide expression profile, it is not surprising that NPY plays a crucial role in a number of physiological functions including the central control of energy homeostasis and food intake, circadian rhythm, cognition, vasoconstriction in many vascular beds, seizure suppression and relevant to this work, a key component of the stress response, producing anxiolytic activity (Heilig, 2004, El Bahh et al., 2005, Eaton et al., 2007, Chee et al., 2010, Giesbrecht et al., 2010, Morin, 2013).

To date, 5 NPY receptors (Y1, Y2, Y4, Y5 and y6) have been described in mammals that mediate the effects of NPY and its related peptides, however, the y6-receptor is non-functional in humans and primates, and is not expressed in rats, while the Y4-receptor is preferentially activated by PP and NPY itself has low affinity for this subtype (Blomqvist and Herzog, 1997, Dumont et al., 1998, Bromee et al., 2006). The Y1- and Y2-receptors are widely distributed in the brain with the highest densities observed in the frontal cortex, lateral septum, NAc, BNST, hypothalamus, amygdala, hippocampus and NTS (Kask et al., 2002, Kopp et al., 2002). The Y5-receptor is less abundant than the Y1- and Y2-receptors, but is found in many limbic brain regions, and is often found co-expressed within the same cell

bodies and fibers as the Y1-receptor (Dumont et al., 1998, Wolak et al., 2003). Immunohistochemical analysis has revealed co-localization of NPY and the Y2-receptor together on GABAergic terminals, suggesting the Y2 is a presynaptic auto-receptor for NPY (Caberlotto et al., 2000, Stanic et al., 2011). All NPY receptors are type 1 G-protein-coupled receptors, nominally coupled to G_i/G_0 proteins and associated with several downstream signaling pathways. Activation of NPY receptors results in inhibition of adenylate cyclase, which reduces cyclic adenosine monophosphate (cAMP), thereby reducing activation of PKA and the phosphorylation of downstream molecules (Wan and Lau, 1995). Furthermore, NPY receptor activation can lead to alterations in gene transcription through ERK or cAMP response element-binding protein (CREB) signaling (Narvaez et al., 2015). Mobilization of intracellular Ca^{2+} stores through phospholipase C/phosphatidylinositol 3-kinase (PLC/PI3K) activity has also been shown in response to NPY receptor activation (Wan and Lau, 1995). Finally, a number of ion channels are also regulated by NPY, likely by direct intractions with βγ-subunits activated by G_i or G_o, with actions including the inhibition of voltage-gated Ca^{2+} and hyperpolarization-activated cyclic nucleotide-gated (HCN) channels and activation of G-protein-coupled inwardly-rectifying potassium (GIRK) channels (Sun et al., 2001, Wang, 2005, Giesbrecht et al., 2010). Differences in responses mediated by individual NPY receptor subtypes seen in specific neurons in the same or different brain regions are likely to result from the presence of different signaling pathways in individual neurons, the differential distribution of NPY receptors on soma, dendrites or presynaptic terminals and the presence of different effector systems. An overview of NPY receptors, their endogenous ligand preferences, selective agonists/antagonists, as well their cell signaling pathways is summarized in Table 1.1.

NPY's Anxiolytic Properties

The coordinated actions mediated by the NPY system on cardiovascular, sympathetic, metabolic, neuroendocrine and immune systems, has resulted in its identification as a major component in the physiological and behavioral aspects of the stress response, and an accumulating body of literature supports an anxiolytic function (Heilig, 2004, Tasan et al., 2015). Central administration of NPY produces anxiolytic-like effects in a number of behavioral paradigms including the EPM, Vogel's drinking conflict test, social interaction, fear conditioning/extinction as assessed by contextual and cued freezing as well as fear-potentiated startle (Heilig et al., 1989, Broqua et al., 1995, Sajdyk et al., 1999b, Gutman et al., 2008, Fendt et al., 2009). Consistent with these findings, NPY knockout mice are more anxious in EPM, OFT and light-dark tests, and have accelerated fear acquisition, while NPY overexpression renders animals less anxious (Bannon et al., 2000, Thorsell et al., 2000, Primeaux et al., 2005, Karl et al., 2008, Lin et al., 2010, Verma et al., 2012). A number of studies suggest the anxiolytic actions of NPY are primarily mediated by the amygdala, although other brain regions such as the hippocampus and BNST likely contribute to its actions as well (Kask et al., 2002, Kash and Winder, 2006, Smialowska et al., 2007).

Although NPY itself is uniformly anxiolytic, the receptor or receptors mediating these actions is unclear. There is general consensus that Y1-receptor activation is responsible for the majority of the acute anti-anxiety actions, as intra-amygdalar injection of the Y1-receptor antagonist BIBP3226 is anxiogenic, while administration of the Y1-receptor selective agonist ([D-His26]NPY) is anxiolytic in both the EPM and OFTs (Sorensen et al., 2004, Primeaux et al., 2005). Furthermore, the anxiolytic actions of NPY can be inhibited by prior- or co-injection of the Y1-antagonist BIBO3304, as assessed in the SI test (Sajdyk et al., 1999b).

Genetic studies corroborate these findings as Y1-receptor knockout mice have an anxiogenic phenotype (Karl et al., 2006). To date there are only a few studies that have investigated the potential cellular mechanisms for NPY-evoked anxiolysis by the Y1-receptor. An early study suggested the protein phosphatase calcineurin, which is implicated in synaptic plasticity and colocalizes with Y1-receptors in principal neurons of the BLA to be involved, as inhibition of calcineurin blocked the long-term anxiolytic effects of repeated NPY injections (Sajdyk et al., 2008, Leitermann et al., 2012). Moreover, in acute brain slices, NPY acting via the Y1-receptor hyperpolarizes principal neurons of rat BLA and deminish excitability by reducing a hyperpolarizing activated-depolarizing current (I_h, carried by HCN channels) (Giesbrecht et al., 2010). Because excitatory output from the BLA is anxiogenic, this action of NPY is consistent with an anxiolytic action. In a more recent study again studying BLA neurons in acute rat brain slices, application of the Y1-agonist [Leu^{31},Pro^{34}]-NPY increased the amplitude of evoked $GABA_A$-mediated inhibitory postsynaptic currents (IPSCs), while concurrently reducing evoked NMDA-mediated excitatory postsynaptic currents (EPSCs) (Molosh et al., 2013). The overall effect resulted in inhibition of principal cells, which is consistent with the anxiolytic effects of NPY.

Interestingly, in contrast to Y1-receptor activation, activation of the Y2-receptor system in the amygdala appears to mediate anxiogenic-like behavior, possibly as a result of its presynaptic localization and its ability to act as an auto-receptor to inhibit the release of NPY (Caberlotto et al., 2000, Sajdyk et al., 2002b). Intracerebroventricular (ICV) and intra-amygdala injection of the Y2-preferring agonists NPY_{3-36} and NPY_{13-36} produced anxiogenic activity in both SI and EPM tests, while treatment with the Y2-antagonists BIIE0246 and JNJ-31020028 both have anti-anxiety effects (Bacchi et al., 2006, Cippitelli et al., 2011, Kallupi et

al., 2014). Genetic studies have supported these findings, as reduced anxiety is observed in Y2-receptor knockout mice (Redrobe et al., 2003, Tschenett et al., 2003). The role this receptor plays in mediating emotional responses becomes obscured, as one study found that in Y2-receptor deficient mice, anti-anxiety activity was not observed (Zambello et al., 2011). Furthermore, injection of a Y2-selective agonist into the CeA resulted in reduced fear conditioning and promoted fear extinction, while injection into the LC or lateral septum increased open arm entries in the EPM (Kask et al., 1998, Trent and Menard, 2013, Verma et al., 2015). These studies suggest that there may be brain-region dependent interactions with the Y2-receptor and genetic background of the animals studied may influence the behavioral effects of Y2-receptor activation.

By far, the least well studied of the NPY receptors in the context of anxiety-related behavior is the Y5-receptor. Controversy still remains as to the role this receptor plays in the regulation of emotion. Originally, it was suggested the Y5-receptor did not play a functional role as administration of the Y5-antagonist CGP71683A did not modify anxiety in the EPM or SI tests (Kask et al., 2001b). Later, a number of studies suggested Y5 may mediate anxiolytic activity as the selective Y5-agonist, [cPP1–7,NPY19–23,Ala31,Aib32,Gln34]hPP (cPP), decreased anxiety-like behavior in the EPM, OFT and SI tests (Sorensen et al., 2004, Morales-Medina et al., 2012). Human studies also indicate a role for the Y5-receptor in mediating anxiolytic activity, as a number of genetic variants of the Y5 gene are associated with panic disorder in male, but not female subjects (Domschke et al., 2008). Conversely, injection of a novel Y5-antagonist, Lu AA33810, was reported to produce anxiolytic-like effects in the SI test (Walker et al., 2009). Genetic studies have yet to resolve the paradox these pharmacological studies have produced, as Y5-receptor knockout mice and mice with

overexpression of the Y5-receptor in the hippocampus and amygdala do not differ in anxiety-related behavior (Olesen et al., 2012a, Ito et al., 2013). It appears there may be some interaction with the Y5- and Y1-receptors as conditional knockout of the Y1-receptor in Y5-receptor-expressing principal neurons resulted in elevated anxiety-like activity in mice as assessed by the EPM and OFT (Longo et al., 2014). Another study by the same group using the same conditional knockout animal model confirmed these results and further showed that responses to chronic social stress, group-housing animals or housing animals in isolation, were not affected in these conditional knockout animals (Longo et al., 2015). From the above studies, it is clear that more work needs to be done to elucidate how this receptor regulates emotional behaviors in the brain.

NPY in Stress Resilience

Resilience has been defined as achieving a positive outcome in the face of adversity, and in relation to stress, it is simply the ability to better cope with stress (McEwen et al., 2015b). As discussed in the allostasis section, there are a number of genetic, epigenetic, psychological and environmental factors that determine the amount of allostatic load an individual can tolerate before overload occurs. Both genetic and pharmacological studies in rodents, as well as several lines of evidence from human studies attest to the resilience-promoting properties of NPY. An early study in transgenic rats made to globally overexpress NPY showed insensitivity to the normal anxiety promoting behavior of restraint stress on the EPM and did not produce fear suppression in a punished drinking test (Thorsell et al., 2000). In a pharmacological study that implicates the BLA in NPY-mediated stress resilience, repeated daily injections of NPY directly into the BLA for 5 consecutive days protected these animals from the negative consequences of prior restraint stress in the SI test, and this effect

persisted up to 8 weeks following the first injection (Sajdyk et al., 2008). This effect was suggested to be calcineurin-dependent downstream of NPY-receptor activation, as co-injection of calcineurin-inhibitory peptide attenuated this response. Furthermore, intranasal infusion of NPY in rats, prior to exposure of a single prolonged stress (an animal model of PTSD), reduced anxiety like behavior on the EPM and on acoustic startle responses (Serova et al., 2013). Analysis of NPY expression levels also indicate a role for the peptide in resilience, as there are observed reductions in the quantity of NPY in the amygdala following recovery from chronic variable stress, which could explain the exaggerated fear responses in rats subjected to chronic variable stress (McGuire et al., 2010, McGuire et al., 2011). Moreover, just as there is significant inter-variability in human populations to develop PTSD following severe emotional trauma, responses of experimental animals to the same psychological trauma can also vary widely. A number of studies have determined that animals expressing a stress resilient phenotype are correlated with higher NPY levels in various brain regions including the hippocampus, amygdala and BNST (Hawley et al., 2010, Bardi et al., 2012, Cohen et al., 2012).

NPY's role in stress resilience in humans is often studied in military subjects along with PTSD patients. PTSD develops in a subpopulation of people in the aftermath of an extremely traumatic event, such as car crashes, environmental disasters or following combat in war, and these patients often re-experience the event in the form of disturbing flashbacks or dreams, acquire avoidance behaviors to the experience and show increased nervousness, irritability and arousal (Benedek, 2011). In an early study examining military survival training and extreme interrogation, subjects with higher plasma NPY levels were more resilient to stress as seen with better performance scores, while individuals with lower NPY levels

showed symptoms of dissociation (Morgan et al., 2000). Furthermore, basal plasma levels of NPY are lower in PTSD patients and in combat-exposed individuals with PTSD compared to non-PTSD subjects (Rasmusson et al., 2000, Morgan et al., 2003). As plasma NPY levels may not accurately reflect the concentration exposed at the site of action in the brain, a number of studies evaluated NPY levels in the cerebrospinal fluid (CSF). Using this approach, it was shown that combat-exposed veterans with PTSD have lower CSF levels of NPY compared to healthy men and compared to veterans without PTSD (Sah et al., 2009, Sah et al., 2014). Finally, a genetic study examining the inter-individual variation in NPY expression has linked low NPY expression to heightened amygdala activity and emotional reactivity following exposure to threat-related facial expressions (Zhou et al., 2008).

Corticotropin-releasing Factor

CRF (also known as corticotropin-releasing hormone, CRH) is a 41-amino-acid neuropeptide that mediates the autonomic, neuroendocrine, and behavioral responses to stress via activation of the HPA-axis, as well as extrahypothalamic limbic forebrain structures (Krohg et al., 2008). CRF is a member of a peptide family that includes urocortin (UCN), urocortin II (UCN II) and urocortin III (UCN III), whose effects are mediated via activation of two G-protein-coupled receptors (G_s): CRF-R1 and CRF-R2 (Dautzenberg and Hauger, 2002). The highest density of CRF containing neurons is found in the PVN; however, other brain regions express this neuropeptide, including the CeA, BNST, LC, hippocampus and brainstem, as well as a number of peripheral tissues (Krohg et al., 2008). The highest density of CRF receptors is in the corticotrophs of the anterior lobe of the pituitary, but they are also broadly distributed in similar brain regions as CRF itself. CRF-R1 is more abundant than CRF-R2 and both are implicated in regulating behavioral stress responses; however, they

appear to act in opposition to each other, with CRF-R1 activating and CRF-R2 inhibiting, respectively, the CRF-mediated stress response (Heinrichs et al., 1997, Bale and Vale, 2004).

CRF's Role in Mediating Anxiety-like Behavior

A number of studies have shown anxiogenic responses to central administration of CRF using several different behavioral paradigms, including OFT, acoustic startle, operant-conflict, EPM and SI tests (Britton et al., 1982, Britton et al., 1985, Swerdlow et al., 1986, Heinrichs et al., 1992, Sajdyk et al., 1999a). CRF-R1 antagonists have been identified as a potential treatment option for stress-induced anxiety disorders, as administration of these compounds decreases anxiety-like behavior in rats and mice, as well as in human subjects diagnosed with depression or PTSD (Zobel et al., 2000, Keck et al., 2001, Ducottet et al., 2003, Adamec et al., 2010). Experimental genetic studies confirm these findings as CRF-R1 knockout in mice results in decreased anxiety and impaired stress responses whereas CRF-R2 knockout mice display anxiety-like behaviors (Smith et al., 1998, Bale et al., 2000). Furthermore, in a non-human primate model of PTSD and in human patients with PTSD, there are significant increases in CRF levels in the CSF compared to controls (Coplan et al., 1996, Baker et al., 1999).

Accumulating evidence suggests the amygdala and particularly the BLA are critical sites for CRF-mediated, stress-related behavioral responses. The BLA is a major extrahypothalamic source of CRF-neurons, while a minor element is derived from GABAergic projections from the CeA (Swanson et al., 1983). Within the BLA, mRNA for CRF-R1, but not for CRF-R2, is present, suggesting the majority of the neuronal and behavioral effects of CRF in this nucleus result from activation of the CRF-R1 (Chalmers et

al., 1995). In preclinical animal studies, acute stress increases both CRF release and CRF mRNA expression within the amygdala (Kalin et al., 1994, Merlo Pich et al., 1995, Merali et al., 1998). Furthermore, lesions of the CeA attenuate the excitatory effects of CRF on the acoustic startle reflex (Liang et al., 1992). Pharmacological studies corroborate these findings. Thus, intra-BLA injection of CRF or UCN induces anxiety-related behavior, which could be blocked via injection of CRF-R1 antagonists (Sajdyk et al., 1999a, Sajdyk and Gehlert, 2000, Roozendaal et al., 2002, Rainnie et al., 2004, Gehlert et al., 2005). Moreover, CRF action within the BLA also appears to play a prominent role in stress vulnerability as repeated injection of a subthreshold dose (i.e., one that specifically did not elicit an acute anxiogenic response) of CRF or UCN directly into the BLA for 3 consecutive days induced an elevated state of anxiety-like behavior (UCN-induced priming) by the third day, as assessed in SI tests (Shekhar et al., 2003). Furthermore, these authors reported that chronic UCN application also increased excitatory, and decreased inhibitory synaptic drive onto BLA principal neurons as seen by an increase and decrease in spontaneous EPSPs and spontaneous IPSPs, respectively. In a follow-up study, this group reported that injecting the same subthreshold dose of UCN for 5 consecutive days induced a persistent state of anxiety-like behavior that lasted up to 5 weeks (Rainnie et al., 2004). In both the above studies, the effect was dependent on CaMKII, as co-administration of UCN with a CaMKII inhibitor (KN-62) abolished its effects. Furthermore, in the latter study, the UCN effect was seen to be dependent on NMDA-receptor activation, as an NMDA receptor antagonist prevented the long-term behavioral effect. Finally, electrophysiological experiments in this study revealed a UCN-mediated reduction in GABAergic-mediated evoked IPSPs and spontaneous IPSPs. Therefore, the CRF-mediated

pathological anxiety observed was suggested to depend on long-term synaptic plasticity, likely in the form of LTP.

In addition to the investigations above, other studies have examined the molecular mechanisms that result in altered BLA activity due to activation of the CRF-R1 *in vitro*. CRF increases excitability of BLA principal neurons by a number of different mechanisms. As excitatory output from the BLA is known to be anxiogenic, this increase in excitability is likely the cause of CRF-mediated increases in anxiety-related behavior. Acutely, CRF increases excitability by reducing the amplitude of a calcium sensitive potassium conductance which mediates the slow afterhyperpolariztion following evoked action potential firing (Rainnie et al., 1992). In acute brain slices, field potentials recorded in the BLA via evoked electrical stimulation in the LA showed that CRF increased the amplitude of the postsynaptic component of the field potential by activating CRF-R1, suggesting increased postsynaptic responsiveness (Ugolini et al., 2008). CRF also depolarizes BLA principal neurons in acute slices by increasing the amplitude of I_h, the exact opposite of the action seen with NPY application to the same cells (Giesbrecht et al., 2010). Overall, it appears the neuronal and behavioral effects of CRF on the BLA act in an opposing fashion to NPY, which is consistent with contrasting actions on cAMP production due activation of G_s and $G_{i/o}$ proteins.

Interactions Between NPY and CRF

The studies described so far have investigated NPY and CRF independently of each other, which have provided strong and consistent evidence as to their reciprocal role in regulating stress-related behavior. However, data suggests these neuropeptide systems can and do interact with each other. In 1994, Heilig et al. first proposed this concept, (Fig.1.3A),

suggesting the initial phase of the amygdala stress response is mediated by rapid activation of CRF release, followed by a slower activation of NPY transmission, acting to counteract the effects of CRF and facilitate maintenance of allostatic balance, protecting against maladaptive overload (Heilig et al., 1994). In addition to the studies discussed above indicating the respective anxiolytic and anxiogenic effects of NPY and CRF, the overlapping expression of CRF and NPY receptors in limbic regions in general and the BLA in particular gives merit to this hypothesis. Moreover, administration of a CRF antagonist blocked the anxiety-like effect of the NPY-Y1-receptor antagonist BIBP3226 in the EPM (Kask et al., 1997). Direct evidence of this interaction stems from studies whereby injection of NPY into the BLA, prior to UCN injection, prevented the development of the avoidance behavior in the two floor choice test and the decrease in SI time that is usually seen following restraint stress (Sajdyk et al., 2006). Furthermore, injection of NPY into the BLA prior to UCN injection for 3 consecutive days blocked the UCN-induced priming of anxiety responses assessed by SI test (Sajdyk et al., 2004). This counter-regulation of NPY and CRF to maintain emotional homeostasis may be due to the reciprocal control of cAMP production and the downstream signal transduction pathways stimulated, as NPY and CRF are coupled to G-proteins ($G_{i/o}$ and G_s, respectively) that have opposing effects on cAMP production (Sheriff et al., 2001). Furthermore, NPY and CRF produce complementary induction of calcineurin and CaMKII, respectively, which may be involved in the opposing effects on the stress response. This hypothesis has since been adapted for other brain regions that are relevant to stress/anxiety pathways such as the hippocampus, BNST, the hypothalamus, LC and the septal nucleus (Thorsell et al., 2000, Hastings et al., 2001, Kask et al., 2001a, Charney, 2004, Kash and Winder, 2006).

Nonetheless, the complexity of GPCR signaling pathways makes this hypothesis one that requires more rigorous mechanistic examination.

Organotypic Slice Cultures

Stress clearly initiates an incredibly complex emotional response, requiring the coordinated effort of many brain areas acting in concert to elicit appropriate actions. In order to understand these multifaceted events, it is necessary to integrate discoveries from different experimental approaches, including animal behavior, immunohistochemistry, imaging, electrophysiology, *in vitro* work, etc. The majority of the *in vitro* work described so far has been performed on acute *ex vivo* slices from rodent brains or on primary dissociated neurons. These studies have been fundamental to our understanding of the cellular basis underlying the production and regulation of emotional responses and are the predominant *in vitro* preparation used in pharmacological and biochemical studies. However, dissociated cell cultures do not reflect the true nature of the organism due to isolation and lack of contact with other cells, while the main drawback of acutely-prepared brain slices is their limited survival time after preparation. Therefore, long-term studies require the use of complementary *in vivo* experimental approaches in addition to the *in vitro* method. What is needed is a model system that best recapitulates the neural circuitry in order to study molecular and cellular mechanisms governing these emotional responses.

Over the past few decades, the organotypic slice culture (OTC) has emerged as a technique offering an alternative to the classical *in vitro* preparations. "Organotypic" refers to the resemblance of the cultured tissues to their counterparts *in vivo*: these thin tissue explants represent an intermediate model between dispersed cell cultures and *in vivo* models. They

retain several features of the original tissue's structural, cytoarchitecture and synaptic organization, while permitting both flexible access and control of specific neural circuits that maintain most of their natural network activities (Pena, 2010). OTCs can be successfully cultured for prolonged periods, even months, which allows the detailed examination of the long-term effects of acute treatments and long-term treatments in a carefully controlled environment.

History of OTCs

OTCs were first described in 1954 in a study investigating differentiation of the eye of the chick embryo (Reinbold, 1954). Since then, a number of other peripheral tissues have been described using the OTC model, however, the first report of CNS tissue being used focused on rat hypophysis and it was not until 1970 that the first detailed description of brain tissue was published using the cerebellum (Bousquet and Meunier, 1962, Wolf, 1970). A breakthrough came in 1981, when Gähwiler et al. cultured cerebellum and hippocampus by means of the "roller tube technique" (Gahwiler, 1981a, b). This technique led to an explosion of studies using this experimental approach for diverse neurobiological investigations including ischemia, long term effects of chemical exposure as well as cell death, proliferation and neurogenesis [for review see, Drexler et al. (2010), Humpel (2015a)]. This method has since been modified and optimized by Stoppini et al., who cultured OTCs on semiporous membrane inserts. This approach has since been adapted by numerous research groups who have cultivated OTCs from various brain regions including neocortex, olfactory bulb, hippocampus, thalamus, basal ganglia, hypothalamus, basal forebrain, midbrain, brain stem, cerebellum, and spinal cord (Stoppini et al., 1991, Drexler et al., 2010, Humpel, 2015a).

Properties of OTCs

Because adult brain tissue in general does not tolerate OTC preparation, OTC neuronal tissue is immature, taken either from embryonic or early postnatal subjects to produce OTCs. However, some remodeling does occur and OTCs develop and differentiate until many morphological and neurochemical features of the neurons resemble those in their mature, *in vivo* counterparts. In culture, the degree of connectivity frequently increases to levels higher than in acute slices, likely due to spatial constraints in which axonal outgrowth and regeneration results in the exuberant development of synaptic connections, often resulting in spontaneous network activity within the culture (Debanne et al., 1995). Still, the physiological and morphological characteristics of different types of recorded neurons frequently matches those of neurons characterized from acute brain slices quite closely for a number of tissues studied (Gahwiler et al., 1997, De Simoni et al., 2003, Stachniak and Bourque, 2006).

The potential to investigate novel biochemical and neuronal processes in physiological and pathophysiological states using OTCs of brain tissue is enormous. OTCs represent an ideal intermediate preparation for a number of applications that have been developed for *in vivo* and classical culture techniques, such as repeated multi-electrode array recordings, gene transfer techniques (including viral-vector based and non-viral methods), retrograde tracing, live-cell imaging, ELISA, RT-qPCR, immunohistochemistry, *in situ* hybridization and calcium-imaging (Ridoux et al., 1995, Jahnsen et al., 1999, Murphy and Messer, 2001, Gerfin-Moser and Monyer, 2002, Gogolla et al., 2006, Ullrich et al., 2011, Ullrich and Humpel, 2011). OTCs coupled with some of the above techniques have been employed to study various mechanisms underlying disease states including Alzheimers and Parkinson's disease, Fragile X syndrome, and Down Syndrome, as well as studying cell therapy and preclinical drug

screening (Humpel and Weis, 2002, Mitrasinovic et al., 2005, Hanson et al., 2007, Hanson and Madison, 2007, Neely et al., 2007, Markou et al., 2009).

To date no reports have indicated that BLA OTCs have been successfully produced, although anecdotal accounts have emerged of unsuccessful attempts by a number of research groups to achieve this. OTCs of BLA would provide a valuable and innovative tool in our ever-expanding repertoire of experimental approaches to study the underlying mechanisms that govern stress/anxiety-related behaviors. Their use can significantly reduce the number of animals required for certain experiments, while also providing a relatively inexpensive and straightforward method for studying molecular and cellular processes of the brain *in vitro*. Furthermore, their use in preclinical drug screening can enhance throughput by providing proof of principal that new drug candidates exert the desired effects not only on individual neurons but on the target brain system, and by helping exclude compounds with significant adverse effects from the drug pipeline, enhancing drug discovery and safety testing. Because of the ease of accessibility, OTCs also permit rigorous early phase testing of innovative, non-conventional therapeutic approaches, such as viral delivery of gene therapies.

Present Study

The purpose of the present study was to develop BLA OTCs as a model to study NPY- and CRF-mediated long-term effects on stress-related behavior. Once viable OTCs are established and their morphological and electrophysiological characteristics are shown to be similar to those from age-matched, acutely prepared slices, novel experimental investigations can proceed. These novel experiments relate to previous findings that *in vivo*, NPY and CRF can induce long-term behavioral stress-resilience and vulnerability, respectively. Although the

mechanisms of action relating to acute applications of NPY and CRF are fairly well established, much remains to be learned of the signaling pathways involved in mediating the stress resilience or vulnerability mediated by these neuropeptides. Furthermore, a number of studies have demonstrated that chronic stress can induce dendritic hypertrophy and increase spine density in BLA principal neurons. Therefore, we sought to use our novel OTC preparation in electrophysiological, pharmacological and morphological studies to investigate the underlying circuitry and molecular mechanisms responsible for NPY- and CRF-mediated stress resilience and vulnerability, respectively, to complement and extend our results from *in vivo* experiments. The following hypotheses follow from the published information outlined above, but also include some, which depend on unpublished information from this and other studies in the laboratory.

Hypotheses

Hypothesis 1: Long-term incubation with NPY and CRF in BLA OTCs reduces and increases, respectively, BLA principal neuron I_h.

NPY and CRF regulate the intensity of I_h in opposing directions (decreased and increased, respectively) following application to acutely prepared brain slices of BLA. These acute actions reversibly affected output neuron excitability in an I_h-dependent manner, and would thus represent a mechanism underlying the corresponding acute behavioral response. Since increased excitatory output from the BLA is anxiogenic, this is consistent with the cellular mechanisms of action of NPY and CRF, respectively. Because prolonged changes in I_h could underlie the long-term actions of these neuropeptides *in vivo*, we therefore hypothesize that a potential mechanism mediating the respective NPY- and CRF-mediated stress resilience and

vulnerability was a neuropeptide-mediated long-term decrease and increase in I_h conductance, respectively.

Hypothesis2: NPY and CRF provide reciprocal regulation of synaptic drive onto principal BLA neurons.

Previous findings in acutely prepared brain slices demonstrated that acute application of a Y1-receptor agonist simultaneously reduced the amplitudes of evoked NMDA-mediated excitatory postsynaptic currents and increased the amplitudes of $GABA_AR$-mediated inhibitory postsynaptic currents. Furthermore, repeated injection of UCN into the BLA increased glutamatergic activity and reduced GABAergic-mediated spontaneous and evoked IPSPs. Thus, we hypothesize that repeated NPY incubations would reduce excitatory neurotransmission and increase inhibitory drive onto BLA OTC principal cells, while CRF would produce the opposite effect.

Hypothesis 3: Chronic NPY treatment results in principal neuron dendritic hypotrophy, while repeated application of CRF causes dendritic hypertrophy in BLA.

Chronic stress is known to result in increased spine density and dendritic hypertrophy of BLA principal neurons *in vivo*. In related work, our laboratory has identified a decrease and increase in spontaneous EPSC frequency following repeated injections with NPY and CRF, respectively (Silveira, et al., unpublished). One potential mechanism could be an increase in the numbers of excitatory synapses. Therefore, we hypothesize that the anxiolytic NPY would cause hypotrophy and a reduction of dendritic spines, while the anxiogenic CRF would result in hypertrophy and an increase in dendritic spines in principal neurons of BLA OTCs.

Hypothesis 4: Repeated incubation with CRF followed by NPY and vice versa, would result in bi-directional synaptic and structural plasticity to counteract the effects of each other in BLA OTCs.

Incubation with NPY and CRF alone in BLA OTCs resulted in dendritic hypotrophy and hypertrophy, respectively. These neuropeptide systems are known to interact with one another *in vivo* to maintain homeostatic emotional balance. Therefore, we hypothesize that incubation with NPY, prior to CRF and vice versa will result in no net effect on neuronal dendritic structure or synaptic drive onto principal neurons in BLA OTCs.

Hypothesis 5: Repeated injection of NPY directly into the BLA in vivo, results in similar morphological changes observed in BLA OTCs.

Repeated activation of principal neuron NPY-receptors in BLA OTCs results in dendritic hypotrophy, while previous studies have shown repeated intra-amygdalar injection of NPY *in vivo,* results in long-term stress resilience. Thus, we hypothesize that similar structural changes would be observed *in vivo* as was described in BLA OTCs, which serve to mediate NPY-induced stress resilience.

Hypothesis 6: Incubation with the Y1-agonists results in reduced excitatory drive, coupled with dendritic hypotrophy in BLA OTCs, while the Y2-agonist results in opposite effects.

The BLA has three NPY receptors present, the Y1, Y2 and Y5 receptors. The acute anxiolytic effects of NPY appear to be mediated predominantly via the Y1-receptor, while the Y2-receptor is reported to paradoxically mediate anxiogenic-like behavior in the BLA. Therefore, we hypothesize that repeated stimulation of these two receptors would result in opposing structural and synaptic effects. Moreover, the Y5-receptor is considered to mediate

some of the anxiolytic effects of NPY, although there is still some controversy as to the exact role it plays. Regardless, we hypothesize that chronic treatment of BLA OTCs with the selective Y5-agonist would mediate dendritic hypotrophy, which is consistent with an anxiolytic effect.

Hypothesis 7: Repeated intra-amygdalar injection of the Y1-agonist in vivo results in no persistent effects on behavior or neuronal structure in the BLA.

Unlike with NPY itself, repeated incubation of the Y1-agonist in BLA OTCs caused no long-term effects on principal cell morphology. Therefore, we hypothesize that NPY-mediated stress resilience *in vivo*, assessed via SI, and dendritic hypotrophy is not mediated by repeated Y1-receptor activation.

Hypothesis 8: The mechanism of action of NPY-mediated dendritic hypotrophy in BLA OTCs is mediated by activation of the protein phosphatase, calcineurin.

NPY-mediated stress resilience was reportedly abolished by pre-injection of the calcineurin inhibitory peptide *in vivo.* Therefore, we hypothesize that blocking calcineurin activity with cyclosporine A, would inhibit NPY-mediated dendritic hypotrophy in BLA OTCs. To ensure that NPY-induced dendritic hypotrophy is not mediated by other protein phosphatases, PP1 or PP2A, we hypothesize that incubation with the Y5-agonist and okadaic acid, a selective PP1 and PP2A inhibitor, would not block Y5-mediated structural remodeling.

Hypothesis 9: The mechanism of action of CRF-mediated dendritic hypertrophy in BLA OTCs is mediated by activation of the protein kinase, CaMKII.

CRF-mediated stress vulnerability was reportedly abolished by pre-injection of the CaMKII inhibitor KN-62 *in vivo.* Therefore, we hypothesize that blocking CaMKII activity with a cell permeable version of Autocamptide-2 Related Inhibitor Peptide, would inhibit CRF-mediated dendritic hypertrophy in BLA OTCs.

Hypothesis 10: Dendritic hypertrophy induced by repeated activation of the Y2-receptor in BLA OTCs is dependent on CRF.

CRF or chronic restraint stress induces activation of the enzyme fatty acid amide hydrolase (FAAH), which causes catalysis of the endocannabinoid anandamide (AEA) and ultimately results in dendritic hypertrophy, within the amygdala. Furthermore, tPA is up-regulated by CRF in the amygdala, resulting in increased spine density in the medial amygdala. Similarly, the Y2-mediated dendritic hypertrophy observed in BLA OTCs may be dependent on CRF actions. Therefore, we hypothesize that the morphological effects of Y2-receptor activation in BLA OTCs, will be blocked by co-incubation with a CRF-antagonist.

Figure 1.1

A

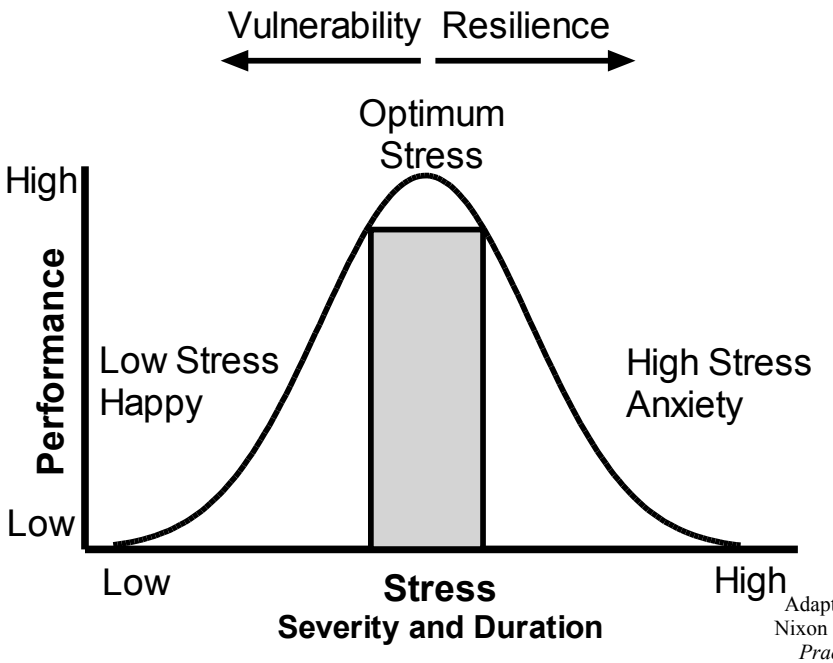

Adapted from
Nixon P., 1976
Practitioner

B

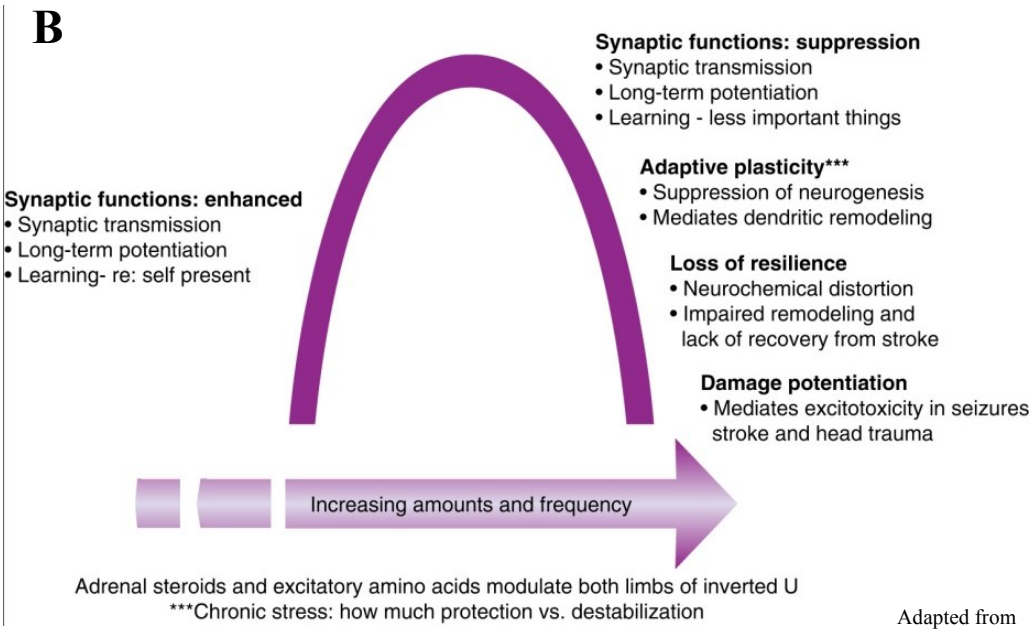

Adapted from
McEwen B., et al., 2015
Neuropsychopharmacology

Figure 1.1 Stress response curves.

(A) The "inverted U" shaped dose-response curve of stress vs. performance illustrates that as the level of stress increases, the performance also increases. There is a narrow range where the level of stress is optimal and facilitates good performance levels. When stress is perceived as overwhelming or excessive, fatigue sets in and performance declines, which can trigger maladaptive stress responses, leading to anxiety-related behavior. Note there are no fixed numbers on the x- or Y-axis, as each individual is unique in their ability to perceive and manage stress. Those individuals who can tolerate more stress than others before it becomes maladaptive are considered stress resilient, while individuals who have a reduced ability to cope are stress vulnerable/susceptible. This is represented on the curve by the arrows at the top, stress resilient or vulnerable individuals would have this curve shifted right and left, respectively (Figure adapted from Nixon P 1976). (B) The effects of stress on synaptic function, adaptive plasticity and damage also operate in an inverted U-shaped manner. Acute stress mediated by excitatory amino acids, CRF, glucocorticoids and others, enhance excitability and promote adaptive fear responses and memory formation in the short term, as long as stress is not overly traumatic. Intense or chronic stress causes neuronal remodeling and synaptic plasticity, typically in a reversible manner, which has adaptive consequences. However, if the stress-mediated effects on synaptic and structural plasticity do not reverse, intervention may be required in the form of behavioral therapy or pharmacotherapy to help reverse the effects of stress. If the stress is allowed to persist further, negative health effects can develop. Figure adapted from McEwen et al., (2015).

Figure 1.2

A

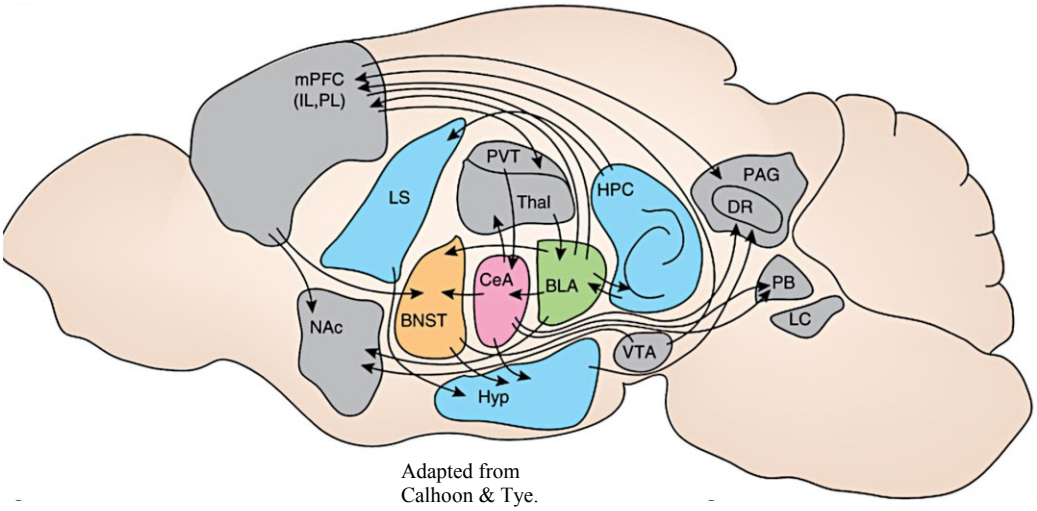

Adapted from
Calhoon & Tye.
2015
Nature Neurosci.

B

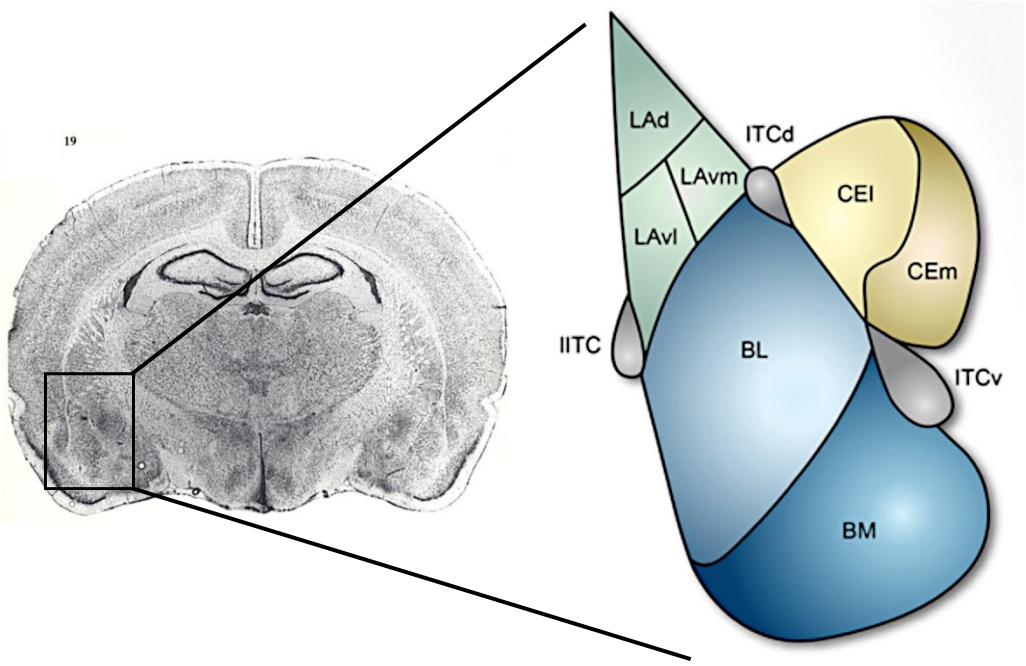

Adapted from
Lee et al., 2013.
Front. Neural Circuits

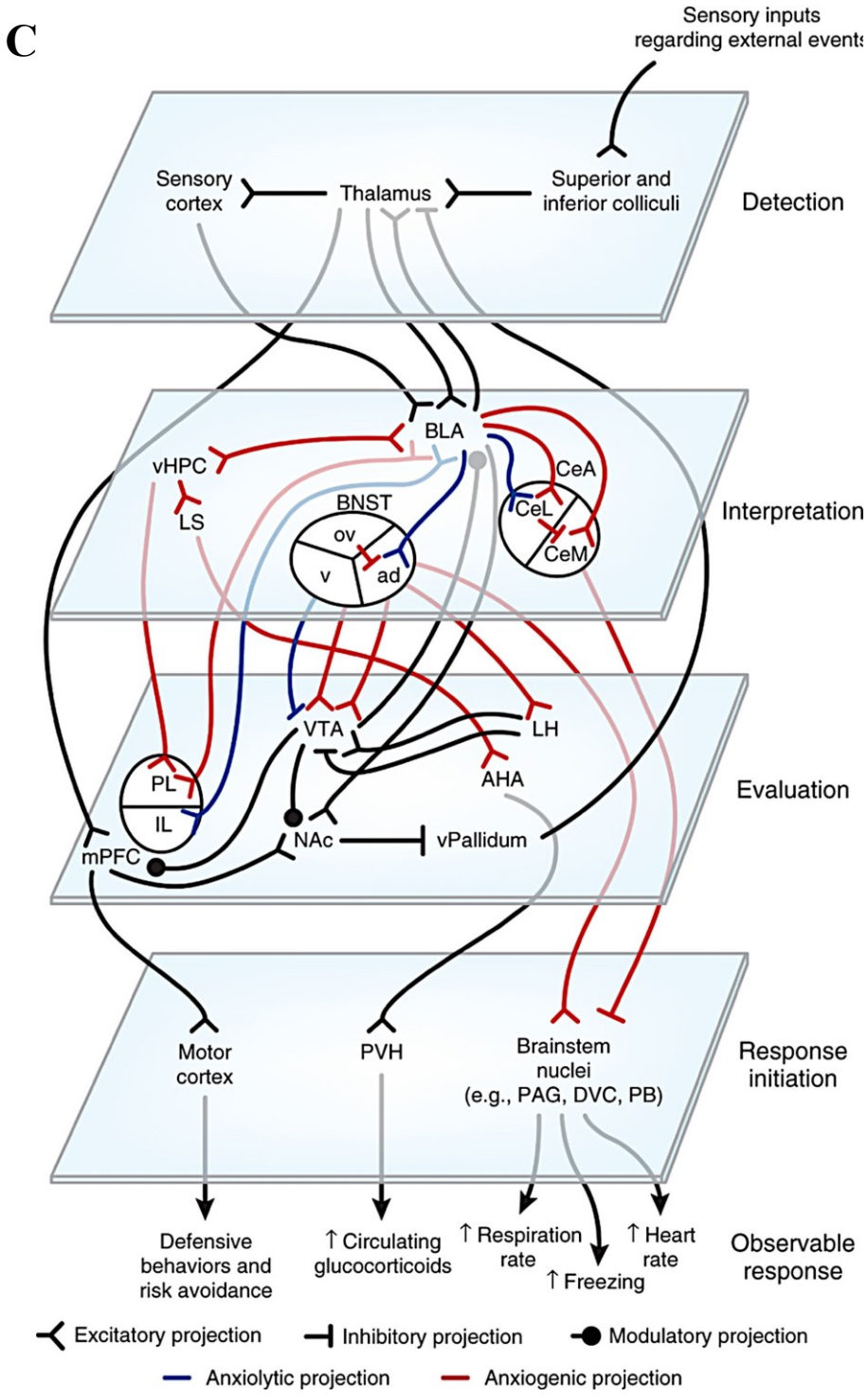
C
Sensory inputs
regarding external events
Sensory
cortex
Thalamus
Superior and
inferior colliculi
Detection
BLA
vHPC
LS
BNST
ov
v
ad
CeA
CeL
CeM
Interpretation
VTA
LH
AHA
PL
IL
mPFC
NAc
vPallidum
Evaluation
Motor
cortex
PVH
Brainstem
nuclei
(e.g., PAG, DVC, PB)
Response
initiation
Defensive
behaviors and
risk avoidance
↑ Circulating
glucocorticoids
↑ Respiration
rate
↑ Freezing
↑ Heart
rate
Observable
response
Excitatory projection
Inhibitory projection
Modulatory projection
Anxiolytic projection
Anxiogenic projection

Figure 1.2 Brain regions and neural circuits involved in mediating anxiety-related behaviors in the rodent brain.

(A) Sagittal view of rat brain depicting major brain structures involved in anxiety/stress-related circuits and their connections (Figure adapted from Calhoon and Tye, 2015). (B) Coronal section of rat brain (left), which includes the amygdala (enclosed box). (Right) Enhanced cartoon depiction of subnuclei of the amygdala including the BL, BM (blue) and LA (green), making up the BLA. The CeA is colored yellow and composed of the CeL and CeM subdivisions. Both lateral- and dorsal-ITC intercalated cell masses (grey) reside at the edge of the BLA defining its boundaries (Figure adapted from Lee et al., 2013). (C) Proposed model of neurocircuitry involved in detecting, interpreting, evaluating and responding to stress. Red, anxiogenic pathway, Blue, anxiolytic projections. Figure adapted from Calhoon and Tye, 2015.

Table 1.1

NPY receptor subtype	Endogenous ligand preference	Selective agonist (antagonist)	Cell signaling pathways
Y1	NPY>PYY>PP	[Leu^{31}, Pro^{34}]NPY) F^{7} P^{34} NPY (BIBO3304,BIBP3226)	cAMP/PKA/PLC-IP3-Ca^{2+} GIRK channel HCN channel
Y2	NPY=PYY>PP	PYY/NPY(3–36) PYY/NPY(13–36) [ahx$^{5-24}$]NPY (BIIE0246, JNJ-3102008, JNJ-5207787)	cAMP-PKA PLC-IP3-Ca^{2+} PI3K-ERK Ca^{2+} channel
Y4	PP>>PYY=NPY	PP, BVD-74D	PLC-IP3-Ca^{2} cAMP-PKA
Y5	NPY>PYY>PP	[CPP$^{1-7}$, NPY$^{19-23}$ Ala^{31}, Aib^{32}, Gln^{34}]hPP (CGP71683A)	cAMP-PKA PI3K-ERK

Table 1.1 An overview of NPY receptors.

A brief summary of NPY receptors, endogenous ligand preference, selective agonists and antagonists and cell signaling pathways activated (Coupled to $G_i/_o$).

Figure 1.3

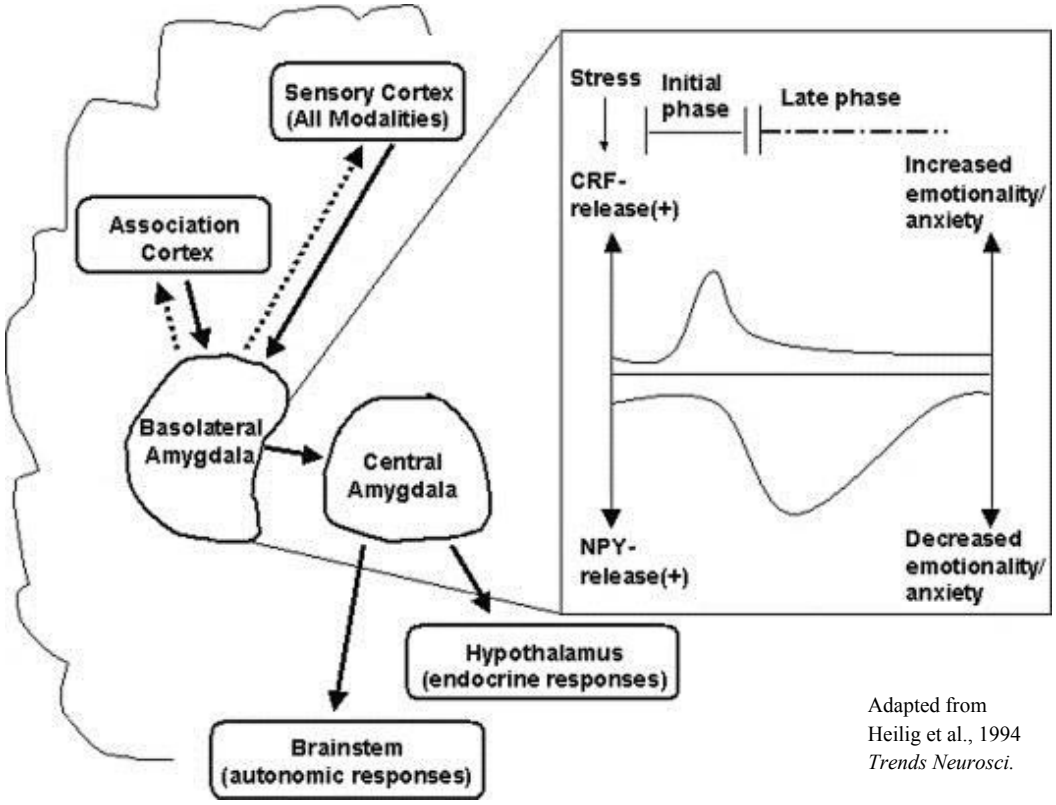

Figure 1.3 Representation of the proposed counter-regulation of emotion and anxiety by CRF and NPY in the amygdala.

The BLA integrates sensory information and provides salience and valence to these inputs, thereby coordinating outputs to downstream brain regions to produce the appropriate physiological and behavioral responses. CRF is released following perception of stress in the initial phase and is primarily responsible for the acute stress response. A slower and sustained release of NPY occurs in the late phase, acting to terminate the stress response and dampen the effects of CRF. Adapted from Heilig et al., 1994.

CHAPTER 2: Methodology and validation of BLA OTCs

Introduction

In this thesis there were two major approaches to elucidating the interactions between NPY and the neurons of the BLA. The first approach using acute brain slices, has been described in detail in Giesbrecht et al., (2010), and will be covered less extensively here, with a focus on the *in vivo* manipulations that preceded the acute brain slice preparations. The second, the organotypic slice culture preparation of the BLA, was developed *de novo* for the present studies, and will be described in greater detail. This section will include detailed methods of preparation, while a second section will focus on the characterization of the properties of BLA principal cells in the OTC slice culture in comparison with neurons from slices of BLA prepared acutely from adult (postnatal 10 weeks) and juvenile (p14 days) rats.

The majority of the *in vitro* work described in Chapter 1 has been performed using acute brain slices from rats, which has significantly enhanced our understanding of the physiological and pharmacological properties of neuronal circuits. Although their ease of preparation, natural cytoarchitecture and neuronal and network properties make acute slice preparations a favored neuropharmacological preparation, these slices are short-lived, precluding long-term studies and necessitate the use of complementary *in vivo* experiments. Over the past few decades, OTCs have been developed that retain the advantages of acute slices in terms of their accessibility, neural circuitry and neuronal properties, but also permit analysis of the effects of chronic treatments in an isolated system [for review see Gahwiler et al. (1997), Humpel (2015a)]. OTCs derived from various brain regions including the hippocampus, spinal cord and cerebellum exhibit conserved properties of synaptic transmission, neuronal morphology and neurochemical phenotype, and gross tissue organization in common with acutely prepared slices of their respective regions (Gahwiler,

1981a, Avossa et al., 2003, De Simoni et al., 2003, Lu et al., 2009). The retention of many of the properties of the acute preparation has been used to validate these OTC models of other brain regions (Gahwiler, 1981a, Stoppini et al., 1991, De Simoni et al., 2003). Interestingly, OTCs have been used for a wide variety of applications using modern technological approaches including network development and plasticity, high-resolution imaging, changes in neuronal networks through gene transfection, synchronous neuronal network activity, morphological changes due to neurodegeneration and have been fundamental in a number of breakthroughs in various disease models including Alzheimer's and Parkinson's disease (Gahwiler et al., 1997, Pena, 2010, Humpel, 2015a).

Classically, slices are cultured in two slightly different ways: 1) OTCs can be prepared using the "roller-tube method", whereby slices are embedded on glass coverslips by a plasma clot, held in a sealed tube containing carbogen and media and subjected to continuous slow rotation so that the cultures are exposed part of the time to the atmosphere inside the tube (Gahwiler, 1981a); 2) Modification to this protocol allowed cultures to grow at the air-medium interface using semipermeable membranes, the "interface method", avoiding the need for rotation (Stoppini et al., 1991). Animal age is important for OTC viability, as embryonic animals typically survive better, yet postnatal (<P12) donors are often preferred due to their relative maturity (Humpel, 2015a). Recently, a number of groups have succeeded in culturing OTCs from adult brain tissues, however, most such studies require special conditions and are largely the exception to the rule (Lossi et al., 2009, Kim et al., 2013, Humpel, 2015b).

The use of early postnatal animals for the preparation of OTCs presents a technical issue with studying changes in disease models, as researchers generally desire a correlate to OTC results with adult pathology. The developing juvenile rodent brain is highly dynamic,

with an array of neurobiological changes. In the BLA, neuronal composition, size and density are not stabilized until P28, which is coupled to alterations in synaptic inputs and electrophysiological properties of principal and interneuron populations (Berdel et al., 1997, Morys et al., 1998, Berdel and Morys, 2000, Bouwmeester et al., 2002, Ehrlich et al., 2012, 2013). The question then arises whether OTCs prepared from young postnatal animals and cultured for an extended period of time are fully representative of the mature adult phenotype?

The present study aimed to develop OTCs of the BLA, a novel culture preparation, as an *in vitro* model to study stress-related circuitry. We plan to use this technique in long-term studies of NPY and CRF actions in the BLA, to further our understanding of anxiolysis and anxiety related to this nucleus. However, the model must first be established by developing and optimizing a protocol, then validated using electrophysiology and immunohistochemistry prior to initiating experimental manipulations. For this, we must first establish viable cultures and second compare directly the properties of neurons and local networks with those in age-matched, acutely prepared slices.

After a number of trials, we determined the "roller-tube method" did not produce viable cultures, likely due to the tissue size preventing adhesion to the glass coverslips. The "interface method" was found to yield much healthier cultures. Additionally, due to the developmental changes that occur within the BLA, we sought to prepare OTC slices from the latest possible postnatal time point, to limit the overall time needed in culture, to age-match our OTCs to previously mentioned *in vivo* studies on stress resilience/vulnerability. OTCs prepared from P28 and P21 were not consistently viable, however, those prepared from P14 rats did very well and could be readily maintained up to equivalent postnatal (EP) 10-weeks (8 weeks in culture). We used this time point for all future studies of OTCs and compared

electrophysiological and morphological data from P14 and 10-week old acutely prepared slices to those obtained from OTCs. Results suggest BLA OTCs develop and behave in a similar fashion to adult 10-week old acutely prepared slices.

Methods

Animals

Two different age groups of male Sprague-Dawley rats were used for experimentation. P14 pups were housed with the dam prior to preparation of OTCs and for a subset of *ex vivo* electrophysiological and morphological studies. The second set of rats, aged five-weeks, were grouped housed (2-3 animals per cage) with 12:12 hours light : dark schedule and food and water were supplied *ad libitum*. All animal procedures were approved by the University of Alberta Animal Care and Use Committee: Health Sciences, in accordance with the guidelines of the Canadian Council on Animal Care.

Experimental setup for OTCs

Traditionally, OTCs of brain tissue are obtained from young P0-P10 animals using the "interface-method" described by (Stoppini et al., 1991), as they take advantage of their ease of preparation and high viability. Previous studies from the Colmers laboratory on the long-term effects of NPY on stress-resilience used ~ 6-week old Sprague-Dawley rats at the time of their injections, and were sacrificied 4-weeks later making them 10-weeks by the end of the experiments. Thus, we sought to age-match our OTCs to the equivalent postnatal time points of these experiments (Fig.2.1). OTCs were prepared from P14 animals and cultured for 7-8 weeks to bring them to equivalent postnatal (EP) 9-10 weeks before further experiments were performed.

Reagents

- D-glucose (Fisher Scientific. Cat # L-10048)

- Minimal Essential Media (MEM) (Gibco. Cat #12360-038)
- Heat-inactivated horse serum (Gibco. Cat # 26050-088)
- Hanks's Balanced Salt Solution (HBSS) (Gibco. Cat # 14025-092
- Kynurenic acid (Abcam. Cat #120064)
- L-ascorbic acid (Sigma. Cat # A4544)
- Glutamax (Gibco. Cat # 35050-061)
- Penicillin-streptomycin (Gibco. Cat # 15070-063)
- Cytosine-β-D-arabino-furanoside (Sigma Cat # C6645)
- Uridine (Sigma. Cat #U3003)
- 5-Fluro-2'deoxyuridine (Sigma. Cat # F0503)
- Agarose (Invitrogen Cat # 16520)

Equipment for OTC preparation

- 70 % ethanol
- Laminar flow cabinet with UV light
- Cell culture incubator set at 37°C, 5% CO_2 and 95% air
- Syringe filter. For large volumes a sterile vacuum filter unit can be used
- Vibratome

- Stainless steel razor blades for vibratome
- Stainless steel razor blades for brain dissection
- Dissection microscope
- Petri dishes
- 24-well culture plates
- Millicell Culture plate inserts (Fisher. Cat # PICMO1250)
- Pipette controller with disposable 10- and 25-mL filter containing, sterile plastic pipettes
- Pipettes with disposable pipette tips
- 1 mL syringe with 25G 5/8" needle
- Ice bucket with ice
- Guillotine
- Surgical scissors, one small straight dissecting scissors, two straight forceps, fine spatula
- Filter paper
- Adhesive cyanoacrylate
- Sterile 15 and 50 mL screw top Falcon tubes
- 1.5 and 5.0 mL microcentrifuge tubes

- HPLC grade ultrapure water
- Paintbrush
- Water bath

Reagent setup

Note: All solutions must be filter-sterilized before aliquoting or use. Prepare all solutions using HPLC grade, ultrapure water and analytical grade reagents.

50% D-glucose solution: Prepare by dissolving 50 g of D-glucose into 100 mL of HPLC grade ultrapure water, sterilize via syringe filter and store at -20°C as 6 and 8 mL aliquots.

Kynurenic acid (3 mM): Prepare the stock solution by dissolving 61.15 mg of kynurenic acid into 100 mL of HBSS, sterile filter and store at as 5 mL aliquots.

L-ascorbic acid (50 mM): Prepare the solution by dissolving 352.24 g of L-ascorbic acid into 40mL of HBSS, sterile filter and store at -20°C as 4 mL aliquots.

Penicillin/streptomycin: From 5000 U/mL stock solution, store at -20°C as 1 mL aliquots.

Slicing solution: To a full 500 mL bottle of HBSS, add one 5 mL aliquot of 3 mM kynurenic acid and one 6 mL aliquot of 50 % D-glucose solution, store at 4°C.

Culture medium (for ~ 400 mL): To a large beaker, add 100 mL heat-inactivated horse serum, 200 mL MEM, 84 mL HBSS, 2 mL Glutamax, 8 mL 50% D-glucose, 2 mL penicillin/streptomycin and 4 mL L-ascorbic acid. Stir and adjust pH to 7.2 using NaOH. If necessary, adjust osmolarity to 320mOsm using HPLC grade ultrapure water. Store at 4°C and discard any unused media after 28 days.

Anti-mitotic stock solution (10^{-4} M): Add 3 mg of each cytosine-β-D-arabino-furanoside**,** uridine and 5-Fluro-2' deoxyuridine to 100 mL HBSS, sterile filter and store at -20°C as 1 mL aliquots.

Equipment setup

Store vibratome razor blades in acetone to remove oil and grease and wash with water before use. Cut the bottom of a capped 50 mL Falcon tube at the 35 mL mark, this will act as a chamber for the liquid agarose and brain block. Sterilize all surgical instruments by autoclaving prior to use including razor blades, scissors, and spatulas. Wear disposable gloves, a mask and a clean lab coat during all procedures. Turn on laminar flow cabinet and clean surface of the hood using 70 % ethanol. Any material entering the laminar flow hood must be sprayed and wiped with 70% ethanol prior to being placed inside. Use UV irradiation to sterilize the hood for ~20 min prior to use. Clean a workspace that will be used for decapitations.

Procedure

Typically, OTCs are prepared from four P14 rats per week. Each animal produces roughly four 350 μm thick BLA containing slices per hemisphere, for a total of eight slices per animal. The procedure can be completed in ~ 1-1½ hours/animal by an experienced individual. Time is vital during the procedure, as a slow dissection will negatively affect the outcome, however, meticulous care must be taken when handling the tissue for optimal health.

Preparation of materials and equipment

1. Sterilize all surgical instruments by placing in a metal container or wrapping in tin foil and autoclave.

2. While autoclaving instruments, place all items required to generate OTCs into the biosafety cabinet including the vibratome, Petri dish, cyanoacrylate, ice bucket with ice, syringe and needle, paintbrush, 24-well plates, paper towel, 50 mL Falcon tubes pipettes and tips.

3. Add slicing solution to 24-well plates, by filling wells half way with a pipette controller and plastic 25 mL pipet. Fill an entire row (6 wells) for each hemisphere of BLA to be sliced. For four animals, add solution to 2 full 24-well plates.

4. Add 15 mL slicing solution to a 50 mL Falcon tube, 1 for each animal and store at 4°C. Store 1 tube at -20°C until slushy for immediate use.

5. Dissolve 400 mg of low melting point agarose in 20 mL slicing solution (2%wt/vol), heat in a microwave or hotplate until completely dissolved and store in water bath at 37°C. This will be enough for two animals and will stay in the liquid phase until the second animal.

6. Add ice to the Petri dish and place in ice bucket.

7. When surgical instruments are autoclaved and cooled, add them to the biosafety cabinet and mount razor blade onto the vibratome.

8. Place tube of slushy slice solution into ice bucket in hood.

Dissection

9. At the clean workbench, spray neck of P14 rat with 70% ethanol, decapitate using the guillotine and remove fur from scalp using surgical scissors.

10. Bring into laminar flow hood for remainder of dissection and slicing.

11. Using small straight dissecting scissors, cut the skull bilaterally along the midline from the foramen magnum to the front and 2 additional cuts to the left and right.

12. Peel away the skull, making sure not to damage the brain and remove the brain into the slushy slice solution.

13. Let brain cool on ice, while preparing Petri dish with ice, covered with wet (slice solution) filter paper.

14. Take warm, liquid agarose and pour 10 mL into cut off 50 mL Falcon tube (cap down), place back into waterbath when finished.

15. After a few minutes in slice solution, remove brain and place on wet filter paper covered petri dish.

16. Remove meninges and major blood vessels with a pair of straight forceps.

17. Take razor blade and make 2 coronal cuts and 1 transverse cut as shown in Figure 2.2A-D.

18. Place brain block into Falcon tube containing liquid agarose and position the brain block to one end of the tube and maintaining correct axis (ventral part facing away). Put tube on ice.

19. Note: agarose needs to be warm enough to stay liquid but not too hot to damage the tissue.

20. Once solidified, remove block by removing cap and loosening, cut block of agarose for a backstop and cut the block making cuts parallel to the edges of the brain block Figure 2.2E.

21. Glue backstop onto slicing chamber and then brain block, using adhesive cyanoacrylate and place onto vibratome. Make sure ventral portion of the brain is facing out (closest to razor blade).

Slice preparation

22. Add ice-cold slicing solution to the slicing chamber and position razor blade rostral to where the amygdala is located and make first cut.

23. Continue cutting 350 μm thick coronal slices containing BLA. After each slice is cut, remove excess agarose and trim slice as shown in Figure 2.2F-G with a bent needle attached to a syringe (the latter is used as a handle).

24. Transfer slices containing BLA, using a cut disposable pipette tip, to 24-well plate containing cold slice solution. If needed, use a dissecting microscope to determine which slices contain BLA. Should obtain four slices per hemisphere for a total of eight slices. Label slices and store at 4°C for ≥1 hr.

25. Repeat for the second animal.

26. Let slices from second animal rest for ≈ 30 minutes before starting plating. If using four animal, make slices from two animals and plate these before continuing on to the next pair of animals.

Plating

27. Add 350 μL of fresh cold culture media to eight wells of a new 24-well plate. Using new sterilized forceps, place culture inserts into these 8 wells, remove and air bubbles under the membrane.

28. Using a new cut pipette tip, transfer slice to the culture insert. Use caution not to puncture membrane and limit amount of slice solution transferred to the insert.

29. Using a fine tipped Pasteur pipette, remove excess slice solution and position slice in the middle of the culture insert using sterile fine watercolor brush. Make sure the slice is not in contact with the side of the membrane insert. Immediately add one drop of fresh media onto slice to prevent slice from drying.

30. Continue to transfer remaining slices to inserts for that animal (Fig.2.2H).

31. Once all slices are positioned, remove the drop of media from inside the insert, label plate and place in incubator (37°C, 5% CO_2, 95% humidity).

32. Repeat for other animals.

Anti-mitotics, feeding and drug incubations

33. After 48 h, incubate cultures with 300 μL of anti-mitotic solution for 24 h to reduce glial proliferation (prepare solution using warmed culture media with stock anti-mitotic solution to a final concentration of 10^{-6} M).

34. Change media 3x/week with 300 μL of fresh warmed media.

35. Culture for 4 weeks and on the 5^{th} week, incubate with drugs per research protocol. Change media daily for 5 consecutive days, adding fresh drug diluted into fresh warmed media each time.

36. Change to drug-free normal media of the 7th day, and continue culture for an additional week with normal media changes for at least 1 week prior to electrophysiological experiments.

Experimental setup for 10-week old acutely prepared slices

To reduce the number of animals used, electrophysiological and morphological properties of BLA principal neurons from 10-week old acutely prepared slices were studied using control, PBS-injected animals from NPY-mediated stress resilience studies that will be mentioned in a future chapter. Figure 2.1 depicts the experimental time course of these animals. All but two of the stereotaxic surgeries and intracranial injections were performed by other members of the Colmers lab, including Dr. Heika Silveira or Ana Miranda.

Stereotaxic surgery

One week of acclimatization was allowed before animals were included in any experimental procedure. During this period all animals were handled daily. Six-week old rats were anesthetized with ketamine/xylazine (90:10 mg/Kg) and placed in a stereotaxic apparatus (Kopf, Tujunga, CA, USA). Bilateral guide cannulas (26 gauge; Plastics One, Roanoke, VA, USA) were implanted into the BLA [anteroposterior (AP): -2.3; mediolateral (ML): ±5.0; dorsoventral (DV): -6.4; incisor bar: -3.2 mm] according to a standard stereotaxic atlas of the rat brain (Paxinos and Watson, 1986). The cannulas were secured to the skull with four stainless steel screws (2.8 mm; Plastics One, Roanoke, VA, USA) and self-curing acrylic resin (Lang Dental Manufacturing Company, Inc., IN, USA). After completion of surgery, all animals received meloxicam (Boerhringer Ingelheim, Burlington, Ontario, Canada; 1 mg/kg, s.c.), 1.0 ml of saline 0.9% s.c., and were placed in a warm environment until they had fully

recovered from the anesthetic. Rats remained singly housed until fully recovery from the surgery.

Intracranial injections

All compounds were delivered via injection cannulas (33 gauge; Plastics One, Roanoke, Virginia, USA) that extended 2 mm beyond the guide cannulas. A 1 μL Hamilton syringe was placed on each side of a dual-channel infusion pump (PHD ULTRA, Harvard Apparatus, Holliston, MA, USA) and were connected to the injection cannulas via a connector assembly tubing (PE50; Plastics One, Roanoke, VA, USA). Delivery rate was set at 100 nL of solution per injection site over 30 s. After drug administration, injection cannulas remained in place for an additional minute to ensure complete delivery of the solution. The cannulas were then removed and tested for proper flow to ensure that they had not become obstructed during drug administration. In these control experiments, rats received a single daily injection of vehicle (PBS), for five consecutive days. All injections were performed between 8:00 AM to 10:00 AM.

Acute slice preparation

P14 or 10-week old rats were decapitated and their brains rapidly submerged in cold (4°C) artificial cerebrospinal fluid (aCSF) slicing solution, containing (in mM): 118 NaCl, 3 KCl, 1.3 MgSO4, 1.4 NaH2PO4, 5.0 MgCl2, 10 glucose, 26 NaHCO3, 2.5 CaCl2 and 1.0 kynurenic acid and bubbled with carbogen (95% O2, 5% CO2). Coronal sections of 300 μm containing the BLA were prepared using a vibratome (Slicer HR2; Sigmann Elektronik, Hüffenhardt, Germany). Brain slices were then transferred to a room temperature (22°C), carbogenated aCSF containing the following (in mM): 124 NaCl, 3 KCl, 1.3 MgSO4, 1.4

NaH2PO4, 10 D-glucose, 26 NaHCO3, and 2.5 CaCl2. Osmolality of was adjusted at 305 mOsm/kg. Slices remained in solution for 1 h prior to any experiment.

Whole-cell patch clamp electrophysiology

Acutely prepared slices or EP 9-10 week OTC slices, were removed from the culture insert with the membrane attached and transferred to a recording chamber attached to a fixed stage upright microscope (Axioskip FS2; Carl Zeiss, Germany). Slices were held submerged using a platinum and polyester fiber "harp" and continuously perfused at a flow rate of 2-3 mL/min for at least 10 minutes before recording, with warmed (32-34°C), carbogenated ASCF containing the following (in mM): 124 NaCl, 3 KCl, 1.3 MgSO4, 1.4 NaH2PO4, 10 glucose, 26 NaHCO3, and 2.5 CaCl2 (300 mOsm/L acute slices and 320mOsm/L adjusted with NaCl for OTCs). Patch pipettes were pulled from borosilicate glass (TW150F; World Precision Instruments, Sarasota, FL, USA) with a two-stage puller (PP-83; Narishige, East Meadow, NY, USA) and had a resistance of 4-6 MΩ when backfilled with an internal solution containing the following (in mM): 126 K-gluconate, 4 KCl, 10 HEPES, 5 MgATP, 0.3 NaGTP, 1 EGTA, 0.3 CaCl2 and 0.2% neurobiotin (pH adjusted to 7.27 with KOH, osmolarity adjusted to 285 mOsm/L for acute slices and 300 mOsm/L for OTCs, using distilled water or K-gluconate).

The BLA was identified under low magnification based on slice morphology and location within the slice. Principal neurons within the BLA were identified under 60x magnification using infrared-differential interference contrast (DIC) optics. Neurons were selected based upon their principal morphology, large soma, presence of a prominent apical dendrite and electrophysiological characteristics (McDonald, 1982, Rainnie et al., 1993). The

locations of recorded principal neurons were chosen randomly throughout the BLA. All recordings were made using a Multiclamp 700A or AxoClamp2A amplifier in conjunction with pCLAMP 10.4 software and a DigiData 1322 interface (Molecular Devices, Sunnyvale CA, USA). Following the establishment of a gigaohm seal, whole-cell patch clamp recordings were obtained and low-pass filtered at 2 kHz and digitized at 10 kHz. Access resistance was measured throughout the experiment, and only those cells with changes less than 20% were kept for further analysis. After recordings were completed, we corrected the nominal membrane potential in voltage- and current-clamp recordings for the calculated 15 mV liquid junction potential (Chee et al., 2010). All potential values reported reflect this correction.

Membrane properties and intrinsic currents

To study the non-specific cation current, I_h, neurons were voltage clamped at a holding potential of -55mV and a family of hyperpolarizing voltage steps was applied (−55 to −145 mV in 10 mV increments; the initial step lasted 1650 ms, and each subsequent step was successively shortened by a 100 ms increment, as the current activated fully within incrementally shorter periods so this prevented damage to the membrane from the stronger hyperpolarizations. The magnitude of I_h at a given potential step was determined as the difference between the initial peak positive current amplitude and the final, steady-state current for each step. A two-term exponential fit, $y(x) = y_0 + A_1 (1 – e^{-x/\tau 1}) + A_2 (1 – e^{-x/\tau 2})$, was used to extract fast (τ_{fast}) and slow (τ_{slow}) time constants of I_h activation. Voltage dependence of I_h activation was calculated for each neuron by expressing the amplitude of I_h at each potential step as a fraction of the maximal I_h value for cell in question and plotting each point against the potential step. The resulting curves were fitted with a Boltzmann function, $I(V)=([A_1 –A_2]/1 + e ([V-V_{1/2}]/k) + A_2$, which resulted in obtaining $V_{1/2}$ values, the

voltage at which half of the maximal current was activated. Capacitance measurements were obtained by recording the capacitive transient in response to a -10 mV hyperpolarizing voltage step from a holding potential of -75 mV. Capacitance was calculated offline with pClamp, from the area under the curve of the current amplitude from the beginning of the step to the steady-state current divided by the voltage change. Amplifiers had no capacitance compensation during these measurements. Spontaneous synaptic activity was assessed in voltage clamp at a holding potential of -55 mV and sampled at 20 kHz. Spontaneous inhibitory postsynaptic currents (sIPSCs) are represented by upward deflections, while spontaneous excitatory postsynaptic currents (sEPSCs) are downward deflections. Compound postsynaptic bursting activity was examined by manually counting the number of burst in a 2 min recording and presented as frequencies in Hz. A burst was identified by the presence of at least one sIPSC and one sEPSC, with at least four individual events within a 100 ms time frame. To determine the effects on rheobase, neurons were held in current clamp and families of up to 10 depolarizing current ramps were swept over a period of 2 s from 0 pA initially to 100 pA; though the initial current remained the same, the peak current was successively incremented by 100 pA per sweep. Resting membrane potential was determined as the average potential during a 60 s current clamp recording. For baseline measurements of each cell (without acute application of drug), 2-3 sets of recordings were taken for each protocol and the mean value was included as an n value of one. Input resistance (R_{in}) was calculated as the change in voltage associated with a transient hyperpolarizing current step (100 pA).

Cell processing and labeling

One to three principal neurons per slice were filled with neurobiotin (Vector Labs, Burlington, Ontario, Canada) during electrophysiological recordings (at least 20 minutes).

Following patch clamp recordings, OTCs and acute slices were fixed with 10 % formalin (Thermo Fisher Scientific, Ottawa, Ontario, Canada) for 24-72 h at 4 °C, and then transferred to 0.2% sodium azide in PBS for subsequent storage at 4 °C. Slices were processed within 4 weeks following patch clamp recordings. Free floating slices were washed for three consecutive 10 min periods in phosphate buffered saline (PBS) solution before blocking and permeabilization for 60 min with 4% normal goat serum (Sigma-Aldrich, Oakville, Ontario, Canada) and 0.3 % Triton X-100 in PBS. Slices were incubated with Alexa Fluor 555- or 546-conjugated Streptavidin (1:1000) (Life Technologies, Grand Island, New York, USA) in 0.3 % Triton X-100 in PBS for 2 h at room temperature. Slices were washed 4 times for 10 min each in PBS, before being slide-mounted onto Superfrost Plus slides and cover slips applied with Prolong Gold mounting media (Thermo Fisher Scientific, Ottawa, Ontario, Canada). Slides were allowed to air dry in the dark at room temperature before being imaged via confocal microscopy.

Imaging and neuronal reconstruction

For morphological analysis of filled neurons, z-stack images were obtained at 20x magnification, 1024 x 1024 resolution and 100 Hz for a series of 0.8 um steps with a laser scanning confocal microscope (Leica TCS SP5; Cell Imaging Centre, University of Alberta). The excitation wavelength used was 543 nm. To determine the position of each neuron within the slice, multiple single plane images were taken at 10x magnification, 512 x 512 resolution and 100 Hz, and stitched together using Leica LAS AF software. Only those neurons whose dendritic arbor was clearly and completely filled and cell body was clearly within the boundaries of the BLA were used for analysis. Neuronal reconstruction was performed using the simple neurite tracer function in FIJI (NIH, Bethesda, MD, USA). Following tracing, Sholl

analysis of the entire 3-demensional dendritic arbor was performed with another module within the FIJI software suite. Total dendritic length and number of dendritic intersections as a function of distance from the soma, dendritic branching, and number of dendrites as a function of branch order was quantified using concentric circles at increasing radii of 10 μm, while number of branches as a function of distance from the soma was measured using shells of 40 μm in radius (Fig.2.10D).

Data analysis and statistics

Recordings were viewed offline using pCLAMP 10.4 software (Molecular Devices, Sunnyvale CA, USA). Raw traces of electrophysiological recordings, statistical analysis and graphs were completed using GraphPad Prism 5 or 6 software (GraphPad, San Diego, CA, USA). Neuronal reconstruction and Sholl analysis was performed using FIJI (NIH, Bethesda, MD, USA). Unless otherwise stated, all data are represented as mean ± SEM. One- and two-way analysis of variance (ANOVA) were used where appropriate and Tukey's post-hoc test was used for multiple comparisons (* $P<0.05$, ** $P<0.01$, *** $P<0.001$, **** $P<0.0001$). For analysis of cumulative probability plots, the Kolmogorov-Smirnov test (K-S) was employed.

Results

Viability of BLA OTCs

As mentioned above, attempts made to culture slices using the "roller-tube method" and from older animals (P21-28) were unsuccessful; slices failed to adhere to the glass coverslips and the health of slices from older animals plated onto membranes deteriorated rapidly enough to discourage further experimentation. Viable BLA OTCs were obtained from P14 animals using the "interface method" described above, and these slices survive well in culture up to at least EP 10 weeks. Slices cut at 350 μm thin over time *in vitro* to ≈ 80-100 μm, the external and internal capsules are greatly diminished, making determination of the boundaries of the BLA using DIC optics at 4x magnification difficult in OTCs (Fig.2.3A-C). However, under higher magnification (60x), the majority of cultures retained traces of these white fibrous tracts, rendering the borders of the BLA resolvable (Fig.2.3D).

Comparison of electrophysiological properties of BLA principal neurons

The neuronal architecture of the amygdala in juvenile rodents is reportedly highly dynamic, and does not reach maturity until after the first postnatal month (Berdel et al., 1997, Morys et al., 1998, Berdel and Morys, 2000, Bouwmeester et al., 2002, Davila et al., 2008, Ehrlich et al., 2012, Ehrlich et al., 2013). This raises the question as to the validity of the use of immature rats for the purpose of making OTCs and investigating neuronal circuitry in the BLA. For OTCs to be considered a useful model of a brain region, they must develop and behave similarly to adult acute brain slices. Therefore, it was critical to compare electrophysiological properties between principal neurons in acutely prepared juvenile (P14) and adult (10 week) BLA principal neurons, and those from OTCs.

Passive membrane properties

Data were collected from a total of 8 rats (58 neurons) for OTCs, acutely prepared slices from 3 P14 (57 neurons) rats and acutely prepared slices from 6, 10-week-old rats, (44 neurons). Comparisons of passive membrane properties were initially made between neurons of these 3 groups of passive neuronal properties including resting membrane potential (RMP), rheobase (a measure of neuronal excitability - the higher the rheobase, the less excitable the neuron is) and input resistance (R_{in}, reflects extent to which membrane channels are open) was first evaluated. Although still significantly different, the RMP, rheobase and R_{in} of BLA OTC principal cells more closely resembles those from 10W acutely prepared slices than from P14 slices (Fig.2.4A-C). Specifically, the RMP of 10W old BLA principal cells was significantly more hyperpolarized compared to P14 principal neurons and from OTC neurons (10W acute: -81.34 ± 0.67 mV, P14 acute: -76.75 ± 0.46 mV (P<0.001), OTC: -77.93 ± 1.03 mV (P<0.01)). The rheobase from BLA OTC principal neurons was reduced, compared to 10-week acute slices, but significantly larger than P14s (OTC: 248.2 ± 24.8 pA, 10W acute: 309.2 ± 13.8 pA (P<0.05), P14 acute: 126.3 ± 5.2 pA (P<0.001)). Lastly, there was an observable reduction in R_{in} in acutely-prepared slices with time, while BLA OTC principal neuron R_{in} falls between the two acute groups (OTC: 103.4 ± 6.3 MΩ (P<0.001 compared to P14, P<0.05 compared to 10W) , 10W acute: 71.50 ± 5.2 MΩ, P14 acute: 176.8 ± 6.4 MΩ (P<0.001).

Development of the H-current (I_h)

Next, the development of an intrinsic current that classically contributes to passive membrane properties, the hyperpolarization-activated cation current, I_h, was examined [for review, see Lewis and Chetkovich (2011)]. I_h, which conducts both Na^+ and K^+, is present in

various cell types in a number of different brain regions, including principal neurons in the BLA (Womble and Moises, 1993, Park et al., 2007). The mean amplitude of I_h in BLA principal neurons has been observed to steadily increase during the entire first postnatal month (Ehrlich et al., 2012). In voltage clamp, successive -10 mV hyperpolarizing steps from -55 mV, revealed the presence of a robust I_h already at P14 which had increased significantly in BLA neurons in acute slices from 10-week old rats (-95 to -135 mV $P<0.001$; Fig.2.5A). Although I_h from OTC principal neurons is still significantly different from 10W acutely prepared slices for similar voltage steps, it does appear to be increasing similarly in amplitude as it would *in vivo*. Cell capacitance is proportional to cell surface area and is deemed as a rough estimate of cell size (Taylor, 2012). To control for possible differences in cell size, we also examined I_h density, by taking the quotient of I_h amplitude and cell capacitance. I_h density was significantly higher in OTC neurons compared to acute P14 cells (-95 to -135 mV ($P<0.001$), -85 mV ($P<0.01$). No significant differences were seen between I_h densities in OTC neurons and acute 10W neurons (Fig.2.5B).

We next studied the voltage-dependency of I_h activation by normalizing I_h amplitude at each step to the peak I_h for the given cell, fit the data to a Boltzmann equation (Fig.2.5C), then calculated $V_{½}$ values for each cell in each group, and presented as mean values (Fig.2.5D). There was no difference in $V_{½}$ values for I_h between OTC, P14 or 10W acutely prepared principal neurons ($P>0.05$). Lastly, we estimated the activation kinetics of I_h by fitting the recorded current trace with a two-term exponential equation to peel two time constants, fast and slow (Fig.2.5E, Tau fast and Tau slow). Fig.2.5F-G illustrates OTC principal neurons had the fastest kinetics, P14 neurons had the slowest kinetics and 10W acute neurons were somewhere in the middle (OTC: tau fast=13.25 ± 0.80 ms, tau slow=93.02 ±

5.13 ms; P14 acute: tau fast=35.06 ± 1.59 ms, tau slow=185.9 ± 8.46 ms; 10W acute: tau fast=25.44 ± 2.22 ms, tau slow= 150.8 ± 12.91 ms). While performing analysis on I_h density, we noticed marked differences in capacitance measurements between the groups (Fig.2.6A). Not surprising, 10W BLA principal cells had the largest capacitance, followed by P14s, while OTC had the smallest capacitance at (OTC: 150.0 ± 5.8 pF, P14 acute: 180.9 ± 3.7 pF, 10W-acute: 230.6 ± 7.3 pF; (P<0.001), Fig.2.6B).

Development of spontaneous inhibitory and excitatory postsynaptic currents

Parvalbumin expressing GABAergic interneurons of the BLA do not reach mature levels until P25-30, while many excitatory inputs to BLA from thalamic and cortical regions are continually being refined until P26 (Berdel and Morys, 2000, Bouwmeester et al., 2002). This parallels the observation that numbers of synaptic contacts there nearly triple during the same time period (Berdel et al., 1997, Morys et al., 1998). We therefore next determined if synaptic connections were being formed in our cultures and to quantify the extent of their development in relation to sIPSCs and sEPSCs.

Spontaneous postsynaptic currents were examined by holding neurons at -55 mV in voltage clamp. Cl^- -mediated sIPSCs mediated by $GABA_A$-receptors, are outward and are seen as upward deflections in the current trace at this potential, while AMPA and NMDA receptor-mediated components of sEPSCs are seen as downward (inward current) deflections at this potential (Fig.2.7A & 2.8A). The mean sIPSC amplitude for OTC principal neurons was significantly greater than that seen in neurons from either P14 or 10W acutely prepared slices (OTC: 49.83 ± 4.95 pA, P14 acute: 25.54 ± 1.12 pA (P<0.0001), 10W-acute: 24.13 ± 1.81 pA (P<0.0001); Fig.2.7B). When plotted as a cumulative probability plot, sIPSC amplitudes were

significantly larger in neurons from OTCs and P14s compared to acute 10W neurons (P<0.0001, Fig.2.7C), which is represented more clearly in the amplitude-frequency histogram (Fig.2.7D). However, the frequency of sIPSCs was not significantly different between OTC principal neurons and those from the 10W acute group while the P14 group's frequency was reduced (increased IEI) compared to the previous two groups (OTC: 155.6 ± 19.3 ms (P<0.0001), P14 acute: 2249 ± 416 ms, 10W-acute: 213.9 ± 22.1 ms (P<0.0001); Fig.2.7E). Cumulative probability plots indicate there was an increase in frequency between OTCs and acute 10W neurons compared to acute P14s, and an increase in frequency between OTCs and acutely-prepared 10W principal neurons (Fig.2.7F).

A similar shift was found when we examined sEPSCs, with OTC principal neurons displaying larger amplitudes than the P14 and 10W acutely prepared slices (OTC: 44.76 ± 2.12 pA, P14 acute: 25.94 ± 0.86 pA (P<0.0001), 10W-acute: 26.87 ± 2.30 (P<0.0001); Fig.2.8B). Cumulative probability plots and amplitude-frequency histograms indicate sEPSC amplitudes from OTCs and acute P14 neurons are larger than those from acute 10W neurons, and acute P14s are larger than 10W acutely prepared slices (Fig.2.8 C-D, P<0.0001). As with sIPSCs, the mean frequency of sEPSCs was similar between OTC principal cells and from acute 10W neurons, while frequency from P14 neurons was markedly reduced compared to the other groups (OTC: 221.5 ± 32.2 ms (P<0.01), P14 acute: 1241 ± 347 ms, 10W-acute: 171.1 ± 26.4 ms (P<0.01); Fig.2.8E). Cumulative probability plots suggest sEPSC IEI is reduced in acute 10W neurons compared to OTCs and acute P14s, while sEPSC IEI from OTCs is smaller compared to acute P14s (Fig.2.8F, P<0.0001).

Finally, an unexpected finding was the occurrence of compound postsynaptic bursting activity within the BLA of OTC slices, which was completely absent from acutely prepared

slices (Fig.2.9). OTC slices generated bursts at a frequency of 0.23 ± 0.022 Hz, while none were present in either group of acutely prepared slices. Compound bursts suggest synchronous network neural activity, requiring both $GABA_A$ receptor activation in projection cells and glutamatergic input to GABAergic interneurons and has been postulated to facilitate emotional states within the BLA (Rainnie, 1999, Chung and Moore, 2009).

Morphological analysis of principal neurons

The dendritic tree is a highly dynamic structure that undergoes extensive remodeling in the first postnatal month, initially with the elaboration of the dendritic architecture, and then its subsequent retraction with postnatal synaptic pruning (Ryan et al., 2014). It is suggested that most of the critical changes in structure and function occur by P28 (Ehrlich et al., 2012, Ehrlich et al., 2013, King et al., 2013, Ryan et al., 2014). Therefore, we aimed to quantify variances in the morphology of principal cells in the three preparations. Neurobiotin-filled neurons from the above electrophysiological experiments were stained and visualized post hoc to make reconstructions (see Methods, above, for detailed description). As depicted in Figure 2.10A, the dendritic arbors of principal neurons from all three groups were similar in general shape and appearance, but differed in their overall extent. Generally, principal neurons from acutely prepared slices increased in size with age, as neurons from 10W old slices were larger than those in P14s. An interesting finding was that BLA OTC principal cells were considerably smaller than neurons either from P14 or 10W acutely prepared slices. A detailed quantification of the observed differences is described below. Note, although electrophysiological data was compiled from three P14 animals, slices from only one animal were processed for morphological analysis.

Using the simple neurite tracer and Sholl analysis functions in FIJI, we first quantified total dendritic length of principal neurons. Total dendritic length of OTC principal cells was considerably smaller compared to acutely prepared P14 and 10W acutely prepared neurons (OTC: 3625 ± 187 μm, P14 acute: 5986 ± 337 μm (P<0.0001), 10W-acute: 8644 ± 284 μm (P<0.0001); Fig.2.11A). Sholl analysis with concentric circles of 10 μm in radii (Fig.2.10D), revealed significant differences in the number of intersections as a function of distance from the soma, for all three groups (Fig.2.11B). Specifically, OTC principal cells exhibited fewer intersections compared to 10W-acute neurons and P14 acute neurons (OTC vs 10W-acute: 30-330 μm (P<0.001), OTC vs P14 acute: 50-190 μm (P<0.001)). Furthermore, the number of intersections increased with age from P14 to 10W acutely-prepared neurons in the region between 60-250 μm (P<0.001). Examining the degree of branching revealed the number of branch points of acutely-prepared BLA principal neurons significantly increased with age, while OTC principal neurons had fewer branches compared to both acute preparations (OTC: 20.54 ± 1.55 (P<0.0001), P14 acute: 37.53 ± 2.28 (P<0.05 vs 10W-acute), 10W-acute: 46.28 ± 1.87; Fig.2.11C). To determine the area along the neuron where branching occurred, we quantified the number of branch points as a function of distance from the soma, which indicated that differences in branching occurred at more proximal sites (Fig.2.11D). Branch points increased with age of acutely prepared slices 20 μm and 60 μm from the soma (20 μm (P<0.001), 60 μm (P<0.05)). Branching was reduced at regions of 20, 60, 100, 140 and 180 μm from the soma between OTCs and 10W acute slices (20 μm (P<0.0001), 60 μm (P<0.0001), 100 μm (P<0.0001), 140 μm (P<0.01), and 180 μm(P<0.05)), while significant reductions were observed between 60 and 100 μm from the soma for OTCs compared to P14 acutely prepared principal cells (60 μm (P<0.0001), and 100 μm (P<0.001)). Finally, we

investigated variations in the specific orders of dendritic branches. Figure 2.11E shows that age of acutely prepared slices only affected 3° dendrites with increases in 10W old neurons compared to P14 neurons (P14 acute: 13.12 ± 1.20 dendrites, 10W-acute: 18.56 ± 1.12 dendrites; (P<0.0001)). However, there were significant reductions in 2°, 3° and 4° branches of OTCs compared to 10W (P>0.0001) and 2° and 3° compared to P14s ((P>0.0001); Fig.2.11E). We did not analyze soma size due potential errors incurred during detaching of patched neurons.

Discussion

In this study, we not only developed and optimized the first known protocol for OTCs of rat BLA, but also were able to functionally characterize and compare principal neurons to those from acutely prepared slices of the developing and adult rat brain. We obtained consistently viable BLA OTCs from P14 rats that have remarkably similar morphological and electrophysiological features of neurons from age-match acute slices. OTCs do undergo some remodeling after culturing is initiated, including loss of anatomical markers and thinning of the slices over time. Flattening, which is common in OTC preparations and a macroscopic criterion of healthy slices, would be consistent with increases in the density of cells in a slice (Guy et al., 2011, Humpel, 2015a). The OTC preparation is an axotomized system, so neurons lose both afferent and efferent connections with distant brain regions. In other OTC models, the degree of connectivity between neurons appears to depart from that of acute slices and approaches the higher levels observed *in vivo* (Holopainen and Lauren, 2003, Pena, 2010, Okamoto et al., 2014). This increase in connectivity may well be attributed to synaptogenesis and neuronal sprouting, which occurs within days to weeks in hippocampal OTCs (Stoppini et al., 1993, Robain et al., 1994). This implies that OTCs may develop altered local synaptic circuits and can be a limitation of the technique. Nevertheless, our comparison of electrophysiological properties of principal cells at different stages of development in acute slices has confirmed others' findings that considerable changes, consistent with normal development occur with time (Ehrlich et al., 2012). The majority of electrical features, RMP, rheobase, input resistance, I_h-amplitude and density, and sIPSC and sEPSC frequency, of BLA OTC principal neurons were more akin to neurons in age-matched acute slices than to those in

acute slices from the age at which OTCs were prepared. This suggests that BLA OTCs mature in a manner comparable, though not exactly, to that seen *in vivo*.

Although neurons from OTCs maintained a similar structural shape to those from acutely prepared slices, there was a dramatic disparity in the extent of the dendritic trees. The likely explanation for this is the intrinsic propensity of OTCs to flatten with time and the corresponding increase in density of cells, paralleled by the loss of extracellular space. Thus, the reduction in neuronal size that accompanies OTCs is likely due to their inability to expand. A recent morphometric analysis of the maturation of rat principal BLA neurons from acutely-prepared slices, revealed a similar growth pattern in the dendritic arbors between P14 and P60 rats as seen here, including comparable total dendritic lengths, spatial extent of dendrites and branch points (Ryan et al., 2014). However, other studies exploring dendritic architecture of adult rat BLA principal neurons are almost uniformly inconsistent with ours. These studies approximate total dendritic length (~ 1000-3000 μm) and number of branch points (~ 5-20) to be far less than what we observe both in acutely-prepared slices from adult BLA (~8600 μm and ~ 46 branch points), but are instead similar to our OTCs (~ 3600 μm and ~ 20 branch points) (Vyas et al., 2002, Vyas et al., 2004, Hill et al., 2011, Adamec et al., 2012, Hill et al., 2013, Padival et al., 2013b). These major differences appear to arise from differences in methods, as these latter studies typically employed a Golgi-Cox stain, which may underestimate the dendritic arbor, either by preferentially staining smaller neurons or by marking only proximal dendritic segments (Ryan et al., 2014). While it is possible that our approach of visualizing neurons for electrophysiological studies could promote overestimates of the dendritic arbor from these neurons, it appears less likely. At this point, it remains unclear if the population of neurons we have chosen to study represents a truly heterogeneous

population of BLA principal neurons, or possibly a population of large, easily identifiable neurons.

The constrained neuronal architecture of BLA OTCs provides a possible explanation for discrepancies in capacitance, I_h activation kinetics and amplitude of spontaneous postsynaptic currents between OTCs and acute slices. As capacitance is proportional to cell surface area, the larger the cell, the larger the capacitance. The apparent altered kinetics of I_h, and of sIPSC and sEPSC amplitudes are likely caused by the more compact physical structures of the OTC neurons. Simply put, the currents are electrical events that happen closer to the recording pipette in the OTC cells.

Space-clamp, is a distortion of the measured current with increased distance, particularly in a non-spherical cell (Spruston and Johnston, 2008). Patching neurons at the cell soma results in the membrane potential being less well voltage-clamped with increasing distance from the pipette. This is exacerbated by the complexity and extent of the dendritic tree. Because of this, the current measured at the soma is slower and smaller in amplitude than the current happening in distal regions of the dendrites (Bar-Yehuda and Korngreen, 2008). Since HCN channels in BLA neurons are likely located distally in the dendrites, as in the hippocampus and other brain regions (Poolos et al., 2002), where we have poor voltage clamp and poor frequency fidelity (dendritic filtering), smaller neurons, would have HCN channels situated closer to the soma, thus the measured currents would appear faster. We consider it unlikely, that there are changes in HCN-subunit expression, since BLA pyramidal cells normally express a very high level of the HCN1 channel, which has the fastest activation kinetics of the 4 HCN subunits (Biel et al., 2009). A similar explanation may be used for the differences observed in the amplitudes of sIPSC and sEPSCs in OTCs relative to the acute

slices; essentially $GABA_A$ and glutamate synapses are physically and electrically closer to the cell soma, making events larger and more rapid. Nonetheless, properties of GABAergic interneurons and their connections with the principal cells or even in the $GABA_A$-receptor subunit composition may also differ significantly the amygdala of OTCs.

Although sometimes presented with the mean ± SEM and analyzed with t-tests or one–way ANOVA, the "gold standard" for analysis of synaptic activity is presenting data as cumulative frequency distributions and analyzing with the K-S test. However, there were marked differences in the level of significance when we analyzed our data for amplitude and frequency of sIPSCs and sEPSCs using mean values followed by one-way ANOVA with Tukey's *post hoc* test versus cumulative probability plots and the K-S test. This discrepancy is likely due to the K-S test being a nonparametric test (does not make any assumptions about the distribution of the data), which computes a P value based on the maximum difference between two cumulative distributions, but does not test for any particular parameter (mean, median, variance, etc) (Lehmann and D'Abrera, 2006). Therefore, although mean values may be non-significantly different, subtle differences in the shape of the cumulative frequency distribution may result in small P values using the K-S test, especially when tens of thousands of events are being evaluated. Alternatively, the mean values may more closely reflect the physiological reality and the K-S analysis may overemphasize trivial differences as significant. Caution must be made when assessing differences based on either of these two methods alone.

We never observed compound postsynaptic bursting activity in acutely prepared slices while almost always present to some degree in our OTCs. While almost always masked or absent in acute BLA slices, phase-locked oscillations in the high delta/low theta frequency

band occur frequently in the *in vivo* BLA, and have been shown to contribute to learning processes (Lesting et al., 2011, Ryan et al., 2012). In BLA of acutely prepared slices, these bursts result from synchronized, rhythmic activity and can be induced by elevations in K^+ concentration in the bath solution or electrical stimulation of the slice (Rainnie, 1999, Chung and Moore, 2009). Furthermore, synchronization of the BLA results from glutamatergic inputs onto interneurons and $GABA_A$ receptor activation in principal cells, as antagonists of either block this activity (Smith and Dudek, 1996, Rainnie, 1999). Studies in cortical OTCs demonstrated that spontaneous activity increases with development *in vitro*, culminating in bursts or "up and down" states with a decrease in intrinsic excitability (Johnson and Buonomano, 2007). Therefore, it seems plausible for bursting activity observed in our OTCs to be a component of normal physiological behavior. However, as OTC preparations normally result in a loss of afferent and efferent projections to and from the culture, there is typically an up-regulation in new, more localized synapses, resulting in enhanced local circuits. Therefore, the observation of bursting activity may be due to enhanced localized circuits, increasing the overall network activity of the slice culture.

Together, the preliminary work presented here gives ample evidence for the similarity of BLA OTCs to the *in vivo* counterpart, and makes them potentially quite attractive as a tool to study stress related circuitry. This *in vitro* preparation appears to have many similarities to age-matched acutely prepared slices, and only modest differences. The OTC model should prevail as a useful tool to generate mechanistic insights into the physiology governing stress, stress resilience and the signal transduction processes underlying plastic changes caused by activation of NPY and CRF receptors.

Figure 2.1

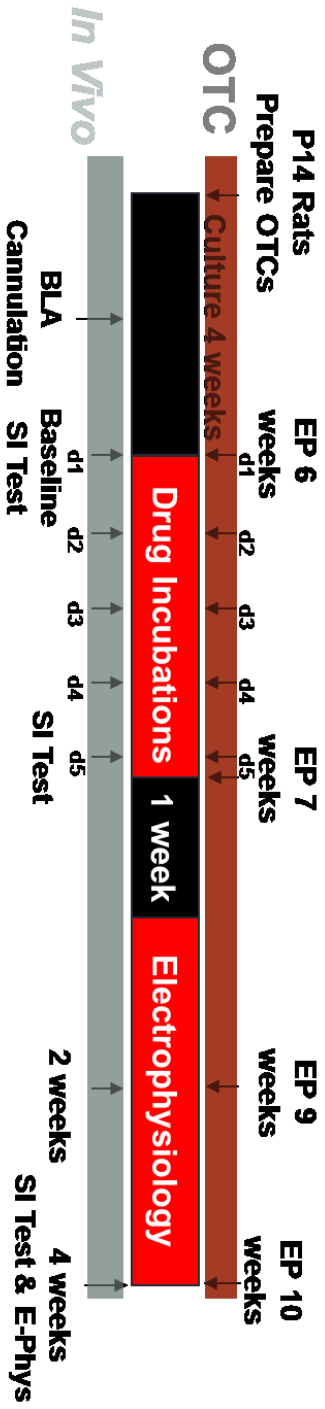
OTC
P14 Rats
Prepare OTCs
Culture 4 weeks
EP 6
weeks
EP 7
weeks
EP 9
weeks
EP 10
weeks
Drug Incubations
1 week
Electrophysiology
In Vivo
BLA
Cannulation
Baseline
SI Test
SI Test
2 weeks
4 weeks
SI Test & E-Phys
d1
d2
d3
d4
d5

Figure 2.1 Comparison of experimental timelines for OTCs and age-matched acutely prepared slices.

Male Sprague-Dawley rats (P14 days) were used for preparation of BLA OTCs using the method of (Stoppini et al., 1991). Slices were grown on membranes in culture in an incubator at 37°C, 5% CO_2, 95% humidity for 7 weeks to bring them to equivalent postnatal (EP) 9 weeks of age before initiating electrophysiological studies. Electrophysiological experiments were performed between EP 9-10 weeks. Media was changed three times per week throughout the culturing period. To compare OTCs to age-matched, acutely prepared slices, we employed PBS injected animals from stress resilience studies. Here, male Sprague-Dawley rats aged 5 weeks were acclimatized, by handling daily for 5 days upon delivery to the laboratory. At this time, baseline social interaction studies were performed prior to animals being implanted with bilateral cannulas targeted to and 2 mm above the BLA. Animals were allowed to recover for 4-7 days before injections began. At 6 weeks of age, PBS vehicle was administered bilaterally directly into the BLA by a syringe pump (100 nL/ 1 min) via an injection cannula inserted into and extending 2 mm beyond the guide cannula for 5 consecutive days and social interaction was measured 30 minutes after the end of the first injection and after the final one on the 5th day. Animals were housed for the following 4 weeks with social interaction being monitored every week. At 10 weeks of age, animals were sacrificed and their brains used for electrophysiological studies. In a subset of experiments, P14 male Sprague-Dawley rats were used to prepare acute slices for electrophysiological and morphological studies.

Figure 2.2

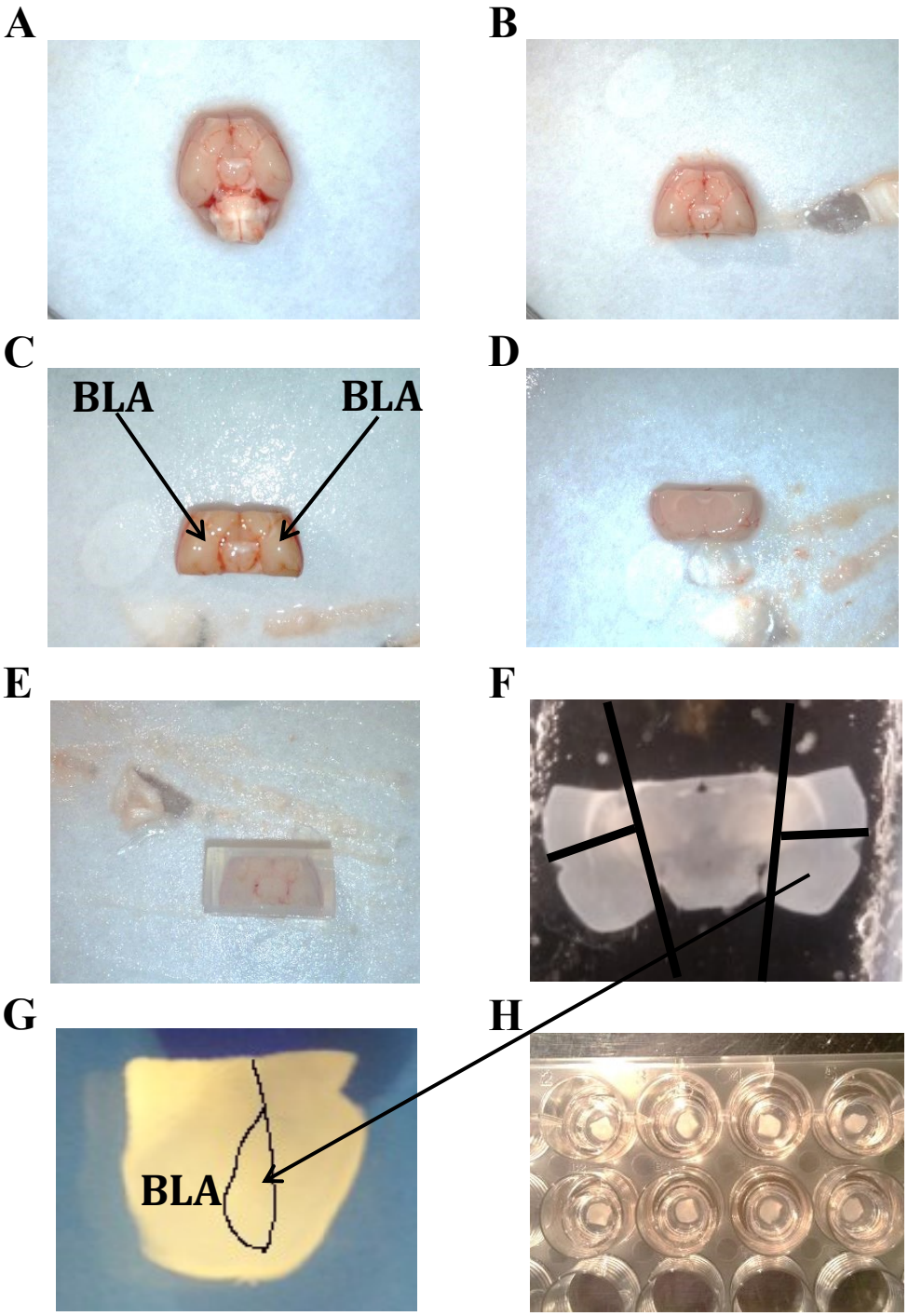

Figure 2.2 Photographs of OTC preparation.

Following decapitation, the whole brain of P14 rats was rapidly removed from the skull and placed ventral side up (A). A brain block was prepared by making 2 coronal cuts (B and C) and one transverse cut to remove part of the dorsal neocortex (D). This brain block is submerged into warm liquid agarose (just above the gel point, <36ºC), which was allowed to harden. Once hardened, the agarose block is trimmed parallel to the edges of the brain block (E). 350 μm thick coronal sections are cut yielding a single slice with both hemispheres still attached (F). Slices are trimmed using a bent 25 G needle and a syringe (cuts are indicated as black lines (F)), dorsal to the rhinal fissure and medial to the medial nucleus of the amygdala (G). When all slices are collected and allowed to rest for some time, the four slices containing the BLA from each hemisphere are plated onto the membrane inserts in a 24-well plate as shown (H).

Figure 2.3

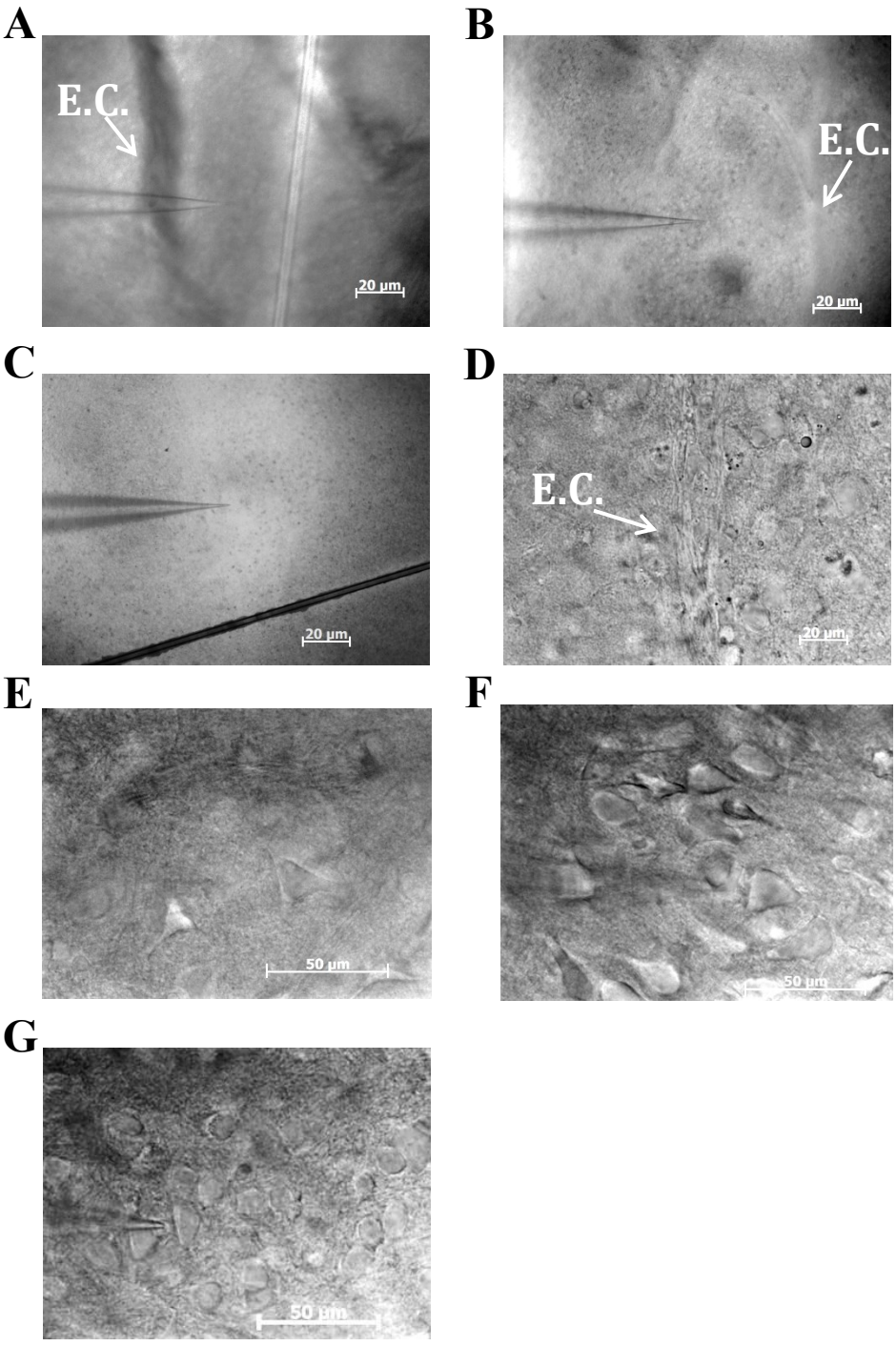

Figure 2.3 DIC images of BLA and BLA principal neurons.

Images at 40x magnification of the BLA from 10-week old acutely prepared rats (A), P14 acutely prepared rats (B) and OTCs (C). Note, the external capsule (white arrow) is easily observable in both acutely prepared slices but is difficult to distinguish in OTC slices. Under 600x magnification, the fibrous white matter tract of the external capsule is visible, delineating the lateral boundary of the amygdala (D). BLA neurons are readily identifiable under 600x magnification in 10-week acutely prepared (E), P14 acutely prepared (F) and OTC slices (G).

Figure 2.4

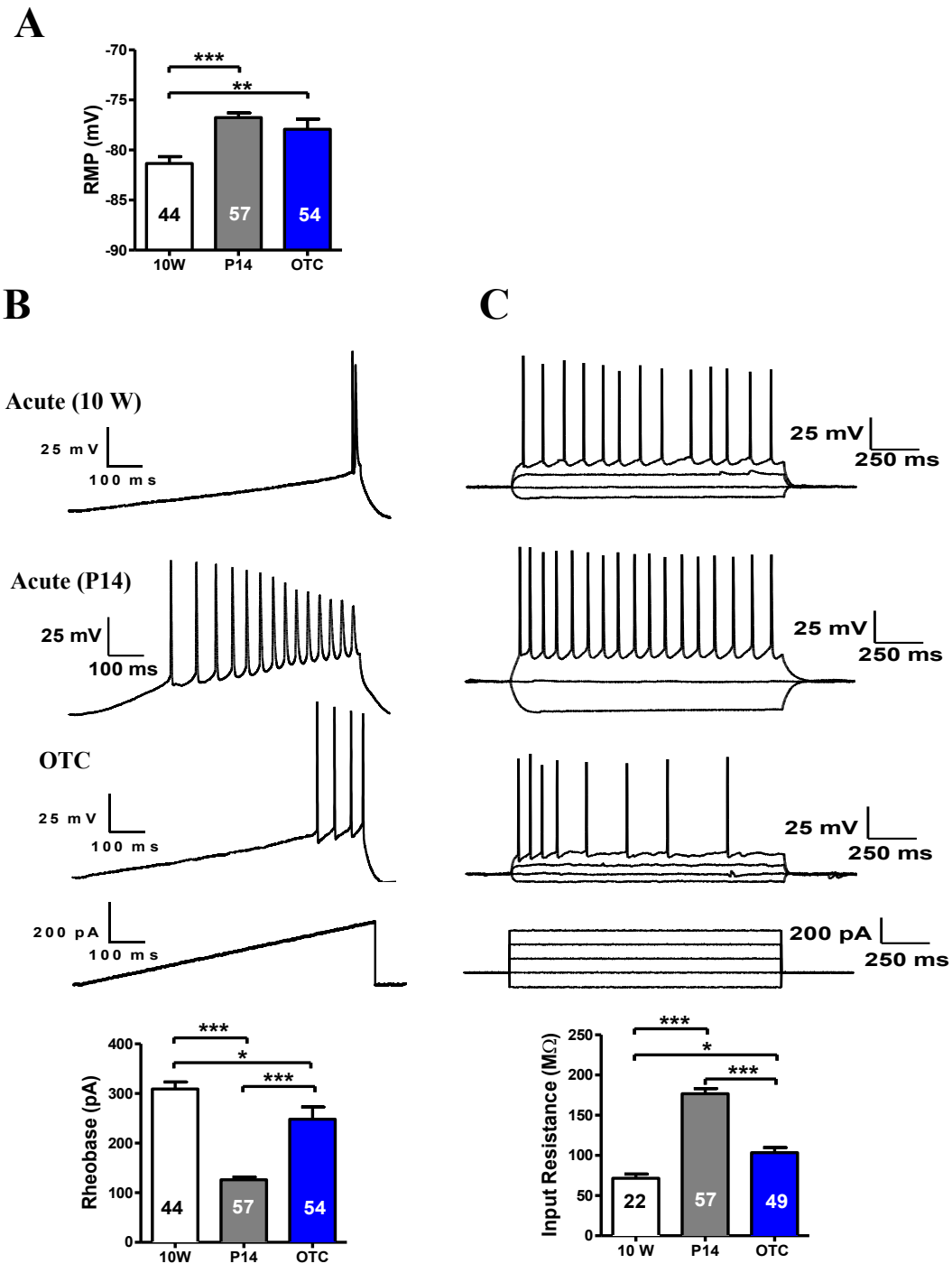
A
RMP (mV)
-70
-75
-80
-85
-90
***
**
44
57
54
10W
P14
OTC
B
Acute (10 W)
25 mV
100 ms
Acute (P14)
25 mV
100 ms
OTC
25 mV
100 ms
200 pA
100 ms
Rheobase (pA)
400
300
200
100
0
***
*
***
44
57
54
10W
P14
OTC
C
25 mV
250 ms
25 mV
250 ms
25 mV
250 ms
200 pA
250 ms
Input Resistance (MΩ)
250
200
150
100
50
0
***
*
***
22
57
49
10 W
P14
OTC

Figure 2.4 Comparison of passive membrane properties with age in acute and OTC BLA pyramidal neurons.

Some but not all passive membrane properties changed significantly with increasing age in acutely prepared slices, and properties of OTC principal neurons appear to develop in a comparable manner. (A) Plotted as mean ± SEM, RMP was significantly more hyperpolarized in BLA principal neurons from 10W acute slices relative to acute P14 and EP 10 week OTCs (***P<0.001; **P<0.01). (B) Representative traces from current clamp recordings of action potential firing in response to depolarizing current ramps (bottom trace). Plotted as mean ± SEM (lower graph), rheobase significantly increased with age in acutely prepared slices (***P<0.001). Rheobase was considerably higher in OTC neurons than in those from P14 slices (***P<0.001), but slightly lower than seen in age-matched, 10W acutely prepared slices (**P<0.01). (C) Input resistance was measured in current clamp following a 100 pA hyperpolarizing current step (bottom) applied from rest. In representative traces as in B. Input resistance (mean ± SEM, bottom graph) was significantly lower in 10W acutely prepared slices and OTCs than in P14 acutely prepared slices (Top, ***P<0.001). OTCs input resistance was slightly greater (*P<0.05) than in acutely prepared 10W slices. Analysis was performed using one-way ANOVA with Tukey's *post hoc* test and significance is denoted by (***P<0.001; **P<0.01). The number of cells analyzed is indicated in individual bars.

Figure 2.5

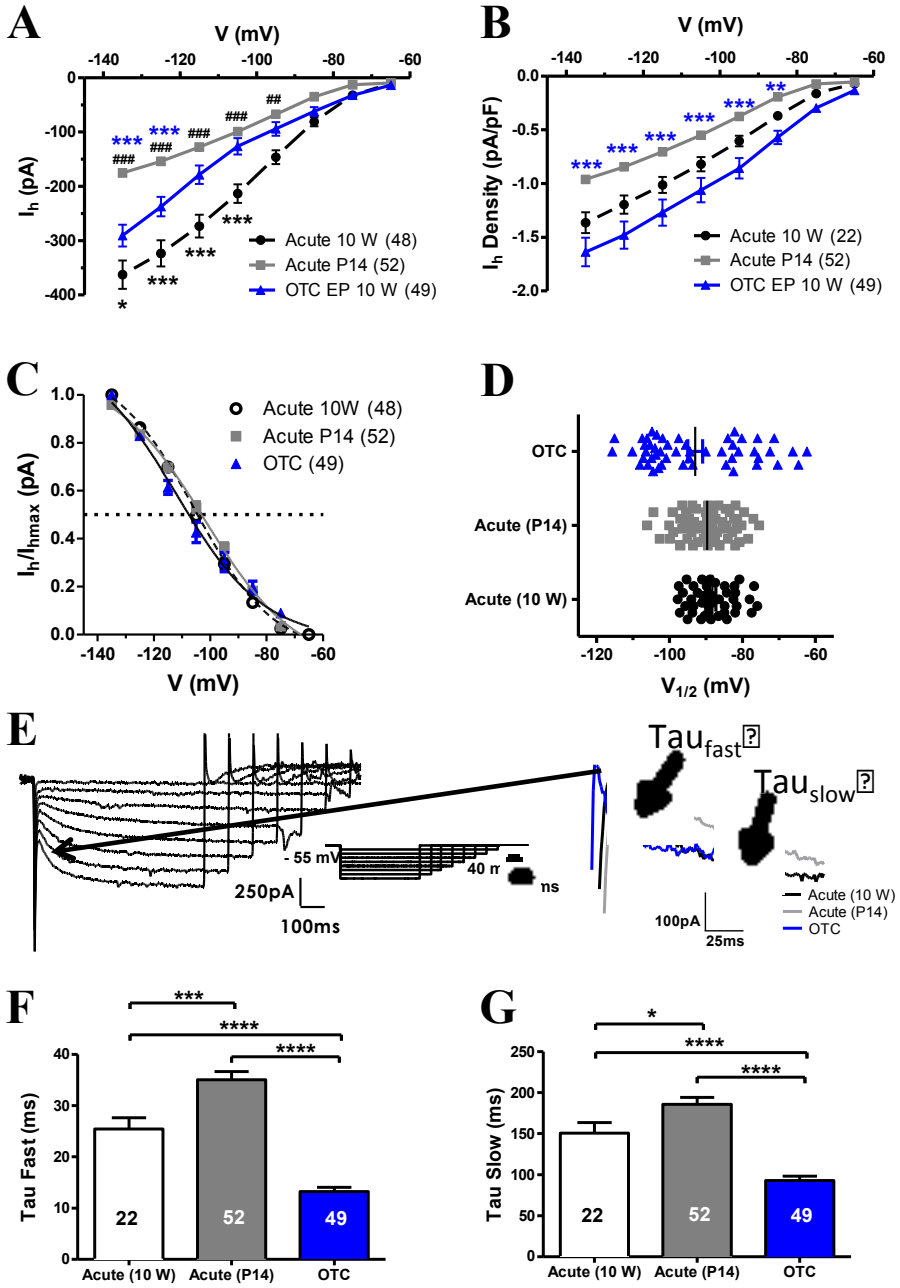
A
V (mV)
-140 -120 -100 -80 -60
0 -100 -200 -300 -400
I_h (pA)
Acute 10 W (48)
Acute P14 (52)
OTC EP 10 W (49)
B
V (mV)
I_h Density (pA/pF)
0.0 -0.5 -1.0 -1.5 -2.0
Acute 10 W (22)
Acute P14 (52)
OTC EP 10 W (49)
C
I_h/I_hmax (pA)
1.0 0.8 0.6 0.4 0.2 0.0
Acute 10W (48)
Acute P14 (52)
OTC (49)
V (mV)
D
OTC
Acute (P14)
Acute (10 W)
V_1/2 (mV)
E
Tau_fast
Tau_slow
- 55 mV
250pA
100ms
100pA
25ms
Acute (10 W)
Acute (P14)
OTC
F
Tau Fast (ms)
22
52
49
Acute (10 W)
Acute (P14)
OTC
G
Tau Slow (ms)
22
52
49
Acute (10 W)
Acute (P14)
OTC

Figure 2.5 Comparison of resting I_h in pyramidal cells from acute 10 week, P14 and OTC slices.

Properties of I_h were examined in current responses to families of 8 hyperpolarizing voltage steps from a holding potential (Vh) of -55 mV to -135 mV in 10 mV increments. (A), I_h amplitude increased significantly with age for voltages between -95 mV and -135 mV (two-way ANOVA, ###P<0.001, ##P<0.01 with Tukey's *post hoc* test). I_h amplitudes from OTCs were significantly larger than in P14s between -125 mV and -135 mV (***P<0.001), however, they were significantly smaller than in age-matched 10W acute slices between -105 mV and -135 mV (***P<0.001, *P<0.05). (B) To control for potential differences in cell size, we expressed I_h density (pA/pF – see Methods). There was no significant difference in I_h density between OTCs and age-match acutely prepared 10W slices, nor was there between P14 and 10W acutely prepared slices. However, I_h density was significantly higher in neurons from OTCs than from acute P14 slices between -85 mV to -135 mV (***P<0.001, **P<0.01, two-way ANOVA with Tukey's *post hoc* test). (C) Comparison of the voltage dependency of I_h activation in pyramidal cells from acute P14, acute 10Wand OTC slices. I_h was normalized to the maximum value at -135 mV and fitted to a Boltzmann function to obtain half maximal ($V_{½}$) values. (D) No significant differences were seen in $V_{½}$ between any of the groups (one-way ANOVA with Tukey's *post hoc* test, P>0.05). (E-G) Kinetics of I_h activation in the 3 populations of cells. (E) (*left)* Representative traces of I_h from an acutely prepared 10W principal cell, elicited by family of current steps (inset). (*right*) I_h onset at -135 mV from representative neurons as indicated. I_h currents were fit with a two-term exponential curve to obtain tau fast and tau slow values. Tau fast and tau slow significantly decreased with age in acute slices (F and G, one-way ANOVA with Tukey's *post hoc* test, ***P<0.001, *P<0.05 respectively). Ih activation was significantly faster in OTC cells than those from acutely

prepared slices. (****P<0.0001, F and G). Grey asterisk = acute P14, blue asterisk = OTC, black # = OTC vs. acute 10W.

Figure 2.6

A

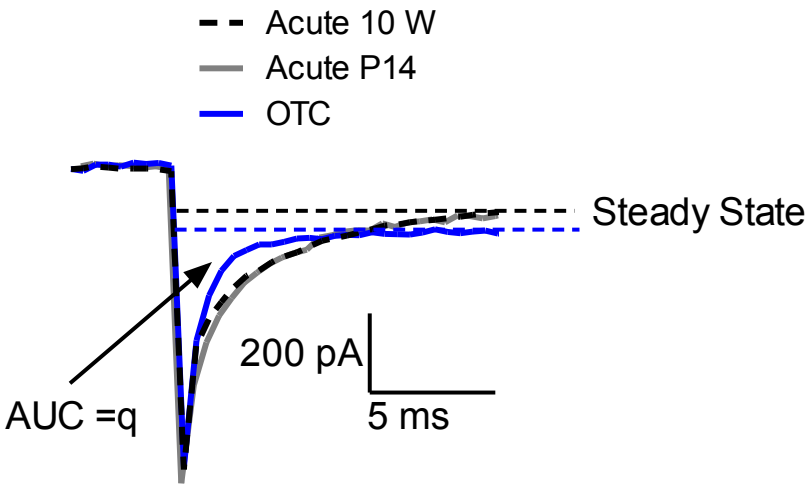

$Cm=AUC/\Delta V$

B

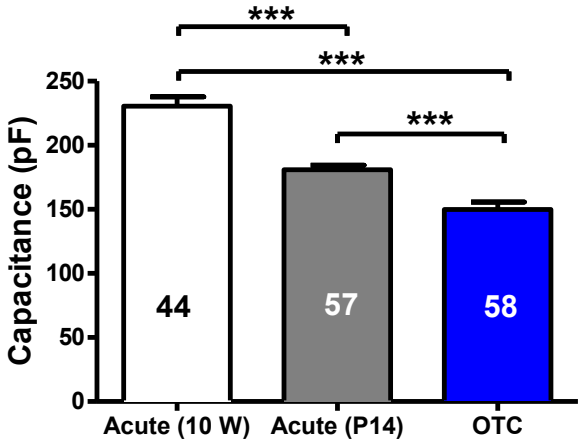

Figure 2.6 Capacitance increases with age but is much smaller in OTCs.

(A) Cell capacitance is proportional to cell surface area, and provides an index of cell size, was measured from capacitative transients from a 10mV hyperpolarizing step using an area under the curve algorithm in pClamp. (B) Neuronal capacitance (mean ± SEM) increased with age in acutely prepared slices (***P<0.001), while it was significantly smaller in OTC principal compared to both groups of cells in acute slices (One-way ANOVA with Tukey's *post hoc* test**,** ***P<0.001).

Figure 2.7

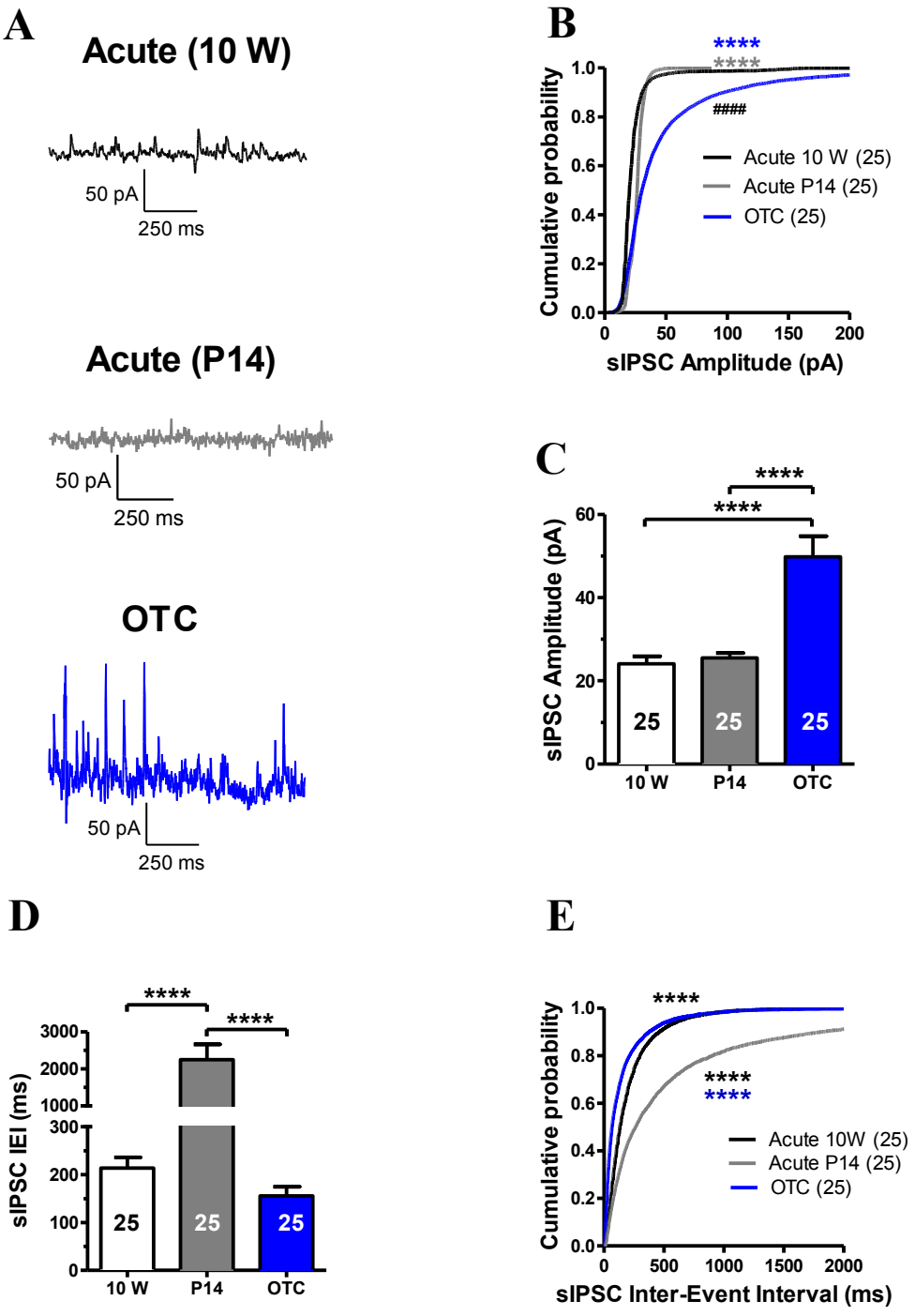
A
Acute (10 W)
50 pA
250 ms
Acute (P14)
50 pA
250 ms
OTC
50 pA
250 ms
B
****
****
####
Cumulative probability
1.0
0.8
0.6
0.4
0.2
0.0
0
50
100
150
200
sIPSC Amplitude (pA)
Acute 10 W (25)
Acute P14 (25)
OTC (25)
C
****
****
sIPSC Amplitude (pA)
60
40
20
0
25
25
25
10 W
P14
OTC
D
****
****
sIPSC IEI (ms)
3000
2000
1000
300
200
100
0
25
25
25
10 W
P14
OTC
E
****
****
****
Cumulative probability
1.0
0.8
0.6
0.4
0.2
0.0
0
500
1000
1500
2000
sIPSC Inter-Event Interval (ms)
Acute 10W (25)
Acute P14 (25)
OTC (25)

Figure 2.7 Development of spontaneous inhibitory postsynaptic currents.

$GABA_A$-mediated spontaneous inhibitory postysynaptic currents (sIPSCs) were measured in voltage clamp at at -55 mV, positive to the chloride equilibrium potential, resulting in outward currents (upward deflections). Data from each cell represents the first 400 inhibitory and excitatory events. (A) sIPSC recordings from principal cells in OTCs and in P14 and 10W-old acute slices (B). Mean amplitudes of OTC cell sIPSCs were considerably greater than in neurons from acute slices of any age (****P<0.0001). (C) Cumulative probability plot of sIPSC amplitude from the 3 populations. (D) Mean sIPSC inter-event interval shows a marked increase in frequency with age of acutely prepared slices; OTCs properties are similar to the 10W slices, ****P<0.0001). (E) Cumulative probability distribution of sIPSC inter-event interval from the 3 populations. The total number of sIPSC events analyzed was 9828 for OTCs, 3372 for acute P14s and 9589 for acute 10W. While sIPSC frequency distributions in neurons from OTC and acute 10W slices were significantly different, the actual differences between them (6.4 Hz and 4.7 Hz, respectively) were relatively minor relative to those from p14 acute slices (0.45 Hz) (**** and ####P<0.0001). Grey asterisk = acute P14 10W, Blue asterisk = OTC vs. acute P14, black asterisk = acute 10W. The number of analyzed cells is presented for each treatment in the bar graph. Mean data were analyzed by one-way ANOVA with Tukey's *post hoc* test, while cumulative probability plots were analyzed using K-S test.

Figure 2.8

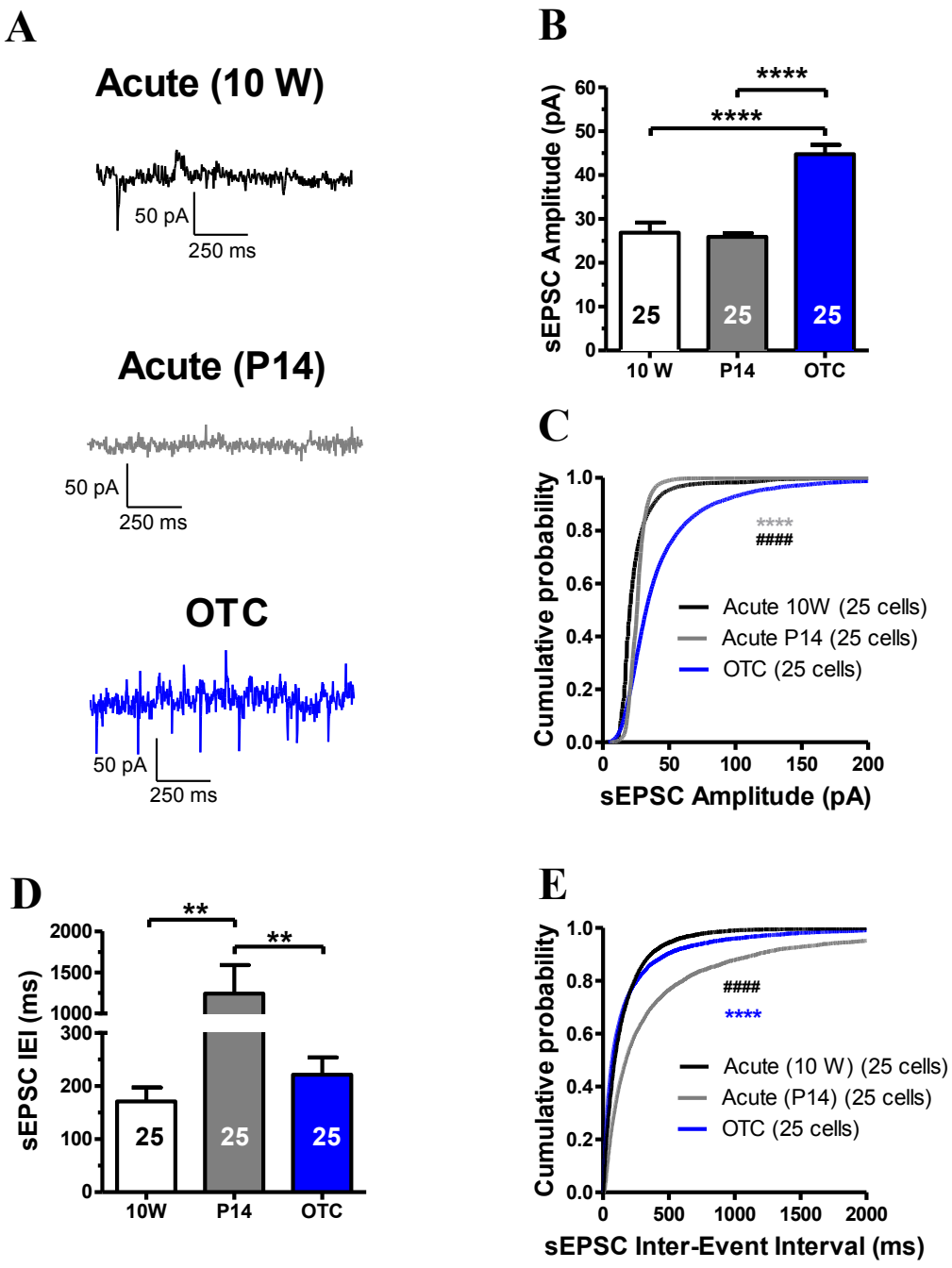
A
Acute (10 W)
50 pA
250 ms
Acute (P14)
50 pA
250 ms
OTC
50 pA
250 ms
B
sEPSC Amplitude (pA)
****
****
25
25
25
10 W
P14
OTC
C
Cumulative probability
****
####
Acute 10W (25 cells)
Acute P14 (25 cells)
OTC (25 cells)
sEPSC Amplitude (pA)
D
sEPSC IEI (ms)
**
**
25
25
25
10W
P14
OTC
E
Cumulative probability
####
****
Acute (10 W) (25 cells)
Acute (P14) (25 cells)
OTC (25 cells)
sEPSC Inter-Event Interval (ms)

Figure 2.8 Development of spontaneous excitatory postsynaptic currents.

(A) Spontaneous excitatory postysynaptic currents (sEPSCs) are mediated by a mixture of both AMPA and NMDA receptor activation and were measured in voltage clamp at -55 mV, resulting in inward (depolarizing) deflections while some (outward) sIPSCs can also be seen. (B) Mean sEPSC amplitudes did not differ significantly in neurons from acutely prepared P14 and 10W slices; however, as with sIPSCs, sEPSCs in cells from OTCs were significantly larger than those from both acutely prepared slice groups (****P<0.0001). (C) Cumulative probability distribution shows large amplitude sIPSCs in OTCs relative to those seen in acutely prepared P14s and 10W slices, while there was a significant but comparatively modest difference between P14s and 10W neurons. (D) As with sIPSCs, mean sEPSC frequencies in OTC principal neurons were comparable to those from age-matched 10W slices, while those from P14 animals were much less frequent; (E) The cumulative probability distribution for sEPSC frequency reflects the differences observed in the mean data. The total number of sEPSC events analyzed was 9776 for acute 10W, 5249 for acute P14s , and 9213 for OTCs. Grey asterisk = acute P14 10W, Blue asterisk = OTC vs. acute P14, black asterisk = acute 10W. The number of analyzed cells is presented for each treatment in the bar graph. Mean data were analyzed by one-way ANOVA with Tukey's *post hoc* test, while cumulative probability plots were analyzed using K-S test.

Figure 2.9

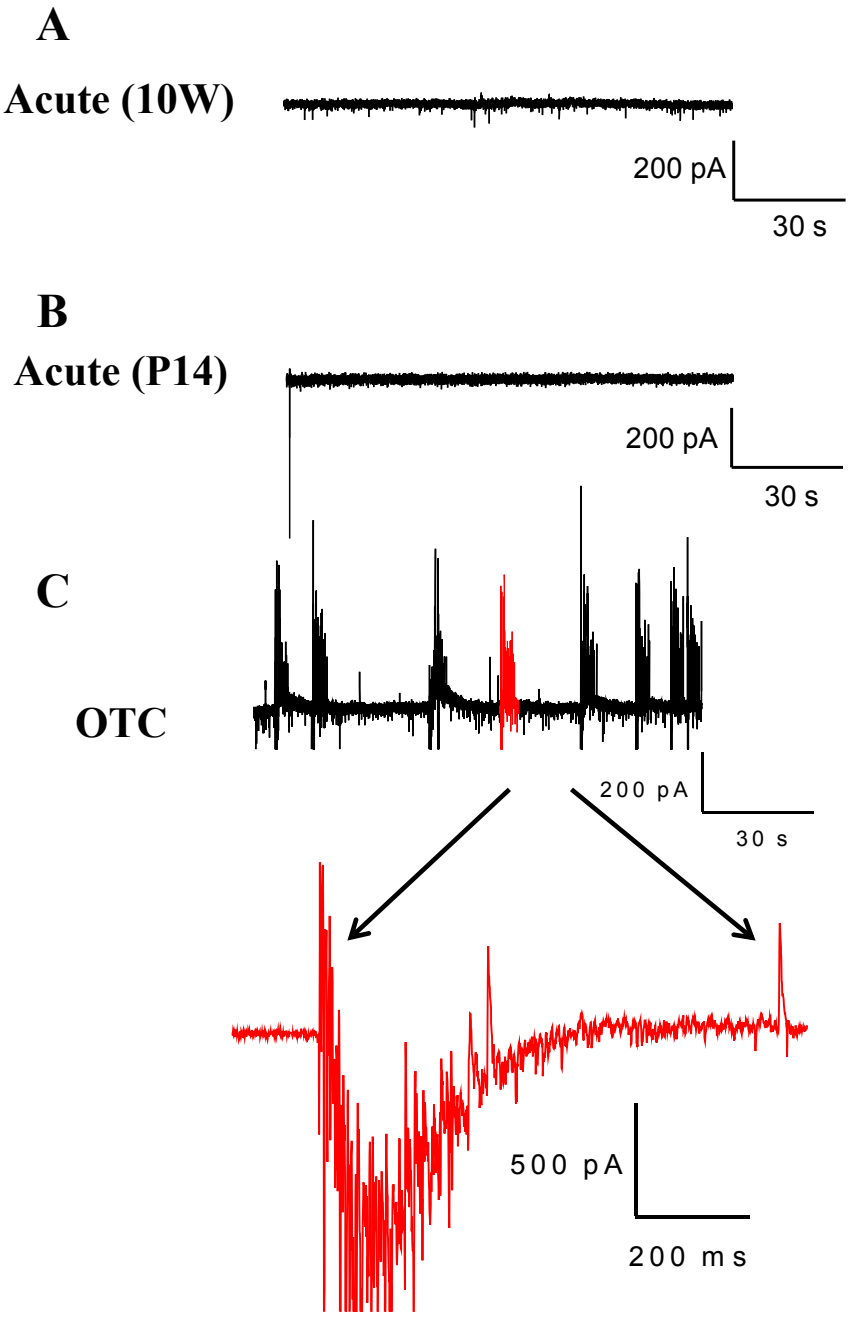
A
Acute (10W)
200 pA
30 s
B
Acute (P14)
200 pA
30 s
C
OTC
200 pA
30 s
500 pA
200 ms

Figure 2.9 OTCs demonstrate compound postsynaptic bursting activity.

Representative slow timescale voltage clamp traces with BLA pyramidal cell held at -55 mV. Acute slices from both 10W (A) and P14 (B) old rats do not display compound postsynaptic bursting activity. (C) Recording from principal neurons from OTC (*upper trace*) shows eight bursts in sequence. For quantitation, bursts were defined as events containing at least one sEPSC and one sIPSC, with a minimum of four total synaptic events that lasted for at least 100 ms in duration (*lower trace*). The average burst frequency for OTCs was 0.23 ± 0.022 Hz, while no bursts were detected for acutely prepared slices (data not shown).

Figure 2.10

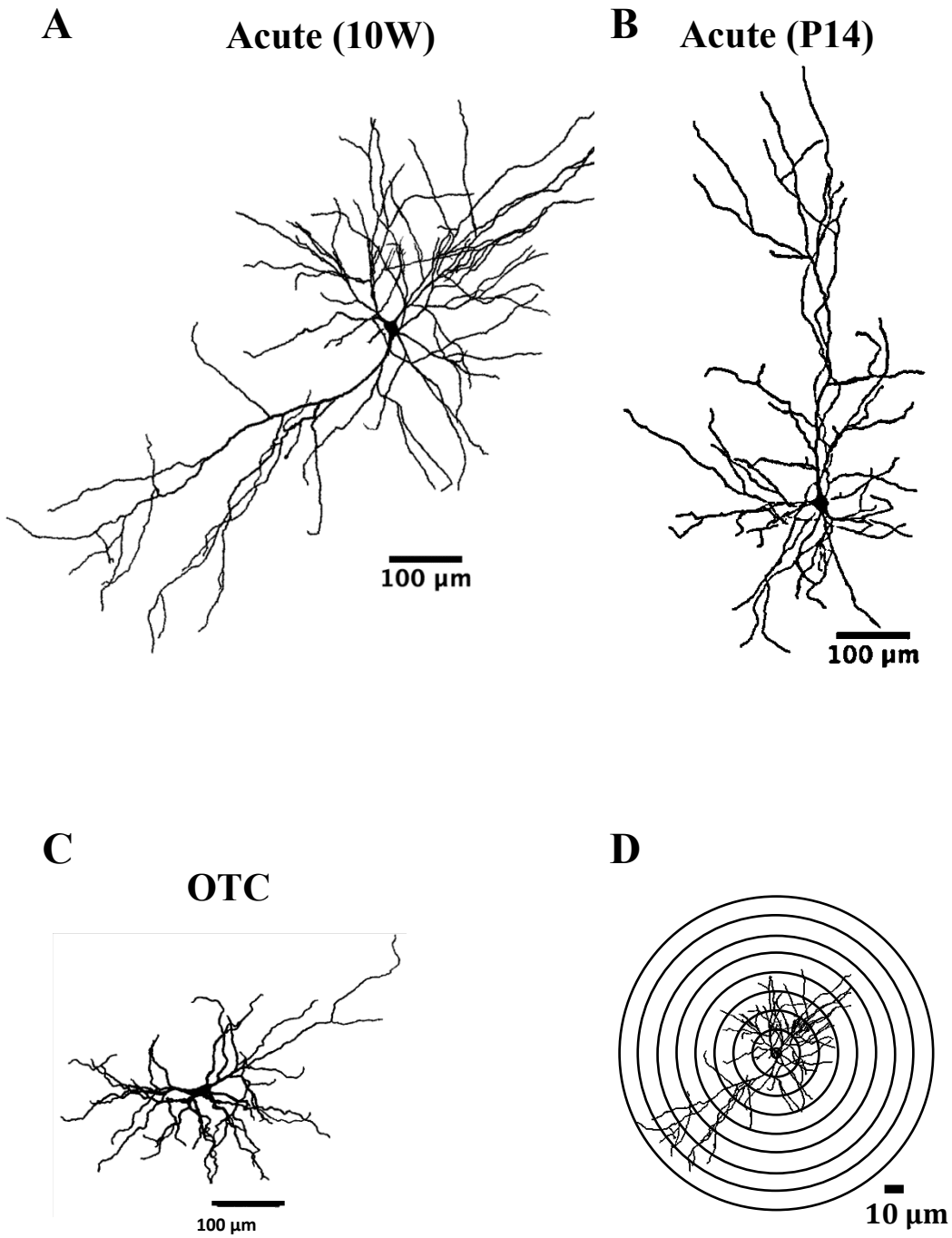

Figure 2.10 Reconstructed BLA principal neurons.

Representative BLA principal neurons reconstructed after recordings in (A) acutely prepared 10W old, and (B) P14 acutely prepared BLA slices and (C) from OTCs. Although principal cells from OTCs are similar in overall shape to those from acute slices, they are much smaller. (D) Example image of Sholl analysis for a 10W acutely prepared BLA principal neuron with successive 10 μm radii concentric circles (D). Neurons were selected based on their mean total dendritic length and mean branching for display.

Figure 2.11

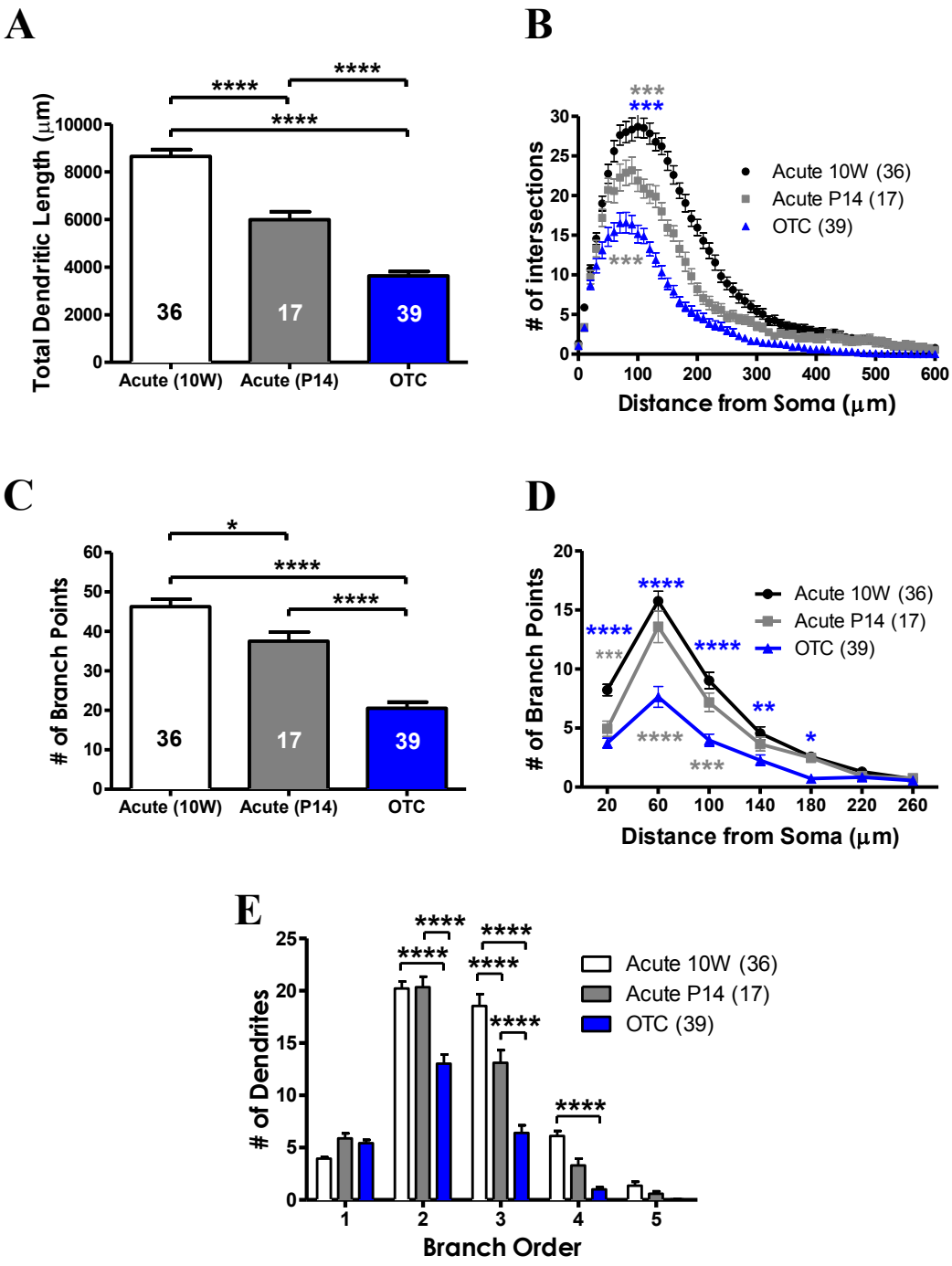
A
Total Dendritic Length (μm)
10000
8000
6000
4000
2000
0
****
****
****
36
17
39
Acute (10W)
Acute (P14)
OTC
B
# of intersections
30
25
20
15
10
5
0
***
***
***
Acute 10W (36)
Acute P14 (17)
OTC (39)
0
100
200
300
400
500
600
Distance from Soma (μm)
C
# of Branch Points
60
50
40
30
20
10
0
*
****
****
36
17
39
Acute (10W)
Acute (P14)
OTC
D
# of Branch Points
20
15
10
5
0
****
****
***
****
***
****
**
*
Acute 10W (36)
Acute P14 (17)
OTC (39)
20
60
100
140
180
220
260
Distance from Soma (μm)
E
# of Dendrites
25
20
15
10
5
0
****
****
****
****
****
****
Acute 10W (36)
Acute P14 (17)
OTC (39)
1
2
3
4
5
Branch Order

Figure 2.11 Morphological analysis reveals principal neurons from OTCs are smaller.

To quantify morphological differences in principal neurons, we reconstructed and analyzed these neurons using FIJI (NIH) and Sholl analysis. (A) Total dendritic length of principal neurons in acutely prepared slices expands with age, however, OTCs were much smaller compared to age-matched 10W and P14 cells (One-way ANOVA, ****P<0.0001). (B) Sholl analysis (see Methods and Figure 2.10D) using concentric circles with 10 μm radii increments returned the number of intersections versus distance from the soma. Expansion of the dendritic arbor with age can be seen in neurons from acutely prepared slices, while neurons of OTCs are smaller than the P14 neurons from which they began (two-way ANOVA with Tukey's *post hoc* test, ***P<0.001 vs. 10W acute, ***P<0.001 vs OTC). (C) Branch point data demonstrates dendritic arbor branching expands with age in acutely prepared slices but is reduced in OTCs (one-way ANOVA with Tukey's *post hoc* test, ****P<0.0001, *P<0.05). (D) Sholl analysis, (concentric circles of 40 μm in radii) and the number of branch points versus distance from the soma (an index of dendritic tree elaboration) illustrates dendritic branch elaboration occurs mostly within 60 – 120 μm from the soma (D, two-way ANOVA with Tukey's *post hoc* test, **** P<0.0001, ***P<0.001, **P<0.01 and *P<0.05 vs OTC). (E) Branching order indicates the complexity of dendrites. Only tertiary branch numbers increased with age in acutely prepared slices (two-way ANOVA with Tukey's *post hoc* test, ***P<0.001). OTCs retained a similar relative distribution of higher-order dendritic branches, but had far fewer than the neurons in acute slices. (****P<0.0001), but only in secondary and tertiary dendrites compared to acute P14s (****P<0.0001, ***P<0.001). Note only one animal was used for reconstructions and morphological analysis of P14 slices. The number of analyzed cells is presented for each treatment in the bar graph.

CHAPTER 3: Counter-regulatory actions of NPY and CRF on the long-term stress response

Introduction

Acute stress is a normal, adaptive reaction that refers to processes involving perception, appraisal and responses to threatening, challenging and potentially harmful stimuli, which can be beneficial for survival and future encounters (Leuner and Shors, 2013). Prolonged, exaggerated, or intense periods of stress, however, can be maladaptive and play a role in the etiology of affective and anxiety disorders (McEwen, 2003). Various brain regions acting in concert mediate and modulate the HPA axis and stress response, though key components such as the hippocampus, PFC, BNST and the amygdala appear to be preferentially involved in the neurocircuitry of anxiety [for review, see Canteras et al. (2010), Shin and Liberzon (2010), Duval et al. (2015)].

The amygdala, which gives salience and valence to sensory inputs, has emerged as a key neural hub for emotional processing and memory consolidation (Schafe et al., 2001, Wood et al., 2003, Phelps and LeDoux, 2005). A specific substructure, the BLA, integrates and responds to stress hormones and neurotransmitters that act to modulate anxiety- and emotionally-driven behaviors through its broad network of efferent projections to other brain regions. Studies indicate that in general excitatory output from the nucleus induces anxiogenic-like activity, and BLA hyperexcitability is evident in most human and rodent forms of anxiety (Rauch et al., 2003, Roozendaal et al., 2009, Rosenkranz et al., 2010, Felix-Ortiz et al., 2015). Furthermore, animal models suggest that in response to acute and chronic stress, the BLA undergoes various forms of synaptic, structural and functional plasticity (Schafe et al., 2001, Wood et al., 2003, Pape and Pare, 2010, Rosenkranz et al., 2010, Hill et al., 2011). Generally, stress-induced neuronal activity and synaptic transmission are enhanced through mechanisms involving both glutamatergic excitation and reductions in GABAergic

inhibition (disinhibition) of BLA neurons [for review, see Roozendaal et al. (2009)]. These mechanisms can result in the structural remodeling both of synapses and of the dendritic arbors of principal neurons. Numerous factors govern the overall effect of stress on structural plasticity, including the age of the subject, type and duration of stress. Thus, an acute (immobilizing) stress in rats induced an increase in dendritic spines (small protrusions from the surfaces of the dendritic processes of neurons, which receives input from one excitatory synapse, and contain postsynaptic densities rich in neurotransmitter receptors, and signaling systems essential for synaptic function and plasticity) on BLA principal neurons after a delay of 10 days, accompanied by no changes in overall dendritic morphology, while chronic stress not only initiated a robust increase in spines, but also dendritic hypertrophy (Vyas et al., 2002, Mitra et al., 2005, Vyas et al., 2006, Hill et al., 2011, Adamec et al., 2012, Padival et al., 2013b). Furthermore, variability in an individual's predisposition to maladaptive stress responses can affect the morphological outcome to chronic stress, as spontaneously anxious animals are more susceptible to alterations in BLA principal neuronal morphology in response to stress (Adamec et al., 2012, Cohen et al., 2014). It is worthy to note that unlike the hippocampus and medial prefontal cortex, where the morphological effects of chronic stress are transient, stress-induced hypertrophy in the BLA is persistent (Vyas et al., 2004).

Though there are numerous neuromodulators that regulate and fine-tune the activity of the BLA, it has been suggested that neuropeptide systems may offer superior targets for the treatment of anxiety disorders due to their limited tonic activity compared to other classical neurotransmitter systems, which could provide improved, state-specific modulation and efficacy (Thorsell, 2010). Since their initial discovery, there is a large body of evidence that suggests two neuropeptide systems: NPY and corticotropin-releasing factor CRF orchestrate

opposing regulation of responsiveness to stressful stimuli in the BLA, and prolonged activation of one or the other can ultimately result in anxiolysis and anxiogenesis, respectively. In addition to the findings that these neuropeptides can reciprocally modulate anxiety- and stress-related behaviors independently of each other, evidence suggests that CRF and NPY directly interact to maintain emotional balance, whereas disruption of this homeostatic mechanism could contribute to maladaptive stress responses and anxiety [for review see Heilig et al. (1994), Sajdyk et al. (2004)]. The dogma of this relationship suggests that following an acute stress, CRF is released and is responsible for the initial phase of the stress response, while a slower but sustained release of NPY acts to dampen and terminate this reaction in the late phase (Heilig et al., 1994). The effects of these neuropeptides are not limited to acute stress, as the association appears to be involved in paradigms of chronic stress as well. Injection of NPY directly into the BLA daily for 3 days prior to UCN injection, blocks induction and expression of UCN-mediated anxiogenic responses (Sajdyk et al., 2006).

Conventionally, researchers study the negative effects of stress by isolating molecular, cellular and neurocircuits that jeopardize normal physiological responses to stress and predispose individuals to enhanced maladaptive behavior: stress vulnerability or susceptibility. A classic example of this involved repeated (5 day) injection of UCN directly into the BLA, which elicited long-lasting neuronal alterations and anxiogenic responses as assessed by social interaction, which persisted for 5 weeks (Rainnie et al., 2004). This CRF receptor-mediated stress vulnerability required activation of an NMDA receptor-mediated, CaMKII-dependent second messenger cascade. This state of behavioral sensitization was accompanied by increases in BLA excitability, stemming from a loss of GABA-mediated inhibition.

Studies both in animal, and human, indicate populations of subjects that fail to exhibit adverse responses to similar acute and chronic stressors, or whose stress response does not become maladaptive: a state of **stress resilience** (Cooper et al., 2015). A recent surge in the number of studies has identified key aspects that make individuals less susceptible to stressful stimuli, and NPY has been implicated as one pathway involved (Sah and Geracioti, 2013). In soldiers, higher plasma NPY levels are associated with better performance following extreme interrogation stress, while lower NPY-expressing individuals show higher amygdala activity and increased emotional reactivity (Morgan et al., 2000, Zhou et al., 2008). Animal studies have also addressed the role of NPY in resilience to stress, using both genetic and pharmacological interventions. Transgenic rats that overexpress NPY do not demonstrate the normal anxiogenic-response to restraint stress, as assessed by the EPM (Thorsell et al., 2000). Furthermore, once-daily injection of NPY directly into the BLA for 5 consecutive days results in anxiolytic-like effects, as assessed by SI, that persisted for up to 8 weeks (Sajdyk et al., 2008). These NPY-mediated, stress-resilient rats were also resistant to restraint-induced changes in SI for the same time points that was not due to alterations in corticosterone or ACTH levels. This study also provided a potential mechanism mediating NPY-induced stress resilience, as inhibiting the synaptic plasticity-associated protein phosphatase, calcineurin (Lin et al., 2003a, Lin et al., 2003b) abolished NPY's long-term anxiolytic effects.

It is clear that NPY and CRF can elicit long-term, bi-directional plasticity in the BLA, such that neurons and animals can become less or more susceptible to a stressor. Moreover, stress can induce persistent hypertrophy of the dendritic architecture of BLA neurons. To date, the potential association between these neuropeptides and their ability to alter morphology of BLA neurons has not been explored. Therefore, we aimed to further understand the

mechanisms of long-term changes in BLA principal neurons underlying stress resilience and vulnerability caused by repeated treatment with NPY and CRF. We hypothesize that repeated application of NPY or CRF to OTCs will result in hypotrophy or hypertrophy of BLA principal neurons, respectively.

To address our hypothesis, we employed our novel BLA OTCs. To mimic the *in vivo* responses, we incubated age-equivalent OTC cultures for 5 consecutive days with NPY or CRF, applied over a range of concentrations. Following at least one week of washout with control media, we made electrophysiological recordings from OTC principal neurons, characterized thoroughly their properties, and later assessed changes to the dendritic arbors of the filled and stained neurons. Our results indicate that repeated application of NPY increases inhibitory, and decreases excitatory drive onto BLA principal neurons, while decreasing synchronous activity within the slice cultures. Examination of the dendritic architecture using Sholl analysis revealed hypotrophy of the dendritic arbor. Conversely, repeated activation of CRF receptors results in a modest decrease in inhibitory, and a robust increase in excitatory drive onto principal neurons, while enhancing synchronized activity within the BLA slice cultures. Structural plasticity also occurs with chronic CRF treatment, but in the opposite direction as NPY, with hypertrophy of the dendritic arbor and increases in branching. All effects were dose-dependent of the respective agonists applied.

We next determined if these two neuropeptides interact with each other as they do *in vivo*. We therefore incubated BLA OTCs with CRF for one week and NPY the following week; we also performed the converse experiment. We observed that BLA principal neurons do undergo bi-directional structural plasticity, as subsequent incubation with the opposing neuropeptide reversed the morphological changes to similar levels seen with control neurons.

Finally, we wanted to confirm our results obtained with OTCs by analyzing neurons from rats that were rendered stress resilient by repeated injection of NPY. Indeed, BLA principal neurons from NPY-induced stress resilient animals possessed smaller dendritic trees compared to PBS-injected controls, thus, confirming our findings with OTCs and further validating the OTC model.

Methods

Animals

Two different age groups of male Sprague-Dawley rats were used for all experiments. P14 pups were housed with the dam prior to preparation of OTCs. The second set of rats, aged five-weeks, were grouped housed (2-3 animals per cage) with 12:12 hours light : dark schedule and conventional rat chow and water were supplied *ad libitum*. All animal procedures were approved by the University of Alberta Animal Care and Use Committee: Health Sciences, in accordance with the guidelines of the Canadian Council on Animal Care.

Experimental setup

As described in the previous chapter, we have previously developed and optimized the OTC protocol, which will be used for experiments highlighted in this chapter. Brain slices from P14 animals were used and cultured for 4 weeks to bring them to EP 6-weeks. At this time, drug incubations, consisting of 5 consecutive daily changes of drug- or vehicle (saline) containing media were performed and cultures then returned to normal media for 1-2 weeks. Electrophysiological experiments were performed between EP 9-10 weeks.

Preparation of organotypic slice cultures

Organotypic cultures were prepared using the interface method described by Stoppini et al. (1991) with minor modifications, as explained in Chapter 2. In short, P14 rats were decapitated and their brains rapidly removed and submerged in ice-cold slice solution. The brain was cut into blocks, which were placed in melted agarose, just above the gel point (the temperature at which an aqueous agarose solution forms a gel as it cools), that was allowed to

harden. The trimmed, agarose-supported brain blocks were secured to a custom slicing chamber with cyanoacrylate adhesive and immersed in cold (<4ºC) slice solution. 350 μm thick slices were cut serially from rostral to caudal using a vibratome and trimmed to size (Chapter 2). Only slices containing the BLA were used for plating and were visualized using a dissecting light microscope. Typically, 4 slices were obtained from each hemisphere, for a total of 8 slices used per animal. Slices were allowed to rest in fresh slice solution for 30-45 minutes at 4°C, before being mounted on individual semiporous membrane inserts and placed in 24-well plates with 300 μL of culture media. After 48 hours in culture, an anti-mitotic solution of 1:1:1 cytosine-β-D-arabino-funanoside, uridine, and 5-Fluro-2'-deoxyuridine was added to the media (0.5 μM final concentration) for 24 hours to prevent glial proliferation. Slices were cultured in a sterile environment at 37°C in 5%/95% CO2/air. Media was changed three times per week for the duration of the experiment, except for drug incubations. All procedures were carried out in a laminar flow hood, using aseptic techniques and all solutions were sterile filtered before use.

OTC drug incubations

Drug incubations were performed during the fifth week of culture (EP 7 weeks). Fresh media containing either 0, 0.1, 1, 10 or 100 nM NPY (Polypeptide Group, San Diego, CA, USA) or 0, 0.3, 3 or 30 nM CRF (Phoenix Pharmaceuticals Inc, Burlingame, CA, USA) was changed daily for five consecutive days; the last change remained on the slice until the normal media change at day 7. In experiments where NPY and CRF were utilized, incubations were identical as stated above starting with one compound, and the other compound was applied in an identical manner at the beginning of week 6. In these experiments, maximal concentrations of both peptides were studied. To control for slight alterations in osmolarity and for

nonspecific peptide effects, we incubated a subset of cultures with NPY-free acid (100 nM), which has no affinity for any known receptor. After incubations, media changes were again performed three times per week.

Whole-cell patch clamp electrophysiology

For complete methodology of electrophysiological recordings, refer to Chapter 2. Briefly, OTC slices were transferred to a recording chamber and continually perfused at a flow rate of 2-3 mL/min with warmed (32-34°C), carbogenated ASCF. Patch pipettes were pulled from borosilicate glass and had a tip resistance of 4-6 MΩ when backfilled with a K-gluconate based internal solution containing 0.2% neurobiotin (pH 7.27, osmolarity 300 mOsm/L). Principal neurons within the BLA were identified under 60x magnification using infrared-differential interference contrast (DIC) optics and selected based upon previously described criteria. All recordings were made using a Multiclamp 700B amplifier in conjunction with pCLAMP 10.4 software and a DigiData 1322 or 1440 (Axon, Molecular Devices). Nominal membrane potential in voltage- and current-clamp recordings were compensated offline for the calculated 15mV liquid junction potential (Chee et al., 2010). All potential values reported reflect this correction.

Membrane properties and intrinsic currents

Similar electrophysiological characteristics were examined as detailed in Chapter 2. Passive membrane properties studied routinely included RMP, rheobase, capacitance and input resistance, as well as characteristics of I_h. Spontaneous inhibitory and excitatory postsynaptic currents were also studied, in addition to compound postsynaptic bursting activity.

Cell processing, labeling, imaging and neuronal reconstruction

Detailed descriptions for processing, immunohistochemistry, imaging and morphological analysis can be found in Chapter 2. Briefly, neurobiotin-filled neurons were fixed with 10% formalin for 24-72 h at 4°C, then stored at 4°C in PBS-azide and processed within four weeks. Free floating sections still attached to the membrane substrate were labeled with streptavidin pre-conjugated to Alexa Fluor 555 or 546, mounted on microscope slides and imaged using confocal microscopy. For morphological analysis of filled neurons, z-stack images were obtained at 20x magnification. Quantification of dendritic spine density was achieved by manually counting dendritic spines on z-stack images taken at 100x magnification, 1024 x 1024 resolution and 100 Hz for a series of 0.5 μm steps, using the cell counter function in FIJI. For each neuron, we counted spines on three separate, randomly selected dendrite segments (100 μm long) for neurons in each treatment group. Groups were formed to assess spine density in functional subdivisions based on distance from the soma and dendrite order. Groups were formed for dendrite segments consisting of 0-100, 100-200 and 200-300 μm from the soma, as well as for primary, secondary and tertiary dendrites. All protrusions that were connected to the dendrite segment were considered as spines and we made no attempt to differentiate between spine morphologies. Estimation of the total spine number was accomplished for each neuron by taking the product of the average spine density and total dendritic length for individual neurons.

Experimental setup for acute slices from 10-week old, BLA-cannulated rats.

To verify our morphological results with NPY, we utilized slices from *in vivo* stress resilient experiments, which were referred to in Chapter 2. Briefly, 6-week old male Sprague-

Dawely rats received injections of either PBS or NPY (10 pmoles) in PBS via syringe pump and cannula, directly into the BLA once daily, for five consecutive days. Animals were individually assessed in SI tests as described in Chapter 2. Four weeks following the first injection, animals were sacrificed, brain slices were obtained and electrophysiological recordings were obtained (Giesbrecht et al. (2010). The neurobiotin-filled neurons were processed, stained, imaged, reconstructed and subjected to the same morphological analysis as OTC slices.

Data analysis and statistics

Recordings were analyzed offline using pCLAMP 10.4 software. Raw traces of electrophysiological recordings, statistical analysis and graphs were completed using GraphPad Prism 5 or 6 software. Neuronal reconstruction, Sholl analysis and dendritic spine analysis was performed using FIJI. Unless otherwise stated, all data are represented as mean ± SEM. One- and two-way analysis of variance (ANOVA) with Tukey's post-hoc test was used for multiple comparisons to determine dose-dependent effects and Student's t-test used to determine the effect of sequential incubations versus controls (*P <0.05, ** P <0.01, ***P <0.001, **** P<0.0001). Data sets for cumulative probability plots of amplitude and inter-event intervals of sIPSCs and sEPSCs were created by pooling all events and analyzed using the Kolmogorov-Smirnov (*K-S*) test for overall effect. All groups of OTCs contained cells from 4-10 animals, unless otherwise stated, *n* represents the number of independent cells analyzed.

Results

Postsynaptic effects of repeated NPY treatment of BLA OTCs

A number of mechanisms have been postulated for the acute anxiolytic effect of NPY in the BLA (Chapter 1), however, the manner in which NPY-mediates behavioral stress resilience remains poorly understood. Our novel BLA OTCs were developed expressly to investigate the mechanisms underlying long-term effects of repeated NPY application. Repeated incubation with NPY produced a dose-dependent reduction in RMP producing neurons that were hyperpolarized compared to controls (Ctrl: -79.05 ± 1.00 mV, 1 nM NPY: -84.40 ± 1.34 mV (P<0.01), 10 nM NPY: -83.89 ± 1.10 mV (P<0.05); Fig.3.1A), although we observed no change in the rheobase of these cells (Fig.3.1B, P>0.05). While we did not study the input resistance in all cell populations, at least we observed no significant difference in this value between controls and cells receiving 100 nM NPY incubations (Fig.3.1C, P >0.05). There was no significant difference between controls and 0.1 nM NPY or NPY-free acid (P>0.05) for any passive membrane properties studied in all groups.

Because the acute anxiolytic effect of NPY is mediated in part via a reduction in I_h (Giesbrecht et al., 2010), we next examined this current in NPY-treated BLA cells in OTCs. OTC BLA cells treated with any concentration of NPY or the free acid showed no significant change in I_h amplitude, I_h density or half-maximal voltage activation of I_h compared to controls (Data not shown, P>0.05). Interestingly, however, we observed that increasing doses of NPY resulted in faster activation rates of I_h. Kinetic analysis resolved to rate constants in the activation curve of I_h, a fast component (τ_{fast}) and a slower one (τ_{slow}) (Fig. 3.2A inset). Specifically, incubation with 10 nM and 100 nM NPY resulted in significantly faster

activation rates of the fast component compared to controls and to cells treated with 0.1 nM NPY (Ctrl: 12.50 ± 0.60 ms, 0.1 nM NPY: 12.69 ± 0.85 ms, 10 nM NPY: 8.47 ± 0.59 ms (P<0.001), 100 nM NPY: 9.071 ± 0.71 ms (P<0.01); Fig.3.2A), while for tau slow, the 10 nM and 100 nM NPY groups displayed more rapid kinetics compared to controls (Ctrl: 100.1 ± 5.9 ms, 10 nM NPY: 62.21 ± 5.93 ms (P<0.001), 100 nM NPY: 60.88 ± 5.04 ms (P<0.001); Fig.3.2B). NPY at concentration of 10 nM or greater therefore altered the activation kinetics, but not the magnitude or voltage dependence of I_h, an unexpected finding (Data not shown).

In examining the data from the I_h voltage step protocol, it became evident that an instantaneous, current preceded the activation of I_h (Fig3.3A). The voltage steps also allowed a clear separation between the two currents, in addition to helping isolate both currents from the effects of the spontaneous, synaptically-driven bursts observed in the cultures, unlike the slow voltage ramp protocol we also employed. This inwardly-rectifying (IIR) current was not significantly different in BLA neurons from control or NPY (100 nM)- treated OTCs (P>0.05; Fig. 3.3B). Finally, we observed a prominent reduction in cell capacitance that increased with increasing concentrations of NPY (Fig. 3.3C). Notably, repeated application of 1 nM, 10 nM and 100 nM NPY reduced cell capacitance compared to controls (Ctrl: 153.5 ± 7.1 pF, 1 nM NPY: 115.0 ± 3.9 pF, (P<0.001), 10 nM NPY: 111.9 ± 4.3 pF, (P<0.001), 100 nM NPY: 105.1± 4.7 pF, (P<0.0001)). There was no significant difference in treatment with 0.1 nM NPY or NPY-free acid, compared to controls for any of the electrophysiological characteristics mentioned above (P>0.05).

NPY reduces excitatory, and increases inhibitory, synaptic input onto BLA OTC principal cells

Acute activation of NPY Y1-receptors alters synaptic transmission within the BLA, with increases and decreases in evoked IPSC and EPSC amplitudes, respectively (Molosh et al., 2013). We next characterized the effects of repeated NPY application on synaptic transmission in neurons of OTCs. Voltage clamp recordings of spontaneous synaptic currents were made at a holding potential of -55 mV, to permit simultaneous visualization of GABAergic sIPSCs (upward deflections) and glutamatergic sEPSCs (downward deflections). We analyzed events from 25 principal neurons from OTCs prepared from at least 3 animals each from control and 100 nM NPY-treated groups, (Fig 3.4A-B). The mean sIPSC amplitude increased following 100 nM NPY treatment, compared to controls (Ctrl: 49.83 ± 4.95 pA, 100 nM NPY: 66.68 ± 5.87 pA, ($P< 0.05$); Fig.3.4C). The cumulative probability distributions and amplitude-frequency histograms illustrate that NPY treatment resulted in a loss of smaller, and an increase in larger amplitude sIPSCs (Fig.3.4D-E). Mean sIPSC inter-event interval was unaffected following repeated treatment with NPY relative to controls (Data not shown, $P>0.05$). We observed no significant effect following NPY treatment compared to controls for sEPSC amplitude (Data not shown, $P>0.05$). However, the mean sEPSC frequency was significantly decreased by the NPY treatment, as inter-event interval increased in in 100 nM NPY-treated neurons compared to controls (Ctrl: 139.0 ± 16.21 ms, 100 nM NPY: 218 ± 23.40 ms ($P<0.01$); Fig.3.4F). The cumulative probability histogram confirmed these findings (Fig.3.4G, $P<0.0001$). Finally, assessment of compound postsynaptic bursting activity revealed that spontaneous bursts were reduced in NPY-treated neurons compared to controls (Ctrl: 0.23 ± 0.022 Hz, 100 nM NPY: 0.15 ± 0.018 Hz ($P<0.05$); Fig.3.5H-J). Overall, the data

suggests treatment of BLA OTCs with NPY results in increased inhibitory drive and decreased excitatory drive onto principal neurons, resulting at least in part in a reduction in synchronous activity within the BLA, ultimately suppressing excitatory output from the BLA.

Dendritic pruning of BLA OTC principal neurons following NPY treatment

Principal neurons undergo structural as well as synaptic plasticity in response to various forms of acute and persistent stress paradigms (Vouimba et al., 2004, Vouimba et al., 2006, Padival et al., 2013a, Padival et al., 2013b, Cohen et al., 2014). Stress induces BLA principal neuron dendritic hypertrophy and proliferation of spine density that is persistent (Leuner and Shors, 2013, Farrell et al., 2015). Furthermore, genetic modifications that reduce BLA principal neuronal dendritic length result in attenuation of anxiety-related behavior (Mitra et al., 2009). Therefore, we sought to determine if long-term treatment of BLA OTCs with NPY results in persistent hypotrophy of the dendritic arbor.

Tracing, reconstruction and Sholl analysis revealed extensive remodeling with NPY treatment of the dendritic architecture of BLA OTC principal neurons, (Fig.3.5). The total dendritic length was reduced by nearly 25% compared to controls following incubations with NPY at 1 nM, 10 nM, and 100 nM NPY (Ctrl: 3911 ± 240 μm, 1 nM NPY: 2800 ± 177 μm (P<0.05), 10 nM NPY: 2811 ± 284 μm (P<0.05), 100 nM NPY: 2875 ± 283 μm, (P<0.05); Fig.3.6A), while NPY-free acid was, as expected, without effect. Sholl analysis using concentric circles with 10 μm radii revealed (Fig.3.6B) that reductions occurred at intermediate dendritic locations of the neuronal structure following NPY treatment at 1 nM, 10 nM and 100 nM compared to controls (NOTE; only data is shown for controls, 100 nM NPY and NPY-FA; 1nM NPY: 70-140 μm from soma (P<0.01), 10 nM NPY: 80-160 μm

from soma (P<0.01), 100 nM NPY: 80-190 μm from soma (P<0.01). The number of branch points declined nearly 30% following incubation with 1 nM, 10 nM, and 100 nM NPY compared to controls (Ctrl: 23.77 ± 1.88 branches, 1 nM NPY: 15.36 ± 0.97 branches, 10 nM NPY: 16.52 ± 1.78 branches, 100 nM NPY: 16.42 ± 1.33 branches (P>0.05); Fig.3.6C). To determine the location along the dendritic arbor of NPY's effect on branch points, we performed Sholl analysis with concentric rings of 40 μm in radius, and grouped all dendrites whose branching initiated within each ring. Figure 3.6D demonstrates there was a significant reduction in the number of dendrites at proximal and intermediate branches along the dendritic arbor for 1 nM, 10 nM and 100 nM NPY treated BLA OTC neurons compared to controls (1 nM NPY: 60 μm (P<0.0001) and 100 μm (P<0.01) from the soma, 10 nM NPY: 60 μm from the soma (P<0.01), 100 nM NPY: 60 μm (P<0.05) and 100 μm (P<0.01) from the soma; Note only data for control, 100 nM NPY and NPY-FA is illustrated). We also quantified the number of dendrites as a function of branch order (Fig.3.6E). While primary dendrites were unaffected, the greatest reductions were observed in secondary and tertiary dendrites following incubation with NPY compared to controls (1 nM NPY: 2º (P<0.0001), 3º (P<0.05), 10 nM NPY: 2º (P<0.001), 100 nM NPY 2º (P<0.001), 3º (P<0.001)). There was no significant effect for incubations with 0.1 nM NPY or NPY-free acid (Fig.3.7B,D,F,H,J) compared to controls.

Repeated NPY treatment does not affect spine density or total spines in BLA OTCs

Dendritic spines, important sites of excitatory synaptic input to many central neurons, are highly dynamic structures located along the length of the dendritic arbor. Both acute and chronic stress leads to increases in dendritic spine density in BLA principal neurons (Mitra et al., 2005, Vyas et al., 2006), but the effects of long-term treatment of BLA with NPY on

dendritic spines is unknown. We thus assessed dendritic spine density of control and NPY-treated BLA neurons in OTCs, expressed as a function of distance from the soma and dendrite order, as well as estimated total number of spines following incubation with 100 nM NPY in BLA OTCs. Dendritic segments were chosen for analysis as described in the methods section of this chapter. Images of representative dendrite segments from control and NPY-treated BLA OTCs are shown in Figure 3.7A-B. Repeated incubation with NPY had no effect on dendritic spine density, or total number of spines compared to control principal neurons, although there was a trend of decreased total spines (Fig.3.7C-F, $P>0.05$).

Postsynaptic effects of repeated treatment of BLA OTCs with CRF

Because NPY and CRF have opposing long-term effects on stress-related behavior *in vivo*, we next studied, in identical experiments if long-term treatment with CRF of BLA OTCs also has opposing actions on principal neurons to those of NPY.

Unlike NPY, repeated application of CRF did not affect RMP of BLA OTC principal neurons (Fig.3.8A, $P>0.05$), but did alter their excitability. Rheobase was significantly increased following treatment with 30 nM CRF compared to controls (Ctrl: 166.5 ± 22.5 pA, 30 nM CRF: 308.1 ± 43.1 pA ($P<0.05$); Fig.3.8B). This treatment also resulted in a reduction in input resistance compared to controls (Ctrl: 109.7 ± 7.85 MΩ, 30 nM CRF: 76.82 ± 7.27 MΩ ($P<0.01$); Fig.3.8C). Incubation with 30 nM CRF also resulted in an increase in an IIR current compared to controls (-145 mV ($P<0.0001$), -135 mV ($P<0.0001$), -125 mV ($P<0.001$) and -115 mV ($P<0.05$); Fig.3.9A-B). The net current elicited is represented in Figure.3.9C; This current had an apparent reversal potential of around -70 mV. Finally, analysis of cell capacitance revealed significant increases following incubation with CRF at 30 nM compared

not only to controls but also to CRF at 0.3nM and 3 nM nM (Ctrl: 138.6 ± 5.6 pF, 0.3 nM CRF: 164.8 ± 8.0 pF, 3 nM CRF: 162.0 ± 6.3 pF, 30 nM CRF: 198.7 ± 11.4 pF vs Ctrl (P<0.001), vs 0.3 nM CRF (P<0.05), vs 3 nM CRF (P<0.05); Fig.3.9D).

Next, we analyzed the effect of repeated CRF treatment on I_h properties. There was a small but significant increase in mean I_h amplitude in response to the -145 mV voltage step in cells treated with 30 nM CRF compared to cells in control slices (Ctrl: -260.20 ± 30.02 pA, 30 nM CRF: -361.36 ± 42.79 pA, (P<0.05); Fig.3.10A). However, when we calculated I_h density, there was no significant difference between CRF-treated and control cells (Data not shown, P>0.05). Although there appeared to be a trend toward a hyperpolarizing shift in the voltage dependence of I_h activation, it was not significant (Data not shown, P>0.05). Figure 3.10B illustrates the activation kinetics of I_h, and estimates revealed that both tau fast and tau slow are increased in neurons receiving CRF treatment (Fig.3.10C-D). Specifically, there was an increase in tau fast following incubation with 3 nM and with 30 nM CRF compared to control principal neurons (Ctrl: 14.20 ± 1.38 ms, 3 nM CRF: 22.58 ± 2.76 ms (P<0.05), 30 nM CRF: 23.14 ± 2.14 (P<0.05). Additionally, tau slow values increased following incubation with 3 nM and 30 nM CRF compared to controls (Ctrl: 86.77 ± 6.25 ms, 3 nM CRF: 145.0 ± 12.2 ms (P<0.01), 30 nM CRF: 181.6 ± 14.3 ms (P<0.0001)).

30 nM CRF increases excitatory drive onto BLA OTC principal neurons

Repeated injection of CRF directly into the *in vivo* BLA results in a concurrent reduction of $GABA_A$ receptor-mediated inhibition and increase of glutamatergic excitation onto BLA principal neurons (Rainnie et al., 2004). Thus, we investigated the long-term effects of chronic application of CRF in BLA OTCs on spontaneous postsynaptic activity of principal

cells. A total of 25 individual neurons were analyzed from OTCs derived from at least three different animals. Incubation with 30 nM CRF had no effect on either mean sIPSC amplitude or frequency or sEPSC amplitude compared to controls (Data not shown, $P>0.05$). However, the most prominent action of CRF on spontaneous postsynaptic transmission was a robust increase in mean sEPSC frequency, illustrated as a significant reduction in sEPSC inter-event interval following 30 nM CRF incubations compared to controls [Ctrl: 221.15 ± 32.2 ms, 30 nM CRF: 121.8 ± 13.8 ms ($P<0.01$)], which was credibly confirmed by the K-S test (Fig.3.11C-D). Finally, the effect on bursting activity within BLA OTCs of 30 nM CRF was opposite to that of NPY, with increases in 30 nM CRF treated cultures compared to controls (Ctrl: 0.19 ± 0.0057 Hz, 30 nM CRF: 0.24 ± 0.0022 Hz ($P<0.01$); Fig.3.11E-G). Overall, the data suggests chronic incubation of BLA OTCs with 30 nM CRF has limited effects on GABAergic inhibition, while robustly augmenting excitatory drive onto BLA principal neurons.

Chronic treatment with CRF results in hypertrophy of principal neurons in BLA OTCs

Tracing, reconstruction and Sholl analysis revealed extensive hypertrophy of the dendritic architecture in BLA OTC principal neurons following CRF treatment, as exemplified by the representative reconstructions in Figure 3.12. There was a dose-dependent effect on aggregate dendritic length following incubation with CRF. Specifically, the total dendritic length increased in 3 nM and 30 nM treated cultures compared to controls (Ctrl: 3539 ± 198 μm, 3 nM CRF: 4889 ± 368 μm ($P<0.05$), 30 nM CRF: 5779 ± 406 μm ($P<0.0001$); Fig.3.13A). Cells treated with 30 nM CRF also were significantly larger than those treated with 0.3 nM CRF (4141 ± 274 μm, ($P<0.01$). Compared to controls, there were significant increases in the number of intersections at intermediate regions of the dendritic

arbor following 3 nM and 30 nM CRF treatment (3 nM CRF: 100-190 μm from the soma (P<0.01), 30 nM CRF: 60-250 μm from the soma (P<0.001); Fig.3.13B). Branching was also significantly increased both with 3 nM and 30 nM CRF incubations, compared to controls (Ctrl: 18.88 ± 1.43 branches, 3 nM CRF: 23.35 ± 2.82 branches (P<0.05), 30 nM CRF: 34.11 ± 2.78 branches (P<0.0001); Fig.3.13C). The positions along the dendritic tree where increases in branching arose are illustrated in Figure 3.13D. Treatment with 30 nM CRF resulted in significant increases in numbers of branch points at 60 μm (P<0.01) and 100 μm (P<0.01), and 140 μm (P<0.05) from the soma, compared to controls. Additionally, branch order analysis (Fig.3.13E) revealed that mean numbers of branch points increased in secondary and tertiary branches for 3 nM and 30 nM CRF concentrations tested, at quaternary branches for 30 nM and only secondary for 0.3 nM CRF compared to controls (0.3 nM CRF: 2º (P<0.05), 3 nM CRF: 2º (P<0.05), 3º (P<0.05), 30 nM CRF: 2º (P<0.0001), 3º (P<0.0001), 4º (P<0.01)).

Analysis of dendritic spines from CRF-treated BLA OTCs

Representative segments of dendrites from control and 30 nM CRF-treated BLA OTCs are shown in Figure 3.14A-B. Incubation with CRF had no significant effect on spine density for any of the dendritic groups examined compared to control OTCs (Fig3.14C-E, P>0.05). However, analysis reveals that repeated incubation with 30 nM CRF caused an increase in the total number of spines per neuron compared to controls (Ctrl: 2661 ± 385 spines, 30 nM CRF: 5158 ± 597.8 spines (P<0.01); Fig.3.14F). The cause of the increase in total spine number is likely due to an increase in the number and length of dendrites with CRF treatment while the spine density per segment remained the same.

Interaction of CRF and NPY: counter-regulatory signals to regulate emotionality

In the amygdala, the stress response is initiated by the release and activity of CRF, to activate endocrine and autonomic stress responses, however, NPY's actions during the late phase acts to terminate the physiological consequences of CRF release (Heilig et al., 1994). The opposing actions of NPY and CRF thus may act as a buffer to prevent exaggerated reactions to threatening stimuli and allow a highly dynamic stress response. It has been postulated that disruption of this homeostatic mechanism may in part underlie some anxiety-related disorders (Heilig et al., 1994, Sajdyk et al., 2004, Sajdyk et al., 2006).

Postsynaptic effects of opposing neuropeptide activation

For visual comparison, mean values of the actions of monophasic incubations with either 100 nM NPY or 30 nM CRF are represented as dashed lines. Following incubation as described above, the RMP of the CRF , NPY group was hyperpolarized compared both to controls and the NPY , CRF group (Ctrl: -75.89 ± 1.17 mV , CRF , NPY: -81.54 ± 1.24 mV (P<0.01), NPY , CRF: -77.42 ± 1.9 mV (P<0.05); Fig.3.15A). Furthermore, rheobase was increased in the CRF , NPY group compared both to controls and the NPY , CRF group (Ctrl: 241.2 ± 28.9 pA (P<0.01), CRF , NPY: 409.3 ± 43.7 pA (P<0.01), NPY , CRF: 273.9 ± 30.7 pA (P<0.05); Fig.3.15B). Input resistance was measured to be decreased in the CRF , NPY group compared to controls (Ctrl: 109.7 ± 7.9 MΩ, CRF, NPY: 74.26 ± 7.17 MΩ (P<0.01); Fig.3.15C). The I_h protocol (Fig.3.16A) was used to extract values for the I/V plot in Figure 3.16B, which demonstrates the CRF , NPY incubations resulted in the increase of an IIR (3.16A insert) that was significantly greater with this treatment than either controls or the NPY , CRF group at the two most negative potentials studied here (-145 mV (P<0.001

compared to both), -135 (P<0.01 compared to NPY , CRF) (P<0.05 compared to controls). The net IIR current increase relative to controls is represented in Figure 3.16C, which reversed around -105 mV. There was no difference in measured cell capacitance from control OTCs and the CRF , NPY or NPY , CRF treated groups (Fig.3.16D, P>0.05). Overall, the passive electrophysiological properties of both the CRF , NPY and NPY , CRF treated groups suggest BLA OTCs can experience bi-directional plasticity in response to CRF and NPY, to limit the effects of each other.

The I_h responses to hyperpolarizing voltage steps revealed no significant change in mean I_h amplitude or density for either the CRF , NPY or NPY , CRF treated groups compared to each other or controls (Fig.3.17A,, P>0.05). Analysis of the activation kinetics revealed a small but significant decrease in tau fast values in CRF , NPY groups compared to controls (Ctrl: 14.20 ± 1.38 ms, CRF , NPY: 9.98 ± 0.80 ms (P<0.05); Fig.3.17C), but no difference was observed in tau slow values for either the CRF , NPY or NPY , CRF treated groups compared to each other or controls (Fig.3.17D, P>0.05). Consistent with the passive membrane properties, results of I_h and its intrinsic properties suggest NPY and CRF can restrict the effects of each other following prolonged application.

Counter-regulation of synaptic events

A total of 25 separate neurons under each treatment were analyzed in OTCs prepared from at least 3 different animals and statistical analysis was performed between CRF , NPY and NPY , CRF groups versus controls on raw mean values (Fig.3.18A). The results indicate that there were no observable effects on sIPSC frequency and amplitude or on sEPSC frequency and amplitude following treatment with groups of peptides (Data not shown).

Due to variability in some of the mean values of control groups for the NPY and CRF alone experiments, we normalized these data to their respective controls, and compared NPY-treated, CRF-treated and NPY, CRF- and CRF, NPY-treated OTCs. Normalized sIPSC amplitude was significantly different between 100 nM NPY and 30 nM CRF (100 nM NPY: 133.8 ± 11.8 % of control, 30 nM CRF: 93.04 ± 9.0 % of control (P<0.05)), but the CRF, NPY- or NPY, CRF- treated groups did not differ from each other or from either CRF or NPY alone (P<0.05; Fig.3.18B). The normalized sEPSC frequency was reduced in 100 nM NPY neurons compared to 30 nM CRF alone and the CRF, NPY- and NPY-CRF-treated groups (100 nM NPY: 156.9 ± 16.8 % of controls (P<0.001 vs CRF), (P<0.001 vs CRF, NPY), (P<0.01 vs NPY, CRF), 30 nM CRF: 55.0 ± 6.2 % of controls, CRF, NPY; 78.4 ± 10.2 % of controls, NPY, CRF; 97.0 ± 13.11 % of controls; Fig.3.18E). There was no difference in the normalized mean sIPSC IEI or mean sEPSC amplitude between the four groups (Fig.3.18C-D, P>0.05). Finally, there was no observable change in the incidence of compound bursts between the CRF , NPY group, NPY, CRF group and controls (Fig.3.19A-B, P>0.05), however, the mean burst incidence as a percent of control was significantly smaller for the 100 nM NPY group compared to the CRF, NPY group, the NPY, CRF group and the 30 nM CRF group (100 nM NPY: 54.7 ± 7.0 % of control, CRF, NPY: 112.8 ± 6.2 % of control, NPY, CRF: 103.0 ± 6.4 % of control, 30 nM CRF: 124.7 ± 12.4 % of control, (P<0.001); Fig.3.19C). Collectively, it appears that opposing neuropeptide treatment, limits the effects on synaptic transmission of the rival peptide treatment alone.

CRF and NPY offset each others' effects on dendritic morphology

Representative reconstructions of BLA principal neurons are shown in Figure 3.20. There were no significant differences in any of the measured morphological properties of

CRF, NPY or NPY, CRF-treated principal neurons compared to controls (Fig.3.21A-E, $P>0.05$). Results indicate that BLA OTC principal neurons have the capacity to undergo bi-directional structural plasticity in response to counter-regulatory neuropeptides. For reasons already stated, mean ± SEM values are included for 100 nM NPY and 30 nM CRF incubations, however, they were not included for statistical analysis.

Repeated injection of NPY in vivo yields comparable morphological effects to BLA OTCs

Treatment of BLA OTCs with CRF or NPY results in profound effects on principal cell dendritic architecture. These results and the BLA OTC model itself are of academic interest only if the *in vitro* effects cannot be reproduced *in vivo*. Thus, we sought to confirm our findings of NPY-mediated dendritic hypotrophy of BLA OTC principal neurons *in vivo*. We examined filled neurons from acutely prepared BLA slices of previous NPY-mediated stress resilience studies performed by other members of the Colmers laboratory, as well as freshly prepared animal subjects (see methods and Figure.3.1 for experimental setup). In total, 8 control (PBS) and 9 NPY-treated animals were used for morphological analysis and representative reconstructions are depicted in Figure 3.22.

Consistent with findings from OTCs, repeated injections of NPY directly into the BLA resulted in a decrease of cell capacitance, and concurrent reduction in extent and branching of principal neuron dendrites. Specifically, cell capacitance was reduced in NPY-treated compared to vehicle-treated animals (Vehicle: 226.1 ± 7.6 pF, NPY: 179.6 ± 8.9 pF ($P<0.001$); Fig3.23A). There was a 21% reduction in total dendritic length in neurons from NPY-treated rats compared to controls (Vehicle: 8644 ± 284 µm, NPY: 6802 ± 329 µm

(P<0.0001); Fig.3.23B). Similar to the OTC experiments, Sholl analysis revealed that differences in *in vivo*-treated neurons were due to reductions at proximal to intermediate locations (40-160 μm from the soma, (P<0.001); Fig.3.23C). Repeated NPY injections prompted a 32 % reduction in branch points compared to vehicle-injected animals (Vehicle: 46.28 ± 1.87 branch points, NPY: 31.50 ± 1.37 branch points (P<0.0001); Fig3.23D). Again, fewer branches were observed at proximal regions of the dendritic arbor, with significant reductions at 20 μm, 60 μm, and 100 μm from the soma (20 μm (P<0.0001), 60 μm (P<0.0001), 100 μm (P<0.0001); Fig.3.23E). Furthermore, NPY-mediated loss of branch points was limited to tertiary (P<0.0001) and quaternary (P<0.0001) branches (Fig.3.23F).

Discussion

Although it is well established that NPY and CRF provide counter-regulatory modulation of the stress response, this study presents a structural correlate of stress resilience and susceptibility. When incubated with either NPY or CRF alone, BLA OTC principal neurons respond with reduced and increased excitatory synaptic drive and dendritic hypo- and hyper-trophy, respectively, that is consistent with the corresponding changes in levels of anxiety normally mediated by these neuropeptides. Subsequent incubation of the opposing neuropeptide appears to reverse the response to the competing peptide, which is a crucial physiological response for organisms to respond to stress, despite being stress resilient and conversely, to constrain the stress response, even in the face of chronic bouts of stress. Confirmation of our results in BLA OTCs by repeated NPY injections *in vivo,* further validates our OTC model and suggests the results reflect a true biological significance.

Surprisingly, NPY and CRF produced few postsynaptic effects on BLA OTC principal neurons. There was a small hyperpolarization of the RMP following NPY-treatment, which is consistent with the notion that reducing excitatory output from the BLA is anxiolytic and complements findings that acute activation of NPY Y1-receptors in *ex vivo* slices causes hyperpolarization of the RMP (Giesbrecht et al., 2010). The Giesbrecht et al. study also revealed that acute application of NPY and CRF to acutely prepared adult BLA slices results in a reduction and augmentation, respectively, of I_h in principal neurons. Furthermore, unpublished work from the Colmers and Urban labs suggests I_h to play a role in NPY-mediated stress resilience, as there was a lasting decline in I_h following repeated injections of NPY directly into the BLA and lentiviral-induced shRNA knockdown of HCN1 (major subunit contributing to HCN channels in the BLA), results in increases in social interaction

(Silveira et al., Unpublished). However, we found no significant changes in the amplitude or density of I_h following repeated NPY treatment and only a minor increase in amplitude for the largest hyperpolarizing step following the highest dose of CRF-treatment in BLA OTCs. This minor affect disappeared when we controlled for cell size and examined I_h density. This is likely a result of uncoupling of the intracellular signal transduction mechanism in BLA OTCs compared to the *in vivo* situation, or perhaps internalization of HCN channels. Previous reports from members of the Colmers lab indicates fewer acute responses to NPY in acutely prepared brain slices from younger (P21-P28) compared to older (6 week) animals. This suggests the signal transduction mechanism linking NPY-receptor activation to reductions in I_h may not develop until maturity is reached, and may be uncoupled in our OTCs. Regardless, NPY and CRF incubations resulted in faster and slower activation kinetics of I_h (changes in space clamp, as discussed in Chapter 2 would predict this) and reductions and increases in cell capacitance, respectively, which gave us the first clue for remodeling of the dendritic structure of principal neurons.

Analysis of the IIR current following hyperpolarizing voltage steps indicates that prolonged CRF treatment increases an inwardly rectifying conductance that reverses around -70 mV, while subsequent prolonged application of NPY failed to limit the effect of CRF on this conductance (reversed around -100 mV) in the CRF, NPY treated group (Fig.3.9B-C and Fig.3.16B-C). The observation of a reduction in input resistance following CRF treatment further supports the notion of an increased conductance. NPY and NPY, CRF treatment appeared to have no effect on this conductance. Although we did not investigate this finding any further, we suspect this to be a result of activation of a GIRK-current, as the reversal potential of the conductance was close to the K^+ equilibrium potential. GIRK-mediated

currents are known to be present at least the LA and acute application of NPY has been shown to activate them (Sosulina et al., 2008). This result is counterintuitive as activation of a GIRK would likely cause hyperpolarization of the membrane potential and make these neurons less excitable. However, this could be a compensatory consequence of the networks overall heightened excitability, in an attempt to return the system to a less active state. Regardless, future studies would be needed to identify the exact ion channels involved, which could among other experiments would involve bath application of Ba^{2+} or the compound SCH23390, both of which potently block GIRK channels (Sodickson and Bean, 1996, Chee et al., 2010).

The effects of NPY and CRF on synaptic activity in the BLA OTCs are consistent with their known anxiolytic and anxiogenic tendencies, respectively. The observation of NPY increasing sIPSC amplitude and decreasing sEPSC frequency would result in a net reduction of excitatory output from BLA principal neurons, which has been shown to decrease anxiety-like behavior and increase social interaction (Felix-Ortiz and Tye, 2014, Felix-Ortiz et al., 2015). Conversely, chronic CRF incubation of BLA OTCs increased excitatory drive onto principal neurons as assessed by increases in the frequency of sEPSCs. This would predict an increase in excitatory output, and correlate with increased stress-related behavior (Padival et al., 2013a, Felix-Ortiz and Tye, 2014, Felix-Ortiz et al., 2015). Changes in the frequency of spontaneous postsynaptic events are consistent with a presynaptic site of action that directly alters release of neurotransmitter from the presynaptic terminal, while altered amplitude suggests a direct postsynaptic mechanism. However, alterations in synapse density could modulate event frequency, thus the effects in BLA OTCs with chronic neuropeptide treatment could be a result of changes in the number of synapses. Indeed following CRF treatment we

found an increase in the estimated total number of spines, the sites of most excitatory synapses, while there was a (non-significant) trend toward decreased total spines with NPY treatment.

The existence of compound postsynaptic bursts in OTCs indicates the presence of synchronous neuronal activity, and is typically not observed under baseline conditions in acutely prepared BLA slices. However, this effect can be generated via excitation of the slice through electrical or pharmacological means and require both glutamate- and $GABA_A$-receptor activation (Rainnie, 1999, Chung and Moore, 2009, Ryan et al., 2012). Acutely, neuropeptides have been shown to modulate compound postsynaptic bursting activity in acute BLA slices, with NPY decreasing, and CRF increasing compound bursts (Chung and Moore, 2009). We observe regular compound bursts at rest in our OTCs and results with chronic NPY and CRF treatment reveal a similar anti- and pro-excitatory modulation of network activity, as noted above. As mentioned in Chapter 2, it is important to consider the discrepancies observed with the different statistical analyses performed on sIPSC and sEPSC amplitudes and IEIs, with mean values combined with t-tests producing different degrees of significance versus plotting cumulative probability plots and using the K-S test. Also, considering the axotomized nature of the OTC preparation, the observed changes in synaptic activity likely represent changes to newly developed local circuits that may not fully represent how NPY and CRF exert their effects *in vivo*. Nevertheless, the direction of sEPSC frequency alterations seen with NPY and CRF fit the hypothesis that these neuropeptides can decrease, and increase, excitatory output from the BLA, respectively.

Both the developing and adult mammalian brain have a remarkable ability to adapt to environmental stimuli and show reversible structural and functional plasticity in the form of

neurogenesis, dendritic remodeling and synapse regulation (McEwen et al., 2015a). In BLA principal neurons, the association between stress and hypertrophy of the dendritic architecture and increase in spine density is well established; but unlike the hypotrophic, stress-related changes seen in the hippocampus and prefrontal cortex, hypertrophy in the BLA appears to be persistent in nature. Therefore, recovery from stress, or in our BLA OTCs, chronic CRF-induced changes to the dendritic architecture appears to require active neuroplastic mechanisms, rather than an autonomous reversal of these neuroadaptations as CRF-meditated effects were persistent and NPY was required to reverse the effects. Furthermore, a state of resilience to stress can be thought of in a similar manner, being mediated not only by a lack of pathological irregularities which occur in susceptible individuals, but also by novel, restorative neural mechanisms, such as seen with repeated NPY treatment in our BLA OTCs (Russo et al., 2012). The persistent nature of the hypertrophic effects in the BLA following stress or CRF incubations suggest that the hypertrophic effects and increases in spine numbers prepare the BLA for an elevated response to stressors, and is adaptive in the context of a prolonged exposure to a risky environment. Thus, our results support the hypothesis that the NPY-mediated hypotrophic effects represent a safeguard towards increased excitatory input resulting from stressful stimuli.

One inconsistency we found in our morphological analysis was that incubation with CRF did not induce an increase in spine density, as occurs in acute and chronic stress paradigms. However, when we calculated the total spine average for each of our treatments, there was a significant increase and a non-significant trend of decreased spines following CRF and NPY incubations, respectively. This demonstrates CRF and NPY treatment likely results in more, and less glutamatergic synapses, respectively, which corroborates our findings with

altered excitatory neurotransmission in BLA OTCs. A possible explanation for the lack of effect on spine density could be the time course of our experiments, as there may be a transient shift in spine density that occurs, thus altering excitatory drive on principal neurons, which could play a role in the initiation of dendritic remodeling. Following the expansion or contraction of the dendritic arbor, spine density may return to a pre-incubation level, providing a new set-point optimized for the state of resilience or vulnerability. Although, it could be that these neuropeptides simply do not affect dendritic spine density at all.

The association between NPY and CRF represents a critical homeostatic mechanism that promotes maintenance of a balanced emotional state. Deviations in the equilibrium of theses neuropeptides can therefore result in resilience or vulnerability. Interestingly, in the experiments with subsequent incubation with the opposing neuropeptide, most electrophysiological and all morphological results suggest that in BLA OTCs this homeostatic mechanism is preserved and individual principal neurons can undergo bi-directional structural and synaptic plasticity. This occurrence would predict animals made stress resilient with NPY to possess the ability to respond to stress in a physiologically-relevant manner (NPY , CRF studies). By the same logic, chronically stressed animals should be able to limit the maladaptive effects through enhanced NPY signaling (CRF , NPY experiments).

To our surprise, the NPY-mediated morphological effects did not follow a typical dose-dependent shift. Incubation with 0.1 nM NPY did not produce alterations to the morphology of BLA OTC principal neurons, however, capacitance and morphology measurements of all higher doses (1, 10 and 100 nM NPY) resulted in similar changes. An unlikely explanation could be that the Hill slope of the concentration effect curve is extremely steep, suggesting a small increase in NPY concentration could dramatically affect the response

and the maximal effect is near 1 nM NPY. A more attractive hypothesis is that NPY could be acting on multiple receptor subtypes that display opposing effects on the dendritic structure. Numerous pharmacological and genetic studies have demonstrated that the anxiolytic action of NPY is primarily mediated by Y1, and to a smaller degree Y5-receptors, while the selective activation of the presynaptic Y2-receptor is anxiogenic in the BLA (Reichmann and Holzer, 2015). Thus, the Y1- and/or Y5-receptors may be responsible for the hypotrophic effects observed with NPY, while activation of the Y2-receptor may be limiting the overall effect and preventing a true dose-dependent effect.

A close comparison of the morphological effects of NPY and CRF treatment in BLA OTCs, as well as repeated NPY injections *in vivo*, reveals that remodeling occurs at similar regions along the dendritic tree, at intermediate domains roughly 50-200 μm from the soma (Fig.3.24). This suggests that inputs from similar regions are likely affected by both CRF and NPY. There are a number of intra- and inter-amygdala regions that make electrical connections with principal neurons in the BLA, and future studies aimed at resolving which inputs are affected would be valuable to enhancing our knowledge of the circuitry involved. As a starting point, examining intra-amygdala connections may be worthwhile, as the axotomized nature of the OTCs would preclude inputs from regions excluded from the cultured slice. Alternatively, it may be possible that these principal neurons initiate the synaptic stress-related remodeling; certainly their robust responses to the neuromodulators studied here strongly suggest that they are capable of undergoing synaptic remodeling despite the removal of many of their endogenous afferent connections.

Figure 3.1

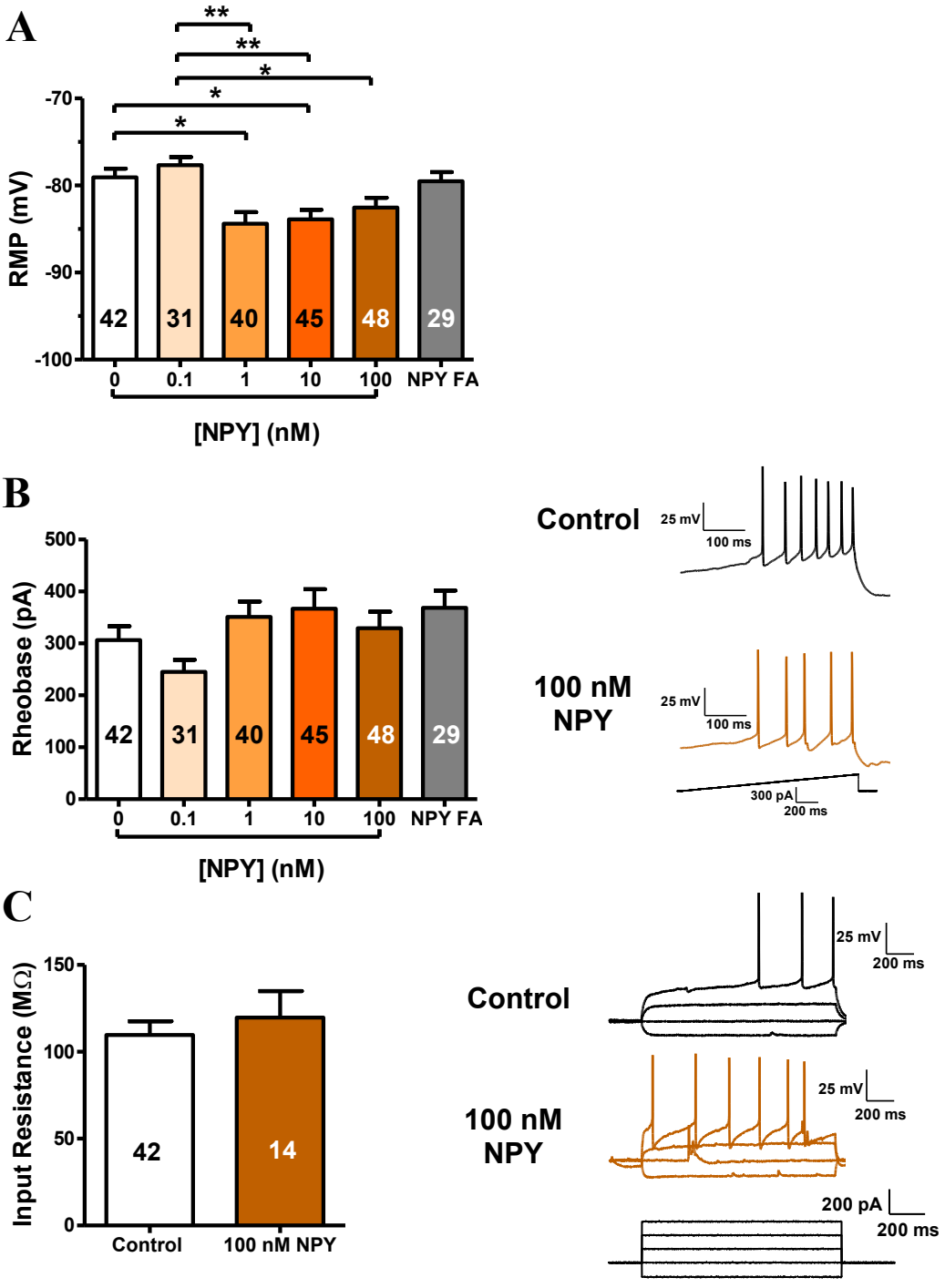
A
**
**
*
*
*
-70
-80
-90
-100
RMP (mV)
42
31
40
45
48
29
0
0.1
1
10
100
NPY FA
[NPY] (nM)
B
500
400
300
200
100
0
Rheobase (pA)
42
31
40
45
48
29
0
0.1
1
10
100
NPY FA
[NPY] (nM)
Control
25 mV
100 ms
100 nM
NPY
25 mV
100 ms
300 pA
200 ms
C
150
100
50
0
Input Resistance (MΩ)
42
14
Control
100 nM NPY
Control
25 mV
200 ms
100 nM
NPY
25 mV
200 ms
200 pA
200 ms

Figure 3.1 Postsynaptic effects of repeated NPY incubation in BLA OTCs.

(A) Incubation with 1 and 10 nM NPY resulted in a significant hyperpolarization of the resting membrane potential (RMP) compared to controls, while 100 nM NPY was trending in the same direction, it did not reach significant levels (*P<0.05, **P<0.01, one-way ANOVA with Tukey's *post hoc* test). There was no difference observed between controls and 100 nM NPY-free acid (P>0.05, t-test). (B) There was no difference in excitability of neurons following any incubation with NPY or NPY-free acid compared to controls (P>0.05, one-way ANOVA with Tukey's *post hoc* test). (Right) Representative voltage traces following a series of current ramps. (C) Analysis of input resistance revealed no difference between controls and 100 nM NPY incubations (P>0.05, t-test). (Right) Representative voltage traces following a series of current steps. The number of analyzed cells is presented for each treatment in the bar graph.

Figure 3.2

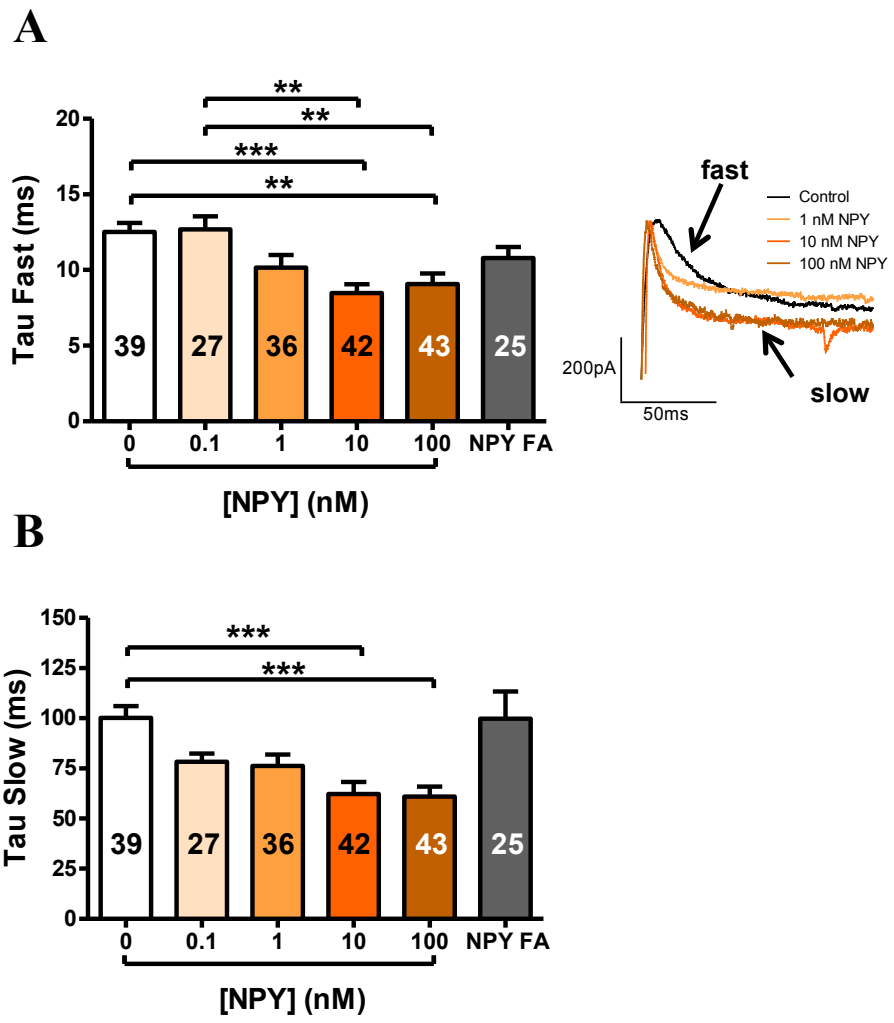
A
**
**
***
**
Tau Fast (ms)
20
15
10
5
0
39
27
36
42
43
25
0
0.1
1
10
100
NPY FA
[NPY] (nM)
fast
Control
1 nM NPY
10 nM NPY
100 nM NPY
200pA
50ms
slow
B
***
***
Tau Slow (ms)
150
125
100
75
50
25
0
39
27
36
42
43
25
0
0.1
1
10
100
NPY FA
[NPY] (nM)

Figure 3.2 Incubation with NPY results in faster I_h activation kinetics with no change in I_h amplitude or density in BLA OTCs.

(A) Representative current trace of I_h depicting faster activation kinetics following NPY incubation (right). Analysis of the time constants tau fast (A) and tau slow (B), reveal incubation with 10 and 100 nM NPY caused an acceleration in activation kinetics of I_h compared to control (**P<0.01, ***P<0.001, one-way ANOVA with Tukey's *post hoc* test). There was no change in activation kinetics with NPY-free acid compared to controls (P>0.05, t-test). The number of analyzed cells is presented for each treatment in the figure legend or bar graph.

Figure 3.3

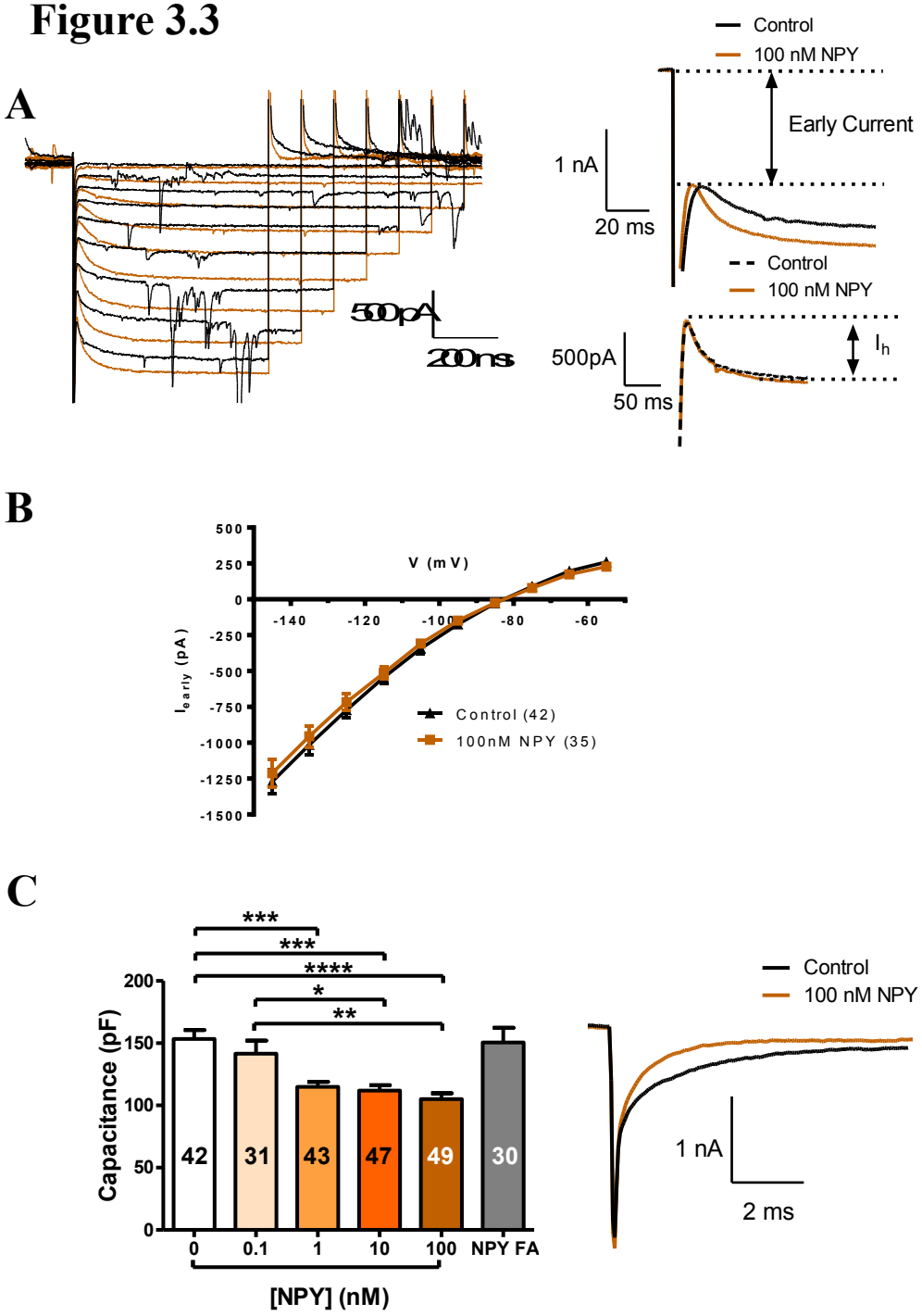
A
Control
100 nM NPY
Early Current
1 nA
20 ms
500pA
200ns
Control
100 nM NPY
I_h
500pA
50 ms
B
V (mV)
500
250
0
-140
-120
-100
-80
-60
-250
-500
-750
-1000
-1250
-1500
I_{early} (pA)
Control (42)
100nM NPY (35)
C
***
***
****
*
**
200
150
100
50
0
Capacitance (pF)
42
31
43
47
49
30
0
0.1
1
10
100
NPY FA
[NPY] (nM)
Control
100 nM NPY
1 nA
2 ms

Figure 3.3 NPY does not alter an early current but results in reductions of cell capacitance.

(A) Representative current traces of control and 100 nM NPY incubated principal cells following a family of increasing hyperpolarizing voltage steps from -55 mV (left). Magnified current traces from the largest (-145 mV) voltage step depicting the early current and I_h (right). (B) Analysis of the current traces, reveals no significant effect following NPY incubations. (C) NPY incubation results in reduced cell capacitance compared to controls (left, **P*<0.05, ** *P*<0.01, *** *P*<0.001, **** *P*<0.0001, one-way ANOVA with Tukey's *post hoc* test), with NPY-free acid having no effect (*P*>0.05, t-test). (Right) Representative current traces of the capacitive transient following a -10 mV voltage step from -55 mV of control and 100 nM NPY treated neurons. The number of analyzed cells is presented for each treatment in the figure legend or bar graph.

Figure 3.4

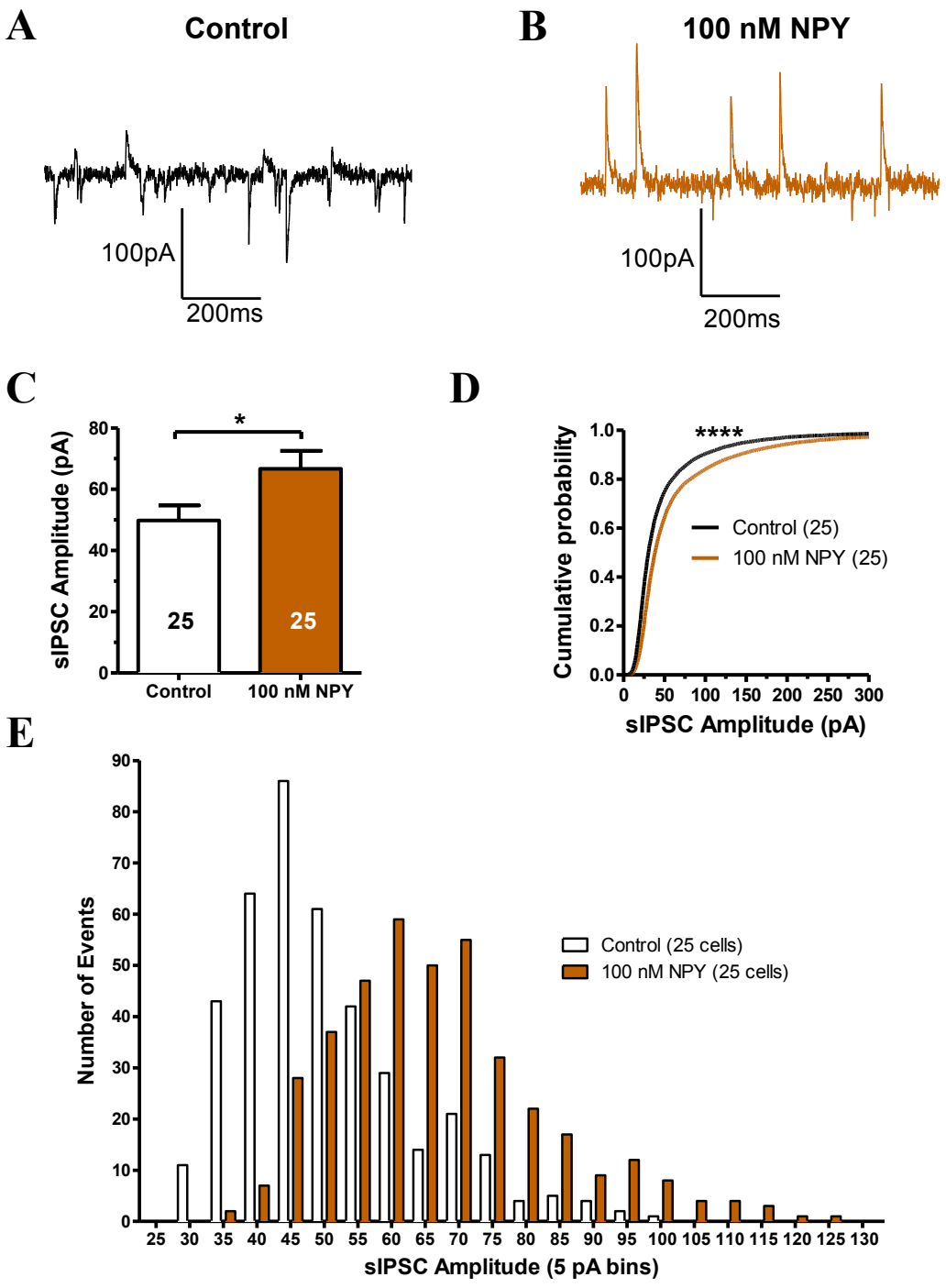
A
Control
100pA
200ms
B
100 nM NPY
100pA
200ms
C
sIPSC Amplitude (pA)
*
25
25
Control
100 nM NPY
D
Cumulative probability
****
Control (25)
100 nM NPY (25)
sIPSC Amplitude (pA)
E
Number of Events
Control (25 cells)
100 nM NPY (25 cells)
sIPSC Amplitude (5 pA bins)

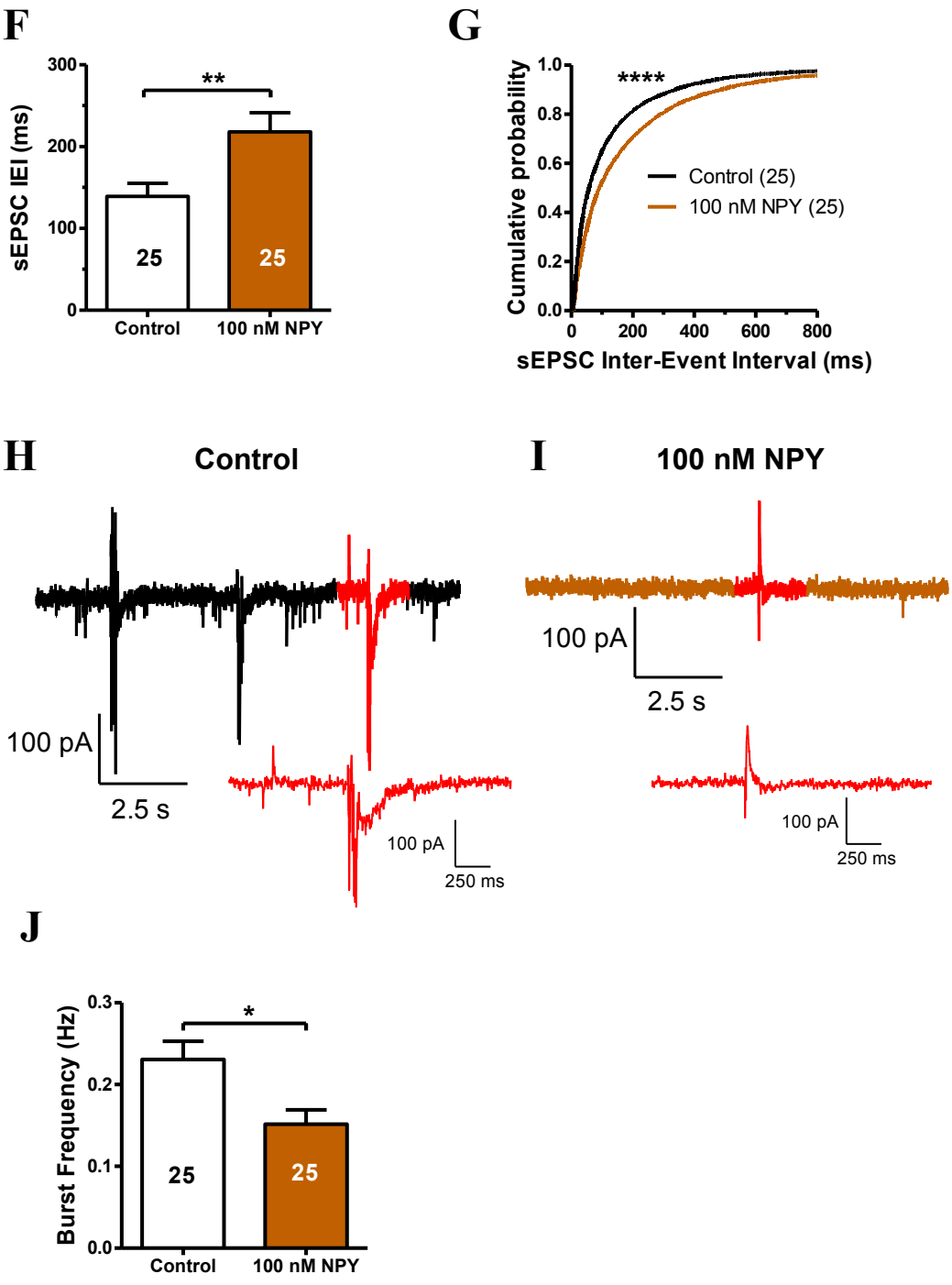
F
sEPSC IEI (ms)
300
200
100
0
**
25
25
Control
100 nM NPY
G
Cumulative probability
1.0
0.8
0.6
0.4
0.2
0.0
****
Control (25)
100 nM NPY (25)
0
200
400
600
800
sEPSC Inter-Event Interval (ms)
H
Control
100 pA
2.5 s
100 pA
250 ms
I
100 nM NPY
100 pA
2.5 s
100 pA
250 ms
J
Burst Frequency (Hz)
0.3
0.2
0.1
0.0
*
25
25
Control
100 nM NPY

Figure 3.4 100 nM NPY incubation results in decreased excitatory and increased inhibitory drive onto BLA OTC principal neurons.

(A-B) Representative current traces of sIPSCs (upward deflections) and sEPSCs (downward deflections) from control and 100 nM NPY incubated principal neurons held at -55 mV. (C) Analysis of mean sIPSC amplitude revealed an increase in amplitude following 100 nM NPY incubation (*P<0.05, t-test). (D) Cumulative probability plot of raw sIPSC amplitudes, depicting the increase in sIPSC amplitude following 100 nM NPY treatment (****P<0.0001, K-S test). (E) Frequency distribution histogram of mean sIPSC amplitudes, grouped in 5 pA bins shows the shift to higher amplitude events following incubation with 100 nM NPY. (F) Analysis of mean sEPSC IEI revealed a decrease in frequency (increase in IEI) of sEPSCs following 100 nM NPY incubations compared to controls (**P<0.01, t-test). (G) Cumulative probability plot of raw sEPSC IEI, depicting a robust increase in sEPSC IEI following 100 nM NPY treatment compared to controls (****P<0.0001, K-S test). (H-I) Representative current traces of neurons from control and 100 nM NPY incubated groups illustrating the frequency of compound postsynaptic bursts. Area illustrated in red represents an enhanced view of a single bursting event. (J) Analysis of bursting frequency suggests 100 nM NPY incubation, reduces bursting activity in BLA OTCs (*P<0.05, t-test). A total of 9828 sIPSCs and 9975 sEPSCs were analyzed for control neurons and 9931 sIPSCs and 9527 sEPSCs for 100 nM NPY incubated neurons. The number of analyzed cells is presented for each treatment in the figure legend or bar graph.

Figure 3.5

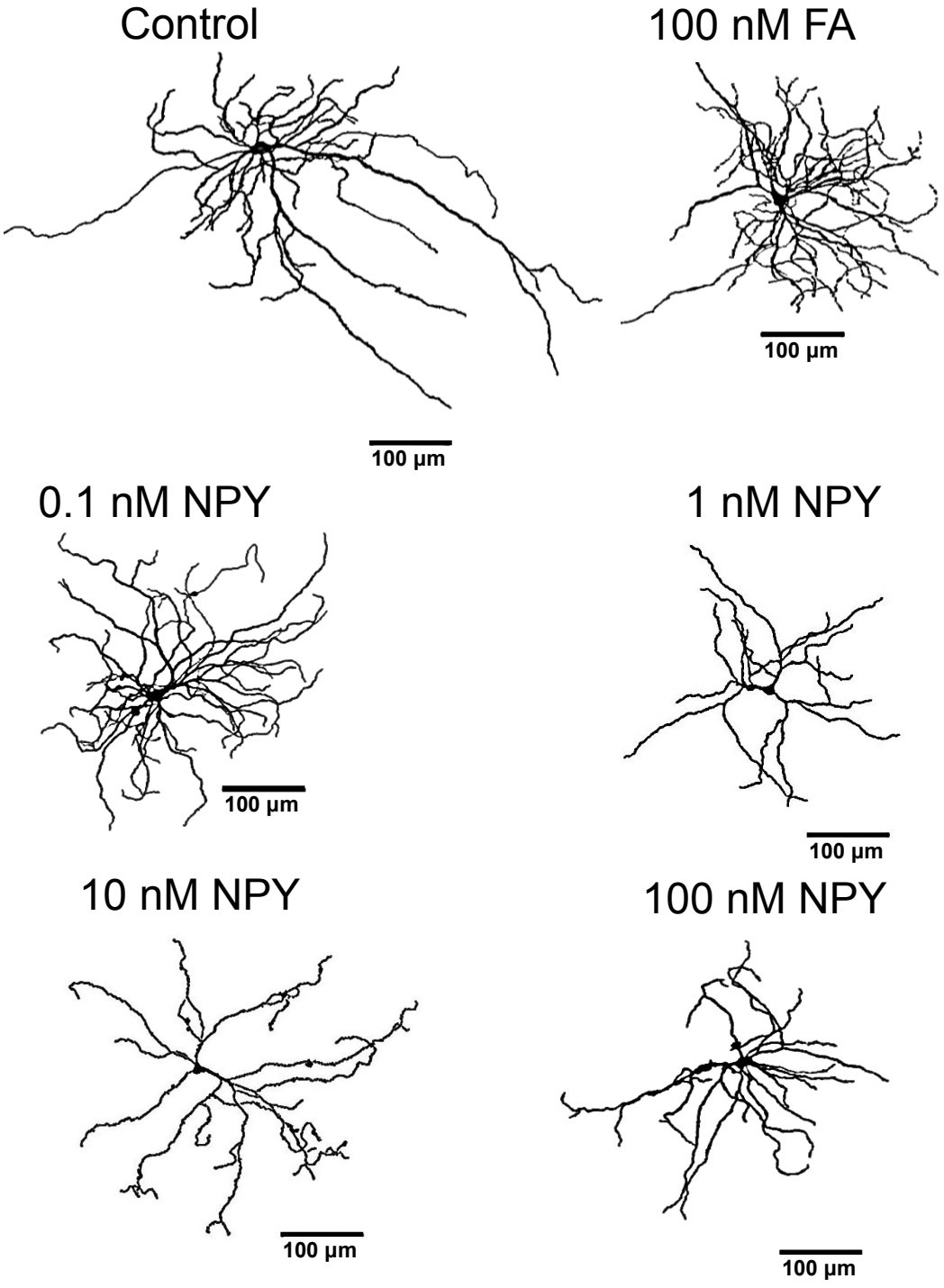
Control
100 µm
100 nM FA
100 µm
0.1 nM NPY
100 µm
1 nM NPY
100 µm
10 nM NPY
100 µm
100 nM NPY
100 µm

Figure 3.5 Representative reconstructed principal neurons following NPY incubations in BLA OTCs.

Following electrophysiological recordings and filling of cells with neurobiotin, OTCs were fixed, stained and imaged. Reconstructions were made using the simple neurite tracer function in FIJI. Representative tracings of the total dendritic tree of principal neurons from control, various concentrations of NPY and NPY-free acid treated BLA OTCs. Sample neurons were chosen based on the mean total dendritic length.

Figure 3.6

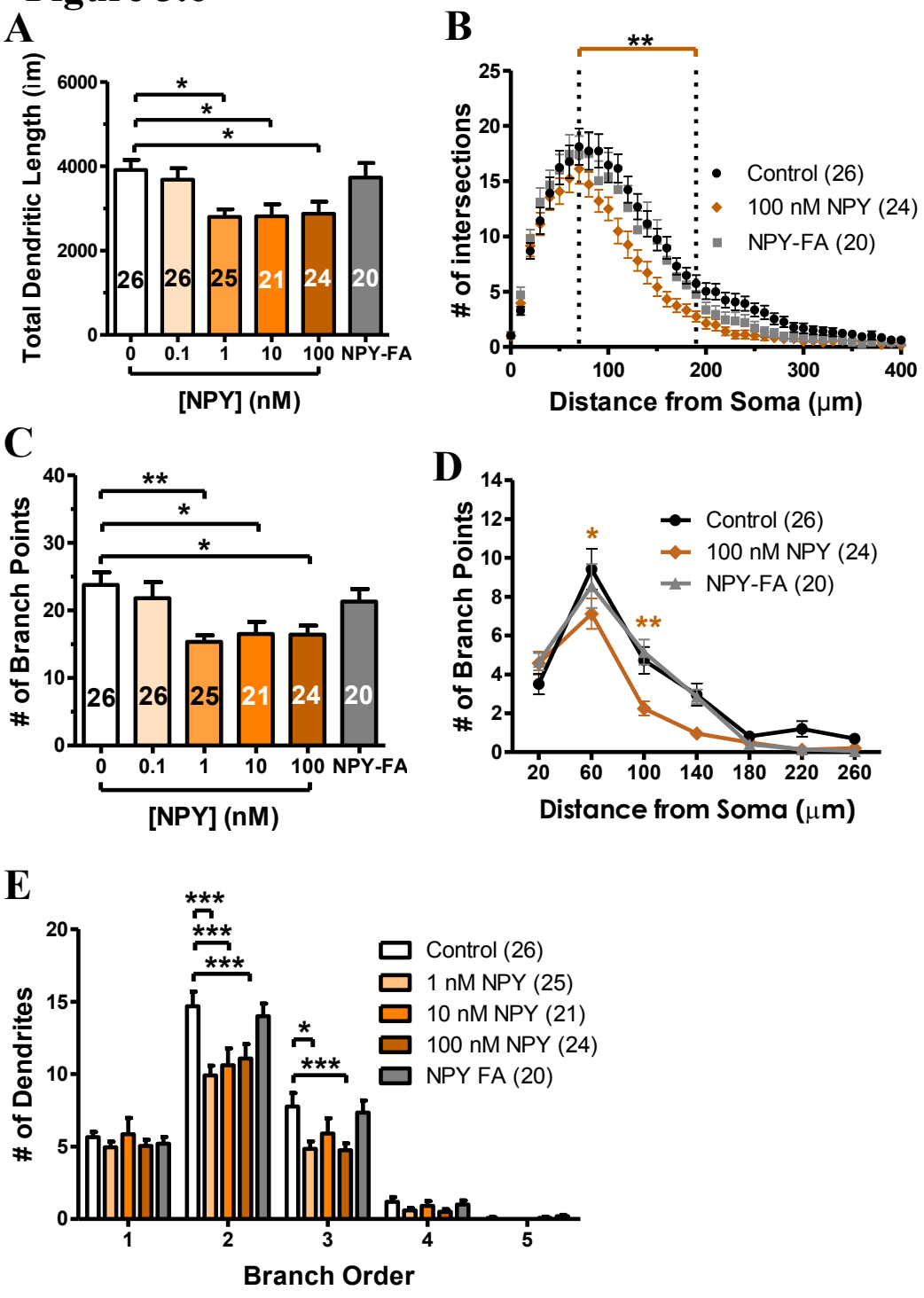
A
Total Dendritic Length (μm)
6000
4000
2000
0
*
*
*
26
26
25
21
24
20
0
0.1
1
10
100
NPY-FA
[NPY] (nM)
B
**
25
20
15
10
5
0
# of intersections
Control (26)
100 nM NPY (24)
NPY-FA (20)
0
100
200
300
400
Distance from Soma (μm)
C
**
*
*
40
30
20
10
0
# of Branch Points
26
26
25
21
24
20
0
0.1
1
10
100
NPY-FA
[NPY] (nM)
D
14
12
10
8
6
4
2
0
# of Branch Points
*
**
Control (26)
100 nM NPY (24)
NPY-FA (20)
20
60
100
140
180
220
260
Distance from Soma (μm)
E
***
***
***
*
***
20
15
10
5
0
# of Dendrites
Control (26)
1 nM NPY (25)
10 nM NPY (21)
100 nM NPY (24)
NPY FA (20)
1
2
3
4
5
Branch Order

Figure 3.6 NPY causes dendritic hypotrophy in principal neurons of BLA OTCs.

(A) Total dendritic length is significantly reduced in principal neurons following NPY incubations of BLA OTC. NPY-free acid, which does not bind to any Y-receptor, had no effect compared to controls ($P>0.5$, t-test). (B) Number of dendritic intersections per distance from the soma plotted from a Sholl analysis (10 μm radii), and analysis revealed the points along the dendritic tree where hypotrophy occurred following NPY incubations (**$P<0.01$, two-way ANOVA with Tukey's *post hoc* test). (C-E) Quantitation of the number and position of dendritic branch points revealed a reduction in dendritic arbor exuberance following NPY incubation compared to controls (*$P<0.05$, **$P<0.01$, one-way ANOVA with Tukey's *post hoc* test), with no change following incubation with NPY-free acid ($P>0.05$, t-test). (D) Consistent with total dendritic length measurements, the branching patterns of NPY-treated BLA OTC neurons are simplified, in the midproximal regions where the number of intersections is also reduced. Treatment with NPY-free acid had no effect on branching (*$P<0.05$, **$P<0.01$, ****$P<0.0001$, two-way ANOVA with Tukey's *post hoc* test). (E) NPY actions on dendritic branching appeared to result in preferential reductions in the numbers of secondary and tertiary dendritic branches, while NPY free acid was without effect. (*$P<0.05$, ***$P<0.001$, ****$P<0.0001$, two-way ANOVA with Tukey's *post hoc* test), while NPY-free acid had no effect ($P>0.05$). The number of analyzed cells is presented for each treatment in the figure legend or bar graph.

Figure 3.7

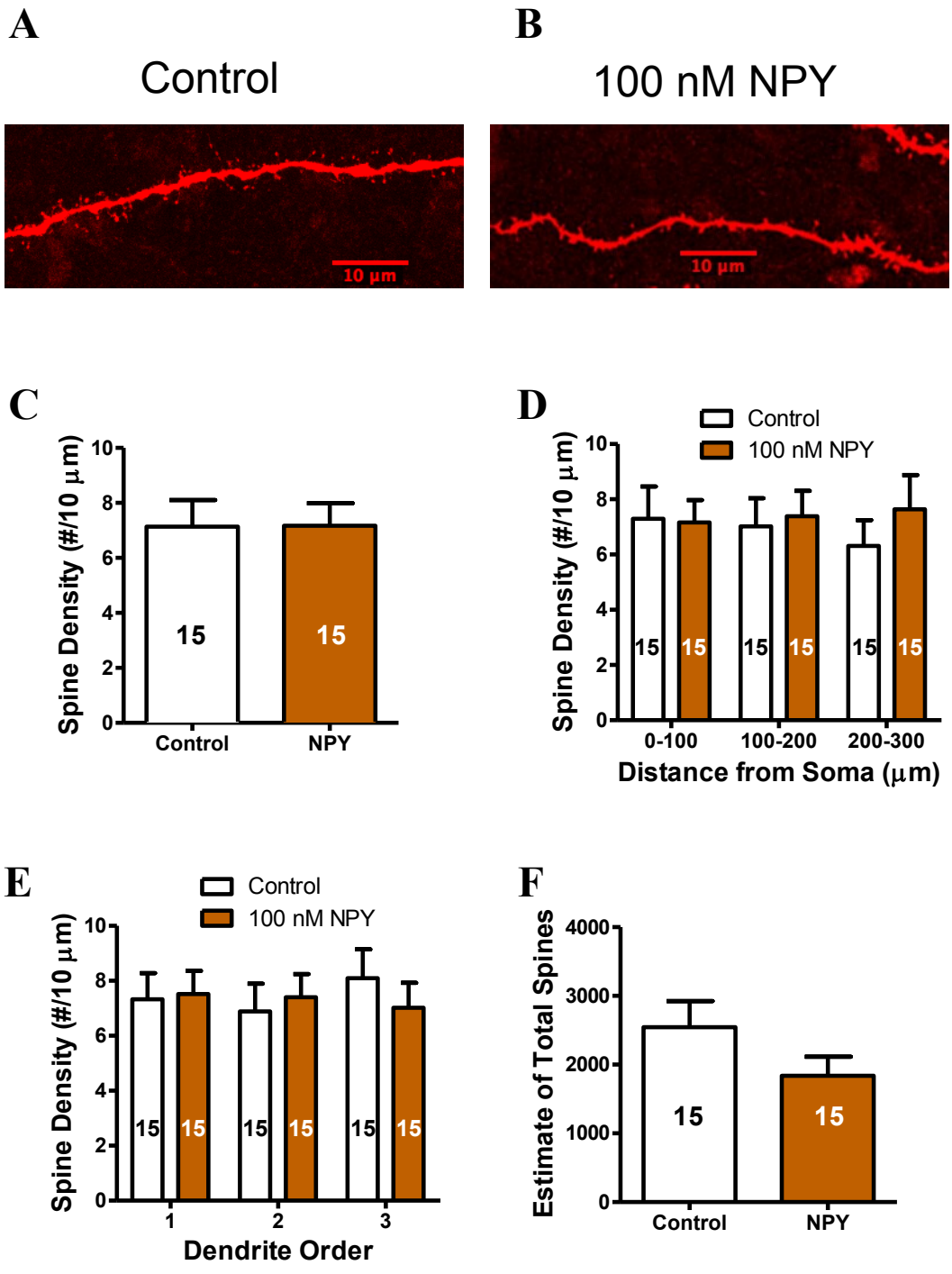
A
Control
10 µm
B
100 nM NPY
10 µm
C
Spine Density (#/10 µm)
15
15
Control
NPY
D
Control
100 nM NPY
Spine Density (#/10 µm)
0-100
100-200
200-300
Distance from Soma (µm)
E
Control
100 nM NPY
Spine Density (#/10 µm)
Dendrite Order
F
Estimate of Total Spines
15
15
Control
NPY

Figure 3.7 Treatment with NPY has no significant effect on dendritic spine density in BLA OTCs.

(A-B) Confocal images at 100x magnification of principal cell spines from control and 100 nM NPY treated BLA OTCs. Graphical representation of the effects of NPY treatment on spine density (C), spine density as a function of distance from the soma (D), spine density versus dendrite order (E), and estimates of total spine number (F). NPY had no significant effect on spine density. The apparent reduction in total number of spines per cell was not significant ($P>0.05$, t-test and two-way ANOVA with Bonferroni's *post hoc* test). The number of analyzed cells is presented for each treatment in the figure legend or bar graph.

Figure 3.8

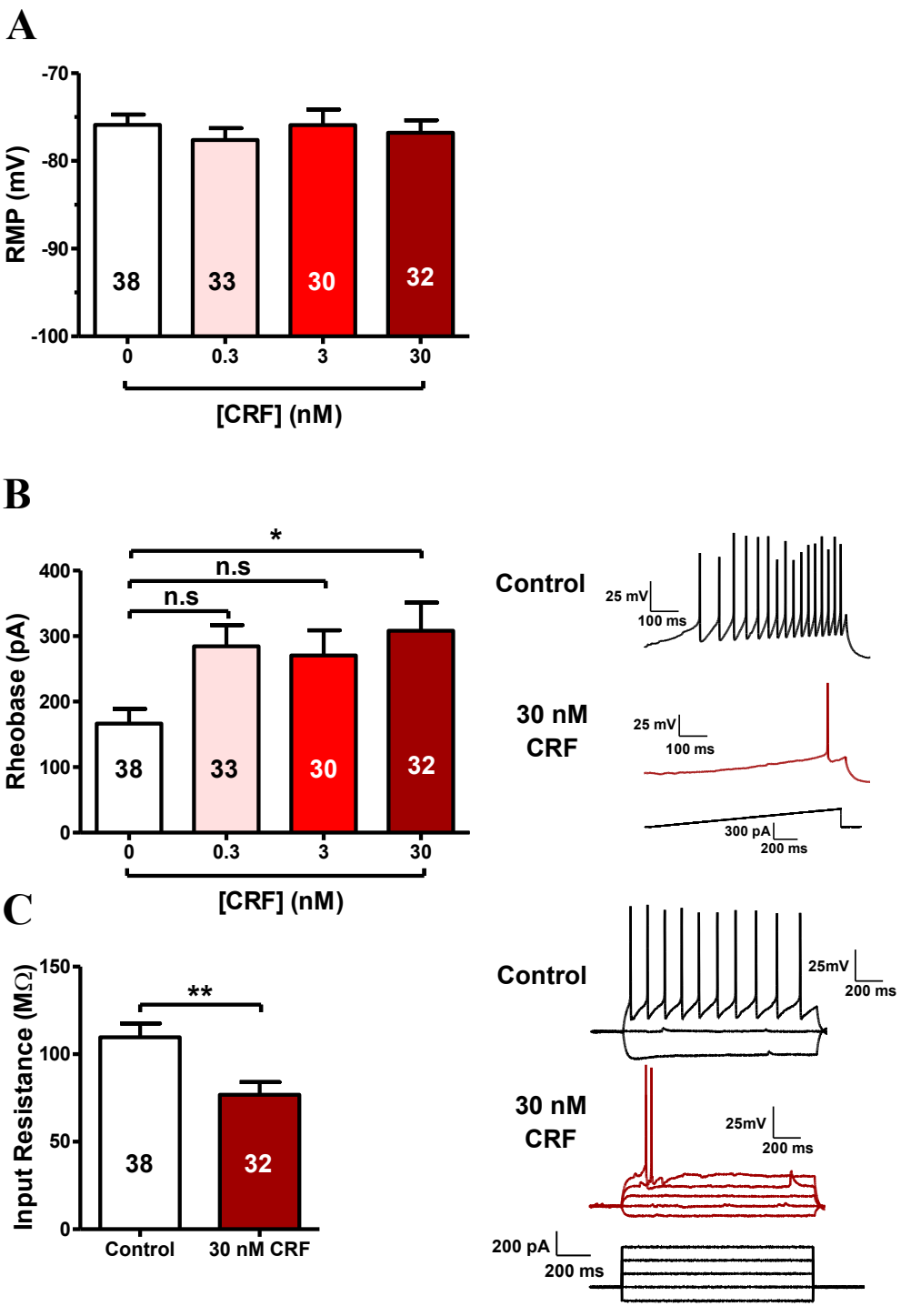
A
-70
-80
-90
-100
RMP (mV)
38
33
30
32
0
0.3
3
30
[CRF] (nM)
B
*
n.s
n.s
400
300
200
100
0
Rheobase (pA)
38
33
30
32
0
0.3
3
30
[CRF] (nM)
Control
25 mV
100 ms
30 nM
CRF
25 mV
100 ms
300 pA
200 ms
C
150
100
50
0
Input Resistance (MΩ)
**
38
32
Control
30 nM CRF
Control
25mV
200 ms
30 nM
CRF
25mV
200 ms
200 pA
200 ms

Figure 3.8 Repeated CRF incubation increases rheobase and reduces input resistance in BLA OTCs.

(A) Incubation with CRF did not alter RMP compared to controls ($P>0.05$, one-way ANOVA with Tukey's *post hoc* test). (B) Treatment in BLA OTCs with 30 nM CRF caused a small decrease in excitability as rheobase was increased (*$P<0.05$, one-way ANOVA with Tukey's *post hoc* test). (Right) Representative voltage traces following a series of current ramps. (C) Analysis of input resistance revealed a reduction following 30 nM CRF incubation compared to controls (**$P<0.01$, t-test). (Right) Representative voltage traces following a series of current steps. The number of analyzed cells is presented for each treatment in the bar graph.

Figure 3.9

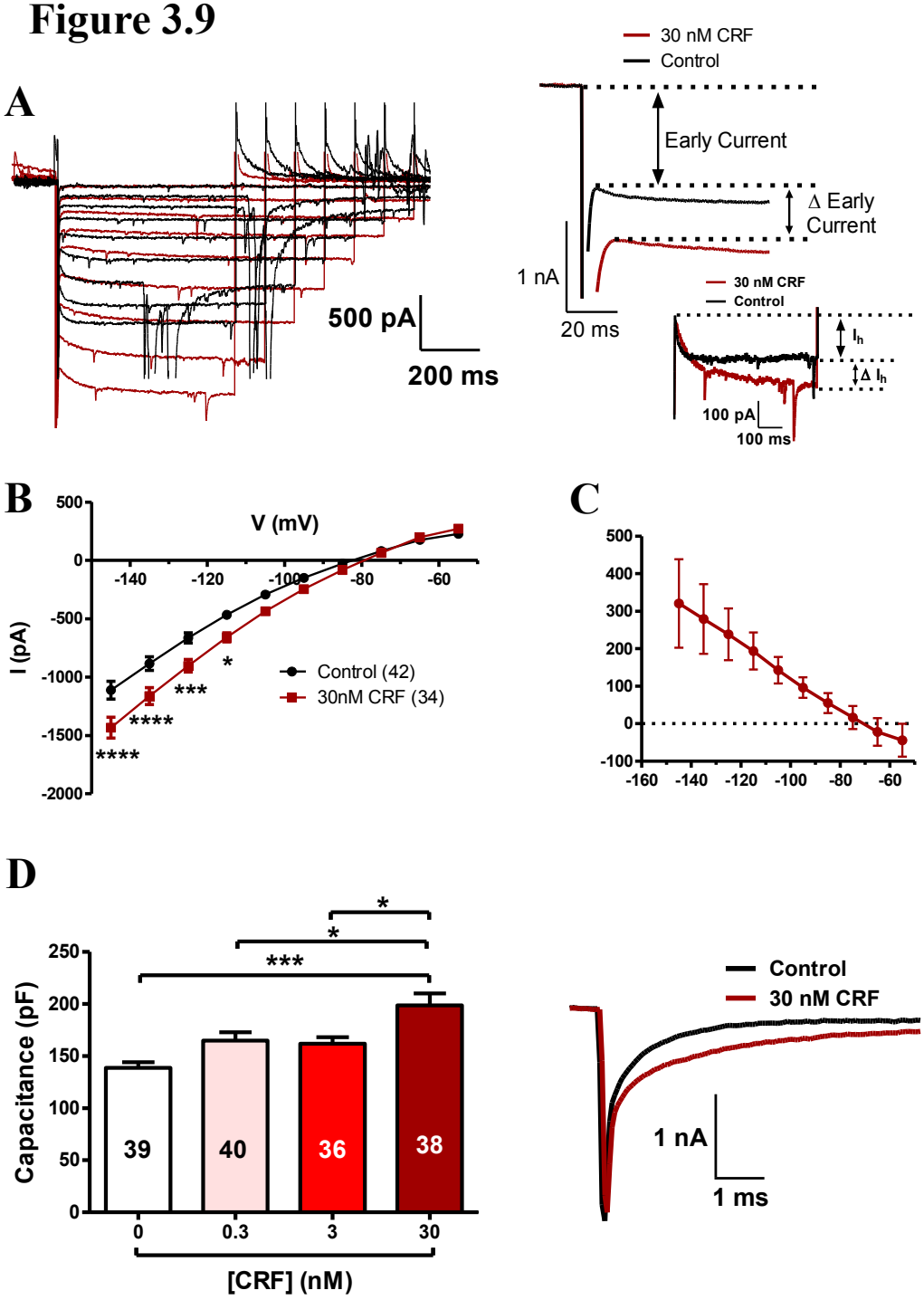
A
500 pA
200 ms
30 nM CRF
Control
Early Current
Δ Early Current
1 nA
20 ms
30 nM CRF
Control
I_h
Δ I_h
100 pA
100 ms
B
V (mV)
I (pA)
Control (42)
30nM CRF (34)
C
D
Capacitance (pF)
39
40
36
38
[CRF] (nM)
Control
30 nM CRF
1 nA
1 ms

Figure 3.9 CRF treatment increases early current and cell capacitance in BLA OTCs.

(A) Representative current traces of control and 30 nM CRF incubated principal cells following a family of increasing hyperpolarizing voltage steps from -55 mV (left). Magnified current traces from the largest (-145 mV) voltage step depicting the early current and I_h (right). (B) Analysis of the current-voltage plot (I/V), reveals a gain in an early current following 30 nM CRF incubations, which reversed around -70 mV (**P*<0.05, ****P*<0.001 *****P*<0.0001, two-way ANOVA with Tukey's *post hoc* test). (C) Subtraction of the current at each potential from the one elicited by 30 nM CRF results in a gain in net current. (D) CRF incubation results in increased cell capacitance compared to controls (left, **P*<0.05, *** *P*<0.001, one-way ANOVA with Tukey's *post hoc* test). (Right) Representative current traces of the capacitive transient following a -10 mV voltage step from -55 mV of control and 30 nM CRF treated neurons. The number of analyzed cells is presented for each treatment in the figure legend or bar graph.

Figure 3.10

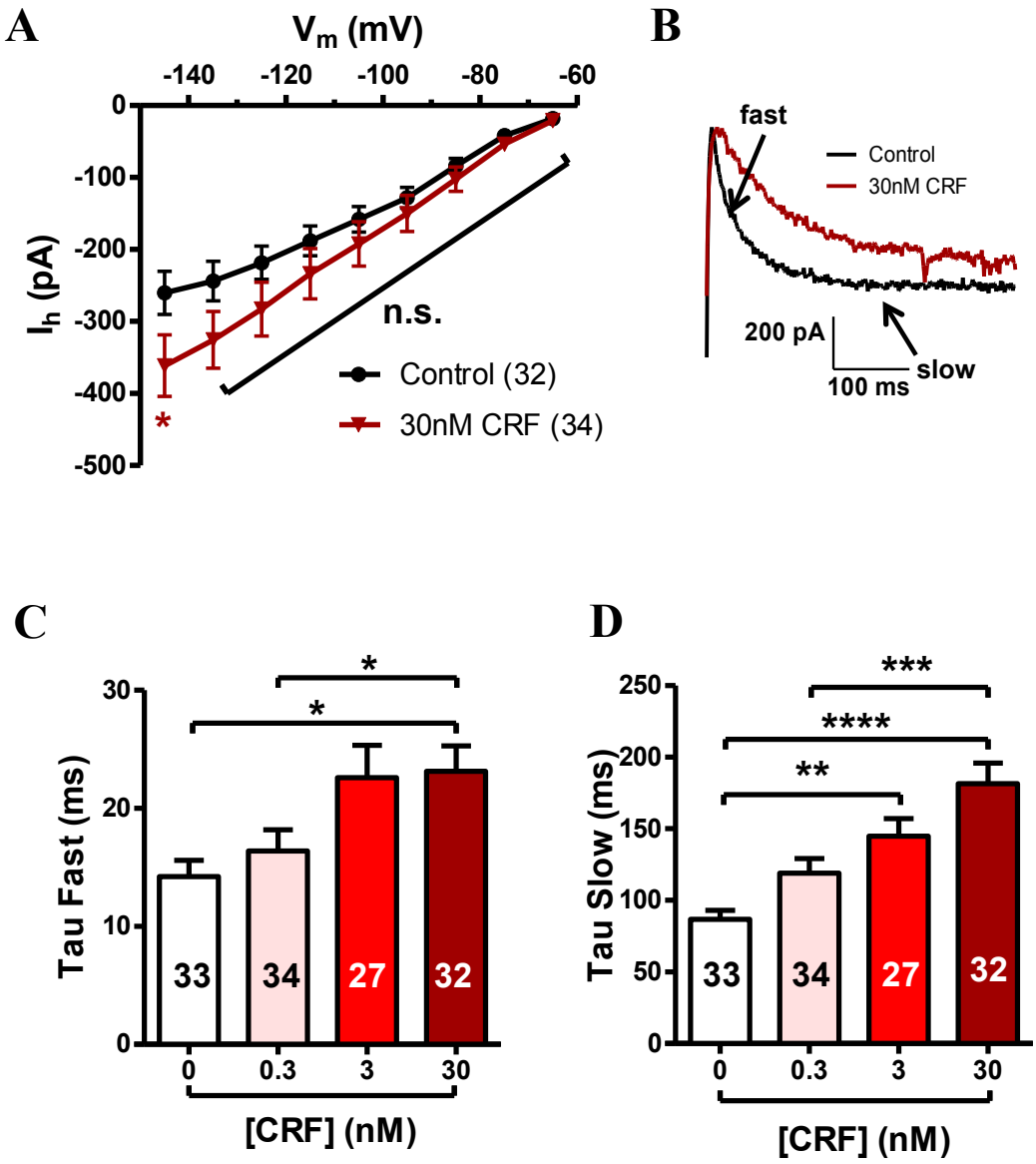
A
V_m (mV)
-140
-120
-100
-80
-60
0
-100
-200
-300
-400
-500
I_h (pA)
n.s.
*
Control (32)
30nM CRF (34)
B
fast
Control
30nM CRF
200 pA
100 ms
slow
C
Tau Fast (ms)
30
20
10
0
*
*
33
34
27
32
0
0.3
3
30
[CRF] (nM)
D
Tau Slow (ms)
250
200
150
100
50
0
***
****
**
33
34
27
32
0
0.3
3
30
[CRF] (nM)

Figure 3.10 Treatment with CRF results in slower I_h activation kinetics.

(A) Following increasing hyperpolarizing voltage steps from -55 mV, analysis revealed incubation with 30 nM CRF resulted in a slight increase in I_h amplitude for the largest (-145 mV) voltage step (*P<0.05, two-way ANOVA with Tukey's *post hoc* test). (B) Representative current trace of I_h depicting slower activation kinetics following CRF incubations. Analysis of the time constants tau fast (C) and tau slow (D), reveal incubation with CRF caused decelerated activation kinetics of I_h compared to control (*P<0.05, **P<0.01, ***P<0.001, ****P<0.0001, one-way ANOVA with Tukey's *post hoc* test). The number of analyzed cells is presented for each treatment in the figure legend or bar graph.

Figure 3.11

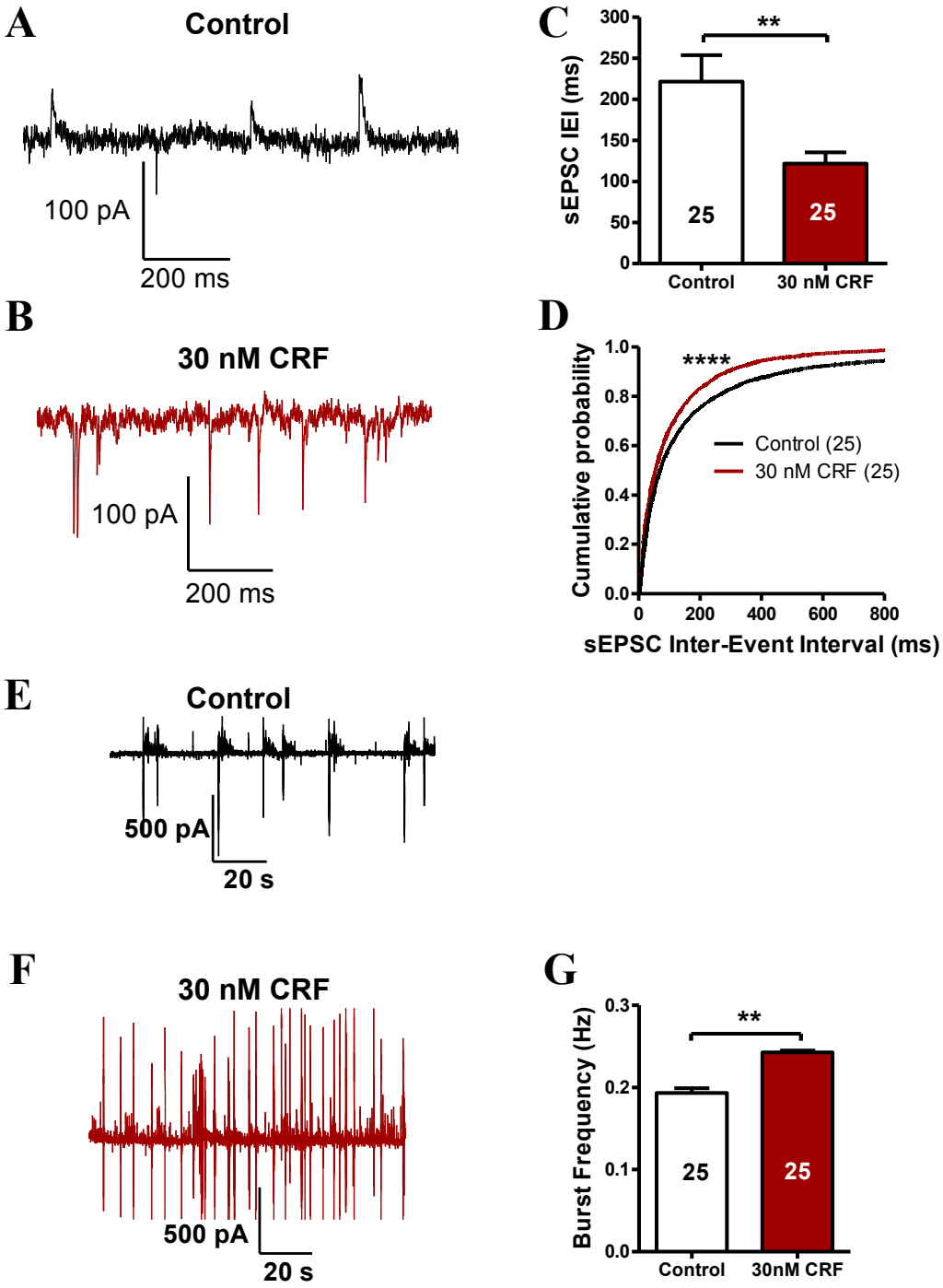
A
Control
100 pA
200 ms
B
30 nM CRF
100 pA
200 ms
C
**
sEPSC IEI (ms)
300
250
200
150
100
50
0
25
25
Control
30 nM CRF
D
****
Cumulative probability
1.0
0.8
0.6
0.4
0.2
0.0
0
200
400
600
800
Control (25)
30 nM CRF (25)
sEPSC Inter-Event Interval (ms)
E
Control
500 pA
20 s
F
30 nM CRF
500 pA
20 s
G
**
Burst Frequency (Hz)
0.3
0.2
0.1
0.0
25
25
Control
30nM CRF

Figure 3.11 30 nM CRF treatment results in increased excitatory and decreased inhibitory drive onto BLA OTC principal neurons.

(A-B) Representative current traces of sIPSCs and sEPSCs from control and 30 nM CRF treated cells held at -55 mV. (C) Analysis of mean sEPSC IEI revealed an increase in frequency (decrease in IEI) of sEPSCs following 30 nM CRF incubations compared to controls (**P<0.01, t-test). (D) Cumulative probability plot of raw sEPSC IEI, depicting a robust decrease in sEPSC IEI following 30 nM CRF treatment compared to controls (****P<0.0001, K-S test). (E-F) Representative current traces of neurons from control and 30 nM CRF incubated groups illustrating the frequency of compound postsynaptic bursts. (G) Analysis of bursting frequency suggests 30 nM CRF incubation, increases bursting activity in BLA OTCs (**P<0.01, t-test). A total of 9833 sIPSCs and 9213 sEPSCs were analyzed for control neurons and 9961 sIPSCs and 9913 sEPSCs for 30 nM CRF incubated neurons. The number of analyzed cells is presented for each treatment in the figure legend or bar graph.

Figure 3.12

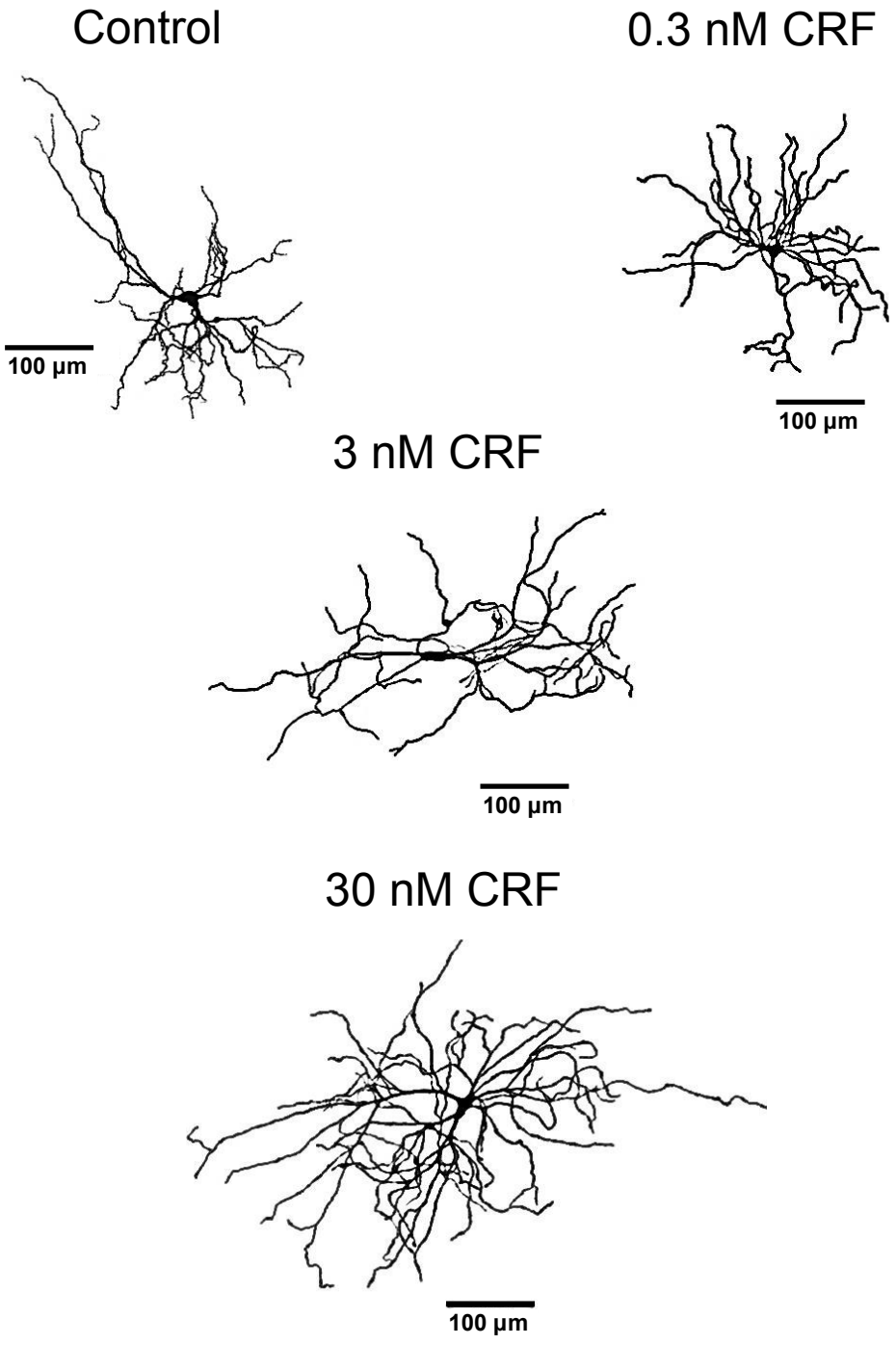

Figure 3.12 Representative reconstructed principal neurons following CRF incubations in BLA OTCs.

Representative tracings of the total dendritic tree of principal neurons from control and various concentrations of CRF-treated BLA OTCs. Sample neurons were chosen based on their mean total dendritic length.

Figure 3.13

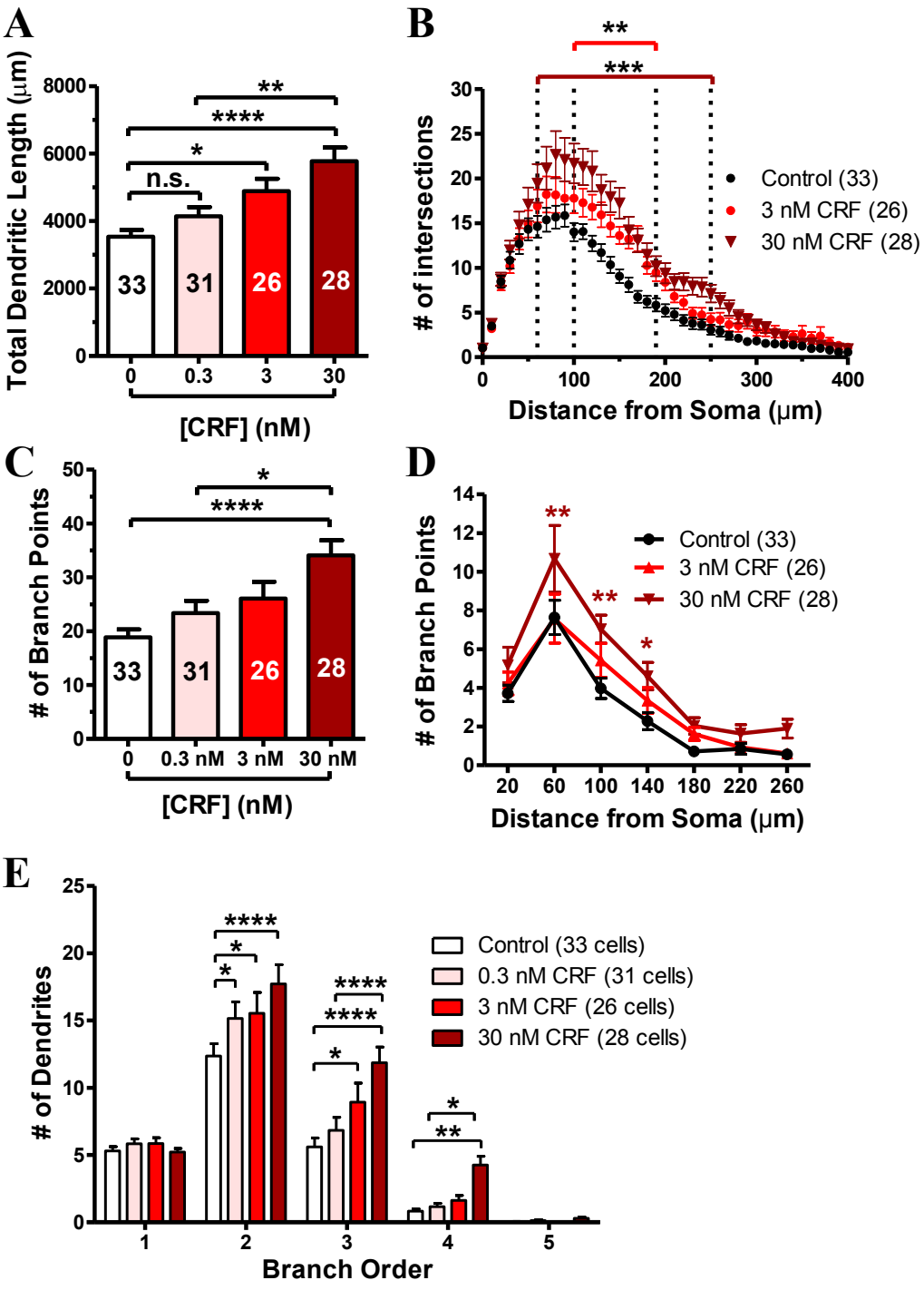
A
Total Dendritic Length (μm)
8000
6000
4000
2000
0
**
****
*
n.s.
33
31
26
28
0
0.3
3
30
[CRF] (nM)
B
# of intersections
30
25
20
15
10
5
0
**
***
Control (33)
3 nM CRF (26)
30 nM CRF (28)
0
100
200
300
400
Distance from Soma (μm)
C
# of Branch Points
50
40
30
20
10
0
*
****
33
31
26
28
0
0.3 nM
3 nM
30 nM
[CRF] (nM)
D
# of Branch Points
14
12
10
8
6
4
2
0
**
**
*
Control (33)
3 nM CRF (26)
30 nM CRF (28)
20
60
100
140
180
220
260
Distance from Soma (μm)
E
# of Dendrites
25
20
15
10
5
0
****
*
*
****
****
*
*
**
Control (33 cells)
0.3 nM CRF (31 cells)
3 nM CRF (26 cells)
30 nM CRF (28 cells)
1
2
3
4
5
Branch Order

Figure 3.13 CRF treatment on OTCs causes dendritic arbor hypertrophy in principal neurons.

(A) Analysis of total dendritic length demonstrates hypertophy of the dendritic tree following CRF incubations (*P<0.05, **P<0.01, ****P<0.0001, one-way ANOVA with Tukey's *post hoc* test). (B) Following Sholl analysis with increasing concentric circles of 10 μm radii, the number of intersections was plotted versus distance from the soma, and analysis revealed the points along the dendritic tree where expansion occurred following CRF incubations (*P<0.05, **P<0.01, ***P<0.001, two-way ANOVA with Tukey's *post hoc* test). (C) Quantification of the number of branch points revealed an increase of branching following CRF incubations compared to controls (*P<0.05, ****P<0.0001, one-way ANOVA with Tukey's *post hoc* test). Alterations in branching along the dendritic tree due to incubation with CRF was examined by Sholl analysis with concentric circles of 40 μm in radii, starting at 20 μm from the soma. (D) Plots of the number of branch points as a function of distance from the soma, revealed CRF incubations enhanced branching at proximal-intermediate distances (*P<0.05, **P<0.01, two-way ANOVA with Tukey's *post hoc* test). To determine if CRF affected the relationship between branching and dendrite order, the number of dendrites was plotted versus branch order. (E) Incubation with CRF resulted in augmentation of 2˚ 3º and 4º dendrites compared to controls (*P<0.05, **P<0.01, ****P<0.0001, two-way ANOVA with Tukey's *post hoc* test). The number of analyzed cells is presented for each treatment in the figure legend or bar graph.

Figure 3.14

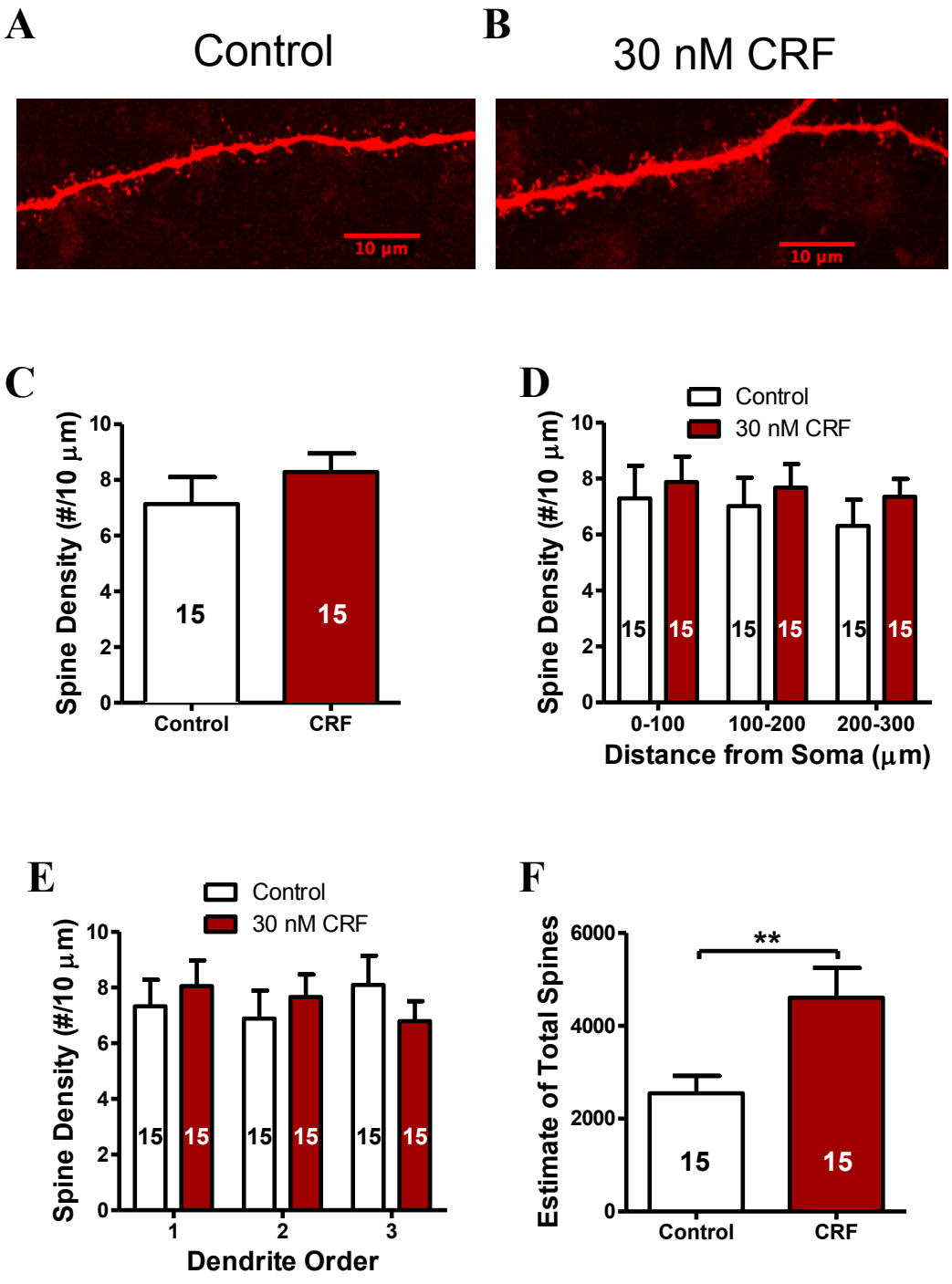
A
Control
B
30 nM CRF
10 µm
10 µm
C
Spine Density (#/10 µm)
15
15
Control
CRF
D
Control
30 nM CRF
Spine Density (#/10 µm)
0-100
100-200
200-300
Distance from Soma (µm)
E
Control
30 nM CRF
Spine Density (#/10 µm)
Dendrite Order
F
Estimate of Total Spines
**
Control
CRF

Figure 3.14 CRF treatment has no effect on dendritic spine density, but increases the total number of spines in BLA OTCs.

(A-B) Confocal images at 100x magnification of principal cell spines from control and 30 nM CRF treated BLA OTCs. CRF treatment had no significant effects ($P>0.05$, t-test and two-way ANOVA with Bonferroni's *post hoc* test) on (C) spine density overall, (D) spine density as a function of distance from the soma, or (E) spine density versus dendrite order while the increased dendritic length resulted in significant increase in (F) estimates of total spine number (**$P<0.01$, t-test). The number of analyzed cells is presented for each treatment in the figure legend or bar graph.

Figure 3.15

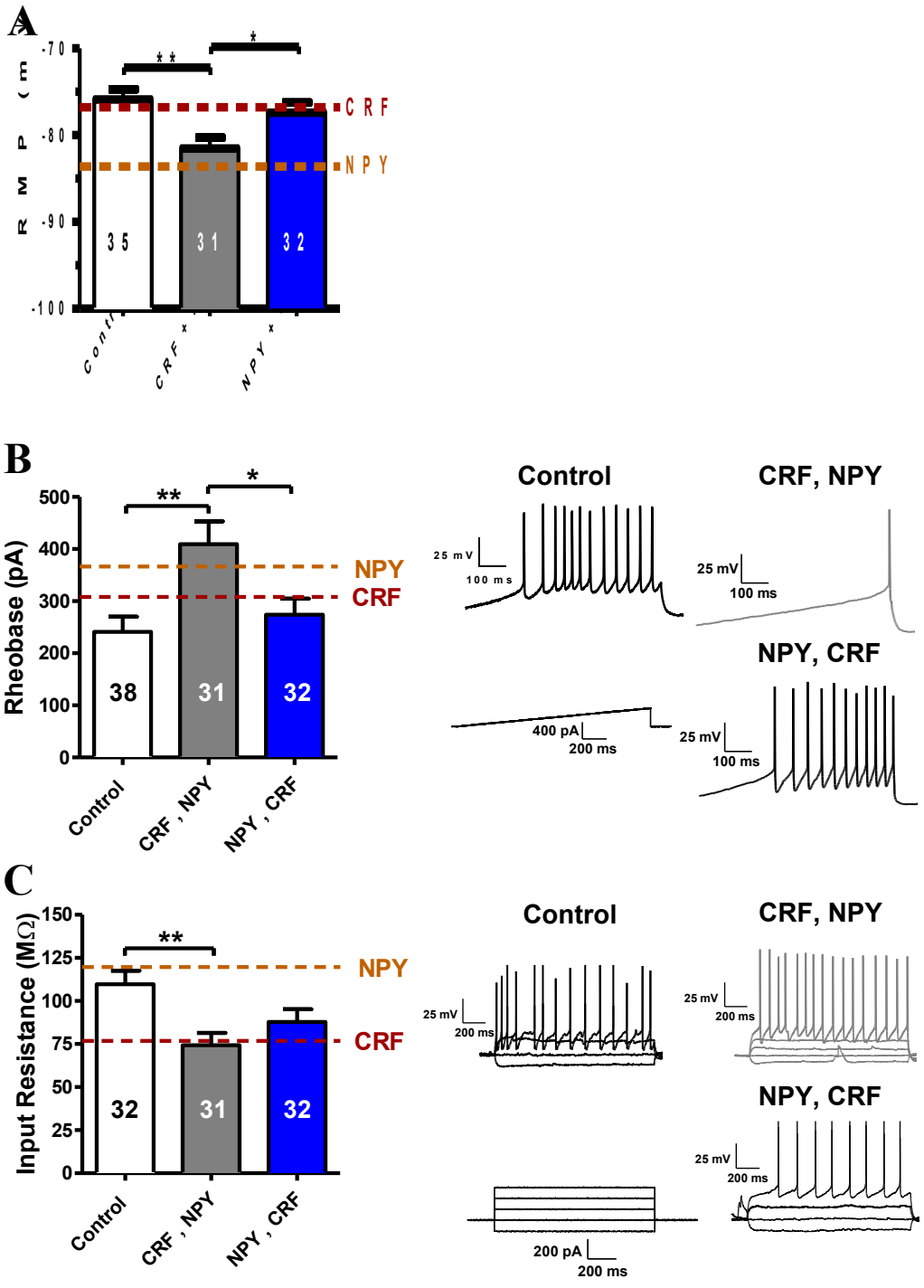
A
-70
-80
-90
-100
CRF
NPY
35
31
32
Cont
CRF *
NPY *
B
Rheobase (pA)
500
400
300
200
100
0
NPY
CRF
38
31
32
Control
CRF , NPY
NPY , CRF
Control
CRF, NPY
25 mV
100 ms
NPY, CRF
400 pA
200 ms
C
Input Resistance (MΩ)
150
125
100
75
50
25
0
NPY
CRF
32
31
32
200 pA
200 ms

Figure 3.15 Counter-regulation of postsynaptic effects by CRF and NPY in BLA OTCs. OTCs were treated as described first with one peptide (CRF or NPY), then in an identical manner with the other. Controls were treated twice with vehicle. (A) The CRF-treated, followed by NPY-treated (CRF, NPY) group's RMP was hyperpolarized compared to controls and the NPY, CRF group (*P<0.05, **P<0.01, one-way ANOVA with Tukey's *post hoc* test). (**B**) Based on rheobase measurements, (*left panel*) the CRF, NPY group was less excitable than either the control or NPY, CRF groups (*P<0.05, **P<0.01, one-way ANOVA with Tukey's *post hoc* test). (*Right panel*) Representative voltage traces from cells treated as indicated in response to a current ramp (lower left trace). (C, *left panel*) Input resistance was significantly reduced in neurons from CRF , NPY slices compared to controls. The NPY , CRF group showed a similar trend, but it did not reach significance (**P<0.01, one-way ANOVA with Tukey's *post hoc* test). (*Right panel*) Representative voltage traces from cells treated as indicated in response to a series of current steps. The mean values of 30 nM CRF (red) and 100 nM NPY (orange) for measurements in A, B and C are denoted by dashed lines in the respective bar graphs, but were not used for statistical analysis. The number of analyzed cells is presented for each treatment in the figure legend or bar graph.

Figure 3.16

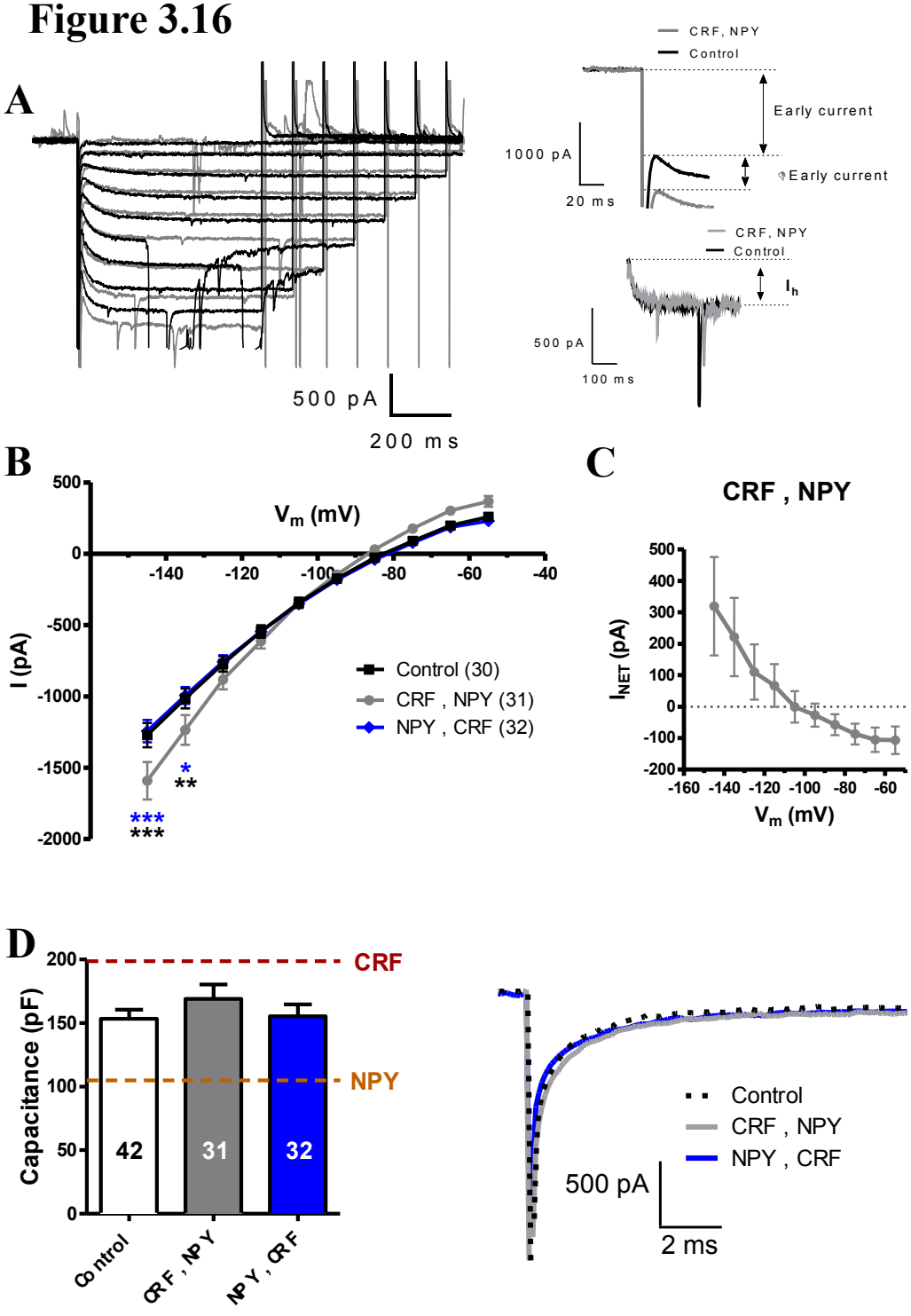
A
500 pA
200 ms
CRF, NPY
Control
Early current
Early current
1000 pA
20 ms
CRF, NPY
Control
I_h
500 pA
100 ms
B
V_m (mV)
I (pA)
Control (30)
CRF , NPY (31)
NPY , CRF (32)
C
CRF , NPY
I_{NET} (pA)
V_m (mV)
D
CRF
NPY
Capacitance (pF)
42
31
32
Control
CRF , NPY
NPY , CRF
Control
CRF , NPY
NPY , CRF
500 pA
2 ms

Figure 3.16 CRF , NPY treatment causes a gain of an early current but no increase in cell capacitance for either NPY , CRF or CRF , NPY in BLA OTCs.

(A, left) Representative current traces of control, CRF , NPY and NPY , CRF treated groups following a family of increasing hyperpolarizing voltage steps from -55 mV. (Right) Enhanced view depicting the early current (top) and I_h (bottom). (B) Analysis of the current-voltage plot (I/V), reveals a gain in an early current in the CRF , NPY treated groups compared to controls and the NPY , CRF treated groups, which reversed around -100 mV (Blue asterisk = CRF , NPY vs. control, black asterisk = CRF , NPY vs. NPY , CRF; **P*<0.05, ***P*<0.0001 *****P*<0.0001, two-way ANOVA with Tukey's *post hoc* test). (C) Subtraction of the control current from the one elicited by CRF , NPY neurons results in a gain in net current. (D) There was no difference in cell capacitance in either CRF , NPY or NPY , CRF treated groups compared to controls (left, *P*>0.05, one-way ANOVA with Tukey's *post hoc* test). (Right) Representative current traces of the capacitive transient following a -10 mV voltage step from -55 mV of control, CRF , NPY and NPY , CRF treated groups. The mean values of 30 nM CRF (red) and 100 nM NPY (orange) for measurements in A, B and C are denoted by dashed lines in the respective bar graphs, but were not used for statistical analysis. The number of analyzed cells is presented for each treatment in the figure legend or bar graph.

Figure 3.17

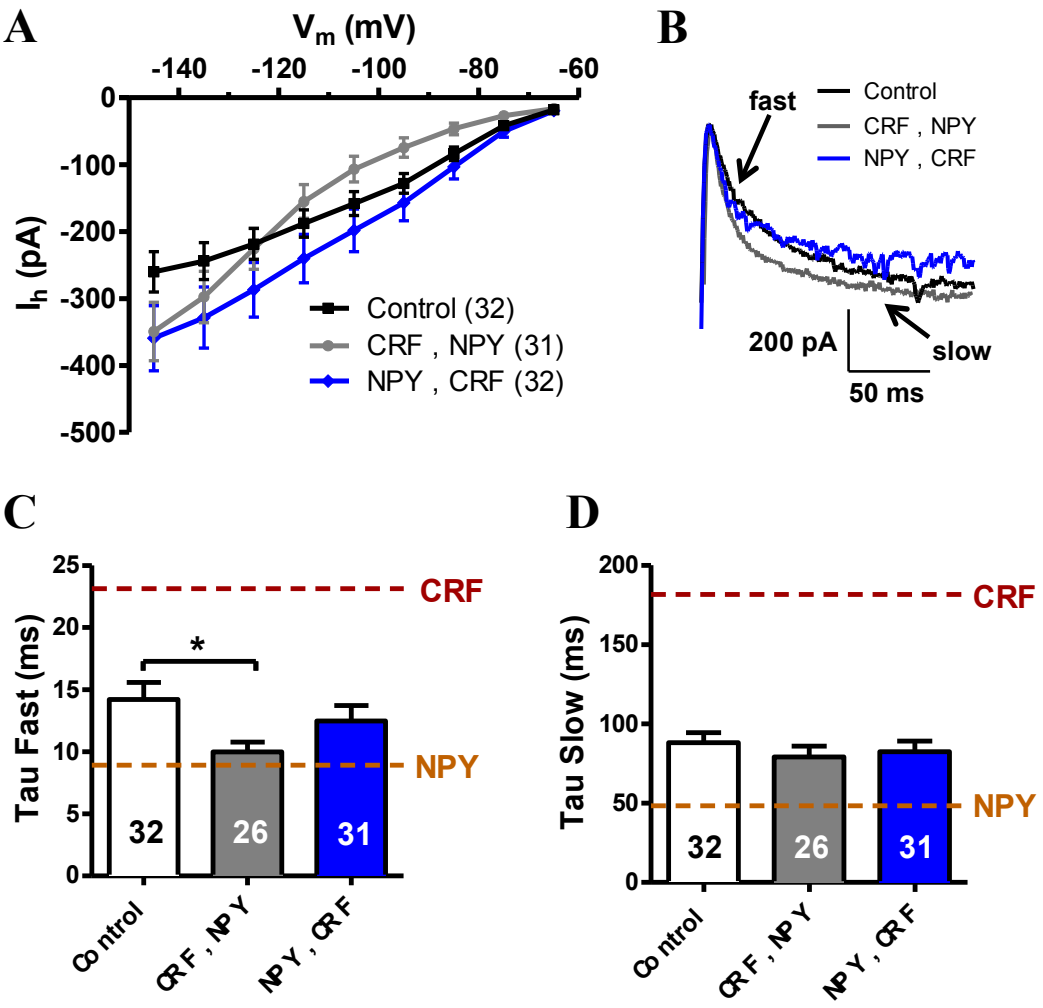
A
V_m (mV)
-140
-120
-100
-80
-60
0
-100
-200
-300
-400
-500
I_h (pA)
Control (32)
CRF , NPY (31)
NPY , CRF (32)
B
fast
Control
CRF , NPY
NPY , CRF
200 pA
slow
50 ms
C
Tau Fast (ms)
25
20
15
10
5
0
CRF
NPY
*
32
26
31
Control
CRF , NPY
NPY , CRF
D
Tau Slow (ms)
200
150
100
50
0
CRF
NPY
32
26
31
Control
CRF , NPY
NPY , CRF

Figure 3.17 Opposing neuropeptide treatment limits the effects on I_h in BLA OTCs.

(A-B) Following increasing hyperpolarizing voltage steps from -55 mV, analysis revealed CRF , NPY and NPY , CRF treated groups had no effect on I_h amplitude (P>0.05, two-way ANOVA with Tukey's *post hoc* test). (B) Representative current trace of I_h depicting similar activation kinetics from BLA OTCs treated with CRF , NPY and NPY , CRF. Analysis of the time constants tau fast (C) and tau slow (D), revealed incubations with CRF , NPY caused accelerated Tau fast compared to controls (*P<0.05, one-way ANOVA with Tukey's *post hoc* test). The mean values of 30 nM CRF (red) and 100 nM NPY (orange) for measurements in A, B and C are denoted by dashed lines in the respective bar graphs, but were not used for statistical analysis. The number of analyzed cells is presented for each treatment in the figure legend or bar graph.

Figure 3.18

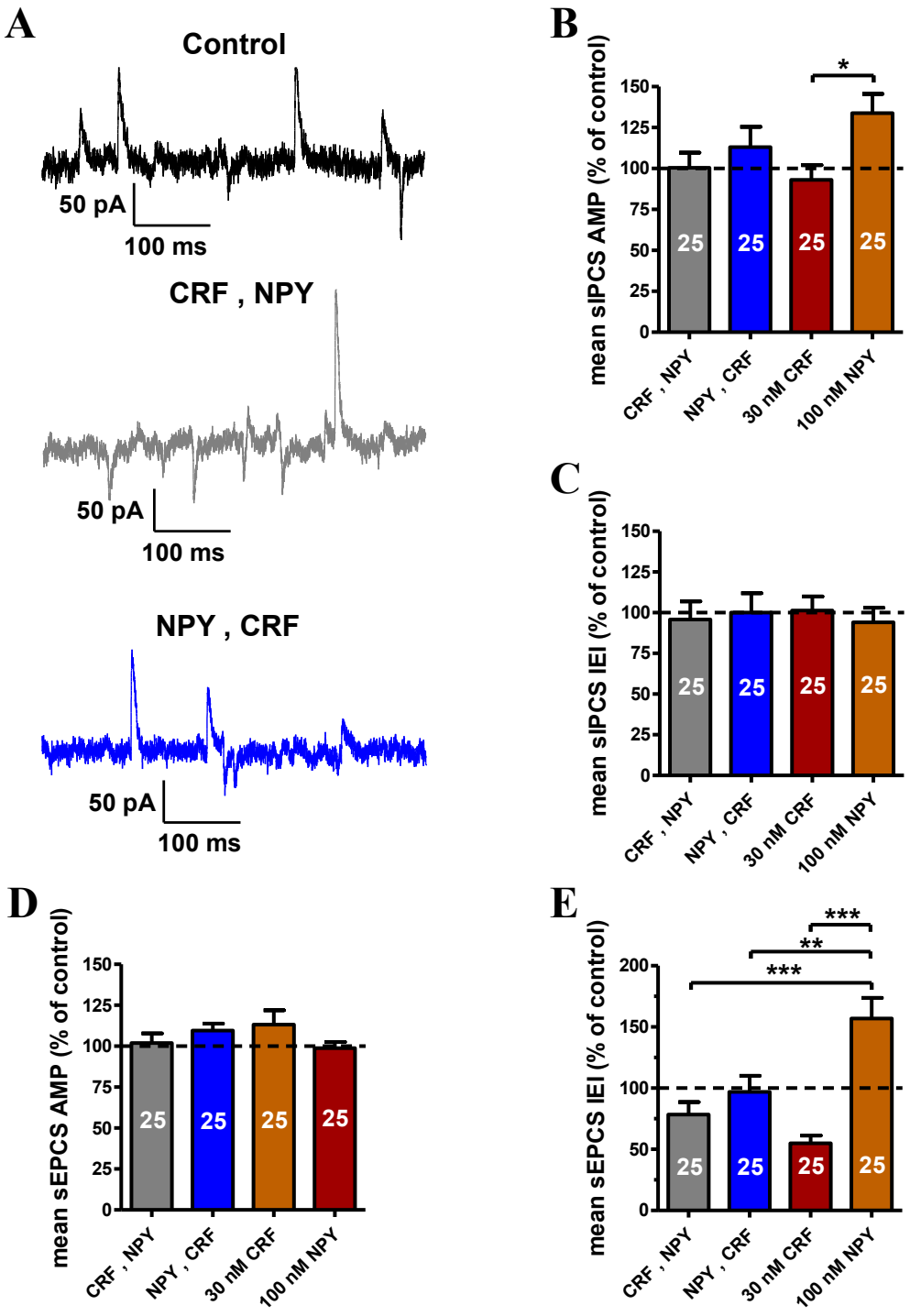
A
Control
50 pA
100 ms
CRF , NPY
50 pA
100 ms
NPY , CRF
50 pA
100 ms
B
mean sIPCS AMP (% of control)
150
125
100
75
50
25
0
*
25
25
25
25
CRF , NPY
NPY , CRF
30 nM CRF
100 nM NPY
C
mean sIPCS IEI (% of control)
150
125
100
75
50
25
0
25
25
25
25
CRF , NPY
NPY , CRF
30 nM CRF
100 nM NPY
D
mean sEPCS AMP (% of control)
150
125
100
75
50
25
0
25
25
25
25
CRF , NPY
NPY , CRF
30 nM CRF
100 nM NPY
E
mean sEPCS IEI (% of control)
200
150
100
50
0
***
**
***
25
25
25
25
CRF , NPY
NPY , CRF
30 nM CRF
100 nM NPY

Figure 3.18 Opposing neuropeptide treatment in BLA OTCs, occludes the effects on synaptic activity.

(A) Representative current traces of sIPSCs and sEPSCs from control, CRF , NPY and NPY , CRF treated neurons held at -55 mV. To reference the observed effects to those of 30 nM CRF and 100 nM NPY alone, mean sIPSC and sEPSC amplitude and frequency is presented as % of controls. (C and D) There was no difference in sIPSC frequency or sEPSC amplitude between any of the groups ($P>0.05$, one- way ANOVA with Tukey's *post hoc* test). (B) There was a significant increase in sIPSC amplitude between 100 nM NPY and 30 nM CRF treated neurons (*$P<0.05$, one- way ANOVA with Tukey's *post hoc* test). (E) The frequency of sEPSCs was reduced in the 100 nM NPY group compared to the 30 nM CRF, CRF , NPY and NPY , CRF treated groups (**$P<0.01$, ***$P<0.001$, one- way ANOVA with Tukey's *post hoc* test). The mean values of 30 nM CRF (red) and 100 nM NPY (orange) for measurements in A, B and C are denoted by dashed lines in the respective bar graphs, but were not used for statistical analysis. The number of analyzed cells is presented for each treatment in the figure legend or bar graph.

Figure 3.19

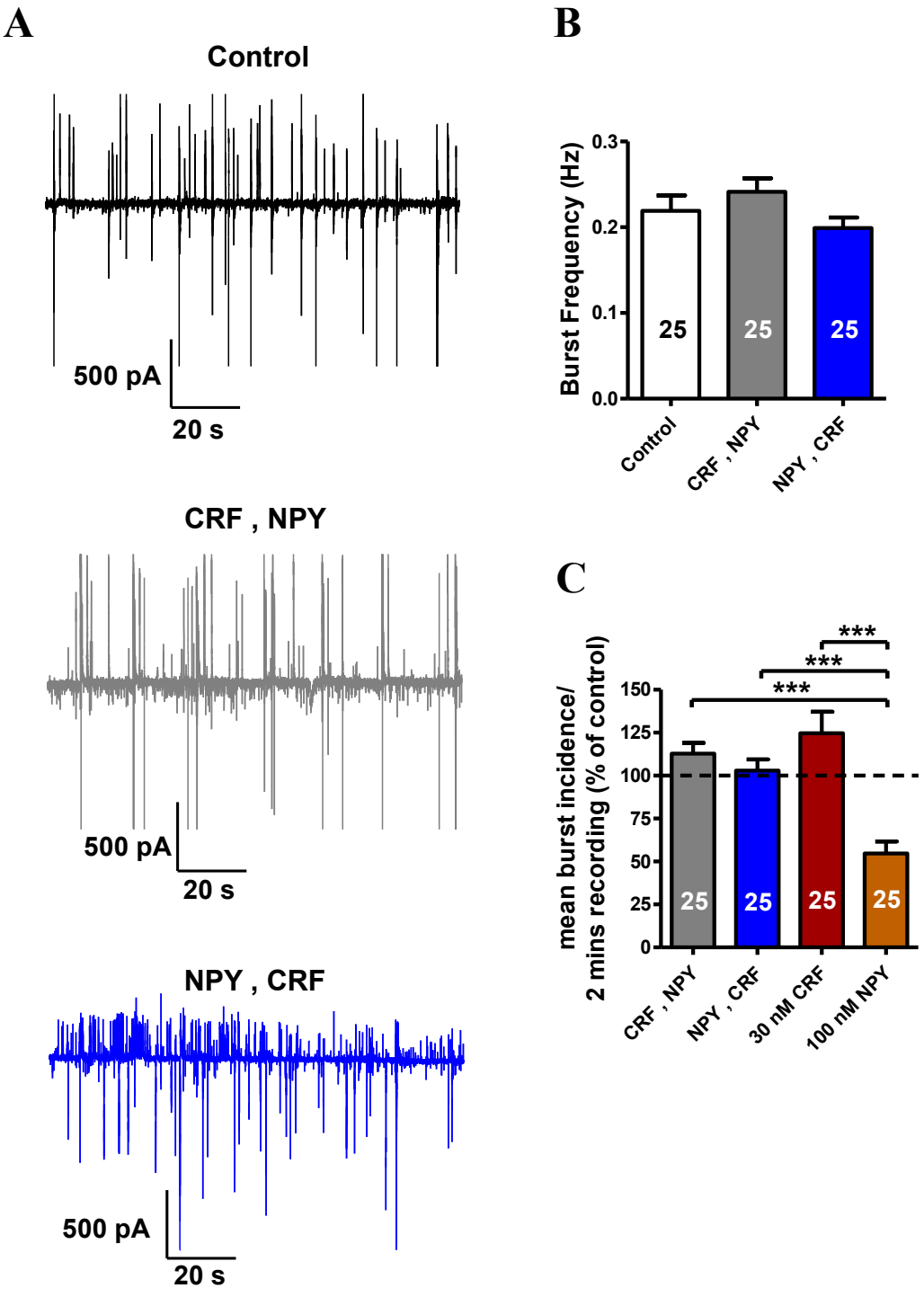
A
Control
500 pA
20 s
CRF , NPY
500 pA
20 s
NPY , CRF
500 pA
20 s
B
Burst Frequency (Hz)
0.3
0.2
0.1
0.0
25
25
25
Control
CRF , NPY
NPY , CRF
C
mean burst incidence/
2 mins recording (% of control)
150
125
100
75
50
25
0
***
***
***
25
25
25
25
CRF , NPY
NPY , CRF
30 nM CRF
100 nM NPY

Figure 3.19 Opposing neuropeptide treatment in BLA OTCs, occludes the effects on compound postsynaptic bursting activity.

(A) Representative current traces of neurons from control, CRF , NPY and NPY , CRF treated groups illustrating the frequency of compound postsynaptic bursts. (B) Analysis of bursting frequency suggests incubations with CRF , NPY and NPY , CRF resulted in no change of bursting activity in BLA OTCs between treated groups or compared to controls ($P>0.05$, one-way ANOVA with Tukey's *post hoc* test). (C) The 100 nM NPY treated group had significant reductions in the burst frequency compared to all other groups (***$P<0.001$, one- way ANOVA with Tukey's *post hoc* test). A total of 9833 sIPSCs and 9213 sEPSCs were analyzed for control neurons, 9870 sIPSCs and 9824 sEPSCs for CRF , NPY neurons and 9948 sIPSCs and 9364 sEPSCs for NPY , CRF treated neurons. The number of analyzed cells is presented for each treatment in the bar graph.

Figure 3.20

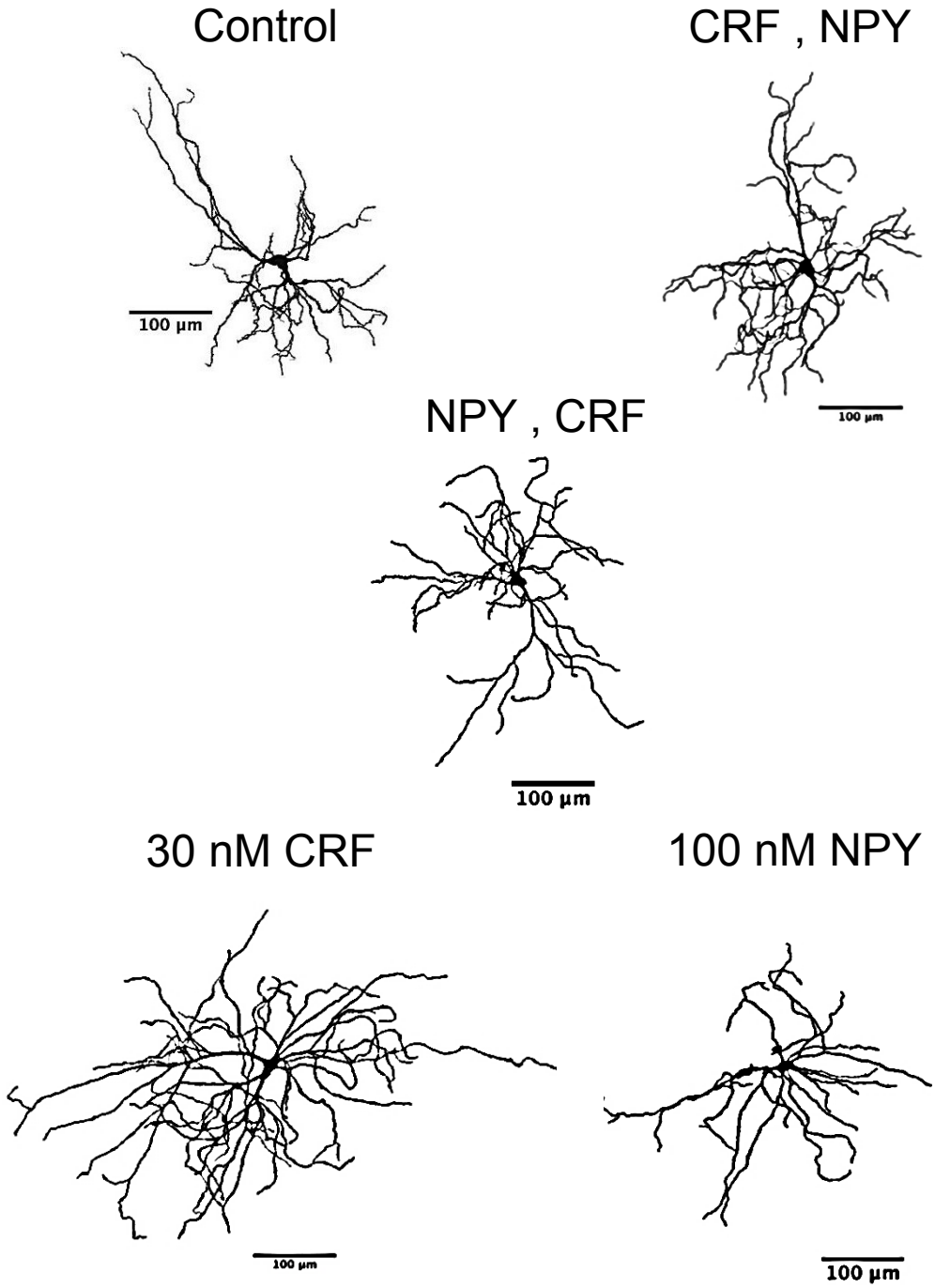

Figure 3.20 Representative reconstructed principal neurons from control, CRF , NPY and NPY , CRF-treated BLA OTCs.

Following electrophysiological recordings and filling of cells with neurobiotin, OTCs were fixed, stained and imaged. Reconstructions were made using the simple neurite tracer function in FIJI. Representative tracings of the total dendritic tree of principal neurons from control, CRF , NPY and NPY , CRF treated BLA OTCs. Neurons were chosen based on the their mean total dendritic length.

Figure 3.21

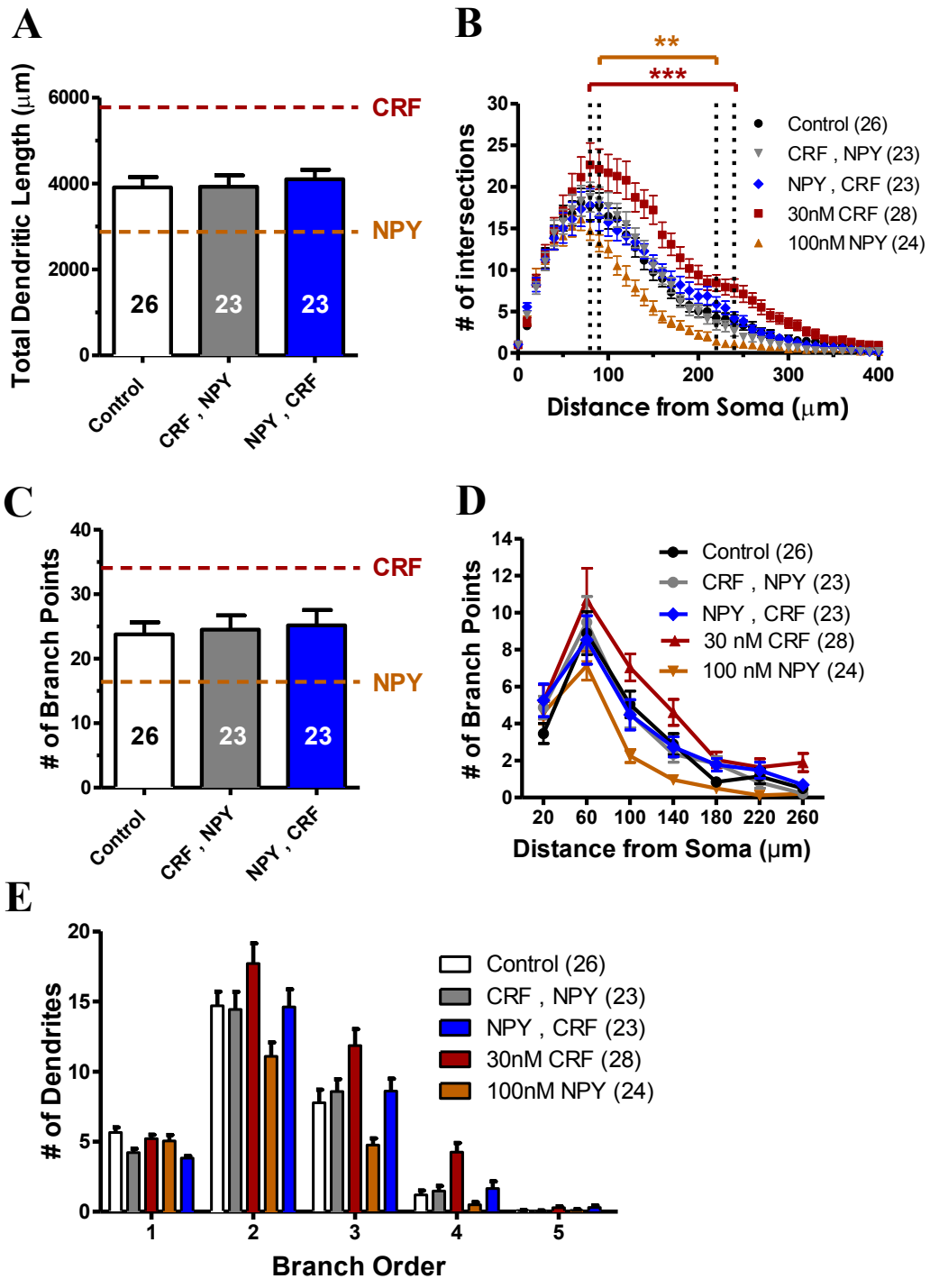
A
Total Dendritic Length (µm)
6000
4000
2000
0
CRF
NPY
26
23
23
Control
CRF , NPY
NPY , CRF
B
**
***
# of intersections
30
25
20
15
10
5
0
0
100
200
300
400
Distance from Soma (µm)
Control (26)
CRF , NPY (23)
NPY , CRF (23)
30nM CRF (28)
100nM NPY (24)
C
# of Branch Points
40
30
20
10
0
CRF
NPY
26
23
23
Control
CRF , NPY
NPY , CRF
D
# of Branch Points
14
12
10
8
6
4
2
0
20
60
100
140
180
220
260
Distance from Soma (µm)
Control (26)
CRF , NPY (23)
NPY , CRF (23)
30 nM CRF (28)
100 nM NPY (24)
E
# of Dendrites
20
15
10
5
0
1
2
3
4
5
Branch Order
Control (26)
CRF , NPY (23)
NPY , CRF (23)
30nM CRF (28)
100nM NPY (24)

Figure 3.21 Opposing neuropeptide treatment has no net effect on principal cell morphology in BLA OTCs.

(A) Analysis of total dendritic length demonstrates no change of the dendritic tree following CRF , NPY or NPY , CRF incubations compared to controls (P>0.05, one-way ANOVA with Tukey's *post hoc* test). (B) Following Sholl analysis with increasing concentric circles of 10 μm radii, the number of intersections was plotted versus distance from the soma, and analysis illustrates incubations with CRF , NPY or NPY , CRF did not result in any dendritic remodeling compared to controls (P>0.05, two-way ANOVA with Tukey's *post hoc* test). (C-E) Quantification of the number and localization of branch points revealed no changes following CRF , NPY or NPY , CRF incubations compared to controls (P>0.05, one-way ANOVA with Tukey's *post hoc* test). For reference, the mean values of 30 nM CRF (red) and 100 nM NPY (orange) alone, are denoted by dashed lines, but were not used in statistical analysis. The number of analyzed cells is presented for each treatment in the figure legend or bar graph.

Figure 3.22

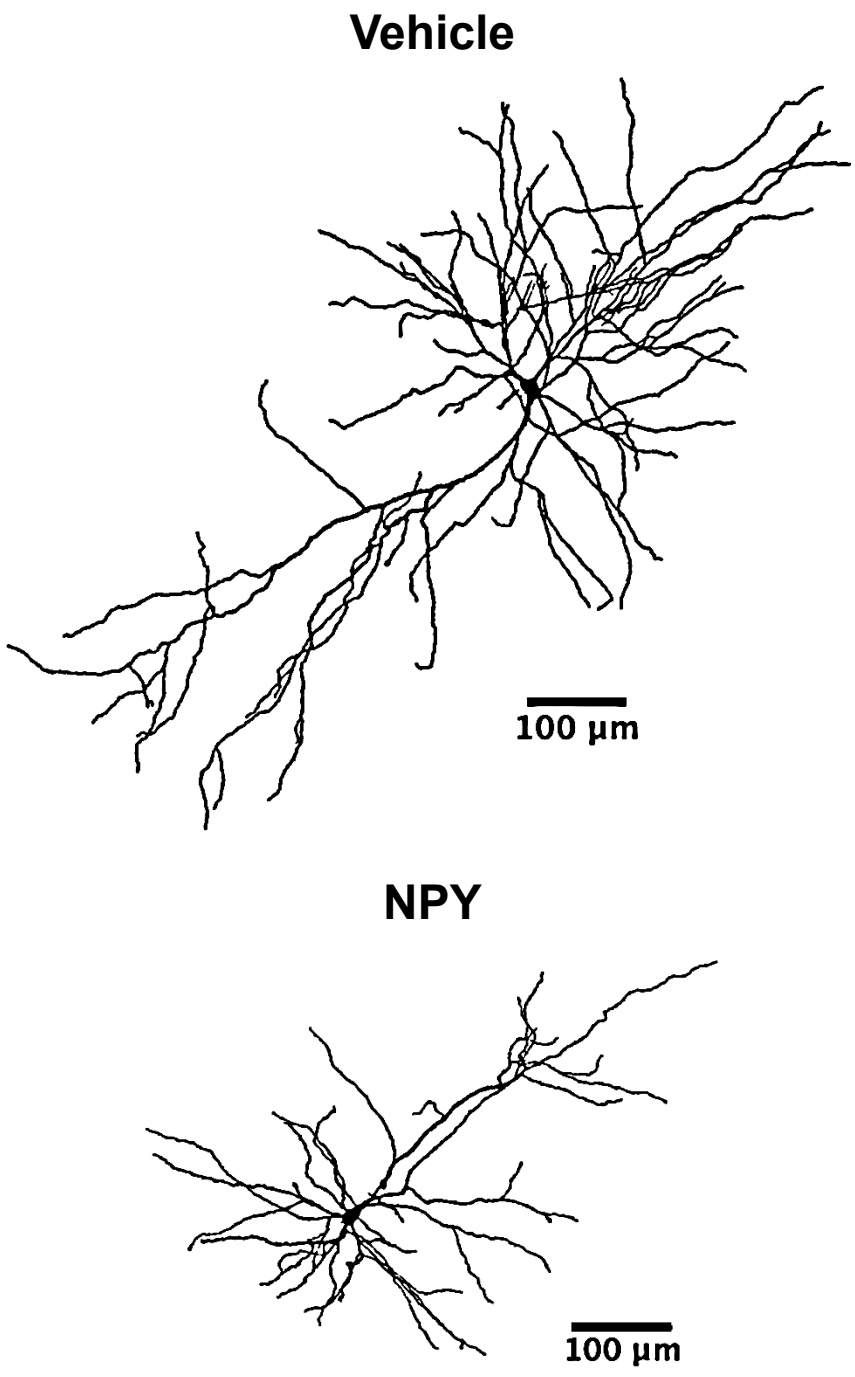

Figure 3.22 Representative reconstructed principal neurons following repeated injection of vehicle or NPY directly into the BLA *in vivo*.

Following electrophysiological recordings and filling of cells with neurobiotin, acutely-prepared slices were fixed, stained and imaged. Reconstructions were made using the simple neurite tracer function in FIJI. Representative tracings of the total dendritic tree of principal BLA neurons from vehicle and NPY injected animals. Representative neurons were chosen based on their mean total dendritic length.

Figure 3.23

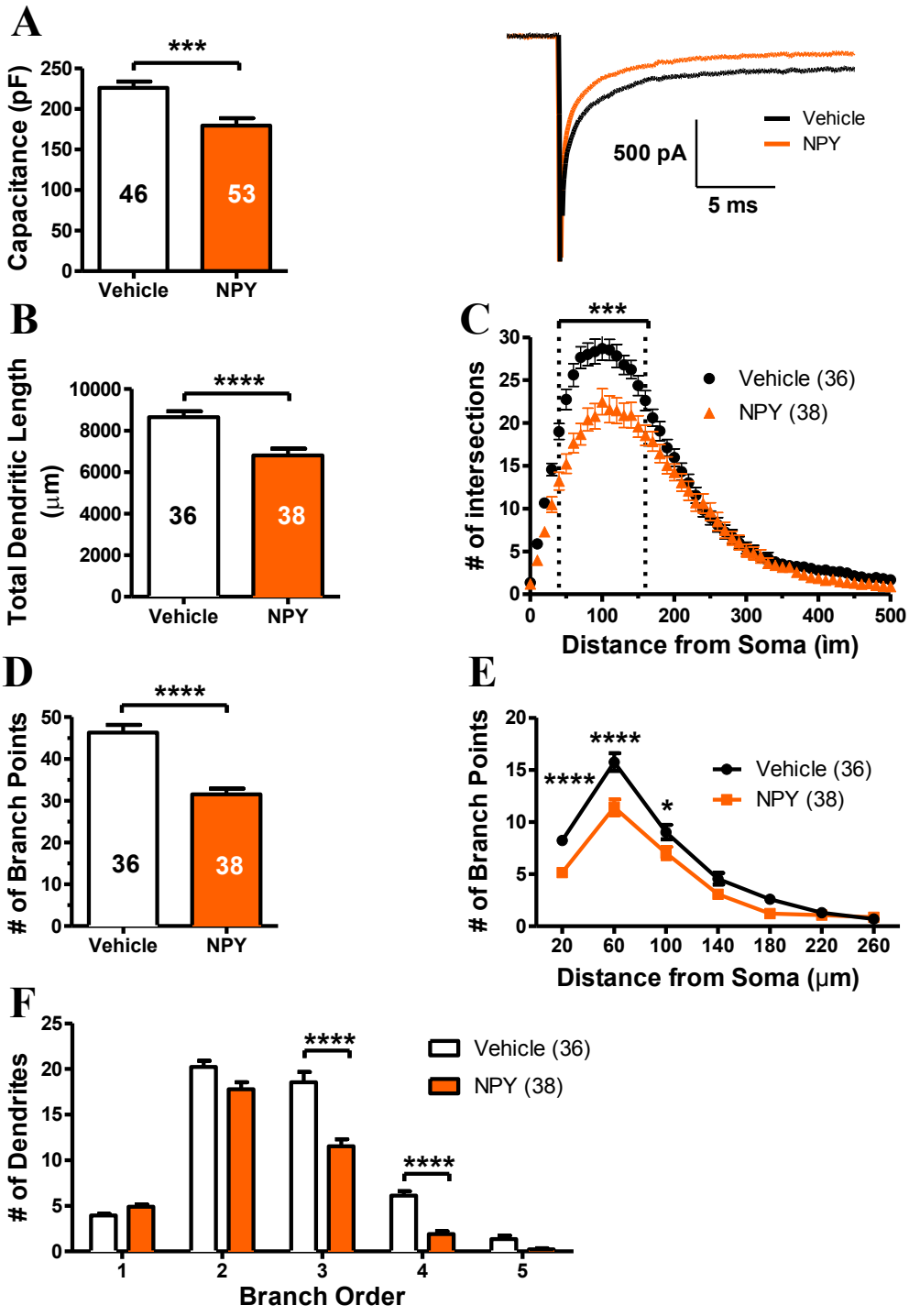
A
***
Capacitance (pF)
250
200
150
100
50
0
46
53
Vehicle
NPY
Vehicle
NPY
500 pA
5 ms
B
****
Total Dendritic Length (μm)
10000
8000
6000
4000
2000
0
36
38
Vehicle
NPY
C
***
# of intersections
30
25
20
15
10
5
0
0
100
200
300
400
500
Distance from Soma (im)
Vehicle (36)
NPY (38)
D
****
# of Branch Points
50
40
30
20
10
0
36
38
Vehicle
NPY
E
****
****
*
# of Branch Points
20
15
10
5
0
20
60
100
140
180
220
260
Distance from Soma (μm)
Vehicle (36)
NPY (38)
F
# of Dendrites
25
20
15
10
5
0
****
****
1
2
3
4
5
Branch Order
Vehicle (36)
NPY (38)

Figure 3.23 Repeated injection of NPY directly into the BLA reduces cell capacitance and the dendritic arbor of BLA principal neurons from *ex vivo* slices.

(A-left) NPY treatment reduced BLA principal neuron capacitance was compared to vehicle injected animals (***P<0.001, t-test). (Right) Representative traces of the capacitive transients following a -10 mV hyperpolarizing voltage step from -55 mV of vehicle and NPY-treated slices. (B) NPY treatment reduced the total dendritic length of BLA principal cells compared to vehicle injected animals (****P<0.0001, t-test). (C) Number of dendritic intersections per distance from the soma plotted from a Sholl analysis (10 μm radii), and analysis revealed the points along the dendritic tree where hypotrophy occurred following NPY injections (***P<0.001, two-way ANOVA with Tukey's *post hoc* test). (D-F) Quantitation of the number and position of dendritic branch points revealed a reduction in dendritic arbor exuberance following NPY injections compared to vehicle treated animals (*P<0.05, ****P<0.0001, two-way ANOVA with Tukey's *post hoc* test and t-test). (E) Consistent with total dendritic length measurements, the branching patterns of NPY-treated BLA OTC neurons are simplified, in the midproximal regions where the number of intersections is also reduced. (F) NPY actions on dendritic branching appeared to result in preferential reductions in the numbers of tertiary and quaternary dendritic branches. The number of analyzed cells is presented for each treatment in the figure legend or bar graph.

Figure 3.24

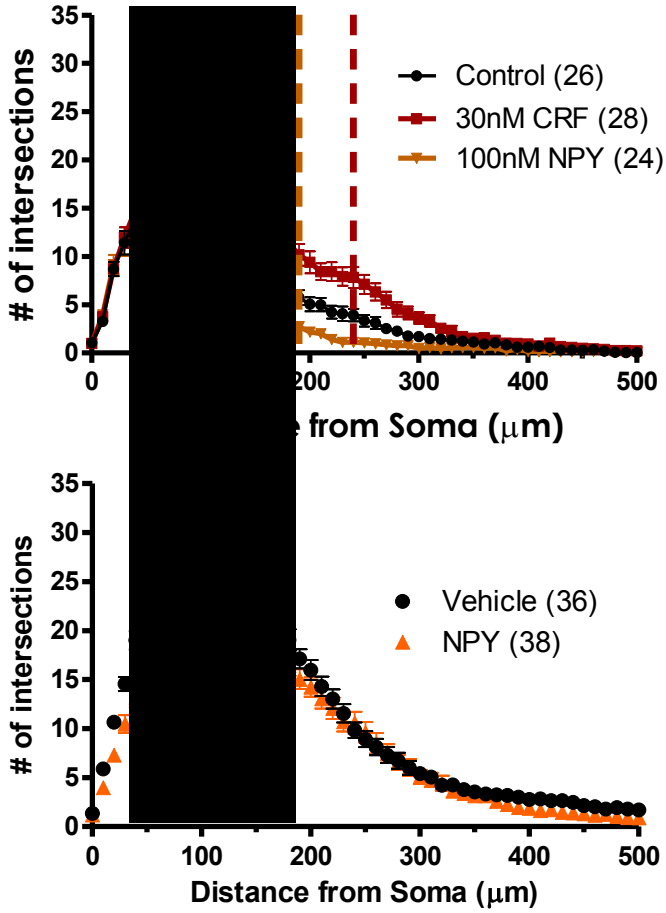

Figure 3.24 Region of principal neuron dendritic remodeling is conserved between BLA OTCs and acutely-prepared BLA slices.

Examination of the regions along the dendritic arbor where NPY- and CRF-mediated remodeling occurs in (top) BLA OTCs corresponds to the same distance from the soma as that of neurons from (bottom) acutely-prepared BLA slices. Note, in neurons from acute slices, this region is at the peak of the number of intersections, while in BLA OTCs, it represents a region on the downslope of the maximum number of intersections.

CHAPTER 4: Differential roles of NPY-receptor subtypes in mediating structural plasticity and long-term anxiolytic-like behavior

Introduction

Neuropeptide Y (NPY) is a 36 amino acid peptide belonging to a family of distinct biologically active peptides comprising NPY, peptide YY (PYY) and pancreatic polypeptide (PP) (Tatemoto et al., 1982, Holzer et al., 2012). NPY is translated from mRNA as a pre-pro-peptide and proteolytically cleaved by various enzymes before exocytotic release from large-dense-core vesicles in response to sustained depolarization. NPY is expressed centrally and in peripheral tissues, while considered to be the most abundant neuropeptide found in the mammalian brain (Lundberg et al., 1990, Kask et al., 2002). The major sites of NPY production in the CNS include the cortex, hippocampus, hypothalamus, basal ganglia and amygdala (Kask et al., 2002, Reichmann and Holzer, 2015). Physiologically, NPY plays a key role in numerous processes including energy homeostasis, food intake, circadian rhythm, processing of pain, seizures, cognition and relevant to our work, the modulation of emotionally affective behaviors and the stress response (for reviews, see (Reichmann and Holzer, 2015, Tasan et al., 2015).

In addition to its distinct expression patterns, the diversity in effects produced by NPY can also be attributed to activation of several different NPY receptor subtypes. To date, five different NPY receptors have been described in mammals (Y1, Y2, Y4, Y5 and Y6), although the Y6-receptor is non-functional in several mammals including non-human primates and humans, and is not expressed in rats (Michel et al., 1998, Bromee et al., 2006). PP is the preferential agonist for Y4-receptors, and NPY itself has very low affinity for this receptor subtype (Alexander et al., 2013). Interestingly, all NPY receptors are G-protein coupled receptors that are linked to G_i/G_o. Just like NPY itself, NPY receptors show distinct regional distributions with Y1- and Y2-receptors achieving the most pronounced expression

throughout the CNS and particular enrichment in limbic brain areas including the hippocampus, amygdala and hypothalamus (Dumont et al., 1998, Kask et al., 2002). Although these two receptors are often found in the same brain regions, their expression pattern shows a complementary distribution, which is likely a result of the postsynaptic and presynaptic localization of the Y1- and Y2-receptors, respectively (Caberlotto et al., 2000, Rostkowski et al., 2009, Stanic et al., 2011). The Y5-receptor is found in similar regions, but far less abundant and expression tends to coincide with that of the Y1-receptor (Wolak et al., 2003).

It is well established that NPY plays a crucial role in the regulation of physiological and behavioral responses in relation to stress and anxiety, fear conditioning and extinction, learning and memory, etc. [for review see, Sah and Geracioti (2013), Reichmann and Holzer (2015), Tasan et al. (2015)]. The anxiolytic action of NPY is primarily attributed to activation of Y1-receptors in the amygdala, although other brain regions do play a role (Heilig et al., 1993). Injection of Y1-selective antagonists BIBO3304 and BIBP3226, block the anxiolytic actions of NPY in several behavioral paradigms, while direct injection of Y1-selective agonists promote anxiolysis (Sajdyk et al., 1999b, Kask et al., 2001a, Sorensen et al., 2004). Genetic manipulations also corroborate the anxiolytic actions of NPY being attributed to Y1-receptor activation, as Y1-receptor knockout mice are anxiogenic, while overexpression renders mice less anxious (Karl et al., 2006, Bertocchi et al., 2011, Olesen et al., 2012b).

Conversely, evidence strongly suggests activation of the Y2-receptor is anxiogenic, likely resulting from its presynaptic localization and ability to function as an autoreceptor to diminish NPY and GABA release (Caberlotto et al., 2000). Y2-selective agonists promote anxiety-like behavior in the EPM, as well as SI paradigms, while blocking the Y2-receptor with selective antagonists or intra-amygdalar deletion of the receptor is anxiolytic (Nakajima

et al., 1998, Sajdyk et al., 2002a, Sajdyk et al., 2002b, Bacchi et al., 2006, Tasan et al., 2010, Kallupi et al., 2014). It should be noted that differences in genetic background of animals tested, brain regions investigated and dose used can produce negative or contradictory findings to the ones stated above, hence further studies are needed to fully elucidate the downstream consequences of Y2-receptor activation (Kask et al., 1998, Sajdyk et al., 2002a, Zambello et al., 2011).

Of the three major receptor subtypes found in limbic regions of the mammalian CNS, the Y5-receptor is by far the least well characterized and effects following activation of this receptor are still somewhat controversial. In an early study, ICV injection of the Y5-selective antagonist CGP71683A failed to produce any effect on anxiety-related behavior in the SI and EPM tests, however, a more recent study revealed a novel Y5-antagonist, LuAA33810, produced anxiolytic activity in the SI test (Kask et al., 2001b, Walker et al., 2009). Activation of Y5-receptors with a selective agonist ([cPP(1-7),NPY(19-23),Ala31,Aib32,Gln34]hPP) appears to mediate anxiolysis in EPM, open field test and SI tests (Sorensen et al., 2004, Morales-Medina et al., 2012). Genetic studies contribute to the confusion, as both Y5-receptor knockout mice and amygdalar overexpression of the Y5-receptor do not produce any effect on anxiety-like behavior, possibly due to global changes in these peptides (Olesen et al., 2012a, Ito et al., 2013). A number of studies indicate the behavioral effects mediated by Y5-receptors may require interaction with other NPY receptor subtypes. Firstly, microinjection of the Y2-selective agonist NPY(3-36) produced a bi-directional dose-response curve with low doses producing anxiogenesis and high doses resulting in anxiolysis. Pretreatment with a Y5-antagonist blocked this effect (Sajdyk et al., 2002a). Furthermore, studies indicate that cells and fibers in the BLA co-localize both Y1 and Y5-receptors and co-expression of these

receptors *in vitro,* can result in heterodimerization, altered pharmacology and slower internalization rates (Wolak et al., 2003, Gehlert et al., 2007). Recently, behavioral analysis of conditional knockout of Y1-receptors in Y5-receptor expressing neurons in mice, resulted in an anxiogenic phenotype suggesting that these receptors do interact to a certain extent *in vivo* (Longo et al., 2014, 2015).

The majority of the acute anxiolytic effects of NPY appear to be mediated via activation of the Y1-receptor, with the potential for the Y5-receptor playing some sort of role. NPY has been identified as a key signaling molecule in the development of stress resilience, both in animals and humans, however, the receptor subtype responsible for mediating its effect on long-term behavior is unknown. In this study, we aimed to determine which NPY receptor(s) are responsible for mediating NPY-induced stress resilience. First, we used our novel OTCs of BLA to determine which receptor(s) mediate the morphological effects of NPY by incubating long-term with NPY-receptor selective agonists and in a subset of experiments, NPY and a selective antagonist or antagonist alone. Lastly, we wanted to confirm our OTC results *in vivo* by injecting NPY, NPY-receptor selective agonists or NPY with selective antagonists directly into the BLA, measuring SI and analyzing morphological data from *ex vivo* filled principal neurons.

Results indicate that incubation with F^{7},P^{34}-NPY, a Y1-selective agonist , does not affect any electrophysiological parameters examined or cause changes in the dendritic structure in BLA OTCs or in acutely prepared slices following repeated injection *in vivo*. Behavioral data from another member of the Colmers, lab Ms. Ana Miranda, suggests that although repeated injection of F^{7},P^{34}-NPY causes an acute increase in SI time (decreased anxiety), this effect does not persist and culminate in long-term anxiolytic-like responses or in

dendritic remodeling. Long-term incubation in BLA OTCs with the Y2-selective agonist [ahx$^{5-24}$]NPY results in similar effects to those observed with CRF incubations, namely increases in cell capacitance, frequency of sEPSCs and dendritic hypertrophy. This is consistent with the concept of Y2-receptor mediating anxiogenic responses in the BLA. Unfortunately, we have not performed repeated injections of this compound *in vivo*, but our collaborator in Chicago, Dr. Janice Urban is currently conducting these experiments. With my expert guidance, Ms. Miranda, conducted experiments with the Y5-selective agonist in OTCs. Although I did have a hand in producing some of this data, I am not incorporating it as results in this thesis. However, the story would not be complete without acknowledging the results and therefore, I am including morphological data in graphical form to be reviewed as part of Appenidx I. Her results indicate cPP incubations in BLA OTC resulted in hypotrophy of the dendritic architecture of principal neurons. Furthermore, the NPY-mediated dendritic hypotrophy can be blocked via co-incubation with a Y5-antagonist CGP71683A (CGP), which confirms the role of the Y5-receptor in mediating NPY's dendritic remodeling. Interestingly, co-incubation with NPY and the Y5-antagonist actually produced hypertrophy, which is harmonious with Y2-receptor activation. Incubation with the Y5-antagonist alone produced mostly non-significant trends of expansion to the dendritic arbor, which suggests there may be some constitutive Y5-receptor activity, or more likely endogenously released NPY within the slice is prevented from activating Y5-receptors. Behavioral data from Ms. Miranda suggests repeated injection of cPP results in a similar acute and long-term anxiolytic-like response as NPY. At this time, there are unsatisfactory numbers of subjects for *in* vivo experiments with NPY and CGP (Y5-antagonist) to make any concrete conclusions but these experiments are in the works. Nevertheless, repeated injection of cPP directly into the BLA

resulted in dendritic hypotrophy that appeared to occur at more distal regions of the dendritic arbor compared to NPY. In collaboration with Ms. Ana Miranda, we have determined that unlike many of the acute anxiolytic effects of NPY that are mediated by the Y1-receptor, NPY-induced stress resilience is not attributed to Y1-receptor activation, rather the Y5-receptor. Furthermore, dendritic remodeling occurs in opposing fashion in response to repeated activation of the Y2- and Y5-receptors causing hypertrophy and hypotrophy, respectively.

Methods

All methods were identical as previously described in Chapter 2 and 3. For detailed description, please refer back to Chapters 2 and 3.

Drugs

Long-term incubation in BLA OTCs were performed with selective agonists for Y1-receptor (F^7,P^{34}-NPY), Y2-receptor ([ahx$^{5-24}$]NPY, (ahx)) and the Y5-receptor (cPP) at 0, 1, 10 and 100 nM (final). In a subset of experiments, 10 nM NPY was co-incubated with the Y5-antagonist CGP (30 nM) and CGP (30 nM) alone. For *in vivo* studies, 10 pmol of F^7,P^{34}-NPY or cPP and in a subset of animals, 10 pmol cPP with 1 pmol CGP was injected bi-laterally each day for 5 consecutive days. The compounds F^7,P^{34}-NPY, [ahx$^{5-24}$]NPY and cPP were generous gifts from Dr. A. G. Beck-Sickinger (Leipzig, Germany), while the rest of test compounds were bought from Polypeptide Group (San Diego, CA, USA).

Results

Long-term incubation with the Y1-agonist F^7,P^{34}-NPY has no effect on postsynaptic properties in BLA OTCs.

Many of the acute anxiolytic effects of NPY are mediated by activation of the Y1-receptor. Therefore, we first incubated our BLA OTCs with increasing concentrations of the Y1-selective agonist F^7,P^{34}-NPY to determine if the Y1-receptor also mediated NPY's long-term electrophysiological and morphological effects. To our surprise, there was no effect on any passive membrane properties including RMP or rheobase of BLA OTC principal neurons (P>0.05, Fig.4.1A-B). Furthermore, F^7,P^{34}-NPY had no effect on any parameter of I_h measured including amplitude, density (data not shown), voltage dependency of activation (data not shown), or activation kinetics (P>0.05, Fig.4.2A-D). Finally, no effect was observed in other intrinsic conductances as measured by the "early current" (data not shown) or on cell capacitance (P>0.05, Fig.4.2E).

Repeated Y1-receptor activation does not produce any substantial effects on synaptic activity in BLA OTCs.

Analysis of synaptic activity following prolonged incubation with F^7,P^{34}-NPY revealed no significant effects compared to controls (P>0.05, Fig.4.3A-C). Analysis of compound postsynaptic bursts revealed F^7,P^{34}-NPY did not significantly affect bursting activity compared to controls (P>0.05, Fig.4.3D-F).

F^7,P^{34}-NPY does not affect morphology of principal neurons in BLA OTCs

Tracing, reconstruction and Sholl analysis revealed long-term incubation with F^7,P^{34}-NPY does not result in remodeling of principal neuron dendritic structure in BLA OTCs (Fig.4.4). There were no significant changes in any morphological parameter measured for BLA OTCs incubated with F^7,P^{34}-NPY including total dendritic length, number of intersections as a function of distance from the soma, number of branch points, number of branch points as a function of distance from the soma or in branching order compared to controls ($P>0.05$, Fig.4.5A-E).

Repeated injection of F^7,P^{34}-NPY directly into the BLA in vivo causes an acute but no long-term behavioral effect or changes in the dendritic architecture.

We were interested in determining if NPY-induced stress resilience and remodeling of the dendritic architecture is mediated by the Y1-receptor *in vivo*, therefore, we analyzed SI and changes to the dendritic arborization of filled neurons from *ex vivo* slices from repeated F^7,P^{34}-NPY, intra-BLA injected rats. Results indicate that repetitive stimulation of the Y1-receptor mediates an acute anxiolytic effect, as SI time was increased at days 1 and 5, however unlike NPY, this effect does not persist past day 5 (Fig.4.6A). Examination of reconstructed principal neurons from control and F^7,P^{34}-NPY treated animals (Fig.4.6B), demonstrates that similarly to BLA OTCs, remodeling of does not occur *in vivo* (Fig.4.7A-F).

Long-term Y2-agonist ([ahx$^{5-24}$]NPY) incubations in BLA OTCs results in similar electrophysiological effects to those from CRF-treated principal neurons in BLA OTCs.

The effects of long-term treatment with the Y2-agonist produced comparable postsynaptic effects to those from CRF treatment. Specifically, there was no change in RMP (P>0.05), but excitability was reduced (increase in rheobase) for the 100 nM ahx treated group compared to controls and the 1 nM ahx group (Ctrl: 214.4 ± 33.38 pA, 100 nM ahx: 364.8 ± 43.3 pA (P<0.05), 1 nM ahx: 188.6 ± 26.2 pA (P<0.01); Fig.4.8A-B). Also, 100 nM ahx reduced input resistance compared to controls, suggesting ahx incubations may result in opening of some unknown ion channels (Ctrl: 108.4 ± 8.3 MΩ, 100 nM ahx: 69.3 ± 6.4 MΩ, (P<0.001), Fig4.8C). Analysis of the intrinsic I_h reveals that repeated Y2-receptor activation enhances the amplitude of I_h at the -145 mV, -135 mV and -125 mV voltage steps (-145 mV: P<0.001, -135 mV: P<0.001, -125 mV: P<0.05; Fig.4.9A). However, when we normalized for potential differences due to changes in cell size and examined I_h density, there was no significant difference observed between any of the ahx groups and controls (P>0.05, Fig.4.9B). Additionally, there was no difference in the estimated voltage dependency of I_h activation (data not shown), or in the kinetics of I_h activation (both Tau_{fast} or Tau_{slow}, P>0.05, Fig.4.9C-E). Similarly to the effects with CRF, incubation with 100 nM ahx also resulted in a gain of an early, IIR at the -145 mV, -135 mV, and -125 mV voltage steps, compared to controls (-145 mV: P<0.001, -135 mV: P<0.001, -125 mV: P<0.05; Fig.4.10A-B). The net current elicited is represented in Figure 4.10C, which reversed around -100 mV. Finally, capacitance was increased in only the 100 nM ahx group compared to controls and all lower ahx concentrations (Ctrl: 151.5 ± 8.9 pF, 100 nM ahx: 205.4 ± 15.6 pF (P<0.001); Fig.4.10D).

100 nM ahx increases excitatory drive onto BLA OTC principal neurons.

sEPSCs and sIPSCs following long-term incubation with ahx were analyzed as previously described. Incubation with 100 nM ahx had no effect on either mean sIPSC amplitude or frequency or on sEPSC amplitude compared to controls (Data not shown; $P>0.05$). The most prominent effect produced by ahx was a robust increase in the mean frequency of sEPSCs compared to controls and was confirmed using cumulative probability plots and the K-S test (Ctrl: 221.5 ± 32.2 ms, 100 nM ahx: 110.6 ± 15.0 ms ($P<0.01$); Fig.4.11C-D). Lastly, bursting activity was increased following incubation with 100 nM ahx compared to controls (Ctrl: 0.19 ± 0.015 Hz, 100 nM ahx: 0.27 ± 0.028 Hz, $P<0.05$, Fig.4.11E-G). Overall, incubation with 100 nM ahx appears to have little effect on sIPSCs, but tends to increase excitatory drive due to increases in the frequency of these events, which also enhances compound bursting activity.

Chronic treatment with ahx results in hypertrophy of the dendritic arbor of principal neurons in BLA OTCs.

Tracing, reconstruction and Sholl analysis revealed extensive hypertrophy of the dendritic architecture in BLA OTC principal neurons following ahx treatment in a similar fashion to CRF treatment. Note the increased complexity in the reconstruction of the 100 nM ahx treated BLA OTC principal neuron compared to control in Figure 4.12. 100 nM ahx incubations of BLA OTCs resulted in increased total dendritic length compared to controls (Ctrl: 3225 ± 438 μm, 100 nM ahx: 4925 ± 551 μm, ($P<0.05$); Fig.4.13A). The increased number of intersections as measured by Sholl analysis revealed hypertrophy was attributed to increased dendrites in the 50 - 200 μm range from the soma in 100 nM ahx compared to

controls (***P<0.001, Fig.4.12B). Additionally, there were significant increases between 130 and 200 μm from the soma between the 10 nM ahx treated groups and controls (**P<0.01, Fig.4.13B). Chronic ahx treatment also resulted in heightened branching as exemplified by increased branching points in the 100 nM ahx treated group compared to controls (Ctrl: 21.4 ± 3.4 branches, 100 nM ahx: 32.7 ± 2.9 branches, (**P<0.001), Fig.4.13C). The alteration in branching was attributed to increased branch points at 20 μm, 60 μm, and 100 μm from the soma (20 μm **P<0.01, 60 μm ****P<0.0001, and 100 μm *P<0.05, Fig.4.13D). Finally, the ahx-induced increases in branch points were preferentially located at secondary and tertiarary branch points compared to controls (Secondary; Ctrl vs. 100 nM ahx: *P<0.05, 10 nM ahx vs 100 nM ahx: **P<0.001; Tertiary; Ctrl vs. 100 nM ahx: ***P<0.001, 1 nM ahx vs. 100 nM ahx: ***P<0.001, 10 nM ahx vs. 100 nM ahx: ***P<0.001; Fig.4.13E).

Discussion

The aim of this study was to investigate the NPY-receptor subtype responsible for mediating dendritic hypotrophy and stress resilience. Although there are two known CRF-receptors, CRF-R1 and CRF-R2, only CRF-R1 is expressed in the BLA (Bale and Vale, 2004). Furthermore, as previous studies indicating the anxiogenic properties of CRF in the BLA are mediated via CRF-R1s, we presume the effects discussed in Chapter 3 are mediated via the CRF-R1, and therefore did not further investigate the CRF-R subtype responsible for our effects in BLA OTCs. At the outset of these experiments, we hypothesized that Y2-receptor activation would result in similar morphological changes to those from CRF-treated neurons, as both of these compounds are known to be anxiogenic in nature. Conversely, we hypothesized that repeated activation of the Y1-receptor would cause dendritic hypotrophy and reductions in the stress-related behavior, as measured by SI. To our surprise, repeated Y1-receptor activation *in vivo* results in an acute anxiolytic response, but does not contribute to long-term stress resilience, nor does it affect the dendritic architecture of principal cells filled from *ex vivo* slices or OTCs. Repeated treatment with the Y2-receptor agonist in BLA OTCs causes enhanced excitatory drive onto principal neurons and dendritic hypertrophy that are similar to the effects observed following CRF exposure, and is consistent with Y2 exhibiting anxiogenic activity. Finally, Ms. Ana Miranda's results suggest that NPY-induced stress resilience is mediated by repeated Y5-receptor activation *in vivo* and is coupled to principal neuron dendritic hypotrophy from *ex vivo* slices and OTCs (Appendix I). Furthermore, the effects of NPY on dendritic morphology can be blocked by co-incubation with the Y5-selective antagonist in OTCs.

With such a high proportion of Y1-receptors in the BLA, and numerous studies showing the Y1-receptor mediates many of the acute anxiolytic effects of NPY, we were amazed to find that it does not contribute to NPY-mediated stress resilience or dendritic remodeling. Although all NPY-receptors primarily couple to $G_{i/o}$ proteins, which leads to a decrease in cAMP, due to inhibition of adenylate cyclase, different receptor subtypes may preferentially activate certain intracellular signal transduction systems, including but not limited to PKA, PI3K, MAPK, and modulation of Ca^{2+} and K^{+} channels, which could account for their diverse responses (Herzog et al., 1992, Cabrele and Beck-Sickinger, 2000). Furthermore, *in vitro* studies indicate the Y1-receptor is more susceptible to desensitization and internalization when bound by agonists, compared to Y2- and Y5- receptors (Parker et al., 2002a, Parker et al., 2002b, Holliday et al., 2005). Although this study did not address this specific question the use of biased agonists and fluorescently tagged receptors could be used to tease out the differences observed between prolonged exposure to Y1- and Y5-selective agonists.

The effects of Y2-agonist incubations in BLA OTCs were similar to those observed for repeated CRF application, thereby providing further evidence as to the anxiogenic nature of this receptor. These results help to explain the lack of a concentration effect noted with prolonged NPY incubation in BLA OTCs, as higher concentrations of NPY would result in activation of a heterogeneous population of receptors. In addition to the effects on synaptic activity and morphology, ahx-treated neurons appear to also gain an inwardly rectifying conductance, which reversed around -95 mV. The reduction in input resistance corroborates this assumption. This is likely a gain of a GIRK current, however, further studies would be needed to fully support this hypothesis.

As mentioned, the experiments involving the Y5-receptor are part of Ms. Miranda's thesis work, but are essential to discuss in this body of work. The effects on capacitance and morphology are similar to those from the NPY studies, which suggest Y5-treated neurons are likely smaller in *ex vivo* slices and OTCs (Appendix I). However, unlike NPY, there appears to be a dose-dependent effect with the Y5-agonist. It is plausible to suggest the lack of a dose-dependent effect of NPY is due to a heterogeneous activation Y2- and Y5-receptors, thereby limiting the overall hypotrophic effects. The regions of the dendritic arbor that remodel in response to the Y5-agonist appear similar to those of NPY-treated principal neurons in OTCs, however, in *ex vivo* principal neurons, the effects appear to be more distal than the effects of NPY. Although it should be noted, there are only 3 animals analyzed for changes in the dendritic structure and 3 have yet to be analyzed.

Co-incubation with NPY and the Y5-antagonist, CGP, prevented NPY-mediated hypotrophy in BLA OTC, and actually caused hypertrophy of principal neurons (Appendix I), likely due to NPY activating Y2-receptors, while being prevented from binding and stimulating Y5-receptors. At this point, we cannot make any conclusions with the co-injection of NPY and CGP *in vivo,* as there is only data from one animal.

For the first time, a collaborative effort by Ms. Ana Miranda and myself, identified the Y5-receptor as the receptor responsible for mediating NPY-induced long-term anxiolytic-like effects and dendritic hypotrophy. This should aid in the development of potential treatment options for patients suffering from various forms of anxiety-related disorders. Also, we expanded on the growing evidence for the link between bi-directional structural plasticity in the BLA and stress-related behavior. This work further validates the OTC model as a suitable

technique to investigate the cellular and molecular mechanisms mediating NPY-induced stress resilience and vulnerability, which will be the topic of the next chapter.

Figure 4.1

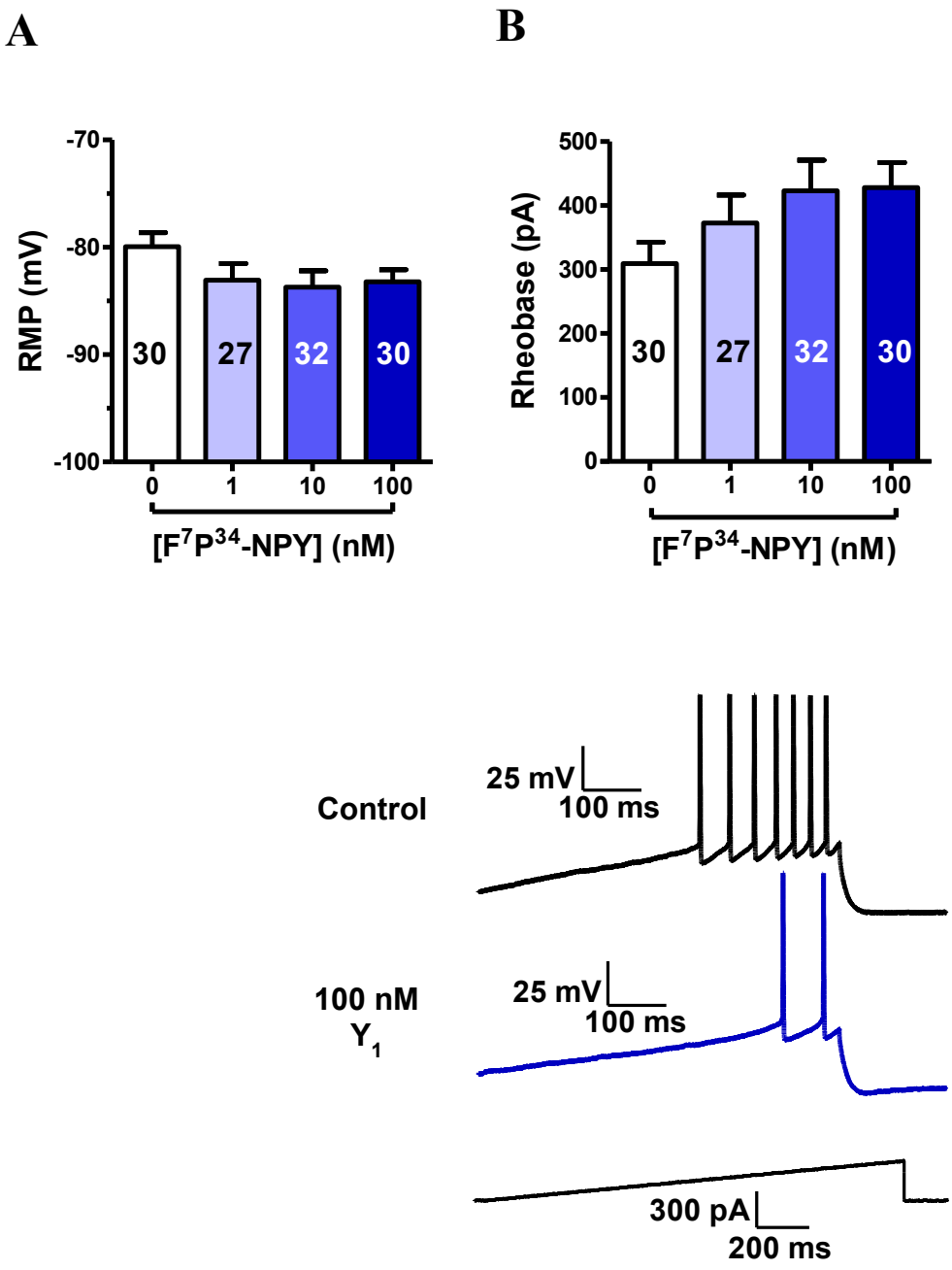
A
B
RMP (mV)
-70
-80
-90
-100
30
27
32
30
0
1
10
100
[F7P34-NPY] (nM)
Rheobase (pA)
500
400
300
200
100
0
Control
25 mV
100 ms
100 nM
Y1
300 pA
200 ms

Figure 4.1 Repeated Y1-receptor incubations does not affect passive membrane properties in BLA OTCs.

Incubations of BLA OTCs with the Y1-agonist, F^7P^{34}-NPY did not alter principal cell (A) RMP or (B, top) rheobase compared to controls (P>0.05, one-way ANOVA with Tukey's *post hoc* test). (B, bottom) Representative voltage traces following a series of current ramps. The number of analyzed cells is presented for each treatment in the figure legend or bar graph.

Figure 4.2

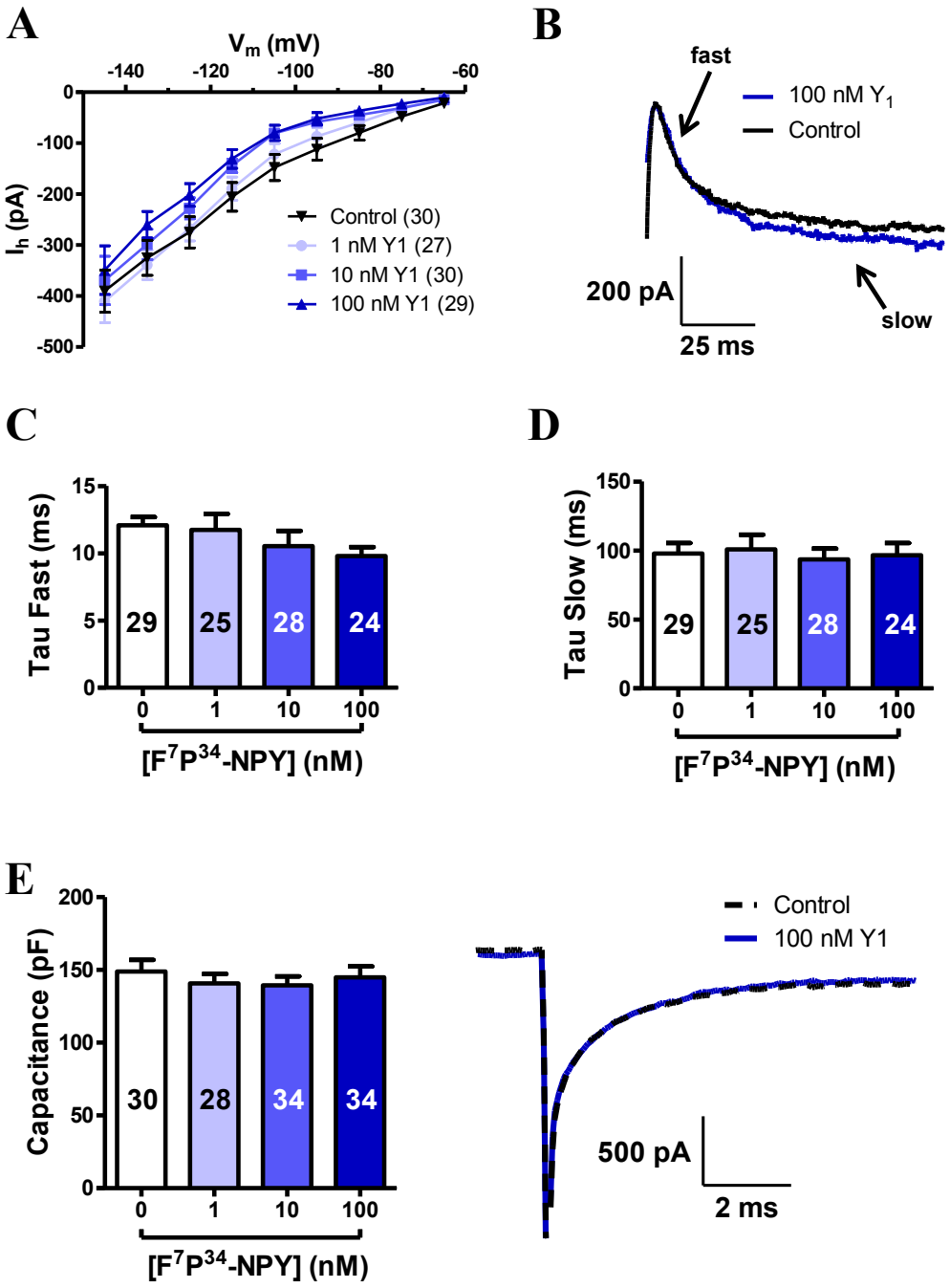
A
V_m (mV)
-140
-120
-100
-80
-60
0
-100
-200
-300
-400
-500
I_h (pA)
Control (30)
1 nM Y1 (27)
10 nM Y1 (30)
100 nM Y1 (29)
B
fast
100 nM Y_1
Control
200 pA
25 ms
slow
C
Tau Fast (ms)
15
10
5
0
29
25
28
24
0
1
10
100
[F^7P^{34}-NPY] (nM)
D
Tau Slow (ms)
150
100
50
0
29
25
28
24
0
1
10
100
[F^7P^{34}-NPY] (nM)
E
Capacitance (pF)
200
150
100
50
0
30
28
34
34
0
1
10
100
[F^7P^{34}-NPY] (nM)
Control
100 nM Y1
500 pA
2 ms

Figure 4.2 Incubation with the Y1-agonist does not affect any property of I_h, or affect capacitance in BLA OTCs.

Following increasing hyperpolarizing voltage steps from -55 mV, analysis revealed incubation with the Y1-agonist did not alter any property of I_h, including; (A) I_h amplitude, (B) activation kinetics such as (C) tau fast or (D) tau slow (P>0.05, two- and one-way ANOVA with Tukey's *post hoc* test). (E, left) Additionally, the Y1-agonist did not cause a reduction in measured capacitance. (E, right) Representative current traces of the capacitive transient following a -10 mV voltage step from -55 mV of control and 100 nM Y1-agonist treated neurons The number of analyzed cells is presented for each treatment in the figure legend or bar graph.

Figure 4.3

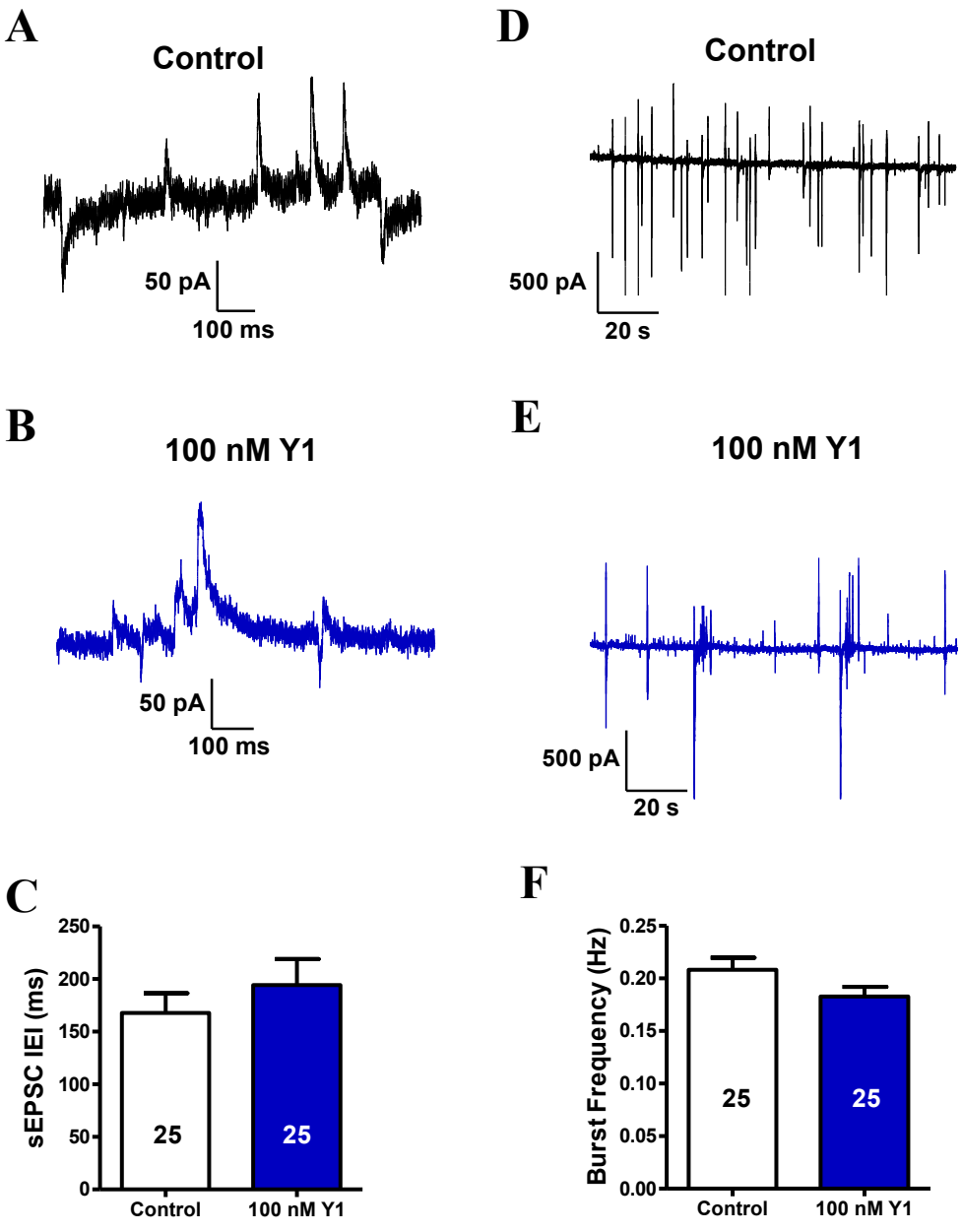
A
Control
50 pA
100 ms
D
Control
500 pA
20 s
B
100 nM Y1
50 pA
100 ms
E
100 nM Y1
500 pA
20 s
C
sEPSC IEI (ms)
250
200
150
100
50
0
25
25
Control
100 nM Y1
F
Burst Frequency (Hz)
0.25
0.20
0.15
0.10
0.05
0.00
25
25
Control
100 nM Y1

Figure 4.3 100 nM Y1-agonist incubations has no affect on synaptic activity of BLA OTC principal neurons.

Representative current traces of sIPSCs and sEPSCs from (A) control and (B) 100 nM Y1-agonist incubated principal neurons held at -55 mV. (C) Analysis of mean sEPSC IEI revealed no change in frequency of sEPSCs following 100 nM Y1-agonist incubations compared to controls ($P>0.05$, t-test). Representative current traces of neurons from (D) control and (E) 100 nM Y1-agonist incubated groups illustrating the frequency of compound postsynaptic bursts. (F) Analysis of bursting frequency suggests 100 nM Y1-agonist incubation, does not significantly affect bursting activity in BLA OTCs ($P>0.05$, t-test). A total of 9828 sIPSCs and 9975 sEPSCs were analyzed for control neurons and 10000 sIPSCs and 9597 sEPSCs for 100 nM Y1-agonist incubated neurons. The number of analyzed cells is presented for each treatment in the figure legend or bar graph.

Figure 4.4

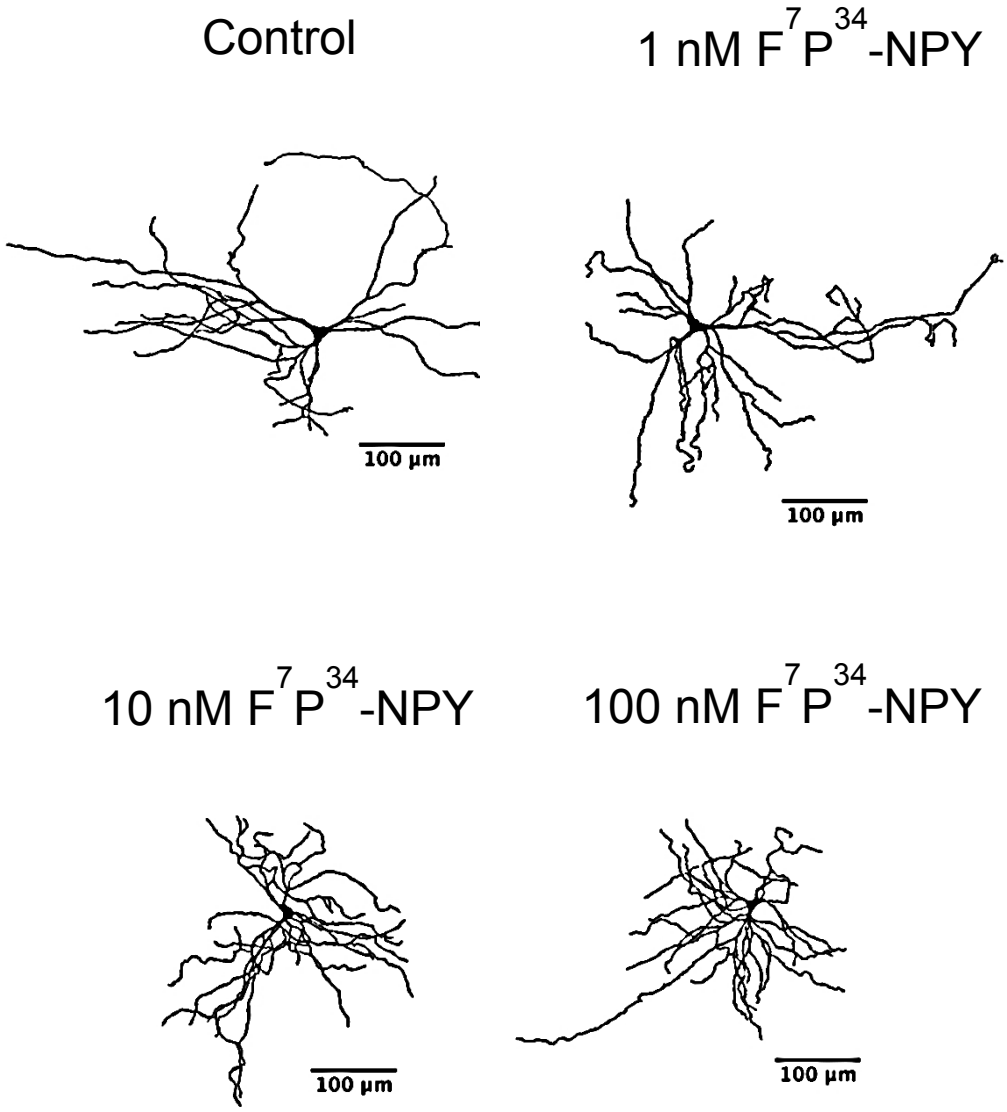
Control
1 nM F7P34-NPY
100 µm
100 µm
10 nM F7P34-NPY
100 nM F7P34-NPY
100 µm
100 µm

Figure 4.4 Representative reconstructions of principal neurons from Y1-agonist-treated BLA OTCs.

Following electrophysiological recordings and filling of cells with neurobiotin, OTCs were fixed, stained and imaged. Reconstructions were made using the simple neurite tracer function in FIJI. Representative tracings of the total dendritic tree of principal neurons from 0, 1, 10 and 100 nM Y1-agonist treated BLA OTCs.

Figure 4.5

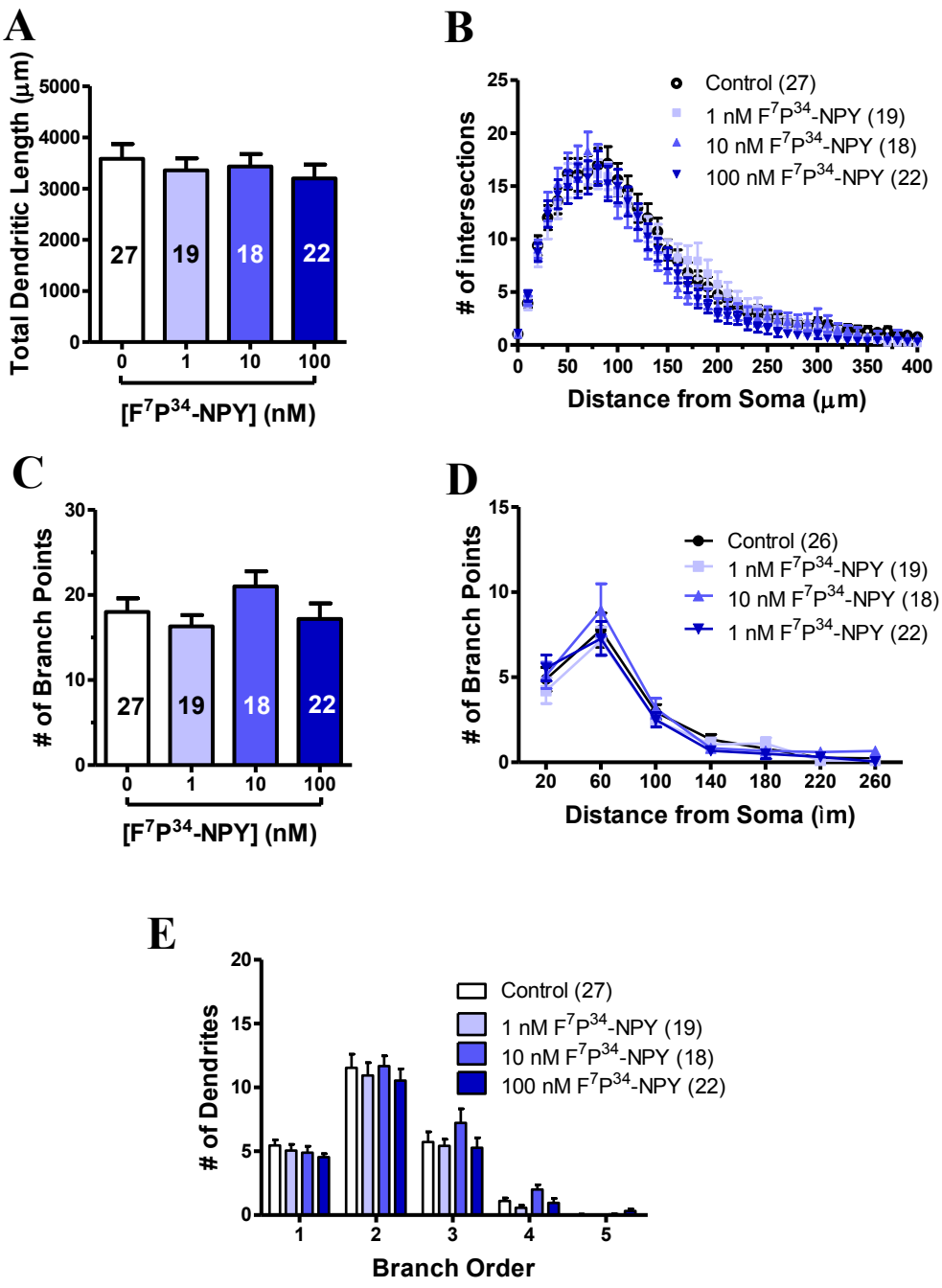
A
Total Dendritic Length (µm)
5000
4000
3000
2000
1000
0
27
19
18
22
0
1
10
100
[F7P34-NPY] (nM)
B
# of intersections
25
20
15
10
5
0
Control (27)
1 nM F7P34-NPY (19)
10 nM F7P34-NPY (18)
100 nM F7P34-NPY (22)
0
50
100
150
200
250
300
350
400
Distance from Soma (µm)
C
# of Branch Points
30
20
10
0
27
19
18
22
0
1
10
100
[F7P34-NPY] (nM)
D
# of Branch Points
15
10
5
0
Control (26)
1 nM F7P34-NPY (19)
10 nM F7P34-NPY (18)
1 nM F7P34-NPY (22)
20
60
100
140
180
220
260
Distance from Soma (im)
E
# of Dendrites
20
15
10
5
0
Control (27)
1 nM F7P34-NPY (19)
10 nM F7P34-NPY (18)
100 nM F7P34-NPY (22)
1
2
3
4
5
Branch Order

Figure 4.5 Treatment with the Y1-agonist does not result in dendritic remodeling of principal neuron in BLA OTCs.

Analysis of principal neuron dendritic arbors from Y1-agonist incubations of BLA OTCs reveals there were no morphological changes in (A) total dendritic length, (B) number of intersections measured by Sholl analysis, (C-E) number of branch points ($P>0.05$, one- and two-way ANOVA with Tukey's *post hoc* test). The number of analyzed cells is presented for each treatment in the figure legend or bar graph.

Figure 4.6

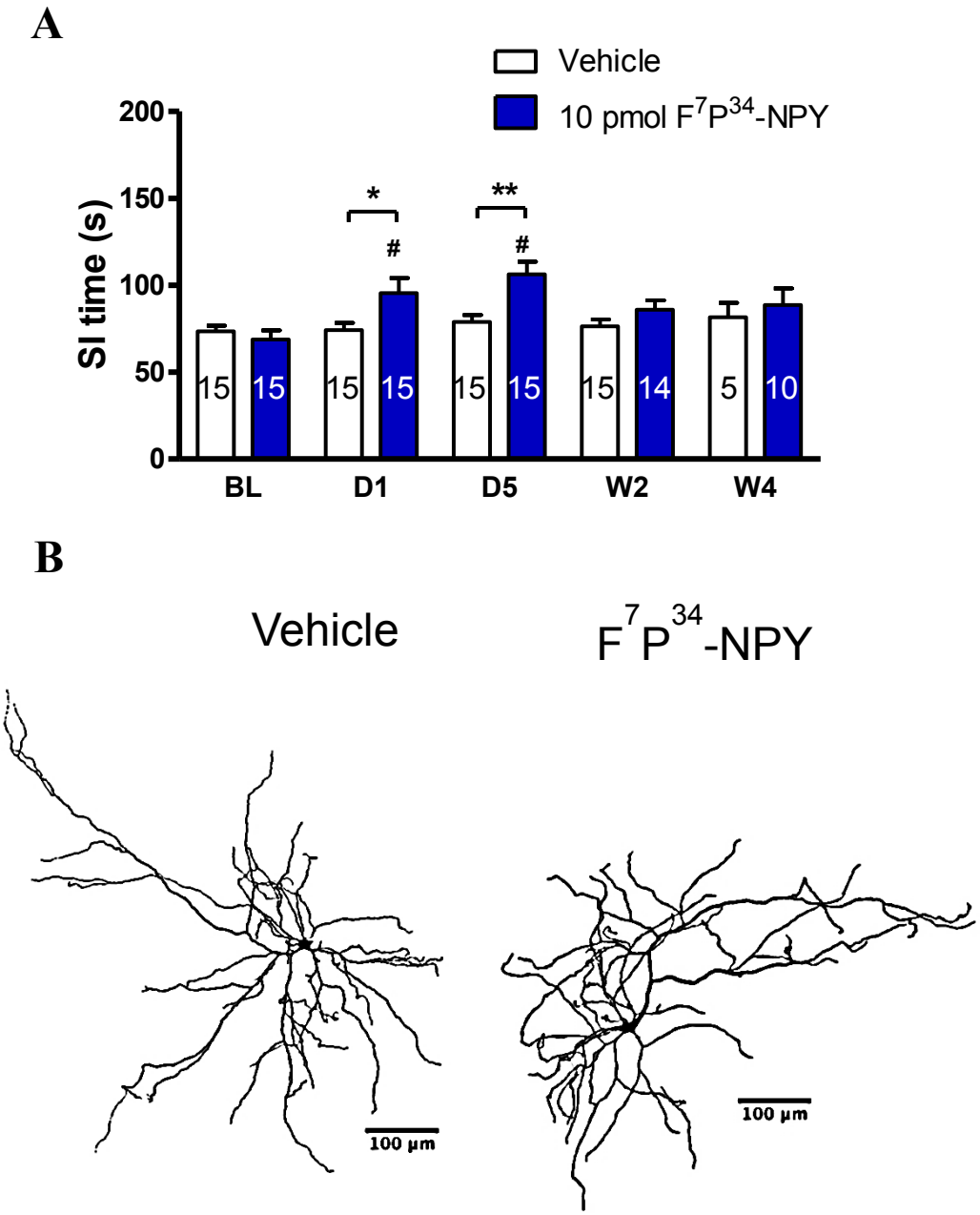
A
Vehicle
10 pmol F7P34-NPY
SI time (s)
200
150
100
50
0
*
**
#
#
15
15
15
15
15
15
15
14
5
10
BL
D1
D5
W2
W4
B
Vehicle
F7P34-NPY
100 µm
100 µm

Figure 4.6 Repeated intra-BLA injection of the Y1-agonist *in vivo* results in an acute, but no long-term anxiolytic effect.

Social interaction (SI) was measured at baseline and at various time points after injection with PBS vehicle or 10 pmol of the Y1-agonist. (A) At days 1 and 5, social interaction time significantly increased compared to vehicle treated animals (*P<0.05, **P<0.01, two-way ANOVA with Tukey's *post hoc* test). This effect was abolished at later time points of 2 and 4 weeks (P>0.05). (B) Representative reconstructions of principal neurons from *ex vivo* BLA slices following repeated injections of vehicle (left) and the Y1-agonist (right).

Figure 4.7

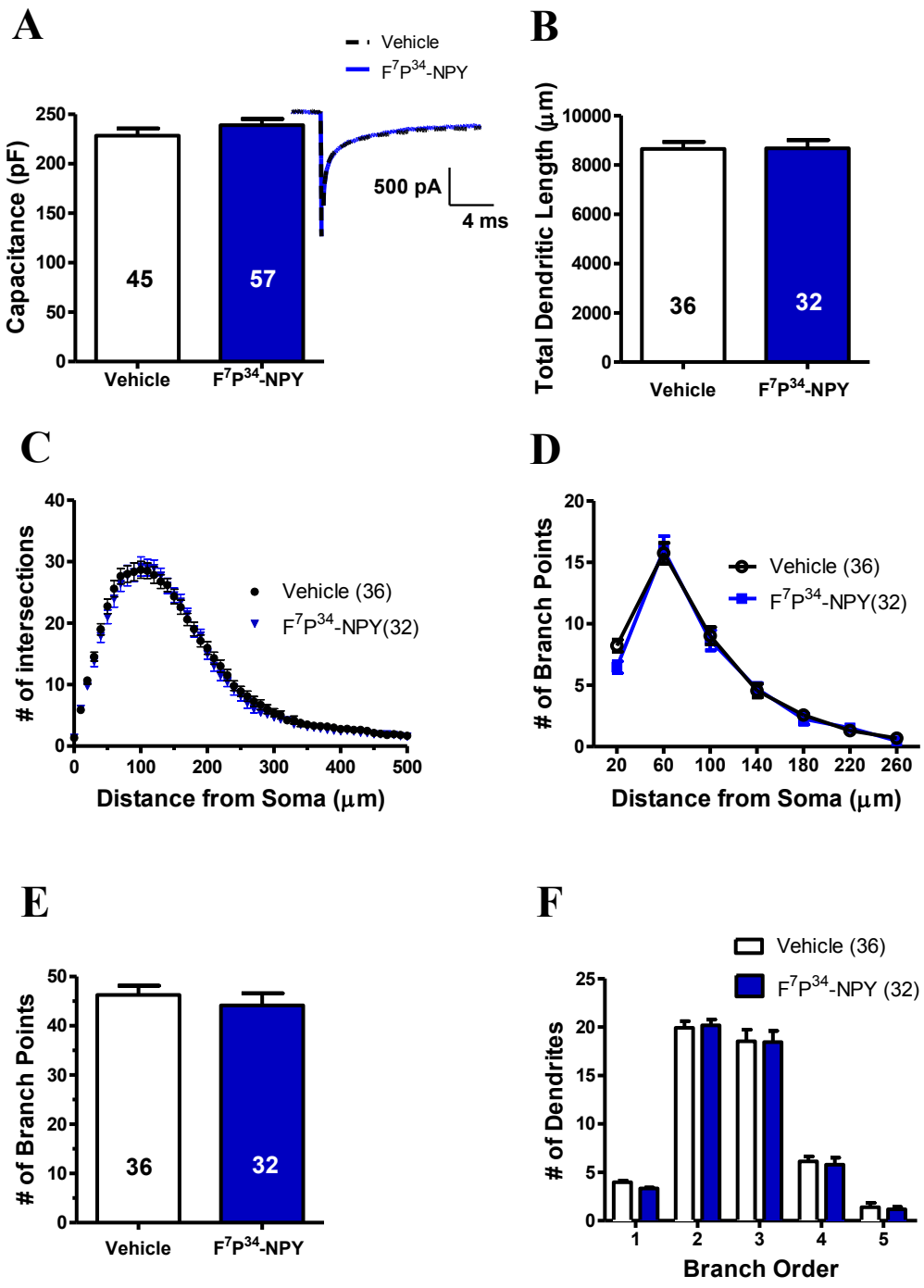
A
Vehicle
F7P34-NPY
Capacitance (pF)
250
200
150
100
50
0
45
57
500 pA
4 ms
Vehicle
F7P34-NPY
B
Total Dendritic Length (µm)
10000
8000
6000
4000
2000
0
36
32
Vehicle
F7P34-NPY
C
# of intersections
40
30
20
10
0
Vehicle (36)
F7P34-NPY(32)
0
100
200
300
400
500
Distance from Soma (µm)
D
# of Branch Points
20
15
10
5
0
Vehicle (36)
F7P34-NPY(32)
20
60
100
140
180
220
260
Distance from Soma (µm)
E
# of Branch Points
50
40
30
20
10
0
36
32
Vehicle
F7P34-NPY
F
Vehicle (36)
F7P34-NPY (32)
# of Dendrites
25
20
15
10
5
0
1
2
3
4
5
Branch Order

Figure 4.7 Repeated intra-BLA injection of the Y1-agonist *in vivo* results in no change in capacitance or morphological remodeling.

(A) Capacitance measurements of principal neurons from *ex vivo* brain slices indicates that repeated injection of the Y1-agoinst does not affect capacitance. (Inset) Representative traces of the capacitive transients following a small -10 mV hyperpolarizing step to vehicle and Y1-agonist treated principal neurons. Consistent with our findings in BLA OTCs, repeated injection of the Y1-agonist did not have an effect on principal neuron morphology. All indices of remodeling following Y1-agonist injections, including total dendritic length (B), number of intersections as a function of distance from the soma (C), number of branch points (D-F), were all not significantly different from vehicle injected animals ($P>0.05$, one- and two-way ANOVA with Tukey's *post hoc* test). The number of analyzed cells is presented for each treatment in the figure legend or bar graph.

Figure 4.8

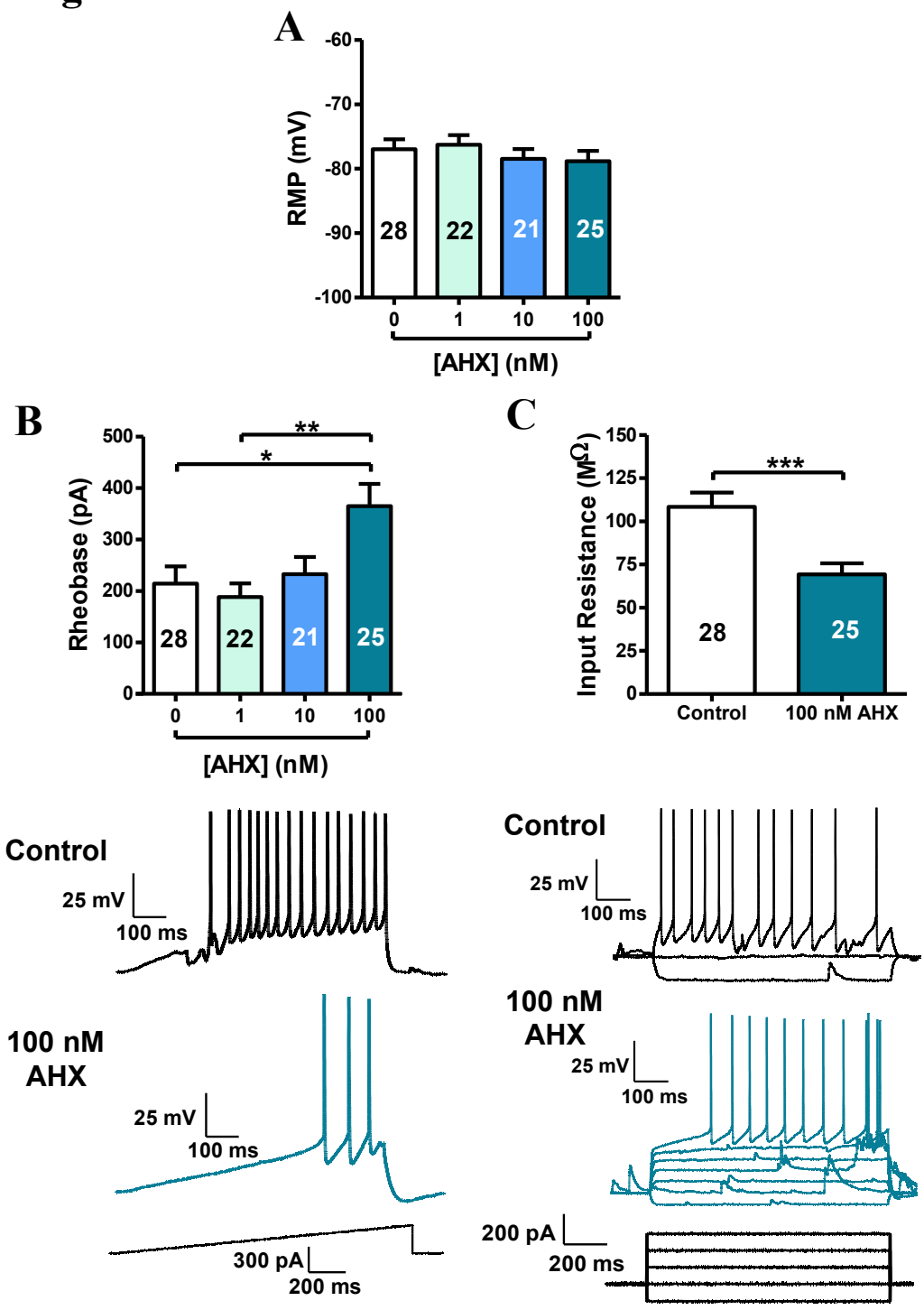
A
RMP (mV)
-60
-70
-80
-90
-100
28
22
21
25
0
1
10
100
[AHX] (nM)
B
Rheobase (pA)
500
400
300
200
100
0
**
*
28
22
21
25
0
1
10
100
[AHX] (nM)
C
Input Resistance (MΩ)
150
125
100
75
50
25
0
***
28
25
Control
100 nM AHX
Control
25 mV
100 ms
100 nM
AHX
25 mV
100 ms
300 pA
200 ms
Control
25 mV
100 ms
100 nM
AHX
25 mV
100 ms
200 pA
200 ms

Figure 4.8 Postsynaptic effects of Y2-agonist incubations in BLA OTCs.

The anxiogenic Y2-selective agonist ahx had similar effects on principal cell postsynaptic responses as CRF in BLA OTCs. There was no changed in (A) RMP compared to controls, but (B) excitability was decreased (increase in rheobase) with 100 nM ahx-treated cultures compared to controls and 1 nM ahx, (one-way ANOVA with Tukey's post hoc test, $*P<0.05$, $**P<0.01$). Finally, repeated Y2-agonist incubations reduced input resistance, suggesting ahx could be opening some subtype of ion channel (C, one-way ANOVA with Tukey's post hoc test $***P<0.001$). The number of analyzed cells is presented for each treatment in the figure legend or bar graph.

Figure 4.9

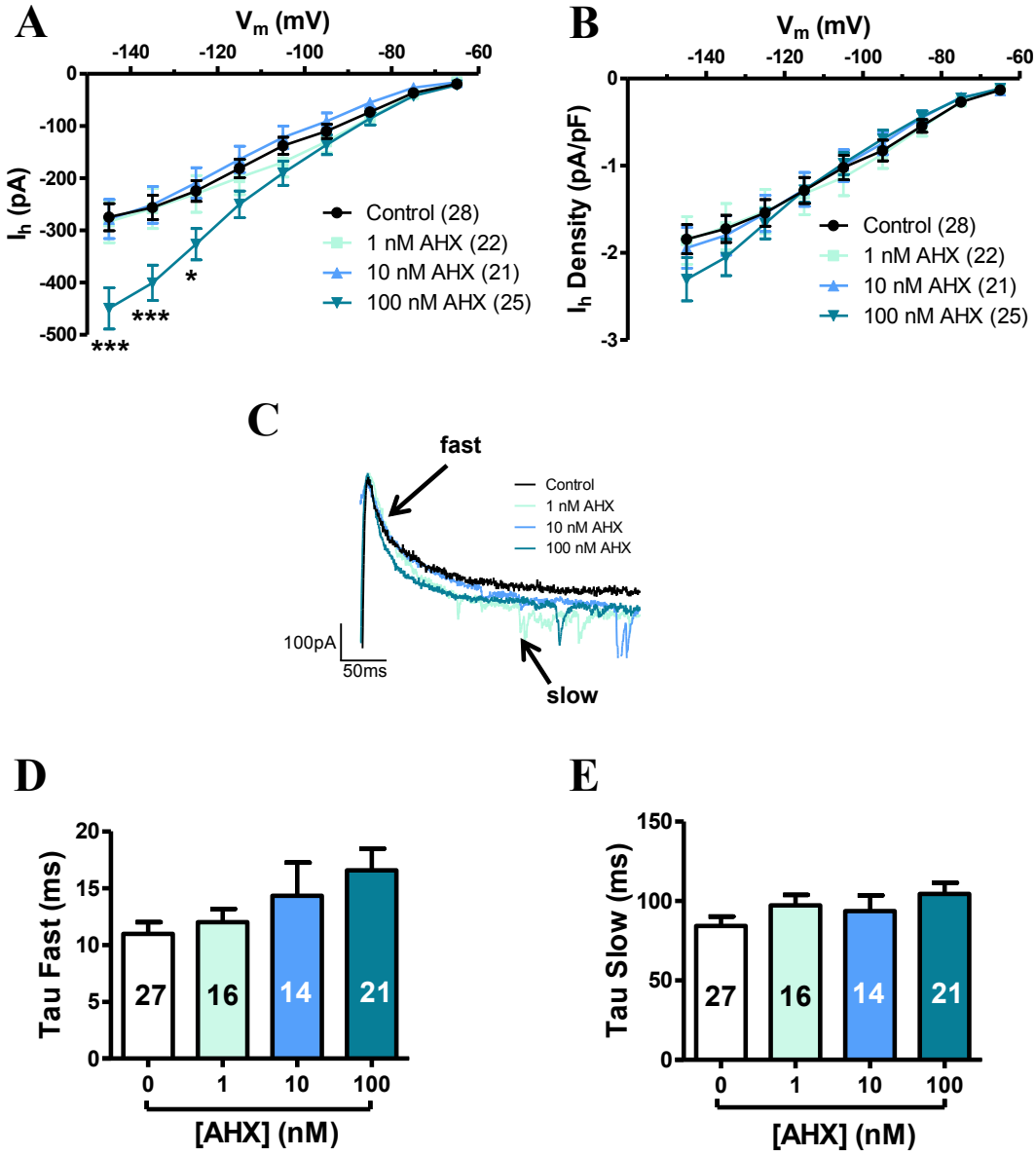
A
V_m (mV)
-140
-120
-100
-80
-60
0
-100
-200
-300
-400
-500
I_h (pA)
Control (28)
1 nM AHX (22)
10 nM AHX (21)
100 nM AHX (25)
*
***
***
B
V_m (mV)
-140
-120
-100
-80
-60
0
-1
-2
-3
I_h Density (pA/pF)
Control (28)
1 nM AHX (22)
10 nM AHX (21)
100 nM AHX (25)
C
fast
Control
1 nM AHX
10 nM AHX
100 nM AHX
100pA
50ms
slow
D
Tau Fast (ms)
20
15
10
5
0
27
16
14
21
0
1
10
100
[AHX] (nM)
E
Tau Slow (ms)
150
100
50
0
27
16
14
21
0
1
10
100
[AHX] (nM)

Figure 4.9 Ahx may modulate I_h in BLA OTCs.

(A) Following increasing hyperpolarizing voltage steps from -55 mV, analysis revealed incubation with 100 nM ahx results in an increase in I_h amplitude for the more hyperpolarized voltage steps (-145: ***P<0.001, -135: ***P<0.001, and -125 mV: *P<0.05; two-way ANOVA with Tukey's *post hoc* test). (B) When we controlled for the potential differences in cell size and analyzed I_h density, this effect was negated (P>0.05, two-way ANOVA with Tukey's *post hoc* test). (C) Representative current trace of I_h (left), with enhanced view depicting slightly slower activation kinetics following ahx incubations. Analysis of the time constants (D) tau fast and (E) tau slow, revealed incubation with ahx caused a trend of decelerated activation kinetics of I_h compared to controls, but this did not reach significant levels (P>0.05, one-way ANOVA with Tukey's *post hoc* test). The number of analyzed cells is presented for each treatment in the figure legend or bar graph.

Figure 4.10

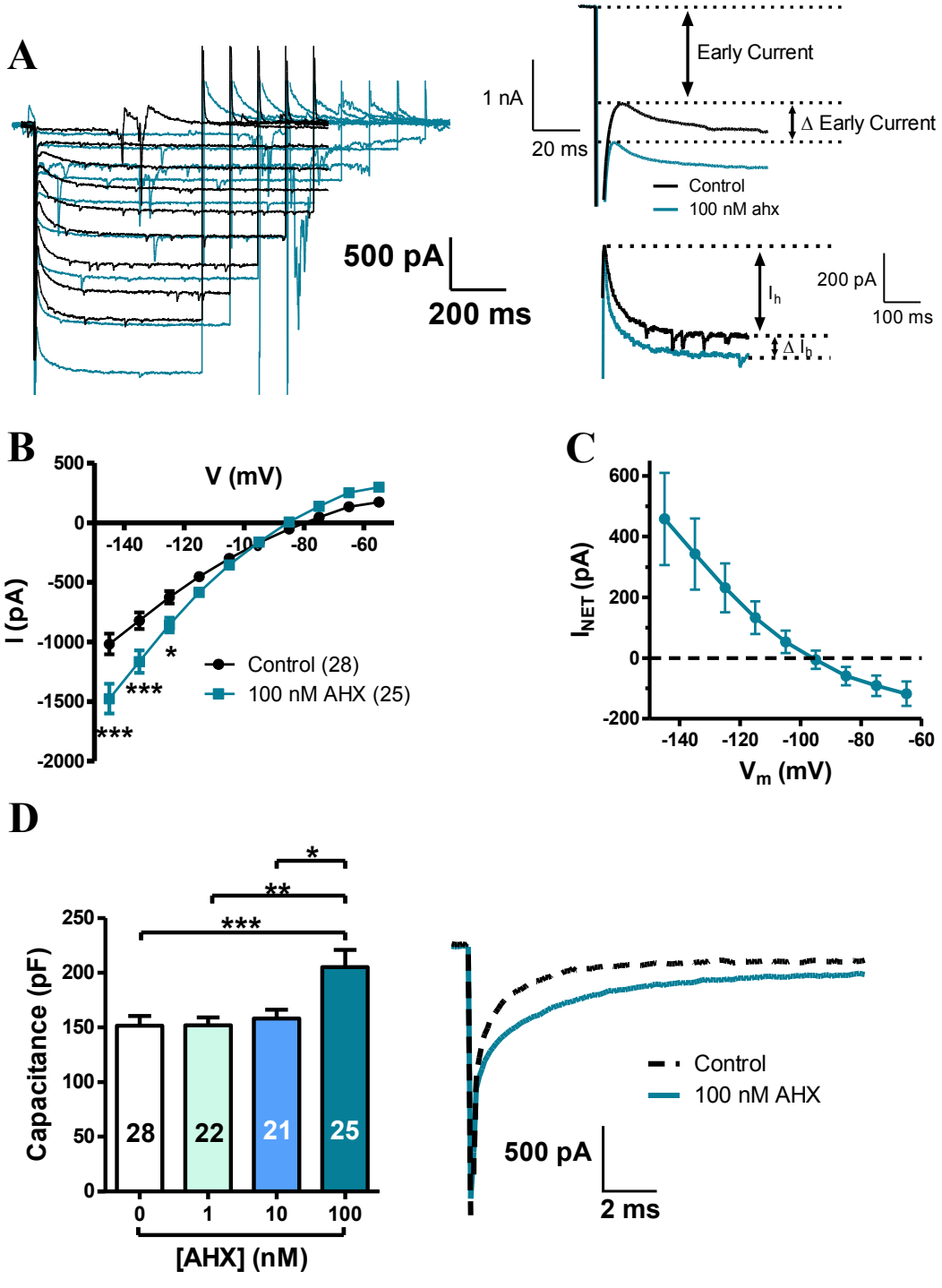
A
Early Current
Δ Early Current
1 nA
20 ms
Control
100 nM ahx
500 pA
200 ms
I_h
ΔI_h
200 pA
100 ms
B
V (mV)
I (pA)
Control (28)
100 nM AHX (25)
C
I_{NET} (pA)
V_m (mV)
D
Capacitance (pF)
28
22
21
25
[AHX] (nM)
Control
100 nM AHX
500 pA
2 ms

Figure 4.10 Ahx incubations resulted in a gain of an early current and increased cell capacitance in BLA OTCs.

(A, left) Representative current traces of control and 100 nM ahx incubated principal cells following a family of increasing hyperpolarizing voltage steps from -55 to -145 mV. (A, right) Enhanced view illustrating the change in (top) IIR and (bottom) I_h amplitude. (B) Analysis of the current-voltage plot (I/V), reveals a gain in an early current following 100 nM ahx incubations, which reversed around -95 mV (*P<0.05, ***P<0.001, two-way ANOVA with Tukey's *post hoc* test). (C) Subtraction of the control current from the one elicited by 100 nM ahx results in a gain of an inward current. (D) Repeated 100 nM ahx incubations resulted in increased cell capacitance compared to controls, 1 nM and 10 nM ahx (left, *P<0.05, **P<0.01, *** P<0.001, one-way ANOVA with Tukey's *post hoc* test). (D, right) Representative current traces of the capacitive transient following a -10 mV voltage step from -55 mV of control and 100 nM ahx treated neurons. The number of analyzed cells is presented for each treatment in the figure legend or bar graph.

Figure 4.11

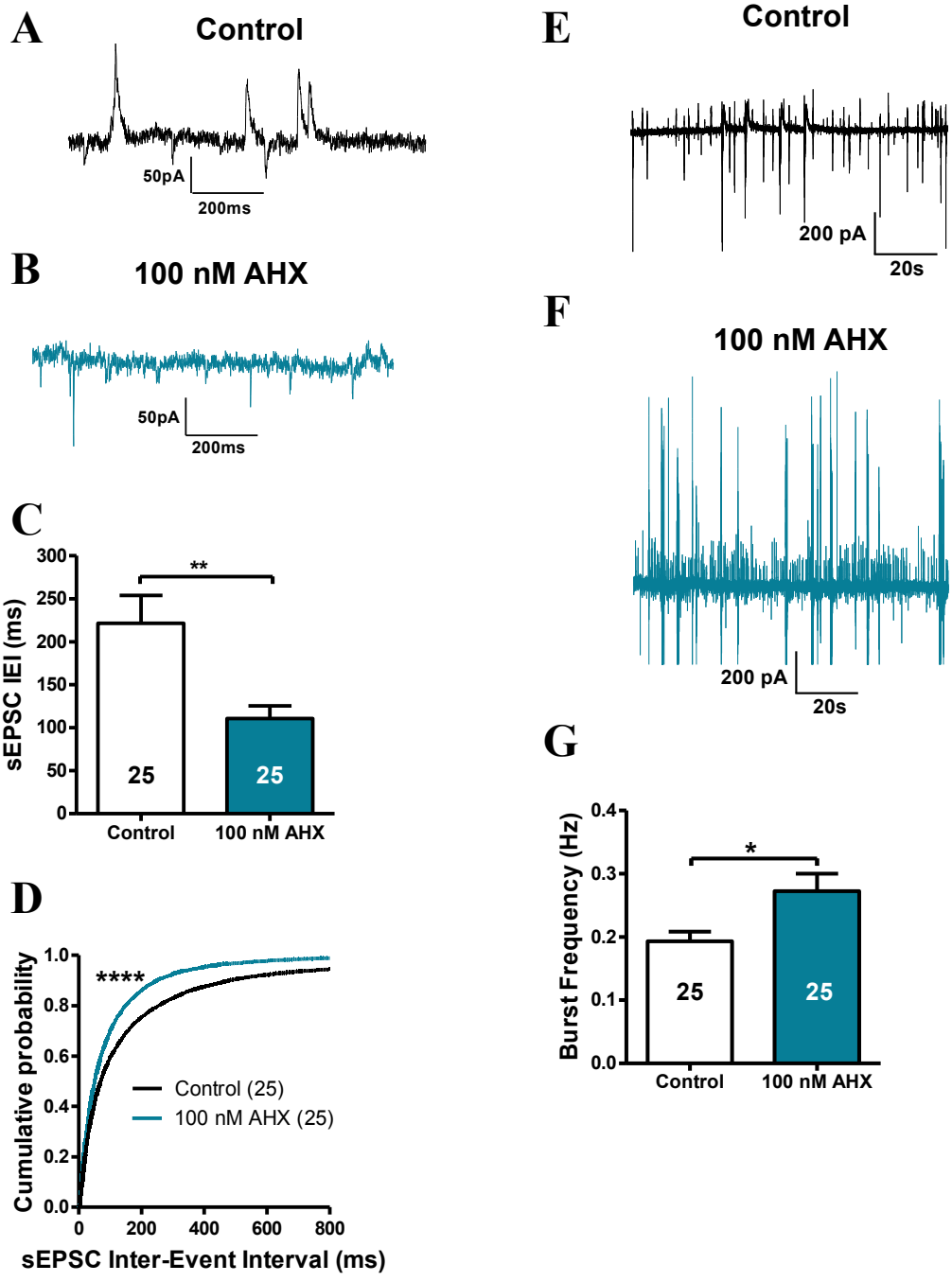
A
Control
50pA
200ms
B
100 nM AHX
50pA
200ms
C
sEPSC IEI (ms)
300
250
200
150
100
50
0
**
25
25
Control
100 nM AHX
D
Cumulative probability
1.0
0.8
0.6
0.4
0.2
0.0
****
Control (25)
100 nM AHX (25)
0
200
400
600
800
sEPSC Inter-Event Interval (ms)
E
Control
200 pA
20s
F
100 nM AHX
200 pA
20s
G
Burst Frequency (Hz)
0.4
0.3
0.2
0.1
0.0
*
25
25
Control
100 nM AHX

Figure 4.11 100 nM ahx incubations resulted in increased excitatory and decreased inhibitory drive onto BLA OTC principal neurons, along with an increase in synchronous activity.

Representative current traces of sIPSCs and sEPSCs from (A) control and (B) 100 nM ahx treated cells held at -55 mV. (C) Analysis of mean sEPSC IEI revealed a robust increase in frequency (decrease in IEI) of sEPSCs following 100 nM ahx incubations compared to controls (**P<0.01, t-test). (D) Cumulative probability plot of raw sEPSC IEI, depicting a robust decrease in sEPSC IEI following 100 nM ahx treatment compared to controls (****P<0.0001, K-S test). Representative current traces of neurons from (E) control and (F) 100 nM ahx incubations illustrating the frequency of compound postsynaptic bursts. (G) Analysis of bursting frequency suggests 100 nM ahx incubations, increases bursting activity in BLA OTCs (*P<0.05, t-test). A total of 9833 sIPSCs and 9213 sEPSCs were analyzed for control neurons and 9772 sIPSCs and 9883 sEPSCs for 100 nM ahx incubated neurons. The number of analyzed cells is presented for each treatment in the figure legend or bar graph.

Figure 4.12

Control

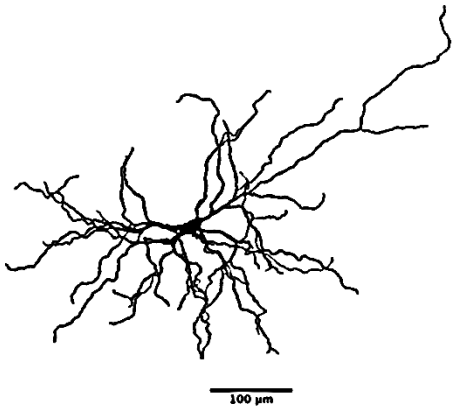

1 nM AHX

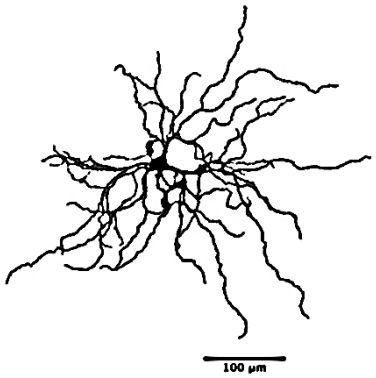

10 nM AHX

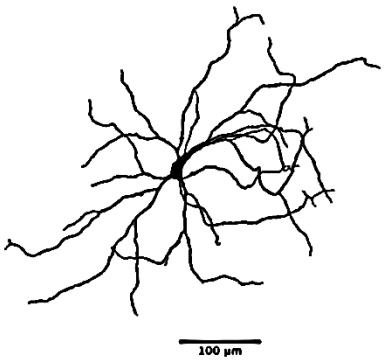

100 nM AHX

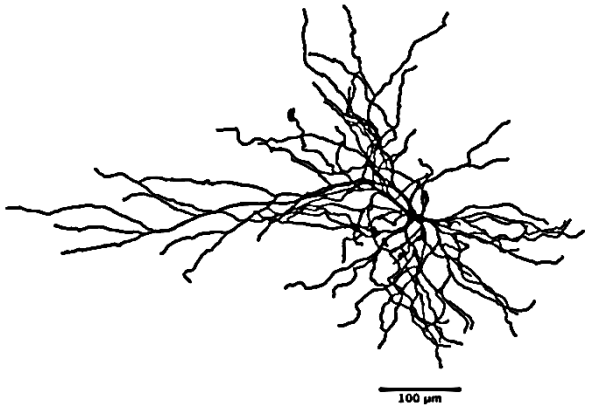

Figure 4.12 Representative reconstructions of BLA OTC principal neurons ahx incubations.

Following electrophysiological recordings and filling of cells with neurobiotin, OTCs were fixed, stained and imaged. Reconstructions were made using the simple neurite tracer function in FIJI. Representative tracings of the total dendritic tree of principal neurons from 0, 1, 10 and 100 nM ahx treated BLA OTCs.

Figure 4.13

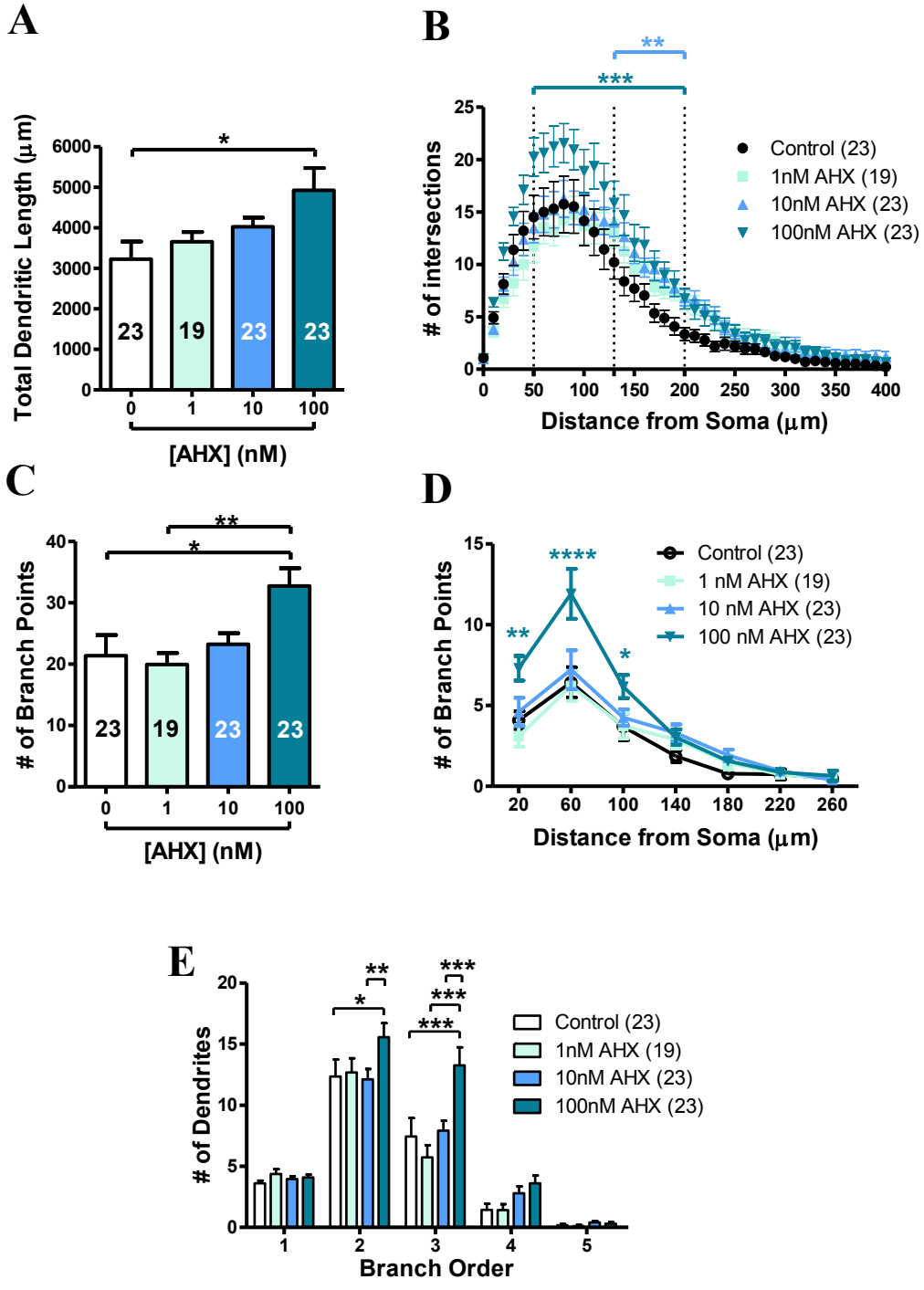
A
Total Dendritic Length (µm)
6000
5000
4000
3000
2000
1000
0
*
23
19
23
23
0
1
10
100
[AHX] (nM)
B
**
***
# of intersections
25
20
15
10
5
0
0
50
100
150
200
250
300
350
400
Distance from Soma (µm)
Control (23)
1nM AHX (19)
10nM AHX (23)
100nM AHX (23)
C
**
*
# of Branch Points
40
30
20
10
0
23
19
23
23
0
1
10
100
[AHX] (nM)
D
# of Branch Points
15
10
5
0
****
**
*
20
60
100
140
180
220
260
Distance from Soma (µm)
Control (23)
1 nM AHX (19)
10 nM AHX (23)
100 nM AHX (23)
E
# of Dendrites
20
15
10
5
0
**
*
***
***
***
1
2
3
4
5
Branch Order
Control (23)
1nM AHX (19)
10nM AHX (23)
100nM AHX (23)

Figure 4.13 Ahx incubations result in dendritic hypertrophy of principal neuron in BLA OTCs.

(A) Analysis of total dendritic length demonstrates hypertophy of the dendritic arbor following 100 nM ahx incubations compared to controls (*P<0.05, one-way ANOVA with Tukey's *post hoc* test). (B) Analysis of the regions of dendritic hypertrophy following Sholl analysis (10 μm radii) reveals dendritic hypertrophy was localized at proximal and intermediate regions of the dendritic arbor (10 nM ahx: **P<0.01, 100 nM ahx: ***P<0.001, two-way ANOVA with Tukey's *post hoc* test). (C) Quantification of the number of branch points revealed an increase of branching with 100 nM ahx incubations compared to controls and 1 nM ahx-treated neurons (*P<0.05, **P<0.01, one-way ANOVA with Tukey's *post hoc* test). (D) Increases in branching was localized to proximal and intermediate regions of the dendritic arbor (*P<0.05, **P<0.01, ****P<0.0001, two-way ANOVA with Tukey's *post hoc* test). (E) Incubation with 100 nM ahx resulted in augmentation of 2˚ and 3º dendrites (*P<0.05, **P<0.01, ***P<0.001, two-way ANOVA with Tukey's *post hoc* test). The number of analyzed cells is presented for each treatment in the figure legend or bar graph.

CHAPTER 5: Mechanisms of dendritic remodeling

Introduction

In addition to triggering a complex neurological response in the brain that prepares an individual for the acute consequences of dangerous and threatening stimuli, stress also induces long-term memories of stressful and emotionally arousing events (Nader et al., 2000). The mechanisms that underlie formation of stress-related memories include activity- and experience-dependent synaptic and structural plasticity, which can contribute to both adaptive and maladaptive changes in the neurocircuitry, and ultimately the behavior of the individual (Collingridge and Bliss, 1995). Individual organisms vary markedly in their perception and response to stress, which can also depend on their genetics, previous stressful encounters, the environment and behavior. While susceptible individuals cope poorly with stressful stimuli and are more likely to express maladaptive responses, possibly later resulting in psychopathology, a similar exposure in resilient individuals can be perceived as minimally disturbing, thus engaging adaptive physiological and psychosocial responses resulting in greater well-being (McEwen et al., 2015b). Although the neural processes that underlie such differences appear to reside in distinct anatomical, functional and molecular connectivity, the exact nature of these networks is still being elucidated.

Previous studies, including those from this thesis, have demonstrated the BLA to be a critical structure in the development and maintenance of stress resilience and vulnerability (Rainnie et al., 2004, Sajdyk et al., 2008). Previous chapters herein demonstrated that bi-directional structural plasticity induced by NPY and CRF, respectively, is an important correlate of stress resilience and vulnerability, in addition to the described alterations in GABAergic and glutamatergic transmission. However, the cellular mechanisms mediating

these opposing plastic effects are still unknown and form the basis for the studies in this chapter.

In addition to its expression of structural plasticity induced by stress and neuropeptide treatment, the BLA is also well-known to express bi-directional synaptic plasticity consisting of both LTP and LTD (McGaugh, 2002, Pape and Pare, 2010). Synaptic plasticity is characterized by a change in synaptic strength at pre-existing synapses following neuronal activation, which can last for seconds, minutes, hours and even days, and is known to be essential in memory processes including fear conditioning and extinction (Johansen et al., 2011). In a simplistic view, the direction of change in synaptic efficacy (LTP vs. LTD) is mediated by the magnitude of calcium elevation in the dendritic spine of the postsynaptic neuron (Citri and Malenka, 2008). LTP, which results in synaptic strengthening, requires high increases of calcium (beyond some critical threshold), which can lead to activation of low-calcium affinity protein kinases, while LTD, a form of synaptic weakening, requires modest increases in calcium, which may activate high-calcium affinity proteins such as calcium-dependent phosphatases (Malenka and Nicoll, 1993, Cummings et al., 1996). The magnitude and influx rate of intracellular calcium and thus the induction of LTP and/or LTD, is generally thought to be mediated by calcium permeable NMDA-receptors that act as coincidence detectors, requiring concurrent binding of glutamate released from the presynaptic terminal and postsynaptic depolarization to relieve magnesium-induced blockade of the channel for maximal efficacy (Citri and Malenka, 2008). However, elevations in intracellular calcium can also be mediated by activation of voltage-gated calcium channels (VGCCs) and through release of calcium from intracellular stores via metabotropic glutamate receptors (mGluRs) (Pape and Pare, 2010).

A number of different kinases have been suggested to play a role in mediating the signal transduction involved in LTP, including PKA, ERK, MAPK, PKC and in particular the atypical PKC isozyme, PKMζ, however, the most robust evidence supports a key role for the enzyme CaMKII (Citri and Malenka, 2008). Conversely, LTD involves the activation of calcium-dependent protein phosphatases, including calcium/calmodulin-dependent phosphatase calcineurin (PP2B) and PP1 (Mirante et al., 2014). Activation of either kinases or phosphatases initiates a number of intracellular signalling cascades that have various effects, including alterations in the trafficking of α-amino-3-hydroxy-5-methyl-4-isoxazole propionic acid (AMPA) receptors and NMDA-receptor and their subunits to and from the plasma membrane, as well as cascades that signal the cell nucleus to control gene transcription (for review see (Mansuy and Shenolikar, 2006, Citri and Malenka, 2008, Pape and Pare, 2010). Altered gene and protein expression allows stabilization of these synaptic changes, which can culminate in structural plasticity by changing the number and/or morphology of spines and is the basis for long-term memories to persist in the brain (Yuste and Bonhoeffer, 2001, Humeau et al., 2005, Suvrathan et al., 2014).

The amygdala plays a central role in the learning events that underlie fear conditioning and extinction, and the majority of studies exploring synaptic plasticity have been conducted in relation to its effects on memory formation. In particular, the LA has been most extensively studied with regards to synaptic plasticity. LTP in the LA is associated with the formation of fear memories, while LTD is thought to underlie the extinction of fear memories (Johansen et al., 2011). An important aspect of this work emerged that the physiological and molecular properties of LTP and LTD differed in different components of the synaptic circuitry. For example, the BLA integrates sensory information from thalamic and cortical afferents,

however, LTP of cortical inputs exhibits larger amplitude changes but persists less long, while LTP at thalamic inputs is initially smaller but it remains stable for longer periods of time (Doyere et al., 2003). Furthermore, using different LTP inducing protocols *in vitro,* coupled with an *in vivo* auditory fear conditioning paradigm, it was demonstrated that VGCCs appear to be involved in long-term memory consolidation, while NMDA-receptors were shown to be critical for fear acquisition (Bauer et al., 2002). Nevertheless, CaMKII appears to be critical in LTP-dependent learning and fear conditioning in the amygdala, as it is upregulated in dendritic spines of the LA following fear learning, and blocking its activity attenuates the acquisition of fear (Silva, 2003, Rodrigues et al., 2004). Conversely, LTD-dependent fear extinction in the LA requires calcineurin, as calcineurin antagonists block the induction of LTD, depotentiation (the reversal of LTP, a form of homeostatic plasticity) and fear extinction; conversely, activation of calcineurin promotes fear extinction (Lin et al., 2003a, Lin et al., 2003b, Mirante et al., 2014)

In addition to its role in fear conditioning and extinction, LTP is significantly enhanced in the amygdala following acute stress, while CaMKII and calcineurin have been shown to play opposing roles in anxiety-related behaviors (Vouimba et al., 2004, Vouimba et al., 2006). Repeated injection directly into the BLA of UCN at a dose of that is subthreshold for inducing acute anxiogenic effects for 5 consecutive days (priming) induces an elevated state of anxiety as assessed by SI, that persists up to 5 weeks. Administration of a CaMKII inhibitor (KN62) 30 min before UCN injection, blocked the development of UCN-induced priming, while acute injection of KN62 after priming was established, failed to block the priming-induced increases in anxiety (Shekhar et al., 2003, Rainnie et al., 2004). The effects on UCN-mediated priming were also abolished by co-application of the NMDA-receptor

antagonist DL-AP-5. Moreover, following exposure to acute predator stress rodents display increases in the expression of the active (phosphorylated) form of CaMKII in the BLA (Zoladz et al., 2012). Building on the work in fear conditioning, these studies further implicate CaMKII as a pro-anxiety mediator and suggest an LTP-like mechanism could play a role in CaMKII's effects on stress responses. Conversely, a growing body of evidence suggests calcineurin acts as an anxiolytic molecule.

Reports in the clinical setting using cyclosporine-A (CsA), a calcineurin inhibitor and immunosuppressant drug used during tissue transplantation, suggests a negative correlation between calcineurin activity and anxiety-related behavior (de Groen et al., 1987, Kahan et al., 1987.). Further studies corroborate these early theories, as intraperitoneal injection of CsA, as well as virally-mediated SiRNA knock-down of calcineurin in the BLA was sufficient to produce anxiogenic- and depression-like behaviors as assessed by EPM, OFT, light-dark, tail suspension test and forced swim tests (Mineur et al., 2014). Finally, in the NPY-mediated stress resilience studies by Sajdyk and colleagues, injection of the calcineurin inhibitory peptide 30 min before the injection of NPY, did not block the acute anxiolytic effect of NPY treatment observed on day 1, but it did prevent the long-term anxiolytic effects in SI perceived on days 5 and 8 (Sajdyk et al., 2008). Together, these studies advocate a role for CaMKII and calcineurin involvement in NPY- and CRF-induced stress resilience and vulnerability, respectively. It appears a regulated balance between calcineurin and CaMKII maintains a homeostatic level of affective behaviors, possibly through a synaptic and structural plasticity-like mechanism. Disruption of this equilibrium could shift this paradigm towards an anxiogenic response if CaMKII activity is elevated or towards an anxiolytic-like state if calcineurin is activated (Fig5.1A). Given that we observed bi-directional structural plasticity

mediated by NPY and CRF that is consistent with the behavioral output mediated by these structural changes, we hypothesized that the morphological changes identified were a result of altered calcineurin and CaMKII activity, respectively. The predicted mechanism is illustrated in Figure 5.1B.

To address our hypothesis of NPY-induced hypotrophy being mediated by calcineurin (=PP2B), we obtained electrophysiological recordings and performed morphological analysis on principal neurons from our BLA OTCs following repeated incubation with CsA (2 μM) and NPY (10 μM) or CsA (2 μM) alone for 5 consecutive days. In order to completely rule out the possibility of other protein phosphatases playing a role, we also performed a similar set of experiment using okadaic acid (OA, 10 nM), which selectively blocks PP1 and PP2A, this time using the Y5-selective agonist cPP. In the converse experiment to determine if CRF-induced hypertrophy is mediated via a CaMKII-mediated pathway, we incubated BLA OTCs with CRF (30 nM) and a myristoylated version of autocamtide-2-related inhibitory peptide (AIP, 40 nM), a cell-permeable CaMKII inhibitor or with AIP alone. Finally, CRF or chronic restraint stress induces activation of the enzyme fatty acid amide hydrolase (FAAH), which causes catalysis of the endocannabinoid anandamide (AEA) and ultimately results in dendritic hypertrophy, within the amygdala (Hill et al., 2013, Gray et al., 2015). Furthermore, tPA is up-regulated by CRF in the amygdala, resulting in increased spine density in the medial amygdala. Similarly, the Y2-mediated dendritic hypertrophy observed in BLA OTCs may be dependent on CRF actions (Matys et al., 2004, Bennur et al., 2007). We reported in the last two chapters that the electrophysiological and morphological effects mediated by CRF and the Y2 agonist [ahx$^{5-24}$]NPY(ahx) were virtually identical, therefore, we hypothesized that the effects of ahx are dependent on CRF-receptor

activation. To investigate this hypothesis we incubated our BLA OTCs with ahx (100 nM) and NBI 27914 hydrochloride (NBI - 100 nM), a selective non-peptide CRF-R1 antagonist or NBI alone and assessed morphological changes.

Results indicate 1) CsA alone had no effect on measured principal cell capacitance or morphological properties. However, co-incubation with CsA and NPY blocked the NPY-mediated hypotrophy and produced hypertrophic effects, likely a result of Y2-receptor activation, 2) that Y5-mediated dendritic hypotrophy is not dependent on other protein phosphatases, as okadaic acid did not preclude structural remodeling. Together, these experiments indicate that NPY-induced dendritic hypotrophy is dependent on calcineurin. Finally, we demonstrate 3) that the Y2-mediated hypertrophic effects are not mediated via CRF, as blockade of CRF-Rs did not occlude the AHX-mediated hypertrophy. Unfortunately, due to time constraints, full morphological analysis of the CRF and AIP experiments could not be completed, however, electrophysiological experiments were completed and capacitance measurements suggest CaMKII may play a role in CRF-mediated dendritic hypertrophy, as blocking CaMKII activity occluded the CRF-mediated increases in cell capacitance.

Methods

All methods were identical as previously described in Chapter 2, 3 and 4. For detailed description, please refer to these chapters.

Drugs

Repeated 5 daily incubations in BLA OTCs were performed with a number of enzyme inhibitors including the calcineurin inhibitor cyclosporine-A (CsA, 2 μM), the PP1 and PP2A inhibitor okadaic acid (OA, 10 nM), and the CaMKII inhibitor, myristoylated-autocamtide-2-related inhibitory peptide (AIP, 40 nM), with and without NPY (10 nM, NPY + CsA), the Y5-agonist (100 nM, cPP + OA) and CRF (30 nM, CRF + AIP). In another set of experiments we incubated the Y2-agonist [ahx$^{5-24}$]NPY, (ahx; 100 nM) with a CRF-R1 selective non-peptide antagonist NBI 27914 hydrochloride (NBI, 100 nM). NPY, AHX and cPP were generous gifts from Dr. A. G. Beck-Sickinger (Leipzig, Germany), while CsA was provided by Dr. Shairaz Baksh (University of Alberta) and OA was provided by Dr. Charles Holmes (University of Alberta). Finally, AIP was purchased from Enzo Life Sciences, Inc (Farmingdale, NY, USA).

Results

In this chapter, we were interested in determining the cellular signaling mechanisms mediating NPY and CRF induced structural plasticity. Although we did collect electrophysiological data from a full repertoire of protocols for every cell, as we did in previous chapters, here we only report our capacitance and morphological measurements.

Blocking basal calcineurin activity with CsA does not produce dendritic hypertrophy, but does block NPY-mediated dendritic hypotrophy in BLA OTCs.

To determine if NPY-mediated dendritic hypotrophy of principal neurons is dependent on calcineurin activity, we co-incubated our BLA OTCs with NPY (10 nM) and CsA (2 μM) for 5 consecutive days and assessed the long-term effects. Incubation with NPY + CsA in BLA OTCs increased cell capacitance compared to controls, however, incubation with CsA alone did not produce an effect compared to controls (Fig.5.3A). Tracing, reconstruction and Sholl analysis revealed hypertrophy of the dendritic architecture in BLA OTC principal neurons following NPY + CSA treatment in a similar fashion to 100 nM AHX treatment, while treatment with CsA alone did not appear to produce an effects (Fig.5.2A-C). All morphological characteristics we examined revealed treatment with CsA blocked NPY-induced hypotrophy, and actually resulted in hypertrophy that was indistinguishable from our ahx experiments (Fig5.3B-F).

Inhibition of PP1 and PP2A with okadaic acid has no effect on Y5-mediated hypotrophy.

Although CsA is a fairly specific inhibitor of calcineurin activity, it is known to also block the activity of other protein phosphatases such as PP1 and PP2A at higher

concentrations. In order to be absolutely confident in our results, we applied okadaic acid to block PP1 and PP2A, at a concentration that would permit calcineurin to act freely in the cytoplasm to mediate its downstream effects. Since the experiments with NPY + CsA resulted in principal neuron hypertrophy, we decided to use the Y5-agonist cPP, so any morphological effects could be attributed to one NPY receptor subtype alone. Capacitance measurements revealed okadaic acid alone had no effect, and when co-incubated with the Y5-agonist, okadaic acid did not suppress the Y5-mediated reduction in capacitance (Fig.5.5A). Furthermore, tracing, reconstruction and Sholl analysis revealed hypotrophy of the dendritic architecture in BLA OTC principal neurons following OA + Y5 treatment for all morphological characteristics we examined, while okadaic acid alone had no effect (Fig.5.4A-C and Fig.5.5B-F). These experiments, coupled with those in which we applied CsA, provides further evidence that calcineurin is the protein phosphatase involved in mediating NPY/Y5-induced dendritic hypotrophy in BLA OTC principal neurons.

Capacitance measurements suggest that CRF-mediated dendritic hypertrophy is dependent on CaMKII activity.

We next wanted to test our hypothesis that CRF mediates its hypertrophic effects by activating intracellular CaMKII. To test this, we blocked CaMKII activity using the cell permeable CaMKII blocker, myristoylated-AIP in our BLA OTCs together with 30 nM CRF. Due to time constraints, we are only able to report the capacitance measurements here, but full morphological analysis will proceed as usual in the near future. Nevertheless, it appears that CaMKII is may be required for CRF-mediated dendritic hypertrophy, as blocking its activity prevented the otherwise very robust CRF-induced increase in capacitance (Fig.5.6A).

Blocking CRF-R1 does not occlude ahx-mediated dendritic hypertrophy.

Because the electrophysiological and morphological consequences resulting with either CRF or ahx treatment were virtually identical, we tested whether ahx mediated its effects via CRF release. We therefore incubated our BLA OTCs with 100 nM ahx and the CRF-R1 antagonist, NBI 27914 hydrochloride. Capacitance measurements suggests that blocking CRF-R1 receptors may not occlude the structural remodeling induced by ahx, as capacitance was increased in NBI + AHX treated neurons compared to controls (Fig 5.8A). Indeed, following reconstruction of patched neurons (Fig 5.7A-B) and Sholl analysis, the NBI + ahx treated group still underwent significant hypertrophic effects for all morphological properties we measured compared to controls (Fig.5.8B-F). These increases are quite consistent with the observed changes following ahx incubations alone in BLA OTCs. Ahx therefore appears to elicit its morphological effects independent of CRF signaling in the BLA.

Discussion

In this chapter, we examined cellular mechanisms that could mediate the structural remodeling associated with NPY and CRF treatment. We show here that NPY Y5-receptor-facilitated hypotrophy requires the calcium-dependent protein phosphatase CaN, but neither PP1 nor PP2A play a role, while CRF-mediated hypertrophy requires CaMKII activity. Although we did not directly test the effects of these neuropeptides on the induction of LTP or LTD, the requirement of the opposing kinase and phosphatase for dendritic remodeling and previous findings that there is altered sEPSC frequency following incubation with CRF and NPY, is consistent with the induction of synaptic plasticity. Taken as a whole, the morphological evidence indeed supports neuropeptide-mediated structural plasticity within the BLA that involves both pre- and postsynaptic structures in a wholesale manner.

This work has provided further evidence that CaN and CaMKII is likely involved in mediating the long-term effects of NPY- and CRF-induced stress-resilience and vulnerability, respectively, and have provided an underlying mechanism, specifically dendritic structural plasticity. Both CaN and CaMKII are dependent on intracellular calcium, although are optimally activated at different $[Ca^{2+}]_i$, however, we have yet to identify the signal transduction mechanism following NPY- and CRF-receptor activation that results in changes to the concentration of intracellular calcium. At this time, we can only speculate as to a few potential candidates. NPY is known to modulate VGCC in a number of brain regions including inhibition in the hippocampal formation and in layer 5 neocortical pyramidal neurons (Qian et al., 1997, Hamilton et al., 2010, Hamilton et al., 2013). Preliminary data from other members of the Colmers lab have suggested that acute application of NPY itself, or the Y5-agonist to acutely prepared BLA slices may block some form of VGCC in the BLA,

which would reduce calcium entry and shift the balance towards CaN activation (Mackay et al., unpublished). Application of ahx or CRF to acutely prepared BLA slices appears to result in disinhibition of the distal dendrites of principal neurons through reduction in a tonic GIRK conductance (Mackay et al., unpublished). This blockade would result in dendrite depolarization, leading to relief of magnesium block on NMDA channels, allowing influx of calcium and shifting the balance towards CaMKII activation. Although speculative at this time, these acute effects could stimulate the cascade of events required for mediating the morphological effects we observed in our BLA OTCs. However, we may have inadvertently already elucidated the potential candidate as the compound postsynaptic bursting activity referred to in earlier chapters, which was modulated by both NPY and CRF, could indeed elicit the fluctuations in Ca^{2+} required for plasticity to take place.

It should be noted that there is an abundance of other potential mechanisms that could play a role in altering intracellular calcium concentrations. For example, the excitatory non-selective cationic, transient receptor potential channels (TRPC) are expressed in the BLA and can pass calcium through their channel pore. A number of studies have indicated that these channels play a role in mediating anxiety-like behavior in the amygdala, as mice lacking both TRPC4 and TRPC5 channels show reduced BLA excitability and decreased anxiety-like behavior and innate fear (Riccio et al., 2009, Riccio et al., 2014). These behavioral effects could arise from diminished calcium entry leading to a shift in the equilibrium towards activation of CaN and dendritic retraction. Furthermore, mGluRs within the BLA are necessary for some forms of fear conditioning and synaptic plasticity (Fendt and Schmid, 2002, Rodrigues et al., 2002). Activation of these receptors can generate the formation of inositol 1,4,5-trisphosphate (IP3) which can release calcium from intracellular stores and

produce propagating calcium waves through the dendritic tree to the soma, where they can have a number of effects including altered gene transcription that regulate and induce synaptic plasticity (Berridge, 1998, Ross et al., 2005). Although this mechanism is thought to be restricted to proximal dendrites, and is not normally observed in the distal spine-dense dendrites, this may be important to our findings as the majority of the morphological effects are compartmentalized to proximal-intermediate locations along the dendritic tree.

A number of mechanisms have been put forth regarding signaling pathways involved in the morphological changes observed following various stress paradigms. For example, tPA, a serine protease, has been shown to be an anxiogenic neuromodulator that reduces spine density in the MeA, but had no effect on BLA neurons (Bennur et al., 2007). Interestingly, CRF was shown to increase release of tPA in the MeA, suggesting the behavioral consequences of CRF are a result of tPA-induced plasticity in spine density (Matys et al., 2004). In addition to the neuropeptides CRF and NPY, the BLA is exposed to numerous neuromodulators that mediate both adaptive and pathophysiological responses following stress. One such class is the endocannabinoids, which act to reduce anxiety-like behavior and alter neuroplasticity. Chronic stress reduces endocannabinoid signaling in the BLA, specifically resulting in reduced concentrations of the endocannabinoid AEA, by enhancing its hydrolysis by fatty acid amide hydrolase (FAAH); this in turn results in increased anxiety-like activity and dendritic hypertrophy (Hill et al., 2013). Blocking the activity of FAAH, either pharmacologically or by genetic manipulations prevented the stress-induced effects on the dendritic architecture. In a follow-up study, CRF acting via the CRF-R1 induced activation of FAAH in the amygdala, driving AEA hydrolysis, thereby reducing its concentration and promoting anxiety-like behavior (Gray et al., 2015). Since both these reports have

demonstrated the effects of distinct neuromodulators interacting with CRF in the amygdala to modulate anxiety-related behavior, we felt our hypothesis that Y2-agonist mediated effects in the BLA were mediated via the CRF-R1 seemed worth testing. Nonetheless, our data suggests this is not the case, as blocking CRF-R1 with AIP did not occlude the morphological effects of Y2-receptor activation. While a minor source of CRF in the BLA stems from GABAergic neurons in the CeA, which should remain intact in our OTC preparation, other possible sources of CRF originating in distant brain regions that are severed during culture production may be absent in our OTC model. While there may be some interaction between Y2-receptors and CRF in the BLA, it appears insufficient to mediate the actions of the Y2 receptor agonist.

As mentioned, we did not directly measure LTD or LTP following CRF and NPY incubations. In addition to CRF-receptor mediated stress vulnerability, both LTP and LTD have been shown to require NMDA-receptor activation in the BLA (Bauer et al., 2002, Rainnie et al., 2004). Unfortunately, time restrictions prevented us from determining if the structural modifications produced by the neuropeptides are dependent on NMDA-receptor activation. Further experiments would be required to test these hypotheses, however, we now have an ideal system to further our understanding of the early events leading to the long-term morphological consequences.

Figure 5.1

A

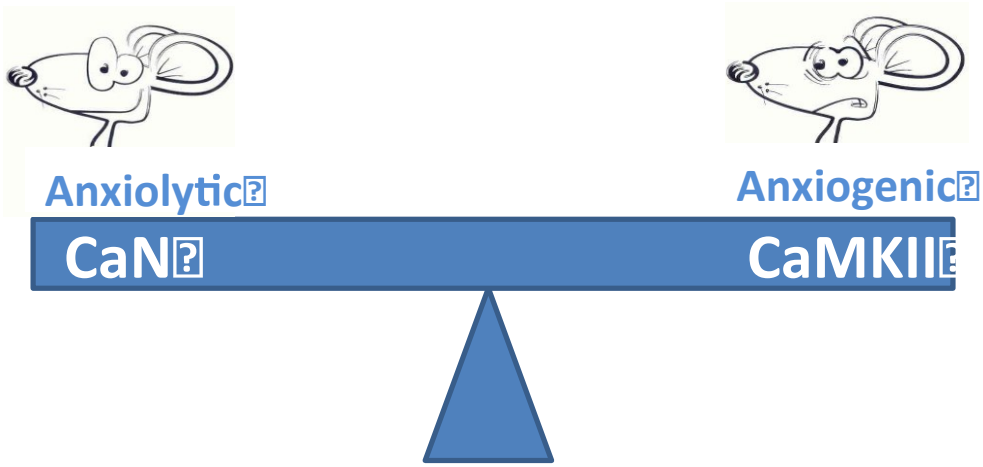
Anxiolytic?
Anxiogenic?
CaN?
CaMKII?

B

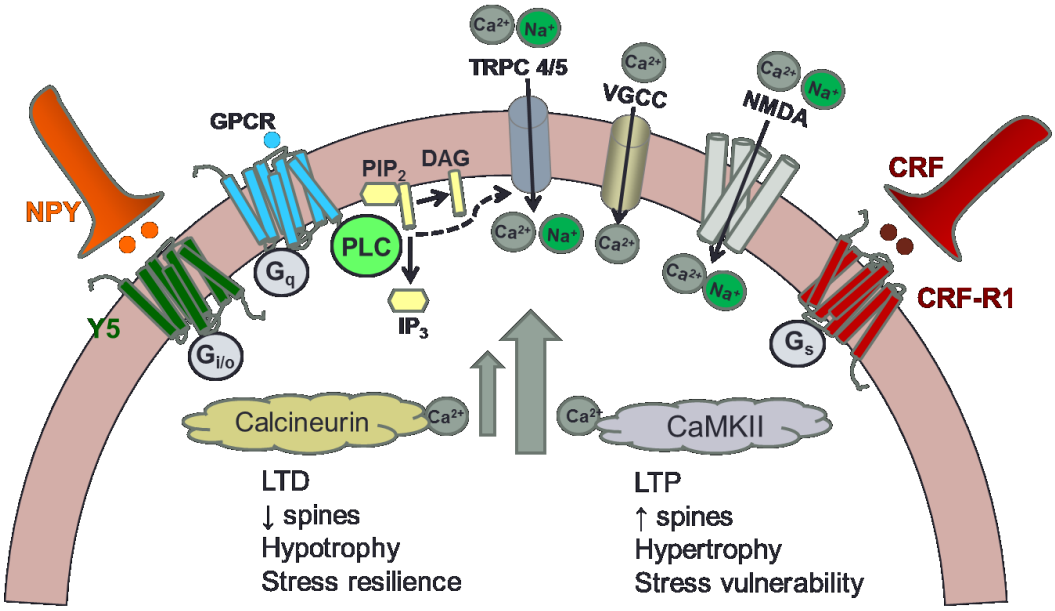
Ca2+
Na+
TRPC 4/5
VGCC
NMDA
GPCR
PIP2
DAG
NPY
PLC
CRF
Gq
IP3
Y5
Gi/o
Gs
CRF-R1
Calcineurin
CaMKII
LTD
↓ spines
Hypotrophy
Stress resilience
LTP
↑ spines
Hypertrophy
Stress vulnerability

Figure 5.1 Proposed mechanism and current model mediating NPY- and CRF-induced dendritic remodeling and alterations in behavior.

(A) Regulated balance between CaN and CaMKII signaling maintains homeostatic affective behavior. Any alterations in signaling that shift the balance of these enzymes will result in modification in emotional behavior. (B) In our proposed model, NPY or the Y5-agonist acting on the Y5-receptor (coupled to $G_{i/o}$) results in a signaling cascade causing decreased calcium entry. The reduction in intracellular calcium activates the high calcium affinity protein phosphatase CaN. Activation of CaN promotes LTD, driving reductions in dendritic spines, dendritic hypotrophy and culminates in altered behavioral responses in the form of stress resilience. Alternatively, CRF acting on the CRF-R1 (coupled to G_s) results in increased intracellular calcium, which activates the low calcium affinity kinase CaMKII. CaMKII phosphorylates its downstream effector molecules, which help promote LTP, leading to structural plasticity in the form of increased dendritic spines, dendritic hypertrophy and stress vulnerability. The alterations in intracellular calcium could be mediated via a number of different mechanisms including changes in the activation of TRPC 4/5, VGCC, or NMDARs, however, this is only speculative at this time.

Figure 5.2

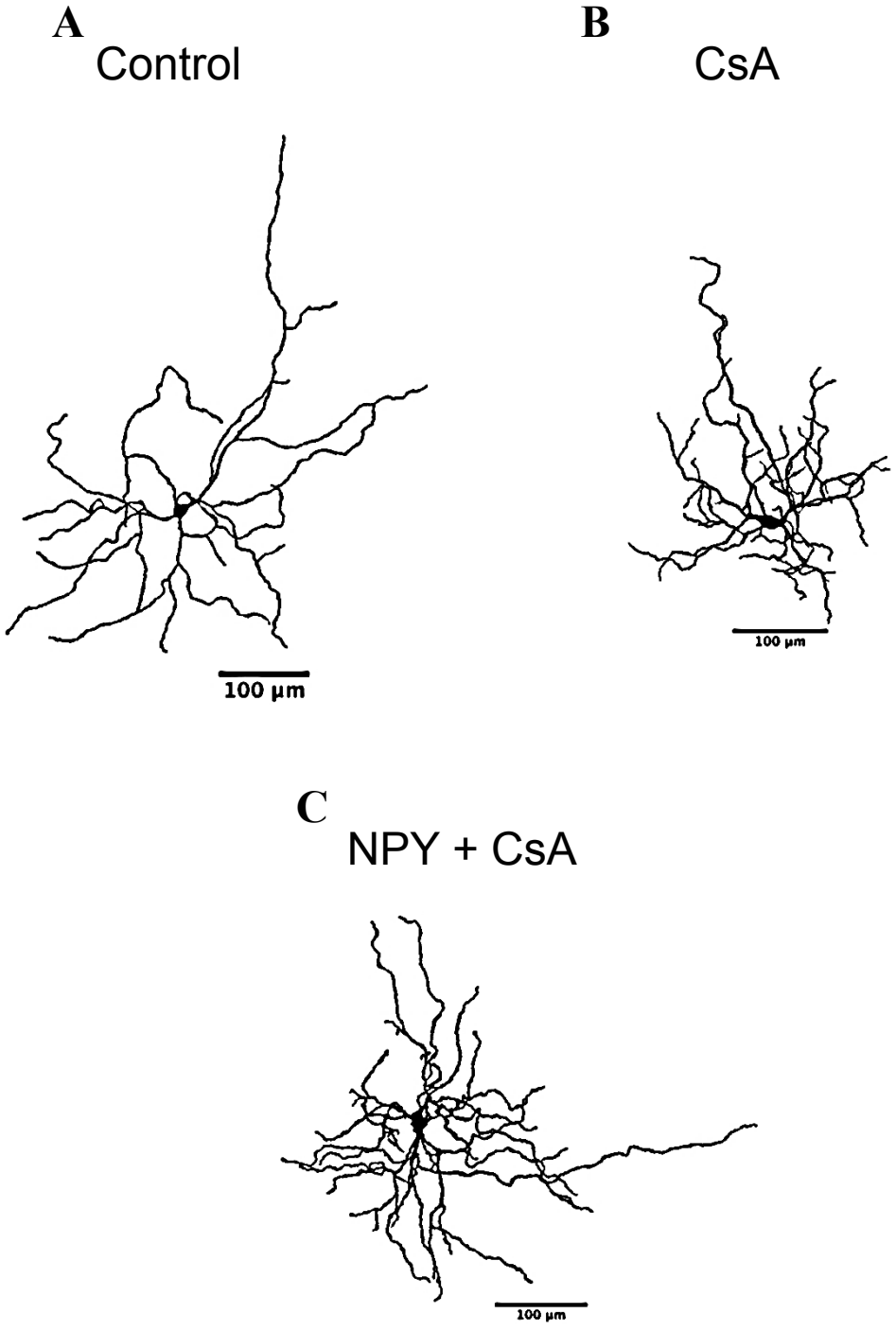

Figure 5.2 Reconstructed BLA OTC principal neurons following incubation with CsA and NPY.

Representative BLA OTC principal neurons reconstructed after recordings from (A) control, (B) CsA (2 μM), and (**C**) NPY (10 nM) + CsA (2μM). Note the increased complexity of the dendritic arbor following NPY + CsA incubations compared to controls.

Figure 5.3

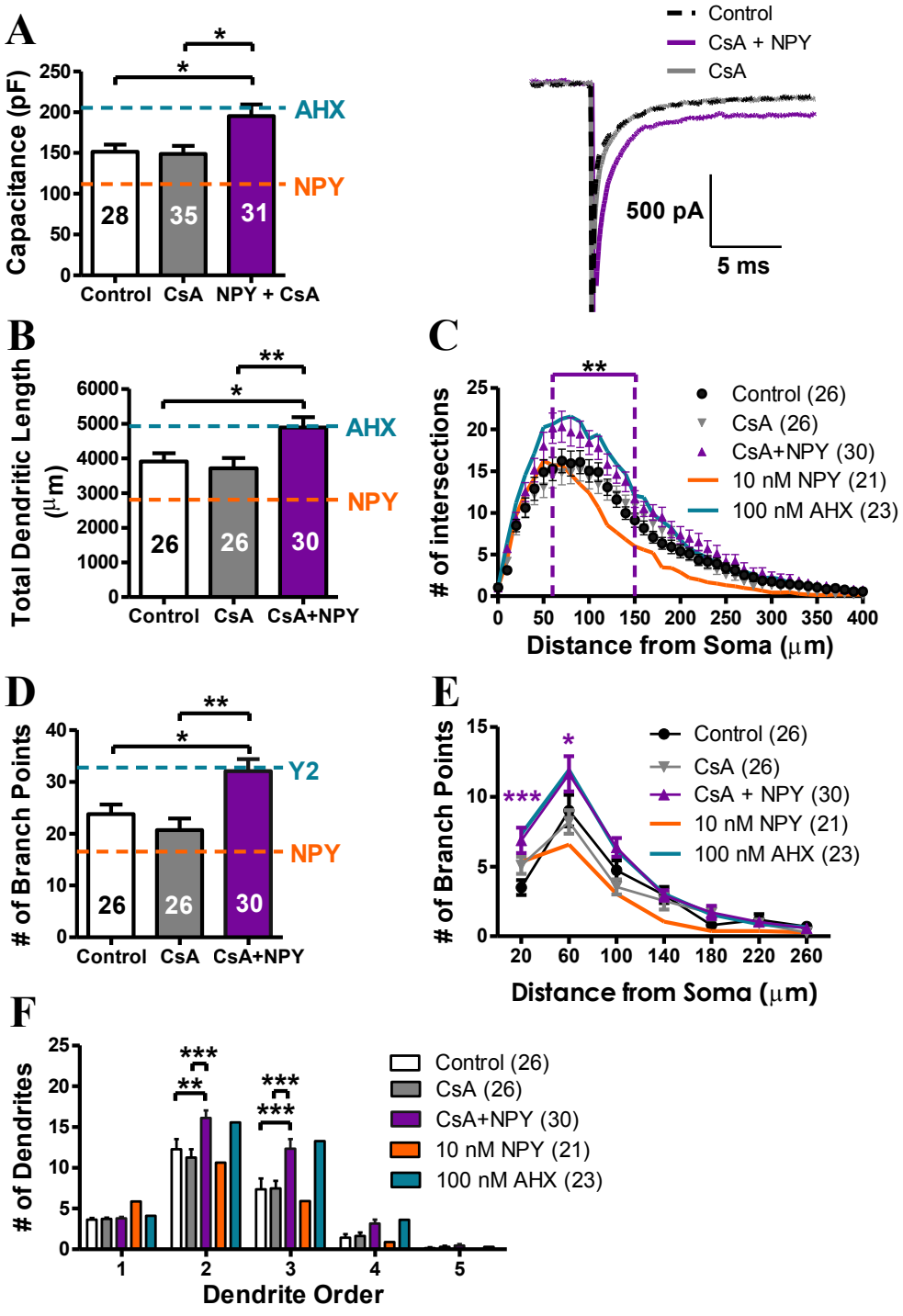
A
Capacitance (pF)
250
200
150
100
50
0
AHX
NPY
28
35
31
Control
CsA
NPY + CsA
*
*
Control
CsA + NPY
CsA
500 pA
5 ms
B
Total Dendritic Length (μm)
6000
5000
4000
3000
2000
1000
0
AHX
NPY
26
26
30
Control
CsA
CsA+NPY
**
*
C
# of intersections
25
20
15
10
5
0
0
50
100
150
200
250
300
350
400
Distance from Soma (μm)
**
Control (26)
CsA (26)
CsA+NPY (30)
10 nM NPY (21)
100 nM AHX (23)
D
# of Branch Points
40
30
20
10
0
Y2
NPY
26
26
30
Control
CsA
CsA+NPY
**
*
E
# of Branch Points
15
10
5
0
20
60
100
140
180
220
260
Distance from Soma (μm)
***
*
Control (26)
CsA (26)
CsA + NPY (30)
10 nM NPY (21)
100 nM AHX (23)
F
# of Dendrites
25
20
15
10
5
0
1
2
3
4
5
Dendrite Order
***
**
***
***
Control (26)
CsA (26)
CsA+NPY (30)
10 nM NPY (21)
100 nM AHX (23)

Figure 5.3 Capacitance and morphological analysis revealed NPY-mediated hypotrophy is dependent on CaN.

(A) Incubation with CsA occludes the observed NPY-mediated decrease in cell capacitance, and on the contrary results in elevated measured capacitance compared to controls (left, **P*<0.05, one-way ANOVA with Tukey's post hoc test). Representative current traces of the capacitive transient following a -10 mV hyperpolarizing voltage step from -55 mV of control, CsA, and CsA + NPY-treated neurons (right). (B) Total dendritic length increased in principal neurons following NPY + CsA incubations of BLA OTCs compared to controls (**P*<0.05, t-test). (C) Number of dendritic intersections per distance from the soma plotted for a Sholl analysis using concentric circles with 10 μm radii increments, and analysis revealed the regions where hypertrophy occurred following NPY + CsA incubations compared to controls (***P*<0.01, two-way ANOVA with Tukey's post hoc test). (D) Quantification of the number and position of dendritic branch points revealed augmented branching in NPY + CsA-treated principal neurons compared to controls (**P*<0.05, t-test). (E) The additional branching observed in BLA OTCs treated with NPY + CsA was localized to proximal-intermediate dendritic regions, where the number of intersections is also elevated (**P*<0.05, *** *P*<0.001, two-way ANOVA with Tukey's post hoc test). (F) The effects of NPY + CsA incubations on principal neuron branching are preferentially attributed to a surge in 2° and 3° dendritic branches (***P*<0.01, ****P*<0.001, two-way ANOVA with Tukey's post hoc test). CsA blocks the NPY-mediated Y5-effect, while permitting the Y2-effect. CsA incubations alone did not generate a response for any morphological characteristic we examined (A-F). For reference, the effects of 100 nM AHX and 10 nM NPY on BLA OTC principal neuron capacitance and morphology is illustrated in turquoise and orange, respectively.

Figure 5.4

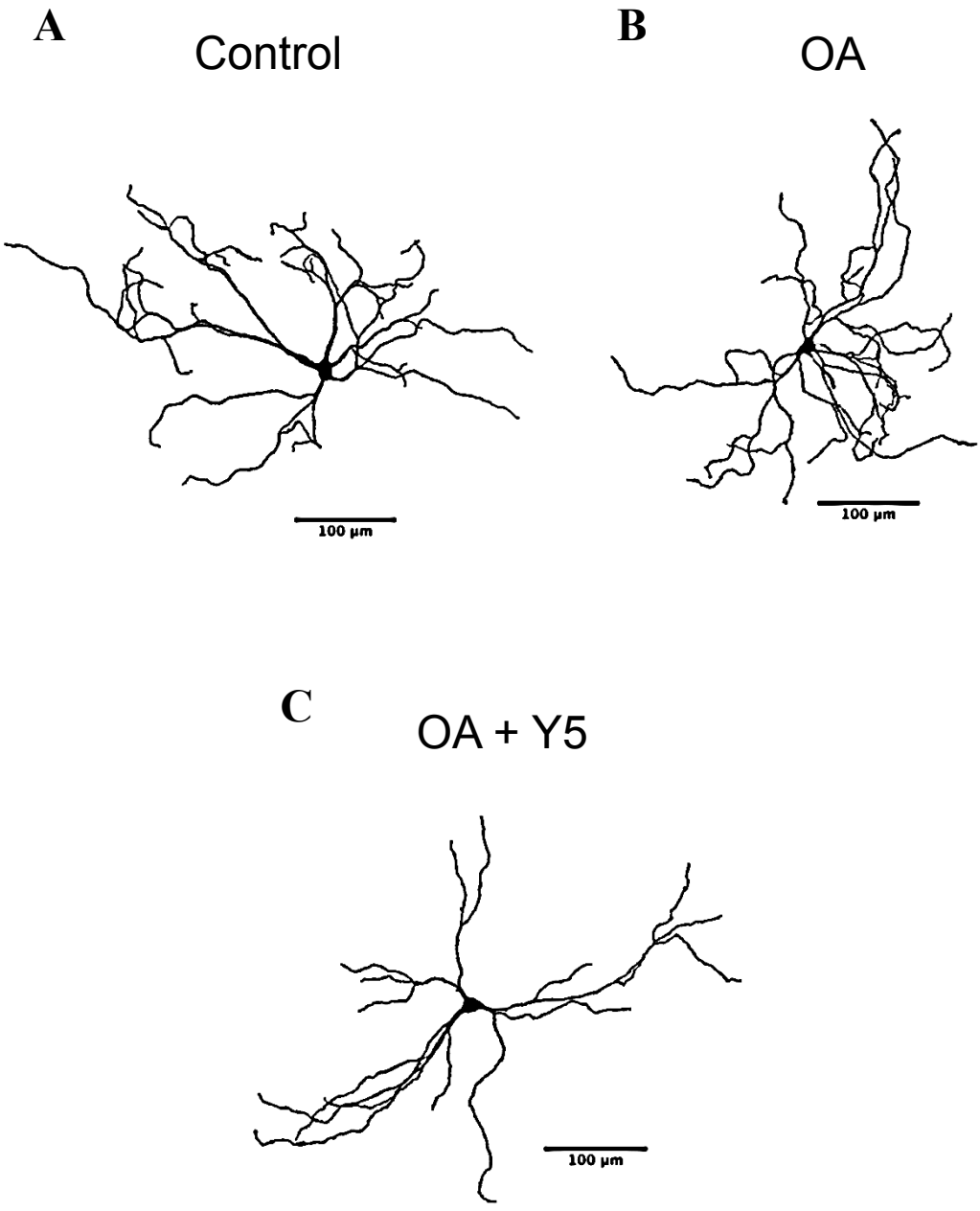

Figure 5.4 Reconstructed BLA OTC principal neurons following incubation with okadaic acid and the Y5-agonist cPP.

Representative BLA OTC principal neurons reconstructed after recordings from (A) control, (B) OA (10 nM), and (C) OA (10 nM) + Y5-agonist (100 nM). Note the simplification of the dendritic arbor following OA + Y5 incubations compared to controls, while OA alone and controls resemble each other.

Figure 5.5

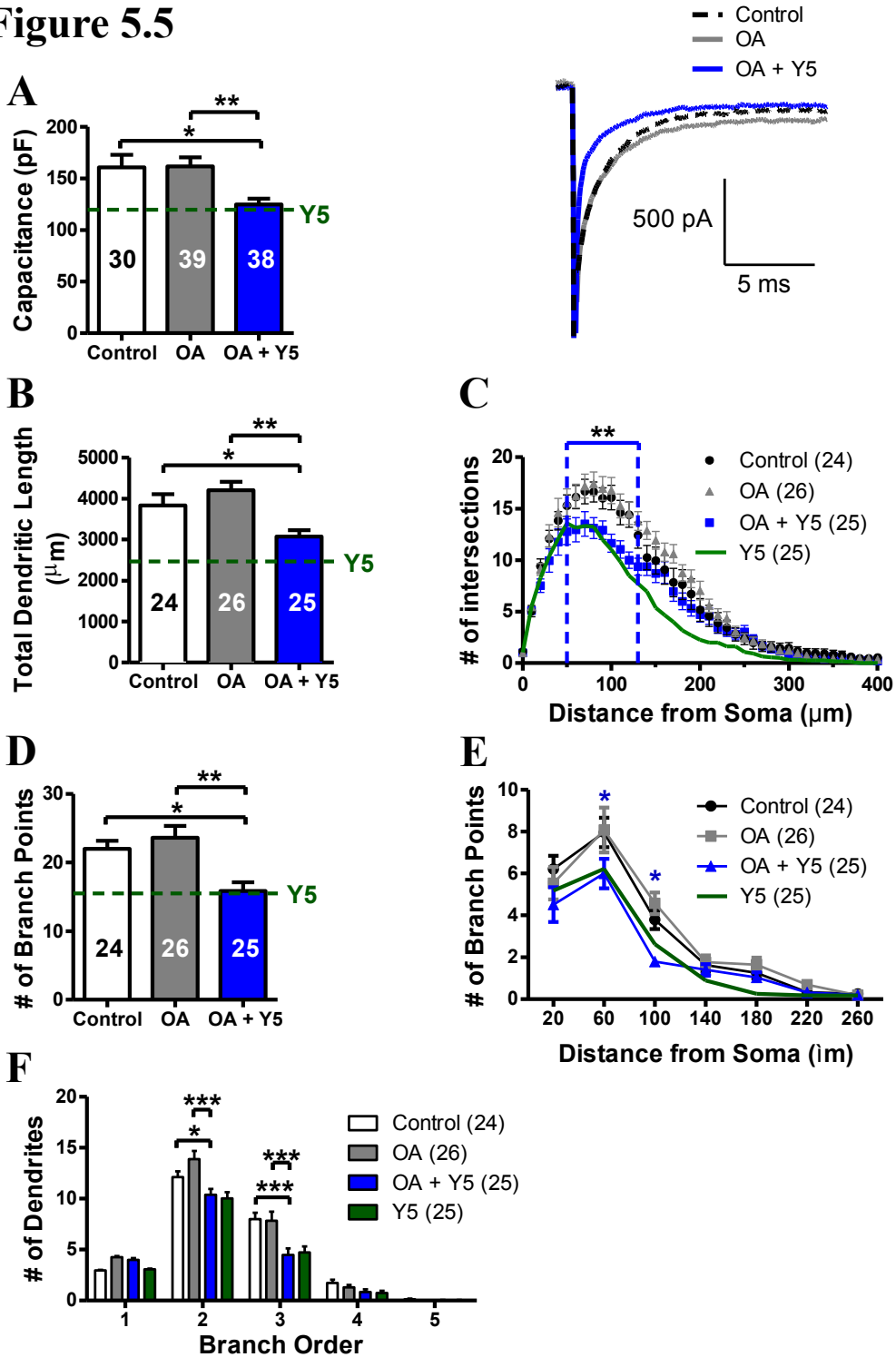
A
Capacitance (pF)
200
150
100
50
0
**
*
Y5
30
39
38
Control
OA
OA + Y5
Control
OA
OA + Y5
500 pA
5 ms
B
Total Dendritic Length (μm)
5000
4000
3000
2000
1000
0
**
*
Y5
24
26
25
Control
OA
OA + Y5
C
# of intersections
20
15
10
5
0
**
Control (24)
OA (26)
OA + Y5 (25)
Y5 (25)
0
100
200
300
400
Distance from Soma (μm)
D
# of Branch Points
30
20
10
0
**
*
Y5
24
26
25
Control
OA
OA + Y5
E
# of Branch Points
10
8
6
4
2
0
*
*
Control (24)
OA (26)
OA + Y5 (25)
Y5 (25)
20
60
100
140
180
220
260
Distance from Soma (ìm)
F
# of Dendrites
20
15
10
5
0
***
*
***
***
Control (24)
OA (26)
OA + Y5 (25)
Y5 (25)
1
2
3
4
5
Branch Order

Figure 5.5 Blocking PP1 and PP2A with OA does not effect Y5-mediated dendritic hypotrophy.

(A) Incubation with OA + Y5 resulted in decreased cell capacitance, while OA alone did not produce an effect (left, **P*<0.05, one-way ANOVA with Tukey's post hoc test). Representative current traces of the capacitive transient following a -10 mV hyperpolarizing voltage step from -55 mV of control, OA, and OA + Y5-treated neurons (right). (B) Total dendritic length declined in principal neurons following OA + Y5 incubations of BLA OTCs compared to controls (**P*<0.05, one-way ANOVA with Tukey's post hoc test). (C) Number of dendritic intersections per distance from the soma plotted for a Sholl analysis using concentric circles with 10 μm radii increments, and analysis revealed the regions where hypotrophy occurred following OA + Y5 incubations compared to controls (***P*<0.01, two-way ANOVA with Tukey's post hoc test). (D) Quantification of the number and position of dendritic branch points revealed diminished branching in OA + Y5-treated principal neurons compared to controls (**P*<0.05, one-way ANOVA with Tukey's post hoc test). (E) The curtailed branching observed in BLA OTCs treated with OA + Y5 was localized to proximal-intermediate dendritic regions, where the number of intersections is also reduced (**P*<0.05, two-way ANOVA with Tukey's post hoc test). (F) The effects of OA + Y5 incubations on principal neuron branching can be attributed to decreased secondary and tertiary dendritic branches (**P*<0.05, ****P*<0.001, two-way ANOVA with Tukey's post hoc test). It appears that okadaic acid does not preclude the Y5-mediated dendritic remodeling. Refinement of the dendritic architecture with OA + Y5 incubation, closely resembles that of 100 nM cPP, which is illustrated in green in the supporting graphs. Note cPP data were not used for statistical analysis.

Figure 5.6

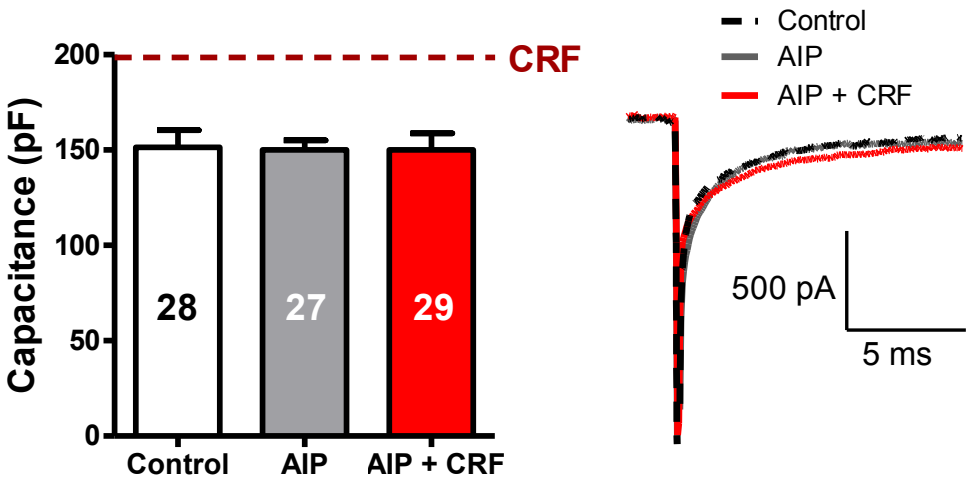

Figure 5.6 Inhibiting CaMKII likely uncouples CRF-R1 activation from dendritic hypertrophy.

(A) Inhibiting the activity of CaMKII by incubating BLA OTCs with AIP (40 nM) prevented the CRF-induced (30 nM) augmentation of cell capacitance, while AIP alone had no effect (left, $P>0.05$, one-way ANOVA with Tukey's post hoc test). Representative current traces of the capacitive transient following a -10 mV hyperpolarizing voltage step from -55 mV of control, AIP, and AIP + CRF-treated neurons (right).

Figure 5.7

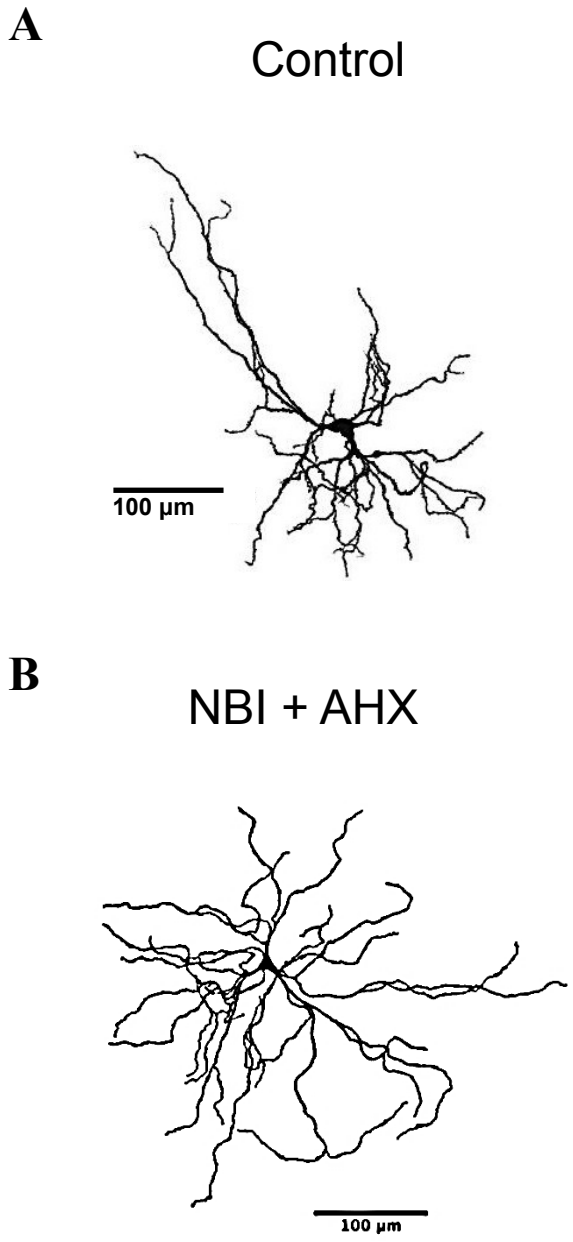

Figure 5.7 Reconstructed BLA OTC principal neurons following incubation with NBI + AHX.

Representative BLA OTC principal neurons reconstructed after recordings from (A) control, and (B) NBI (100 nM) + AHX (100 nM)-treated cultures. Note the apparent increased dendrites in the NBI +AHX-treated reconstructed neuron compared to control.

Figure 5.8

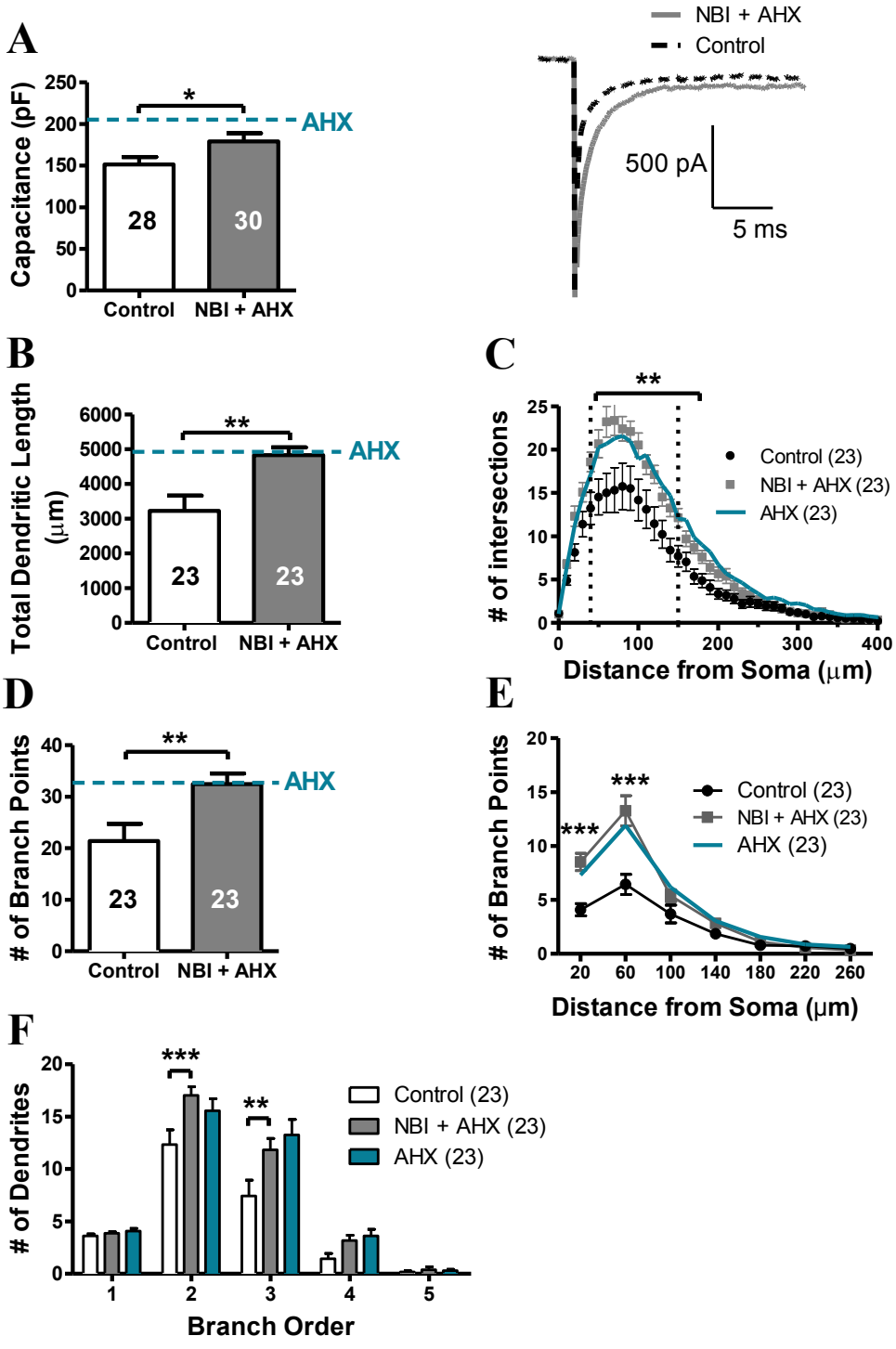
A
Capacitance (pF)
250
200
150
100
50
0
*
AHX
28
30
Control
NBI + AHX
NBI + AHX
Control
500 pA
5 ms
B
Total Dendritic Length (μm)
6000
5000
4000
3000
2000
1000
0
**
AHX
23
23
Control
NBI + AHX
C
# of intersections
25
20
15
10
5
0
**
Control (23)
NBI + AHX (23)
AHX (23)
0
100
200
300
400
Distance from Soma (μm)
D
# of Branch Points
40
30
20
10
0
**
AHX
23
23
Control
NBI + AHX
E
# of Branch Points
20
15
10
5
0
***
***
Control (23)
NBI + AHX (23)
AHX (23)
20
60
100
140
180
220
260
Distance from Soma (μm)
F
# of Dendrites
20
15
10
5
0
***
**
Control (23)
NBI + AHX (23)
AHX (23)
1
2
3
4
5
Branch Order

Figure 5.8 Capacitance and morphological analysis revealed Y2-mediated hypertrophy is not dependent on CRF-R1 activation.

(A) NBI + AHX incubations resulted in increased cell capacitance, which was similar to the observed effect following 100 nM AHX alone (left, **P*<0.05, t-test). Representative current traces of the capacitive transient following a -10 mV voltage step from -55 mV of control and NBI + AHX treated neurons (right). (B) Total dendritic length significantly increased in principal neurons following NBI + AHX incubations of BLA OTCs compared to controls (***P*<0.01, t-test). (C) Number of dendritic intersections per distance from the soma plotted for a Sholl analysis using concentric circles with 10 μm radii increments, and analysis revealed the regions where hypertrophy occurred following NBI + AHX incubations compared to controls (***P*<0.01, two-way ANOVA with Tukey's post hoc test). (D) Quantification of the number and position of dendritic branch points revealed augmented branching in NBI + AHX-treated principal neurons compared to controls (***P*<0.01, t-test). (E) Consistent with the Sholl analysis, the elaborate branching patterns of NBI + AHX-treated BLA OTC neurons was localized to proximal-intermediate dendritic regions, where the number of intersections is also elevated *** *P*<0.001, two-way ANOVA with Tukey's post hoc test). (F) The effects of NBI + AHX incubations on principal neuron branching are preferentially attributed to a surge in secondary and tertiary dendritic branches (***P*<0.01, ****P*<0.001, two-way ANOVA with Tukey's post hoc test). Refinement of the dendritic architecture with NBI + AHX incubation, closely resembles that of 100 nM AHX, which is illustrated in turquoise in the supporting graphs. Note AHX data were not used for statistical analysis.

CHAPTER 6: General discussion

Based on the contributions in this thesis, we are the first group to successfully develop, optimize, and validate BLA OTCs as an *in vitro* model to study the underlying mechanisms governing stress/anxiety-related behavior. Coupled with *in vivo* animal experiments, the use of OTCs should provide an efficacious and seminal tool for exploring cellular processes in an isolated, three-dimensional system where preservation of the cellular architecture exists. The data presented here, using our novel BLA OTCs, adds to the growing body of literature implicating counter-regulation of anxiety-like behavior by two neuropeptide systems in the BLA: NPY and CRF. The results suggest a novel mechanism by which NPY and CRF may exert their effects on contending behavioral responses, that is structural plasticity. Furthermore, we have begun to identify the cellular processes that occur downstream of receptor activation that stimulate BLA principal neuron dendritic remodeling. This chapter will highlight the major findings from previous sections, attempt to explain the significance of the results, and discuss several questions that arise as a consequence of these studies.

Organotypic Slice Cultures of Basolateral Amygdala

Over the past few decades, a technique that has come of age is the OTCs, in which CNS tissue prepared from early postnatal rodents can be maintained in culture for weeks to months. Neurons continue to develop and differentiate into a tissue network organization that closely resembles that observed *in vivo* and represent an attractive alternative and complement to acute slices. We have developed a novel BLA OTC preparation using the "interface method" adapted from Stoppini et al. (1991). OTCs are typically prepared from embryonic or early postnatal animals, however, the aim of our studies was to investigate the neurocircuitry implicated in altered stress responses from adult animals. Therefore, we designed the BLA OTC protocol to age-match our cultures to the equivalent postnatal time points of the

previously mentioned *in vivo* studies. The latest age that resulted in consistently viable cultures was P14, which were maintained for two months in culture bringing them to EP 10 weeks, the age at which our *in vivo* NPY-induced stress resilience experiments ended. The developing juvenile rodent brain and in particular, the BLA, is a highly dynamic structure that experiences a multitude of neurobiological changes that do not stabilize until P28 (Berdel et al., 1997, Morys et al., 1998, Berdel and Morys, 2000, Bouwmeester et al., 2002, Ehrlich et al., 2012, Ehrlich et al., 2013). Therefore, we examined the development of our BLA OTCs by comparing the electrophysiological and morphological properties to age-matched EP 10W and juvenile P14 acute slices.

Summary of Findings and Implications

Validation of BLA OTCs

Classically, OTCs derived from various brain regions exhibit conserved properties of synaptic transmission, neuronal morphology, neurochemical phenotype, and gross tissue organization in common with acutely prepared slices of their respective regions and the retention of many of the properties of the acute preparation has been used to validate these OTC models (Gahwiler, 1981a, Avossa et al., 2003, De Simoni et al., 2003, Lu et al., 2009). Overall, results from our novel BLA OTC model suggest that many of the electrophysiological properties shift away from the immature state and better resemble those in their mature counterparts. The majority of electrical features; RMP, rheobase, input resistance, I_h-amplitude and -density, and sIPSC and sEPSC frequency were shown to be analogous to age-matched EP 10W acutely-prepared slices. However, with any model that attempts to recapitulate an *in vivo* setting, there is always the intrinsic propensity towards distorted neurobiological characteristics. Due to the axotomized nature and inherent susceptibility of OTCs to flatten with time, there were a few inconsistencies that were revealed. Following explantation, OTCs flatten in the first few weeks, increasing neuronal density, and thus diminishing the extracellular space in which the neurons reside. This is likely the cause for reduced dendritic arborization of BLA OTC principal neurons compared to those from acutely-prepared P14 and 10W old animals. The finding of smaller BLA OTC neurons would predict altered kinetics and amplitudes of the resulting ionic currents measured. Due to issues of space-clamp, this is precisely what was observed. As a result of axotomy, there is a loss of afferent and efferent connections with distant brain regions, and although synaptic connections appear to be reestablished and often exceed levels that are

observed in acute slices from 10W old rats, the synaptogenesis that occurs likely results in altered local circuits that may not exist *in vivo*. Furthermore, the increase in local circuitry appears to result in spontaneous network activity exemplified by compound postsynaptic bursting within the OTCs. However, as basal excitability of BLA principal neurons from acutely-prepared slices are typically limited, the presence of bursting activity within BLA OTCs renders it an attractive model to study oscillatory behavior of principal neurons.

A re-emerging question seems to always arise when discussing the use of OTCs: how suitable to simulating the *in vivo* situation are OTCs? This is a complex question and before it can be answered, another similarly critical question must be asked: does studying a 10W old rat housed in a cage all its life, truly represent the sophisticated and often enigmatic behavior of an adult human? We argue that the use of OTCs should provide mechanistic insights in an isolated system that then must be proven through *in vivo* animal models. Similarly, animal models must be proven in human tissue, before translation to live human imaging and therapeutic/diagnostic approaches.

Taken together, we have laid the foundation for the use of BLA OTCs as a potent and innovative *in vitro* system for studying stress-related circuitry. In time, further improvements of the model could be made. The development of adult murine BLA OTCs should be one of the primary goals of future work, as this would limit the amount of time needed in culture and eradicate the controversy surrounding the suggestion that postnatally derived cultures represent only a developing model and in no way compare with a mature phenotype. The use of human tissue from postmortem or biopsied brains would serve as an elegant alternative to animal tissue for modeling various disease states, and indeed a number of groups have successfully prepared OTCs from various human peripheral tissues including the skin, lungs,

breasts and eye (Milani et al., 2013, Frade et al., 2015, Kuehn et al., 2015, Osborne et al., 2015). Recently, OTCs were successfully prepared from the temporal lobe of adult patients with epilepsy following operations to remove part of the hippocampal formation and temporal cortex (Eugene et al., 2014). Moreover, coupling OTCs to an artificial blood brain barrier would be an attractive progression, thereby allowing the study of therapeutically suitable compounds.

Counter-regulation of BLA OTC dendritic remodeling by NPY and CRF

Although the mechanisms mediating the acute actions of NPY and CRF on the stress-response are well-established, we know little pertaining to the long-term effects these neuropeptides have on stress resilience and vulnerability. This work advocates for a novel role of structural plasticity in regulating appropriate and maladaptive emotional responses. Parallel to *in vivo* work, we showed using BLA OTCs that these peptides can work independently of each other, but also interact with one another to dampen the effect of the other, a physiological relevant finding.

Long-term NPY incubations in BLA OTCs did not affect principal cell passive membrane or various I_h properties. We were surprised that NPY failed to reduce I_h, as recent data from the Colmers and Urban labs suggests repeated NPY injections reduce HCN-mediated currents at 4-week time points, and lentivirus-mediated knockdown of the HCN1 subunit (highest expressing subunit in the BLA and the one inhibited by acute application of NPY in *ex vivo* slices) results in attenuated anxiety-like behavior in SI tests (Silveira et. al., unpublished). This is one limitation of the OTC model, in that the biochemical and cell signaling pathways may not be fully established and mature at the time cultures are prepared.

It is widely accepted that acute and chronic stress results in increased spine density, while only chronic stress triggers dendritic hypertrophy in the BLA (Vyas et al., 2002, Hill et al., 2011, Adamec et al., 2012, Padival et al., 2013b, Cohen et al., 2014). This effect is associated with increased excitatory drive on BLA principal neurons and elevated emotional sensitivity (Rosenkranz et al., 2010, Padival et al., 2013a). Our BLA OTCs also produced changes in synaptic activity following NPY or CRF incubations that would predict the appropriate behavioral response, especially on the frequency of sEPSCs. Although our BLA OTCs did respond to chronic peptide treatment with dendritic arbor remodeling in the direction that is consistent with its role in modulating anxiety-related behavior, we never observed a change in the density of dendritic spines, but did detect effects on estimates of total spines that are likely due to alterations in the number of dendrites. This discrepancy could be a result of the time frame and order of changes that occur in the BLA. Alterations in spines would likely come before dendritic remodeling, as their modulation can take place on a faster time scale (Scott and Luo, 2001). Activation of CRF- or NPY-receptors may induce changes in the concentration of intracellular calcium (CRF increases while NPY decreases), which could drive synaptic plasticity resulting in altered protein synthesis during the late-phase of synaptic plasticity. This could culminate in actin (de)-polymerization and the emergence or selective loss of dendritic spines through activation of various small GTPases including RhoA and Rac 1 (Lai and Ip, 2013). Spines are highly dynamic in the developing and mature brain, which are modulated mainly by excitatory inputs from the environment in the form of synaptic activity (Yuste, 2011). If excitatory activity is further modulated, it may lead to additional structural rearrangements in the form of dendritic outgrowth and branching through the coordinated actions of various neurotrophins including BDNF, neurotrophin 3 (NT-3), and

nerve growth factor (NGF) or limiting growth and loss of branches through other mediators such as RhoA and the Notch receptor (Nakayama et al., 2000, Redmond et al., 2000, Scott and Luo, 2001). Interestingly, spinogenesis and dendritic branching share the same initial stages of development, in that both structures originate as transient filipodia (Dailey and Smith, 1996). The brain has an uncanny ability to promote allostasis, therefore, it seems plausible following dendritic hyper- or hypo-trophy, the density of spines reverts back towards its homeostatic level, while the alterations in the dendritic structure remain and serve as a new set point for further modulation by emotionally relevant stimuli. As we were interested in understanding the long-term effects of NPY and CRF treatment, we may have bypassed the early changes in spine density. It would be interesting to investigate the early processes that occur subsequent to NPY- or CRF-receptor activation to initiate remodeling of the dendritic architecture. Our OTCs combined with live-cell imaging using 2-photon microscopy would be an excellent way to study this.

NPY-induced dendritic hypotrophy of BLA principal neurons is mediated via Y5-receptor activation in BLA OTCs and in vivo.

As the majority of the acute anxiolytic effects of NPY are mediated by the Y1-receptor, we were surprised to find that long-term anxiolytic-like behavior is not mediated via repeated Y1-receptor activation. Furthermore, following repeated administration of the Y1-agonist, there were no effects on dendritic morphology in BLA OTCs or in acutely-prepared slices following repeated injections *in vivo*. Instead studyies conducted by Ms. Miranda suggest repeated Y5-receptor activation is the culprit. Surprisingly, the region of dendritic hypotrophy mediated by the Y5-agonist is shifted to more distal regions of the dendritic arbor compared to NPY *in vivo,* but remains similar in BLA OTCs. Although this may be a trivial

finding, it also raises the question of potential cooperativity between NPY-receptors to mediate dendritic hypotrophy *in vivo*. Although in experiments where NPY was coincubated with the Y5-antagonist tested for interactions between the Y1- and Y2-receptors, we did not test for interaction between Y1- and Y5-receptors or Y2- and Y5-receptors. However, this could easily be accomplished in future studies by co-injecting NPY and a Y1- or Y2-antagonist.

Although Y5-receptor containing BLA principal neurons typically co-express Y1-receptors and both are coupled to $G_{i/o}$ proteins that inhibit adenylate cyclase activity, and thus the formation of cAMP, it seems peculiar that they both did not produce the same morphological consequence upon repeated stimulation. One possible explanation is a potential divergence in the preferential intracellular signaling cascade activated by each receptor. With such an exuberant amount of potential intracellular molecules that cooperate to shape the neuronal response, it appears difficult to tease this apart. However, with the advent of novel biased agonists, we may be able to determine if this hypothesis holds any truth and obtain further knowledge of the players involved. Indeed, our collaborator Dr. A. G. Beck-Sickinger (Leipzig, Germany) has provided the Colmers lab with a number of biased agonists that could be employed in future studies. An alternative hypothesis may be enhancement of Y1-receptor desensitization, in the form of faster internalization rates. Indeed, Y1-receptors do exhibit faster internalization rates compared to Y2-receptors or Y5-receptors in mammalian cell cultures transfected to express various NPY-receptors (Parker et al., 2002a, Parker et al., 2002b). The augmented internalization has been postulated to be a result of an essential phosphorylated motif in the C-terminal domain that causes enhanced interaction between agonist-occupied Y1-receptors and the protein β-arrestin2 (Berglund et al., 2003, Holliday et

al., 2005). Again, our collaborator Dr. A. G. Beck-Sickinger (Leipzig, Germany) has developed a biased Y1-agonist that prevents the internalization of the Y1-receptor. Future studies examining the effects of this compound in BLA OTCs should clarify if internalization of the Y1-receptor is responsible for the lack of observable hypotrophy of BLA principal neurons. Finally, Y1- and Y5-receptors are known to form functional heterodimers when cotransfected in cell culture (Gehlert et al., 2007). Interestingly, application of a Y5-agonist enhanced dimerization and produced greater inhibition of adenylate cyclase compared to NPY or the Y1-agonist. Although it is unknown if heterodimer complexes form and function *in vivo,* they may serve as an important modulator of NPY signaling that results in an altered pharmacological profile of the endogenous neuropeptide.

Using our novel BLA OTCs, we have provided evidence that similarly to repeated CRF stimulation, repeated activation of the anxiogenic Y2-receptor results in dendritic hypertrophy of BLA principal neurons. Unfortunately, there was insufficient time to confirm these findings *in vivo* and to examine the long-term effects of repeated ahx injections on behavior, however, current studies are being performed by the Urban lab to address these questions.

Capacitance predicts morphological changes and morphological changes predicts behavior

Throughout all experiments presented in this thesis, a re-emerging trend was identified, and that was measured average capacitance for a given drug treatment was associated with remodeling of the dendritic arbor in the same direction. This may seem obvious when considering that capacitance is proportional to cell surface area, however,

neuronal capacitance measurements classically contain major errors as neurons are non-isopotential cells that have extremely complex dendritic arbors (Golowasch et al., 2009). A common method to measure capacitance and one that we employ is to deliver a small voltage-clamp step that is long enough to reach steady state, and then divide the integrated transient charge by the voltage-clamp step size (Taylor, 2012). The total membrane surface area cannot be accurately calculated from this measured capacitance because in non-isopotential cells, this only measures the "well-clamped" portion of the membrane (poor voltage clamp in distal dendrites) and does not represent total cell capacitance. However, researchers often measure capacitance to express ionic conductances as densities, to control for potential differences in cell size, and indeed this is why we began to measure cell capacitance, to examine I_h density. Although we found no effect on I_h density in response to NPY incubations, we did notice a consistent reduction in cell capacitance, which serendipitously led us on the path to examining alterations in neuronal morphology. With a small sample size, capacitance measurements are not very useful, however, when enough cells are recorded for a particular treatment, a certain trajectory begins to take shape. We found that good estimates of cell size could be acquired with approximately 30 independent observations, and we attempted to meet this standard for every experimental treatment. Figure 6.1 illustrates there is a strong correlation between measured cell capacitance and total dendritic length for BLA OTC principal neurons. A similar graph has not been prepared for comparison of BLA principal neurons from acutely-prepared slices. However, we anticipate a similar trend, although, the correlation may tail off at larger dendritic lengths as errors in capacitance measurements would be intensified in more distally localized dendrites due to poor voltage clamp. Nevertheless, a change in cell capacitance predicts the effects on structural remodeling and the direction of morphological

change is predictive of the behavioral outcome; that is, if the drug treatment results in decreased cell capacitance, dendritic hypotrophy develops, and a stress resilient phenotype emerges (ex. NPY and Y5), whereas if a drug treatment has no effect on measured cell capacitance, dendritic remodeling does not occur, and there is no long-term effect on behavior (ex. Y1). We have yet to identify if this trend persists in the opposite direction of increasing cell capacitance, dendritic hypertrophy and stress vulnerability develops, as no *in vivo* experiments have been completed rendering animals stress susceptible. Regardless, just from measuring and analyzing cell capacitance with an appropriate number of observations, we can accurately predict the morphological and long-term behavioral effects of a given drug treatment. This novel biomarker should provide an effortless and quick means to evaluate potential drug candidates for their ability to alter stress resilience or vulnerability in the BLA.

NPY- and CRF-mediated remodeling of the dendritic architecture is dependent on calcineurin and CaMKII activity, respectively.

Using our novel BLA OTCs, we have begun to unravel the perplexing intracellular signaling mechanisms regulating NPY- and CRF-mediated dendritic remodeling of BLA principal neurons. The results strongly implicate a role for opposing regulation of cytosolic protein phosphorylation by calcineurin and CaMKII, as blocking their activity prevents the effects of NPY and CRF, respectively, on dendritic morphology. As both enzymes are inherently associated with synaptic plasticity in the BLA, the resulting alterations in dendritic morphology due to NPY and CRF incubations likely involve some sort of effect on LTD and LTP, respectively. Although we did not directly examine these processes, future studies should employ techniques to quantitatively measure alterations in synaptic efficacy following repeated neuropeptide incubations. Furthermore, as the polarity of synaptic plasticity is

determined by the magnitude of intracellular calcium, measuring calcium dynamics following acute application of NPY and CRF should be explored to test the hypothesis that calcium flux plays an integral role in initiating dendritic remodeling. Ms Miranda has used our BLA OTCs in calcium imaging experiments using 2-photon microscopy, and preliminary work suggests they work quite well for measuring calcium dynamics. If altered intracellular calcium in response to NPY and CRF application is playing a role in reshaping the dendritic architecture of BLA principal neurons, the question that then arises is how? Preliminary work from other members of the Colmers lab suggests that acute application of both ahx and CRF act to inhibit a GIRK conductance in principal neurons of acutely prepared BLA slices (Mackay et al., unpublished). This would result in depolarization of the membrane, relieving magnesium-induced blockade of NMDA-receptors and influx of calcium through activated NMDA-receptors. Further preliminary evidence suggests acute application of NPY and the Y5-agonist may be inhibiting some subtype of VGCC in BLA principal neurons. Theoretically, any process that disturbs the tightly regulated levels of intracellular calcium could promote synaptic plasticity. Ms. Miranda is currently working on advancing our knowledge of the acute effects of Y5-receptor activation, while Mr. James Mackay is exploring the consequences of acute ahx application in acutely-prepared slices from adult rat brain slices. Together, their work should provide mechanistic insights into their roles in altered calcium flux.

Outstanding Questions

Possible role of the neurotrophic factor BDNF in NPY- and CRF-induced dendritic remodeling of BLA principal neurons.

The neurotrophin, BDNF, is a molecule that is implicated in modulating morphological changes to central neurons in response to and independently of stress, and has received much attention the past couple of decades due to its role in neuroplasticity and supporting neuronal survival. BDNF, like NPY, is translated as a precursor peptide (proBDNF) and requires proteolytic cleavage to its mature BDNF form (Seidah et al., 1996). This mature form primarily binds to tropomyosin-related kinase B (TrkB) receptors, causing receptor dimerization and autophosphorylation, leading to activation of a number of intracellular signaling cascades including MAPK/ERK, PLCϒ, and PI3K that produce a multitude of effects including neuoronal survival and growth, as well as enhancement of memory consolidation (Huang and Reichardt, 2003, Cohen-Cory et al., 2010, Ehrlich and Josselyn, 2015). Alternatively, proBDNF preferentially binds to low-affinity p75 neurotrophin receptors ($p75^{NTR}$) to activate signal transduction mechanisms that appear to have opposite effects to TrkB receptor activation (Lee et al., 2001, Woo et al., 2005). There is high expression of both BDNF and TrkB receptor mRNA throughout the brain and protein levels are particularly enriched in BLA principal cell bodies and processes (Conner et al., 1997, Gray et al., 2013). BDNF release is activity-dependent and many of its downstream effects on axonal and dendritic growth are mediated in a Ca^{2+} dependent manner through changes in local cytoskeletal dynamics, along with alterations in cytoskeletal protein and cell adhesion molecule gene expression (Horch and Katz, 2002, Horch, 2004, Lohmann and Wong, 2005, Mattson, 2008, Boyle, 2013). BDNF is thought to play a prominent role in mediating synaptic

plasticity by enhancing postsynaptic responses to glutamate through stimulation of NMDA receptor phosphorylation, and delivery of NR2B-containing NMDA receptors to the membrane (Caldeira et al., 2007). Furthermore, BDNF is required for learning and memory in the amygdala, as exogenous applied BDNF reduces the stimulation threshold for LTP, and blockade of TrkB receptors prevents LTP *in vitro*, and the acquisition of fear conditioning *in vivo* (Rattiner et al., 2004, Li et al., 2011, Meis et al., 2012).

Similarly to the contrasting effects of stress on the polarity of dendritic morphology and the temporal persistence, the hippocampus and amygdala appear to respond to stress with opposing BDNF expression patterns. The hippocampus responds to chronic immobilization stress by eliciting dendritic atrophy, reducing dendritic spine density and diminishing BDNF expression that is reversible during a 21-day period of post-stress recovery (Luine et al., 1994, Smith et al., 1995, Vyas et al., 2004, Lakshminarasimhan and Chattarji, 2012). Alternatively, the BLA acts in response to chronic stress by inducing principal neuron dendritic hypertrophy, increasing spine density and augmenting BDNF expression that persist past the 21-day post-stress recovery period (Vyas et al., 2004, Lakshminarasimhan and Chattarji, 2012, Padival et al., 2013b). Interestingly, chronic antidepressant treatment prevents stress-induced decreases in BDNF levels and dendritic hypotrophy in the hippocampus, while BDNF infusion or transgenic overexpression of BDNF produces an antidepressant-like effect and prevents stress-mediated dendritic hypotrophy (Nibuya et al., 1995, Chen et al., 2001, Shirayama et al., 2002, Govindarajan et al., 2006). The transgenic mice from the above study, exhibited spinogenesis in the BLA, which could be replicated in control mice by exposure to chronic stress (Govindarajan et al., 2006). Moreover, stress-induced spinogenesis was occluded in these transgenic mice suggesting a direct role for BDNF signaling in stress-induced plasticity

in the BLA. These studies and others have contributed to the "neurotrophic hypothesis", which states that symptoms associated with depression, both pathological and behavioral, are a result of decreased neurotrophic support, and conversely, that increasing neurotrophic support would lead to the resolution of these symptoms (Duman et al., 1997, Nestler et al., 2002, Duman and Monteggia, 2006). With such a wide body of literature establishing a role for BDNF as a compelling regulator of structural plasticity in various regions of the brain [for review see Gray et al. (2013), Bennett and Lagopoulos (2014)], it seems plausible that some of the effects observed with NPY and CRF on BLA principal dendritic morphology, and hence stress resilience or vulnerability could be a result of altered BDNF signaling. Further support for this hypothesis stems from work in the dendate gyrus of the hippocampus, whereby using lentiviral mediated overexpression or knockdown of BDNF in rats, resilience to chronic mild stress was dependent on BDNF expression (Taliaz et al., 2011). Thus, stress resilience in the BLA may develop in opposing fashion, whereby reductions in BDNF expression drives resilience through dendritic hypotrophy. To our knowledge, no study has yet to investigate this possible link between the neuropeptides we studied and BDNF, which would serve as an opportune set of future experiments. However, due to the dichotomy of brain-region specific differences in the regulation of dendritic morphology, as discussed above, targeting BDNF pharmacologically will likely serve as an ineffective treatment option for patients with various neuropsychiatric conditions.

Possible role of autophagy in neuropeptide mediated morphological remodeling.

Autophagy is the major cellular pathway for the degradation of long-lived proteins and cytoplasmic organelles, that involves sequestering material for delivery to the lysosome for degradation and recycling (Levine and Klionsky, 2004). It typically occurs as a cellular

response to both extracellular and intracellular stress conditions, and in mammalian systems, it is thought to play a role in physiological processes such as responding to starvation, cell growth control, anti-aging mechanisms and innate immunity. Conversely, deregulation of autophagy has been suggested to be intimately involved in certain pathologies including cancer, cardiomyopathy, muscular disease, and neurodegenerative disorders (Klionsky and Emr, 2000). It was recently discovered that NPY stimulates autophagy and enhances autophagic flux in rodent hypothalamic neurons (Aveleira et al., 2015). Moreover, the NPY-induced increase in autophagy was mediated by activation of Y1- and Y5-receptors, which was associated with concerted stimulation of PI3K, MEK/ERk and PKA signaling pathways. Additionally, autophagy has been implicated in synaptic remodeling in a number of animal models including those in *C. elegans* and *Drosophila* (Rowland et al., 2006, Shen and Ganetzky, 2009). More recently, in a mammalian model of autism spectrum disorder autophagy deficiency downstream of over-activated mammalian target of rapamycin (mTOR) was shown to contribute to increased spine density with a defect in net postnatal spine pruning, while correcting autophagy signaling normalized developmental dendritic spine pruning defects and social behaviors (Tang et al., 2014). Therefore, it seems plausible that NPY- and CRF-mediated dendritic remodeling of BLA principal neurons could be a result of increased and decreased autophagy, respectively. Our BLA OTCs would serve as a convenient model to test this hypothesis using commercially available kits to study the induction of autophagy.

Concluding Remarks

The development of our novel BLA OTC model provides us with an additional instrument to understand the neurobiology of adaptive and maladaptive stress responses in an isolated system. From the work described in this thesis, it has allowed mechanistic insight underlying the counter-regulation of the stress response due to neuropeptides in the BLA. We have provided the first known evidence of bi-directional synaptic and structural plasticity as a correlate of NPY- and CRF-mediated stress resilience and vulnerability, respectively, and a regulated balance of calcineurin and CaMKII signaling to be essential in these processes. Furthermore, a collaborative effort between Ms. Miranda and myself have established that activation of the Y5-receptor is responsible for mediating NPY's effects on dendritic hypotrophy and long-term anxiolytic behavior. Confirmation of the results obtained from complementary *in vivo* work further legitimizes BLA OTCs as a dependable model to further study the neurocircuitry in anxiety/stress-related behavior. As such, their use should provide an easy and straightforward method to advance our understanding of mechanisms regulating physiological and pathophysiological emotional states, in an effort to expedite rational drug design for the therapeutic treatment of patients with anxiety-related disorders.

Figure 6.1

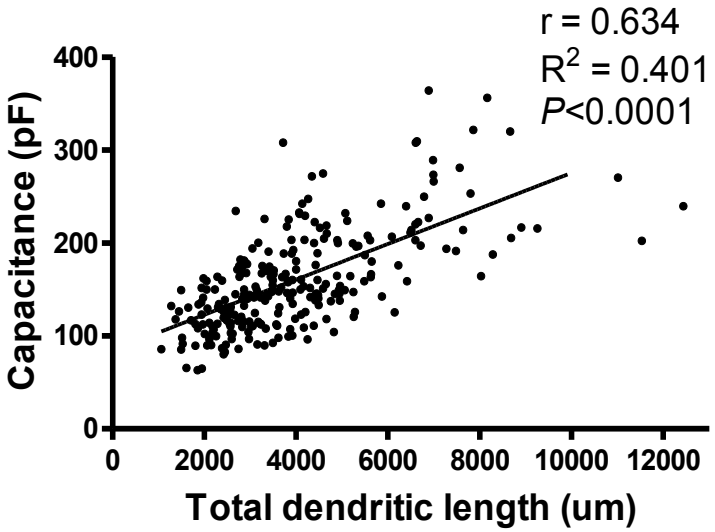

Figure 6.1 Principal neuron capacitance and total dendritic length are correlated in BLA OTCs.

Plotting cell capacitance versus total dendritic length for every principal neuron from BLA OTCs that morphology data was obtained revealed a strong correlation. Alterations in morphology can therefore, be predicted from changes in capacitance.

Table 6.1

	C_m	sEPSC Frequency	Total Dendritic Length	Sholl Analysis	# of Branches	Total Spines
NPY (100 nM)	↓	↓	↓	↓	↓	↓
CRF (30 nM)	↑	↑	↑	↑	↑	↑
NPY (100 nM) , CRF (30 nM)	⊘	⊘	⊘	⊘	⊘	⊘
CRF (30 nM) , NPY (100 nM)	⊘	⊘	⊘	⊘	⊘	⊘
Y1 (100 nM)	⊘	⊘	⊘	⊘	⊘	⊘
Y2 (100 nM)	↑	↑	↑	↑	↑	?
Y5 (100 nM)	↓	?	↓	↓	↓	↓
NPY (10nM) + CsA (2 μM)	↑	?	↑	↑	↑	?
Y5 (100 nM) + OA (10 nM)	↓	?	↓	↓	↓	?
CRF (30 nM) + AIP (40 nM)	⊘	?	?	?	?	?
AHX (100 nM) + NBI (100 nM)	↑	?	↑	↑	↑	?

Table 6.1 Summary of electrophysiological and morphological effects of various drug treatments in BLA OTCs.

A brief summary of electrophysiological, and morphological effects of various drugs in BLA OTCs. Symbols used: ↑ increases, ↓ decreases, ⊘ no change, ? unknown.

Table 6.2

	Acute Social Interaction (time)	Long-term Social Interaction (time)	C_m	Total Dendritic Length	Sholl Analysis	# of Branches
NPY (10 pmol)	↑	↑	↓	↓	↓	↓
Y1 (10 pmol)	↑	⊘	⊘	⊘	⊘	⊘
Y5 (10 pmol)	↑	↑	↓	↓	↓	↓

Table 6.2 Summary of NPY and NPY-agonists on behavior, capacitance and morphology of principal neurons *in vivo.*

A brief summary of repeated NPY and NPY-selective agonist injections *in vivo* on behavior, capacitance, and morphology. Symbols used: ↑ increases, ↓ decreases, ⊘ no change.

References

Adamec R, Fougere D, Risbrough V (2010) CRF receptor blockade prevents initiation and consolidation of stress effects on affect in the predator stress model of PTSD. The international journal of neuropsychopharmacology / official scientific journal of the Collegium Internationale Neuropsychopharmacologicum 13:747-757.

Adamec R, Hebert M, Blundell J, Mervis RF (2012) Dendritic morphology of amygdala and hippocampal neurons in more and less predator stress responsive rats and more and less spontaneously anxious handled controls. Behavioural brain research 226:133-146.

Adhikari A (2014) Distributed circuits underlying anxiety. Frontiers in behavioral neuroscience 8:112.

Adolphs R, Tranel D, Damasio H, Damasio A (1994) Impaired recognition of emotion in facial expressions following bilateral damage to the human amygdala. Nature 372:669-672.

Adrian TE, Allen JM, Bloom SR, Ghatei MA, Rossor MN, Roberts GW, Crow TJ, Tatemoto K, Polak JM (1983) Neuropeptide Y distribution in human brain. Nature 306:584-586.

Alexander SP, Benson HE, Faccenda E, Pawson AJ, Sharman JL, Spedding M, Peters JA, Harmar AJ, Collaborators C (2013) The Concise Guide to PHARMACOLOGY 2013/14: G protein-coupled receptors. British journal of pharmacology 170:1459-1581.

Anderson AK, Phelps EA (2001) Lesions of the human amygdala impair enhanced perception of emotionally salient events. Nature 411:305-309.

Aveleira CA, Botelho M, Carmo-Silva S, Pascoal JF, Ferreira-Marques M, Nobrega C, Cortes L, Valero J, Sousa-Ferreira L, Alvaro AR, Santana M, Kugler S, Pereira de Almeida L, Cavadas C (2015) Neuropeptide Y stimulates autophagy in hypothalamic neurons. Proceedings of the National Academy of Sciences of the United States of America 112:E1642-1651.

Avossa D, Rosato-Siri MD, Mazzarol F, Ballerini L (2003) Spinal circuits formation: a study of developmentally regulated markers in organotypic cultures of embryonic mouse spinal cord. Neuroscience 122:391-405.

Bacchi F, Mathe AA, Jimenez P, Stasi L, Arban R, Gerrard P, Caberlotto L (2006) Anxiolytic-like effect of the selective neuropeptide Y Y2 receptor antagonist BIIE0246 in the elevated plus-maze. Peptides 27:3202-3207.

Baker DG, West SA, Nicholson WE, Ekhator NN, Kasckow JW, Hill KK, Bruce AB, Orth DN, Geracioti TD, Jr. (1999) Serial CSF corticotropin-releasing hormone levels and adrenocortical activity in combat veterans with posttraumatic stress disorder. The American journal of psychiatry 156:585-588.

Bale TL, Contarino A, Smith GW, Chan R, Gold LH, Sawchenko PE, Koob GF, Vale WW, Lee KF (2000) Mice deficient for corticotropin-releasing hormone receptor-2 display anxiety-like behaviour and are hypersensitive to stress. Nature genetics 24:410-414.

Bale TL, Vale WW (2004) CRF and CRF receptors: role in stress responsivity and other behaviors. Annual review of pharmacology and toxicology 44:525-557.

Bandelow B, Reitt M, Rover C, Michaelis S, Gorlich Y, Wedekind D (2015) Efficacy of treatments for anxiety disorders: a meta-analysis. International clinical psychopharmacology 30:183-192.

Bandelow B, Zohar J, Hollander E, Kasper S, Moller HJ, Wfsbp Task Force on Treatment Guidelines for Anxiety O-C, Post-Traumatic Stress D, Zohar J, Hollander E, Kasper S, Moller HJ, Bandelow B, Allgulander C, Ayuso-Gutierrez J, Baldwin DS, Buenvicius R, Cassano G, Fineberg N, Gabriels L, Hindmarch I, Kaiya H, Klein DF, Lader M, Lecrubier Y, Lepine JP, Liebowitz MR, Lopez-Ibor JJ, Marazziti D, Miguel EC, Oh KS, Preter M, Rupprecht R, Sato M, Starcevic V, Stein DJ, van Ameringen M, Vega J (2008) World Federation of Societies of Biological Psychiatry (WFSBP) guidelines for the pharmacological treatment of anxiety, obsessive-compulsive and post-traumatic stress disorders - first revision. The world journal of biological psychiatry : the official journal of the World Federation of Societies of Biological Psychiatry 9:248-312.

Bannon AW, Seda J, Carmouche M, Francis JM, Norman MH, Karbon B, McCaleb ML (2000) Behavioral characterization of neuropeptide Y knockout mice. Brain research 868:79-87.

Bar-Yehuda D, Korngreen A (2008) Space-clamp problems when voltage clamping neurons expressing voltage-gated conductances. Journal of neurophysiology 99:1127-1136.

Baratta MV, Kodandaramaiah SB, Monahan PE, Yao J, Weber MD, Lin PA, Gisabella B, Petrossian N, Amat J, Kim K, Yang A, Forest CR, Boyden ES, Goosens KA (2015) Stress Enables Reinforcement-Elicited Serotonergic Consolidation of Fear Memory. Biological psychiatry.

Bardi M, Rhone AP, Franssen CL, Hampton JE, Shea EA, Hyer MM, Huber J, Lambert KG (2012) Behavioral training and predisposed coping strategies interact to influence resilience in male Long-Evans rats: implications for depression. Stress 15:306-317.

Barrett J, Armony JL (2009) Influence of trait anxiety on brain activity during the acquisition and extinction of aversive conditioning. Psychological medicine 39:255-265.

Bauer EP, Schafe GE, LeDoux JE (2002) NMDA receptors and L-type voltage-gated calcium channels contribute to long-term potentiation and different components of fear memory formation in the lateral amygdala. The Journal of neuroscience : the official journal of the Society for Neuroscience 22:5239-5249.

Baur V, Hanggi J, Jancke L (2012) Volumetric associations between uncinate fasciculus, amygdala, and trait anxiety. BMC neuroscience 13:4.

Benedek DM (2011) Posttraumatic stress disorder from Vietnam to today: the evolution of understanding during Eugene Brody's tenure at the journal of nervous and mental disease. The Journal of nervous and mental disease 199:544-552.

Bennett MR, Lagopoulos J (2014) Stress and trauma: BDNF control of dendritic-spine formation and regression. Progress in neurobiology 112:80-99.

Bennur S, Shankaranarayana Rao BS, Pawlak R, Strickland S, McEwen BS, Chattarji S (2007) Stress-induced spine loss in the medial amygdala is mediated by tissue-plasminogen activator. Neuroscience 144:8-16.

Berdel B, Morys J (2000) Expression of calbindin-D28k and parvalbumin during development of rat's basolateral amygdaloid complex. International journal of developmental neuroscience : the official journal of the International Society for Developmental Neuroscience 18:501-513.

Berdel B, Morys J, Maciejewska B (1997) Neuronal changes in the basolateral complex during development of the amygdala of the rat. International journal of developmental neuroscience : the official journal of the International Society for Developmental Neuroscience 15:755-765.

Berglund MM, Schober DA, Statnick MA, McDonald PH, Gehlert DR (2003) The use of bioluminescence resonance energy transfer 2 to study neuropeptide Y receptor agonist-induced beta-arrestin 2 interaction. The Journal of pharmacology and experimental therapeutics 306:147-156.

Bernard C (1878) Leçons sur les phénomènes de la vie communs aux animaux et aux végétaux. Paris,: J. B. Baillière et fils.

Berridge MJ (1998) Neuronal calcium signaling. Neuron 21:13-26.

Bertocchi I, Oberto A, Longo A, Mele P, Sabetta M, Bartolomucci A, Palanza P, Sprengel R, Eva C (2011) Regulatory functions of limbic Y1 receptors in body weight and anxiety uncovered by conditional knockout and maternal care. Proceedings of the National Academy of Sciences of the United States of America 108:19395-19400.

Biel M, Wahl-Schott C, Michalakis S, Zong X (2009) Hyperpolarization-activated cation channels: from genes to function. Physiological reviews 89:847-885.

Blanchard DC, Blanchard RJ (1972) Innate and conditioned reactions to threat in rats with amygdaloid lesions. Journal of comparative and physiological psychology 81:281-290.

Blechert J, Michael T, Vriends N, Margraf J, Wilhelm FH (2007) Fear conditioning in posttraumatic stress disorder: evidence for delayed extinction of autonomic, experiential, and behavioural responses. Behaviour research and therapy 45:2019-2033.

Blomqvist AG, Herzog H (1997) Y-receptor subtypes--how many more? Trends in neurosciences 20:294-298.

Boehme S, Ritter V, Tefikow S, Stangier U, Strauss B, Miltner WH, Straube T (2014) Brain activation during anticipatory anxiety in social anxiety disorder. Social cognitive and affective neuroscience 9:1413-1418.

Bousquet J, Meunier JM (1962) [Organotypic culture, on natural and artificial media, of fragments of the adult rat hypophysis]. Comptes rendus des seances de la Societe de biologie et de ses filiales 156:65-67.

Bouwmeester H, Smits K, Van Ree JM (2002) Neonatal development of projections to the basolateral amygdala from prefrontal and thalamic structures in rat. The Journal of comparative neurology 450:241-255.

Boyle LM (2013) A neuroplasticity hypothesis of chronic stress in the basolateral amygdala. The Yale journal of biology and medicine 86:117-125.

Brakch N, Rist B, Beck-Sickinger AG, Goenaga J, Wittek R, Burger E, Brunner HR, Grouzmann E (1997) Role of prohormone convertases in pro-neuropeptide Y processing: coexpression and in vitro kinetic investigations. Biochemistry 36:16309-16320.

Britton DR, Koob GF, Rivier J, Vale W (1982) Intraventricular corticotropin-releasing factor enhances behavioral effects of novelty. Life sciences 31:363-367.

Britton KT, Morgan J, Rivier J, Vale W, Koob GF (1985) Chlordiazepoxide attenuates response suppression induced by corticotropin-releasing factor in the conflict test. Psychopharmacology 86:170-174.

Bromee T, Sjodin P, Fredriksson R, Boswell T, Larsson TA, Salaneck E, Zoorob R, Mohell N, Larhammar D (2006) Neuropeptide Y-family receptors Y6 and Y7 in chicken. Cloning, pharmacological characterization, tissue distribution and conserved synteny with human chromosome region. The FEBS journal 273:2048-2063.

Broqua P, Wettstein JG, Rocher MN, Gauthier-Martin B, Junien JL (1995) Behavioral effects of neuropeptide Y receptor agonists in the elevated plus-maze and fear-potentiated startle procedures. Behavioural pharmacology 6:215-222.

Brown JS, Kalish HI, Farber IE (1951) Conditioned fear as revealed by magnitude of startle response to an auditory stimulus. Journal of experimental psychology 41:317-328.

Brown S, Sharpey-Schäfer EA (1888) An investigation into the functions of the occipital & temporal lobes of the monkey's brain. London,: Trübner.

Butler RK, White LC, Frederick-Duus D, Kaigler KF, Fadel JR, Wilson MA (2012) Comparison of the activation of somatostatin- and neuropeptide Y-containing neuronal

populations of the rat amygdala following two different anxiogenic stressors. Experimental neurology 238:52-63.

Caberlotto L, Fuxe K, Hurd YL (2000) Characterization of NPY mRNA-expressing cells in the human brain: co-localization with Y2 but not Y1 mRNA in the cerebral cortex, hippocampus, amygdala, and striatum. Journal of chemical neuroanatomy 20:327-337.

Cabrele C, Beck-Sickinger AG (2000) Molecular characterization of the ligand-receptor interaction of the neuropeptide Y family. Journal of peptide science : an official publication of the European Peptide Society 6:97-122.

Caldeira MV, Melo CV, Pereira DB, Carvalho RF, Carvalho AL, Duarte CB (2007) BDNF regulates the expression and traffic of NMDA receptors in cultured hippocampal neurons. Molecular and cellular neurosciences 35:208-219.

Calhoon GG, Tye KM (2015) Resolving the neural circuits of anxiety. Nature neuroscience 18:1394-1404.

Cannon WB (1915) Bodily changes in pain, hunger, fear, and rage; an account of recent researches into the function of emotional excitement. New York, London,: D. Appleton and Company.

Canteras NS, Resstel LB, Bertoglio LJ, Carobrez Ade P, Guimaraes FS (2010) Neuroanatomy of anxiety. Current topics in behavioral neurosciences 2:77-96.

Cascade E, Kalali AH (2008) Use of benzodiazepines in the treatment of anxiety. Psychiatry 5:21-22.

Chalmers DT, Lovenberg TW, De Souza EB (1995) Localization of novel corticotropin-releasing factor receptor (CRF2) mRNA expression to specific subcortical nuclei in rat brain: comparison with CRF1 receptor mRNA expression. The Journal of neuroscience : the official journal of the Society for Neuroscience 15:6340-6350.

Chapman PF, Kairiss EW, Keenan CL, Brown TH (1990) Long-term synaptic potentiation in the amygdala. Synapse 6:271-278.

Charney DS (2004) Psychobiological mechanisms of resilience and vulnerability: implications for successful adaptation to extreme stress. The American journal of psychiatry 161:195-216.

Chee MJ, Myers MG, Jr., Price CJ, Colmers WF (2010) Neuropeptide Y suppresses anorexigenic output from the ventromedial nucleus of the hypothalamus. The Journal of neuroscience : the official journal of the Society for Neuroscience 30:3380-3390.

Chen B, Dowlatshahi D, MacQueen GM, Wang JF, Young LT (2001) Increased hippocampal BDNF immunoreactivity in subjects treated with antidepressant medication. Biological psychiatry 50:260-265.

Chung L, Moore SD (2009) Neuropeptides modulate compound postsynaptic potentials in basolateral amygdala. Neuroscience 164:1389-1397.

Ciocchi S, Herry C, Grenier F, Wolff SB, Letzkus JJ, Vlachos I, Ehrlich I, Sprengel R, Deisseroth K, Stadler MB, Muller C, Luthi A (2010) Encoding of conditioned fear in central amygdala inhibitory circuits. Nature 468:277-282.

Cippitelli A, Rezvani AH, Robinson JE, Eisenberg L, Levin ED, Bonaventure P, Motley ST, Lovenberg TW, Heilig M, Thorsell A (2011) The novel, selective, brain-penetrant neuropeptide Y Y2 receptor antagonist, JNJ-31020028, tested in animal models of alcohol consumption, relapse, and anxiety. Alcohol 45:567-576.

Citri A, Malenka RC (2008) Synaptic plasticity: multiple forms, functions, and mechanisms. Neuropsychopharmacology : official publication of the American College of Neuropsychopharmacology 33:18-41.

Clugnet MC, LeDoux JE (1990) Synaptic plasticity in fear conditioning circuits: induction of LTP in the lateral nucleus of the amygdala by stimulation of the medial geniculate body. The Journal of neuroscience : the official journal of the Society for Neuroscience 10:2818-2824.

Cohen H, Kozlovsky N, Matar MA, Zohar J, Kaplan Z (2014) Distinctive hippocampal and amygdalar cytoarchitectural changes underlie specific patterns of behavioral disruption following stress exposure in an animal model of PTSD. European neuropsychopharmacology : the journal of the European College of Neuropsychopharmacology 24:1925-1944.

Cohen H, Liu T, Kozlovsky N, Kaplan Z, Zohar J, Mathe AA (2012) The neuropeptide Y (NPY)-ergic system is associated with behavioral resilience to stress exposure in an animal model of post-traumatic stress disorder. Neuropsychopharmacology : official publication of the American College of Neuropsychopharmacology 37:350-363.

Cohen-Cory S, Kidane AH, Shirkey NJ, Marshak S (2010) Brain-derived neurotrophic factor and the development of structural neuronal connectivity. Developmental neurobiology 70:271-288.

Collingridge GL, Bliss TV (1995) Memories of NMDA receptors and LTP. Trends in neurosciences 18:54-56.

Conner JM, Lauterborn JC, Yan Q, Gall CM, Varon S (1997) Distribution of brain-derived neurotrophic factor (BDNF) protein and mRNA in the normal adult rat CNS: evidence for anterograde axonal transport. The Journal of neuroscience : the official journal of the Society for Neuroscience 17:2295-2313.

Conrad CD, LeDoux JE, Magarinos AM, McEwen BS (1999) Repeated restraint stress facilitates fear conditioning independently of causing hippocampal CA3 dendritic atrophy. Behavioral neuroscience 113:902-913.

Cook SC, Wellman CL (2004) Chronic stress alters dendritic morphology in rat medial prefrontal cortex. Journal of neurobiology 60:236-248.

Cooper MA, Clinard CT, Morrison KE (2015) Neurobiological mechanisms supporting experience-dependent resistance to social stress. Neuroscience 291:1-14.

Coplan JD, Andrews MW, Rosenblum LA, Owens MJ, Friedman S, Gorman JM, Nemeroff CB (1996) Persistent elevations of cerebrospinal fluid concentrations of corticotropin-releasing factor in adult nonhuman primates exposed to early-life stressors: implications for the pathophysiology of mood and anxiety disorders. Proceedings of the National Academy of Sciences of the United States of America 93:1619-1623.

Corbit LH, Leung BK, Balleine BW (2013) The role of the amygdala-striatal pathway in the acquisition and performance of goal-directed instrumental actions. The Journal of neuroscience : the official journal of the Society for Neuroscience 33:17682-17690.

Costall B, Jones BJ, Kelly ME, Naylor RJ, Tomkins DM (1989) Exploration of mice in a black and white test box: validation as a model of anxiety. Pharmacology, biochemistry, and behavior 32:777-785.

Crawley JN (1985) Exploratory behavior models of anxiety in mice. Neuroscience and biobehavioral reviews 9:37-44.

Cummings JA, Mulkey RM, Nicoll RA, Malenka RC (1996) Ca2+ signaling requirements for long-term depression in the hippocampus. Neuron 16:825-833.

Dailey ME, Smith SJ (1996) The dynamics of dendritic structure in developing hippocampal slices. The Journal of neuroscience : the official journal of the Society for Neuroscience 16:2983-2994.

Dautzenberg FM, Hauger RL (2002) The CRF peptide family and their receptors: yet more partners discovered. Trends in pharmacological sciences 23:71-77.

Davila JC, Olmos L, Legaz I, Medina L, Guirado S, Real MA (2008) Dynamic patterns of colocalization of calbindin, parvalbumin and GABA in subpopulations of mouse basolateral amygdalar cells during development. Journal of chemical neuroanatomy 35:67-76.

Davis M, Walker DL, Miles L, Grillon C (2010) Phasic vs sustained fear in rats and humans: role of the extended amygdala in fear vs anxiety. Neuropsychopharmacology : official publication of the American College of Neuropsychopharmacology 35:105-135.

De Bellis MD, Casey BJ, Dahl RE, Birmaher B, Williamson DE, Thomas KM, Axelson DA, Frustaci K, Boring AM, Hall J, Ryan ND (2000) A pilot study of amygdala volumes in pediatric generalized anxiety disorder. Biological psychiatry 48:51-57.

de Groen PC, Aksamit AJ, Rakela J, Forbes GS, Krom RA (1987) Central nervous system toxicity after liver transplantation. The role of cyclosporine and cholesterol. The New England journal of medicine 317:861-866.

De Simoni A, Griesinger CB, Edwards FA (2003) Development of rat CA1 neurones in acute versus organotypic slices: role of experience in synaptic morphology and activity. The Journal of physiology 550:135-147.

Debanne D, Guerineau NC, Gahwiler BH, Thompson SM (1995) Physiology and pharmacology of unitary synaptic connections between pairs of cells in areas CA3 and CA1 of rat hippocampal slice cultures. Journal of neurophysiology 73:1282-1294.

Dinan T (2006) Therapeutic options: Addressing the current dilemma. European neuropsychopharmacology : the journal of the European College of Neuropsychopharmacology 16 Suppl 2:S119-127.

Domschke K, Hohoff C, Jacob C, Maier W, Fritze J, Bandelow B, Krakowitzky P, Kastner F, Rothermundt M, Arolt V, Deckert J (2008) Chromosome 4q31-34 panic disorder risk locus: association of neuropeptide Y Y5 receptor variants. American journal of medical genetics Part B, Neuropsychiatric genetics : the official publication of the International Society of Psychiatric Genetics 147B:510-516.

Doyere V, Schafe GE, Sigurdsson T, LeDoux JE (2003) Long-term potentiation in freely moving rats reveals asymmetries in thalamic and cortical inputs to the lateral amygdala. The European journal of neuroscience 17:2703-2715.

Drexler B, Hentschke H, Antkowiak B, Grasshoff C (2010) Organotypic cultures as tools for testing neuroactive drugs - link between in-vitro and in-vivo experiments. Current medicinal chemistry 17:4538-4550.

Ducottet C, Griebel G, Belzung C (2003) Effects of the selective nonpeptide corticotropin-releasing factor receptor 1 antagonist antalarmin in the chronic mild stress model of depression in mice. Progress in neuro-psychopharmacology & biological psychiatry 27:625-631.

Duman RS, Heninger GR, Nestler EJ (1997) A molecular and cellular theory of depression. Archives of general psychiatry 54:597-606.

Duman RS, Monteggia LM (2006) A neurotrophic model for stress-related mood disorders. Biological psychiatry 59:1116-1127.

Dumont Y, Jacques D, Bouchard P, Quirion R (1998) Species differences in the expression and distribution of the neuropeptide Y Y1, Y2, Y4, and Y5 receptors in rodents, guinea pig, and primates brains. The Journal of comparative neurology 402:372-384.

Duval ER, Javanbakht A, Liberzon I (2015) Neural circuits in anxiety and stress disorders: a focused review. Therapeutics and clinical risk management 11:115-126.

Eaton K, Sallee FR, Sah R (2007) Relevance of neuropeptide Y (NPY) in psychiatry. Current topics in medicinal chemistry 7:1645-1659.

Ehrlich DE, Josselyn SA (2015) Plasticity-related genes in brain development and amygdala-dependent learning. Genes, brain, and behavior.

Ehrlich DE, Ryan SJ, Hazra R, Guo JD, Rainnie DG (2013) Postnatal maturation of GABAergic transmission in the rat basolateral amygdala. Journal of neurophysiology 110:926-941.

Ehrlich DE, Ryan SJ, Rainnie DG (2012) Postnatal development of electrophysiological properties of principal neurons in the rat basolateral amygdala. The Journal of physiology 590:4819-4838.

El Bahh B, Balosso S, Hamilton T, Herzog H, Beck-Sickinger AG, Sperk G, Gehlert DR, Vezzani A, Colmers WF (2005) The anti-epileptic actions of neuropeptide Y in the hippocampus are mediated by Y and not Y receptors. The European journal of neuroscience 22:1417-1430.

Engel JA, Hjorth S, Svensson K, Carlsson A, Liljequist S (1984) Anticonflict effect of the putative serotonin receptor agonist 8-hydroxy-2-(di-n-propylamino)tetralin (8-OH-DPAT). European journal of pharmacology 105:365-368.

Etkin A, Wager TD (2007) Functional neuroimaging of anxiety: a meta-analysis of emotional processing in PTSD, social anxiety disorder, and specific phobia. The American journal of psychiatry 164:1476-1488.

Eugene E, Cluzeaud F, Cifuentes-Diaz C, Fricker D, Le Duigou C, Clemenceau S, Baulac M, Poncer JC, Miles R (2014) An organotypic brain slice preparation from adult patients with temporal lobe epilepsy. Journal of neuroscience methods 235:234-244.

Farrell MR, Gruene TM, Shansky RM (2015) The influence of stress and gonadal hormones on neuronal structure and function. Hormones and behavior.

Felix-Ortiz AC, Burgos-Robles A, Bhagat ND, Leppla CA, Tye KM (2015) Bidirectional modulation of anxiety-related and social behaviors by amygdala projections to the medial prefrontal cortex. Neuroscience.

Felix-Ortiz AC, Tye KM (2014) Amygdala inputs to the ventral hippocampus bidirectionally modulate social behavior. The Journal of neuroscience : the official journal of the Society for Neuroscience 34:586-595.

Fendt M, Burki H, Imobersteg S, Lingenhohl K, McAllister KH, Orain D, Uzunov DP, Chaperon F (2009) Fear-reducing effects of intra-amygdala neuropeptide Y infusion in animal models of conditioned fear: an NPY Y1 receptor independent effect. Psychopharmacology 206:291-301.

Fendt M, Schmid S (2002) Metabotropic glutamate receptors are involved in amygdaloid plasticity. The European journal of neuroscience 15:1535-1541.

File SE, Hyde JRG (1978) Can Social-Interaction Be Used to Measure Anxiety. British journal of pharmacology 62:19-24.

Fisher S, Reason JT (1988) Handbook of life stress, cognition, and health. Chichester ; New York: Wiley.

Frade MA, de Andrade TA, Aguiar AF, Guedes FA, Leite MN, Passos WR, Coelho EB, Das PK (2015) Prolonged viability of human organotypic skin explant in culture method (hOSEC). Anais brasileiros de dermatologia 90:347-350.

Gahwiler BH (1981a) Morphological differentiation of nerve cells in thin organotypic cultures derived from rat hippocampus and cerebellum. Proceedings of the Royal Society of London Series B, Biological sciences 211:287-290.

Gahwiler BH (1981b) Organotypic monolayer cultures of nervous tissue. Journal of neuroscience methods 4:329-342.

Gahwiler BH, Capogna M, Debanne D, McKinney RA, Thompson SM (1997) Organotypic slice cultures: a technique has come of age. Trends in neurosciences 20:471-477.

Gehlert DR, Schober DA, Morin M, Berglund MM (2007) Co-expression of neuropeptide Y Y1 and Y5 receptors results in heterodimerization and altered functional properties. Biochemical pharmacology 74:1652-1664.

Gehlert DR, Shekhar A, Morin SM, Hipskind PA, Zink C, Gackenheimer SL, Shaw J, Fitz SD, Sajdyk TJ (2005) Stress and central Urocortin increase anxiety-like behavior in the social interaction test via the CRF1 receptor. European journal of pharmacology 509:145-153.

Gerfin-Moser A, Monyer H (2002) In situ hybridization on organotypic slice cultures. International review of neurobiology 47:125-134.

Giesbrecht CJ, Mackay JP, Silveira HB, Urban JH, Colmers WF (2010) Countervailing modulation of Ih by neuropeptide Y and corticotrophin-releasing factor in basolateral amygdala as a possible mechanism for their effects on stress-related behaviors. The Journal of neuroscience : the official journal of the Society for Neuroscience 30:16970-16982.

Gogolla N, Galimberti I, DePaola V, Caroni P (2006) Long-term live imaging of neuronal circuits in organotypic hippocampal slice cultures. Nature protocols 1:1223-1226.

Golowasch J, Thomas G, Taylor AL, Patel A, Pineda A, Khalil C, Nadim F (2009) Membrane capacitance measurements revisited: dependence of capacitance value on measurement method in nonisopotential neurons. Journal of neurophysiology 102:2161-2175.

Govindarajan A, Rao BS, Nair D, Trinh M, Mawjee N, Tonegawa S, Chattarji S (2006) Transgenic brain-derived neurotrophic factor expression causes both anxiogenic and antidepressant effects. Proceedings of the National Academy of Sciences of the United States of America 103:13208-13213.

Gray JD, Milner TA, McEwen BS (2013) Dynamic plasticity: the role of glucocorticoids, brain-derived neurotrophic factor and other trophic factors. Neuroscience 239:214-227.

Gray JM, Vecchiarelli HA, Morena M, Lee TT, Hermanson DJ, Kim AB, McLaughlin RJ, Hassan KI, Kuhne C, Wotjak CT, Deussing JM, Patel S, Hill MN (2015) Corticotropin-releasing hormone drives anandamide hydrolysis in the amygdala to promote anxiety. The Journal of neuroscience : the official journal of the Society for Neuroscience 35:3879-3892.

Griffin CE, 3rd, Kaye AM, Bueno FR, Kaye AD (2013) Benzodiazepine pharmacology and central nervous system-mediated effects. The Ochsner journal 13:214-223.

Gutman AR, Yang Y, Ressler KJ, Davis M (2008) The role of neuropeptide Y in the expression and extinction of fear-potentiated startle. The Journal of neuroscience : the official journal of the Society for Neuroscience 28:12682-12690.

Guy Y, Rupert AE, Sandberg M, Weber SG (2011) A simple method for measuring organotypic tissue slice culture thickness. Journal of neuroscience methods 199:78-81.

Hall E (1972) Some aspects of the structural organization of the amygdala. In: *The neurobiology of the amygdala*; the proceedings of a Symposium on the Neurobiology of the Amygdala, Bar Harbor, Maine, June 6-17, 1971. New York,: Plenum Press.

Hamilton TJ, Wheatley BM, Sinclair DB, Bachmann M, Larkum ME, Colmers WF (2010) Dopamine modulates synaptic plasticity in dendrites of rat and human dentate granule cells. Proceedings of the National Academy of Sciences of the United States of America 107:18185-18190.

Hamilton TJ, Xapelli S, Michaelson SD, Larkum ME, Colmers WF (2013) Modulation of distal calcium electrogenesis by neuropeptide Y(1) receptors inhibits neocortical long-term depression. The Journal of neuroscience : the official journal of the Society for Neuroscience 33:11184-11193.

Hanson JE, Blank M, Valenzuela RA, Garner CC, Madison DV (2007) The functional nature of synaptic circuitry is altered in area CA3 of the hippocampus in a mouse model of Down's syndrome. The Journal of physiology 579:53-67.

Hanson JE, Madison DV (2007) Presynaptic FMR1 genotype influences the degree of synaptic connectivity in a mosaic mouse model of fragile X syndrome. The Journal of neuroscience : the official journal of the Society for Neuroscience 27:4014-4018.

Hastings JA, McClure-Sharp JM, Morris MJ (2001) NPY Y1 receptors exert opposite effects on corticotropin releasing factor and noradrenaline overflow from the rat hypothalamus in vitro. Brain research 890:32-37.

Haubensak W, Kunwar PS, Cai H, Ciocchi S, Wall NR, Ponnusamy R, Biag J, Dong HW, Deisseroth K, Callaway EM, Fanselow MS, Luthi A, Anderson DJ (2010) Genetic dissection of an amygdala microcircuit that gates conditioned fear. Nature 468:270-276.

Hawley DF, Bardi M, Everette AM, Higgins TJ, Tu KM, Kinsley CH, Lambert KG (2010) Neurobiological constituents of active, passive, and variable coping strategies in rats: integration of regional brain neuropeptide Y levels and cardiovascular responses. Stress 13:172-183.

Heilig M (2004) The NPY system in stress, anxiety and depression. Neuropeptides 38:213-224.

Heilig M, Koob GF, Ekman R, Britton KT (1994) Corticotropin-releasing factor and neuropeptide Y: role in emotional integration. Trends in neurosciences 17:80-85.

Heilig M, McLeod S, Brot M, Heinrichs SC, Menzaghi F, Koob GF, Britton KT (1993) Anxiolytic-like action of neuropeptide Y: mediation by Y1 receptors in amygdala, and dissociation from food intake effects. Neuropsychopharmacology : official publication of the American College of Neuropsychopharmacology 8:357-363.

Heilig M, Soderpalm B, Engel JA, Widerlov E (1989) Centrally administered neuropeptide Y (NPY) produces anxiolytic-like effects in animal anxiety models. Psychopharmacology 98:524-529.

Heinrichs SC, Lapsansky J, Lovenberg TW, De Souza EB, Chalmers DT (1997) Corticotropin-releasing factor CRF1, but not CRF2, receptors mediate anxiogenic-like behavior. Regulatory peptides 71:15-21.

Heinrichs SC, Pich EM, Miczek KA, Britton KT, Koob GF (1992) Corticotropin-releasing factor antagonist reduces emotionality in socially defeated rats via direct neurotropic action. Brain research 581:190-197.

Herzog H, Hort YJ, Ball HJ, Hayes G, Shine J, Selbie LA (1992) Cloned human neuropeptide Y receptor couples to two different second messenger systems. Proceedings of the National Academy of Sciences of the United States of America 89:5794-5798.

Hill MN, Hillard CJ, McEwen BS (2011) Alterations in corticolimbic dendritic morphology and emotional behavior in cannabinoid CB1 receptor-deficient mice parallel the effects of chronic stress. Cerebral cortex 21:2056-2064.

Hill MN, Kumar SA, Filipski SB, Iverson M, Stuhr KL, Keith JM, Cravatt BF, Hillard CJ, Chattarji S, McEwen BS (2013) Disruption of fatty acid amide hydrolase activity

prevents the effects of chronic stress on anxiety and amygdalar microstructure. Molecular psychiatry 18:1125-1135.

Hirschfeld RM (2001) The Comorbidity of Major Depression and Anxiety Disorders: Recognition and Management in Primary Care. Primary care companion to the Journal of clinical psychiatry 3:244-254.

Holliday ND, Lam CW, Tough IR, Cox HM (2005) Role of the C terminus in neuropeptide Y Y1 receptor desensitization and internalization. Molecular pharmacology 67:655-664.

Holopainen IE, Lauren HB (2003) Neuronal activity regulates GABAA receptor subunit expression in organotypic hippocampal slice cultures. Neuroscience 118:967-974.

Holzer P, Reichmann F, Farzi A (2012) Neuropeptide Y, peptide YY and pancreatic polypeptide in the gut-brain axis. Neuropeptides 46:261-274.

Horch HW (2004) Local effects of BDNF on dendritic growth. Reviews in the neurosciences 15:117-129.

Horch HW, Katz LC (2002) BDNF release from single cells elicits local dendritic growth in nearby neurons. Nature neuroscience 5:1177-1184.

Huang EJ, Reichardt LF (2003) Trk receptors: roles in neuronal signal transduction. Annual review of biochemistry 72:609-642.

Humeau Y, Herry C, Kemp N, Shaban H, Fourcaudot E, Bissiere S, Luthi A (2005) Dendritic spine heterogeneity determines afferent-specific Hebbian plasticity in the amygdala. Neuron 45:119-131.

Humpel C (2015a) Organotypic brain slice cultures: A review. Neuroscience 305:86-98.

Humpel C (2015b) Organotypic vibrosections from whole brain adult Alzheimer mice (overexpressing amyloid-precursor-protein with the Swedish-Dutch-Iowa mutations) as a model to study clearance of beta-amyloid plaques. Frontiers in aging neuroscience 7:47.

Humpel C, Weis C (2002) Nerve growth factor and cholinergic CNS neurons studied in organotypic brain slices. Implication in Alzheimer's disease? Journal of neural transmission Supplementum 253-263.

Ito M, Dumont Y, Quirion R (2013) Mood and memory-associated behaviors in neuropeptide Y5 knockout mice. Neuropeptides 47:75-84.

Jahnsen H, Kristensen BW, Thiebaud P, Noraberg J, Jakobsen B, Bove M, Martinoia S, Koudelka-Hep M, Grattarola M, Zimmer J (1999) Coupling of organotypic brain slice cultures to silicon-based arrays of electrodes. Methods 18:160-172.

Janak PH, Tye KM (2015) From circuits to behaviour in the amygdala. Nature 517:284-292.

Jansen AS, Nguyen XV, Karpitskiy V, Mettenleiter TC, Loewy AD (1995) Central command neurons of the sympathetic nervous system: basis of the fight-or-flight response. Science 270:644-646.

Jennings JH, Stuber GD (2014) Tools for resolving functional activity and connectivity within intact neural circuits. Current biology : CB 24:R41-50.

Johansen JP, Cain CK, Ostroff LE, LeDoux JE (2011) Molecular mechanisms of fear learning and memory. Cell 147:509-524.

Johansen JP, Hamanaka H, Monfils MH, Behnia R, Deisseroth K, Blair HT, LeDoux JE (2010) Optical activation of lateral amygdala pyramidal cells instructs associative fear learning. Proceedings of the National Academy of Sciences of the United States of America 107:12692-12697.

Johnson HA, Buonomano DV (2007) Development and plasticity of spontaneous activity and Up states in cortical organotypic slices. The Journal of neuroscience : the official journal of the Society for Neuroscience 27:5915-5925.

Josselyn SA, Shi C, Carlezon WA, Jr., Neve RL, Nestler EJ, Davis M (2001) Long-term memory is facilitated by cAMP response element-binding protein overexpression in the amygdala. The Journal of neuroscience : the official journal of the Society for Neuroscience 21:2404-2412.

Kahan BD, Flechner SM, Lorber MI, Golden D, Conley S, Van Buren CT (1987) Complications of cyclosporine-prednisone immunosuppression in 402 renal allograft recipients exclusively followed at a single center for from one to five years. Transplantation 43:197-204.

Kalin NH, Takahashi LK, Chen FL (1994) Restraint stress increases corticotropin-releasing hormone mRNA content in the amygdala and paraventricular nucleus. Brain research 656:182-186.

Kallupi M, Vendruscolo LF, Carmichael CY, George O, Koob GF, Gilpin NW (2014) Neuropeptide YY(2)R blockade in the central amygdala reduces anxiety-like behavior but not alcohol drinking in alcohol-dependent rats. Addiction biology 19:755-757.

Karl T, Burne TH, Herzog H (2006) Effect of Y1 receptor deficiency on motor activity, exploration, and anxiety. Behavioural brain research 167:87-93.

Karl T, Duffy L, Herzog H (2008) Behavioural profile of a new mouse model for NPY deficiency. The European journal of neuroscience 28:173-180.

Kash TL, Winder DG (2006) Neuropeptide Y and corticotropin-releasing factor bi-directionally modulate inhibitory synaptic transmission in the bed nucleus of the stria terminalis. Neuropharmacology 51:1013-1022.

Kask A, Harro J, von Horsten S, Redrobe JP, Dumont Y, Quirion R (2002) The neurocircuitry and receptor subtypes mediating anxiolytic-like effects of neuropeptide Y. Neuroscience and biobehavioral reviews 26:259-283.

Kask A, Nguyen HP, Pabst R, Von Horsten S (2001a) Neuropeptide Y Y1 receptor-mediated anxiolysis in the dorsocaudal lateral septum: functional antagonism of corticotropin-releasing hormone-induced anxiety. Neuroscience 104:799-806.

Kask A, Rago L, Harro J (1997) Alpha-helical CRF(9-41) prevents anxiogenic-like effect of NPY Y1 receptor antagonist BIBP3226 in rats. Neuroreport 8:3645-3647.

Kask A, Rago L, Harro J (1998) Anxiolytic-like effect of neuropeptide Y (NPY) and NPY13-36 microinjected into vicinity of locus coeruleus in rats. Brain research 788:345-348.

Kask A, Vasar E, Heidmets LT, Allikmets L, Wikberg JE (2001b) Neuropeptide Y Y(5) receptor antagonist CGP71683A: the effects on food intake and anxiety-related behavior in the rat. European journal of pharmacology 414:215-224.

Keck ME, Welt T, Wigger A, Renner U, Engelmann M, Holsboer F, Landgraf R (2001) The anxiolytic effect of the CRH(1) receptor antagonist R121919 depends on innate emotionality in rats. The European journal of neuroscience 13:373-380.

Keller-Wood ME, Dallman MF (1984) Corticosteroid inhibition of ACTH secretion. Endocrine reviews 5:1-24.

Kemppainen S, Pitkanen A (2000) Distribution of parvalbumin, calretinin, and calbindin-D(28k) immunoreactivity in the rat amygdaloid complex and colocalization with gamma-aminobutyric acid. The Journal of comparative neurology 426:441-467.

Kessler RC, Angermeyer M, Anthony JC, R DEG, Demyttenaere K, Gasquet I, G DEG, Gluzman S, Gureje O, Haro JM, Kawakami N, Karam A, Levinson D, Medina Mora ME, Oakley Browne MA, Posada-Villa J, Stein DJ, Adley Tsang CH, Aguilar-Gaxiola S, Alonso J, Lee S, Heeringa S, Pennell BE, Berglund P, Gruber MJ, Petukhova M, Chatterji S, Ustun TB (2007) Lifetime prevalence and age-of-onset distributions of mental disorders in the World Health Organization's World Mental Health Survey Initiative. World psychiatry : official journal of the World Psychiatric Association 6:168-176.

Kim H, Kim E, Park M, Lee E, Namkoong K (2013) Organotypic hippocampal slice culture from the adult mouse brain: a versatile tool for translational neuropsychopharmacology. Progress in neuro-psychopharmacology & biological psychiatry 41:36-43.

King EC, Pattwell SS, Sun A, Glatt CE, Lee FS (2013) Nonlinear developmental trajectory of fear learning and memory. Annals of the New York Academy of Sciences 1304:62-69.

Klionsky DJ, Emr SD (2000) Autophagy as a regulated pathway of cellular degradation. Science 290:1717-1721.

Kopp J, Xu ZQ, Zhang X, Pedrazzini T, Herzog H, Kresse A, Wong H, Walsh JH, Hokfelt T (2002) Expression of the neuropeptide Y Y1 receptor in the CNS of rat and of wild-type and Y1 receptor knock-out mice. Focus on immunohistochemical localization. Neuroscience 111:443-532.

Krettek JE, Price JL (1978) A description of the amygdaloid complex in the rat and cat with observations on intra-amygdaloid axonal connections. The Journal of comparative neurology 178:255-280.

Krohg K, Hageman I, Jorgensen MB (2008) Corticotropin-releasing factor (CRF) in stress and disease: a review of literature and treatment perspectives with special emphasis on psychiatric disorders. Nordic journal of psychiatry 62:8-16.

Kuehn D, Majeed S, Guedj E, Dulize R, Baumer K, Iskandar A, Boue S, Martin F, Kostadinova R, Mathis C, Ivanov NV, Frentzel S, Hoeng J, Peitsch MC (2015) Impact assessment of repeated exposure of organotypic 3D bronchial and nasal tissue culture models to whole cigarette smoke. Journal of visualized experiments : JoVE.

Lai KO, Ip NY (2013) Structural plasticity of dendritic spines: the underlying mechanisms and its dysregulation in brain disorders. Biochimica et biophysica acta 1832:2257-2263.

Lakshminarasimhan H, Chattarji S (2012) Stress leads to contrasting effects on the levels of brain derived neurotrophic factor in the hippocampus and amygdala. PloS one 7:e30481.

Lang PJ, Davis M, Ohman A (2000) Fear and anxiety: animal models and human cognitive psychophysiology. Journal of affective disorders 61:137-159.

LeDoux JE (1992) Brain mechanisms of emotion and emotional learning. Current opinion in neurobiology 2:191-197.

LeDoux JE, Cicchetti P, Xagoraris A, Romanski LM (1990) The lateral amygdaloid nucleus: sensory interface of the amygdala in fear conditioning. The Journal of neuroscience : the official journal of the Society for Neuroscience 10:1062-1069.

Lee R, Kermani P, Teng KK, Hempstead BL (2001) Regulation of cell survival by secreted proneurotrophins. Science 294:1945-1948.

Lehmann EL, D'Abrera HJM (2006) Nonparametrics : statistical methods based on ranks. New York: Springer.

Leitermann RJ, Sajdyk TJ, Urban JH (2012) Cell-specific expression of calcineurin immunoreactivity within the rat basolateral amygdala complex and colocalization with the neuropeptide Y Y1 receptor. Journal of chemical neuroanatomy 45:50-56.

Lesting J, Narayanan RT, Kluge C, Sangha S, Seidenbecher T, Pape HC (2011) Patterns of coupled theta activity in amygdala-hippocampal-prefrontal cortical circuits during fear extinction. PloS one 6:e21714.

Leuner B, Shors TJ (2013) Stress, anxiety, and dendritic spines: what are the connections? Neuroscience 251:108-119.

Levine B, Klionsky DJ (2004) Development by self-digestion: molecular mechanisms and biological functions of autophagy. Developmental cell 6:463-477.

Lewis AS, Chetkovich DM (2011) HCN channels in behavior and neurological disease: too hyper or not active enough? Molecular and cellular neurosciences 46:357-367.

Li C, Dabrowska J, Hazra R, Rainnie DG (2011) Synergistic activation of dopamine D1 and TrkB receptors mediate gain control of synaptic plasticity in the basolateral amygdala. PloS one 6:e26065.

Liang KC, Melia KR, Campeau S, Falls WA, Miserendino MJ, Davis M (1992) Lesions of the central nucleus of the amygdala, but not the paraventricular nucleus of the hypothalamus, block the excitatory effects of corticotropin-releasing factor on the acoustic startle reflex. The Journal of neuroscience : the official journal of the Society for Neuroscience 12:2313-2320.

Lin CH, Lee CC, Gean PW (2003a) Involvement of a calcineurin cascade in amygdala depotentiation and quenching of fear memory. Molecular pharmacology 63:44-52.

Lin CH, Lee CC, Huang YC, Wang SJ, Gean PW (2005) Activation of group II metabotropic glutamate receptors induces depotentiation in amygdala slices and reduces fear-potentiated startle in rats. Learning & memory 12:130-137.

Lin CH, Yeh SH, Leu TH, Chang WC, Wang ST, Gean PW (2003b) Identification of calcineurin as a key signal in the extinction of fear memory. The Journal of neuroscience : the official journal of the Society for Neuroscience 23:1574-1579.

Lin EJ, Lin S, Aljanova A, During MJ, Herzog H (2010) Adult-onset hippocampal-specific neuropeptide Y overexpression confers mild anxiolytic effect in mice. European neuropsychopharmacology : the journal of the European College of Neuropsychopharmacology 20:164-175.

Lohmann C, Wong RO (2005) Regulation of dendritic growth and plasticity by local and global calcium dynamics. Cell calcium 37:403-409.

Longo A, Mele P, Bertocchi I, Oberto A, Bachmann A, Bartolomucci A, Palanza P, Sprengel R, Eva C (2014) Conditional inactivation of neuropeptide Y Y1 receptors unravels the role of Y1 and Y5 receptors coexpressing neurons in anxiety. Biological psychiatry 76:840-849.

Longo A, Oberto A, Mele P, Mattiello L, Pisu MG, Palanza P, Serra M, Eva C (2015) NPY-Y1 coexpressed with NPY-Y5 receptors modulate anxiety but not mild social stress response in mice. Genes, brain, and behavior 14:534-542.

Lossi L, Alasia S, Salio C, Merighi A (2009) Cell death and proliferation in acute slices and organotypic cultures of mammalian CNS. Progress in neurobiology 88:221-245.

Lu VB, Colmers WF, Smith PA (2009) Long-term effects of brain-derived neurotrophic factor on the frequency of inhibitory synaptic events in the rat superficial dorsal horn. Neuroscience 161:1135-1143.

Luine V, Villegas M, Martinez C, McEwen BS (1994) Repeated stress causes reversible impairments of spatial memory performance. Brain research 639:167-170.

Lundberg JM, Franco-Cereceda A, Hemsen A, Lacroix JS, Pernow J (1990) Pharmacology of noradrenaline and neuropeptide tyrosine (NPY)-mediated sympathetic cotransmission. Fundamental & clinical pharmacology 4:373-391.

Makino H, Malinow R (2009) AMPA receptor incorporation into synapses during LTP: the role of lateral movement and exocytosis. Neuron 64:381-390.

Malenka RC, Nicoll RA (1993) NMDA-receptor-dependent synaptic plasticity: multiple forms and mechanisms. Trends in neurosciences 16:521-527.

Mansuy IM, Shenolikar S (2006) Protein serine/threonine phosphatases in neuronal plasticity and disorders of learning and memory. Trends in neurosciences 29:679-686.

Maren S, Ferrario CR, Corcoran KA, Desmond TJ, Frey KA (2003) Protein synthesis in the amygdala, but not the auditory thalamus, is required for consolidation of Pavlovian fear conditioning in rats. The European journal of neuroscience 18:3080-3088.

Markou A, Chiamulera C, Geyer MA, Tricklebank M, Steckler T (2009) Removing obstacles in neuroscience drug discovery: the future path for animal models. Neuropsychopharmacology : official publication of the American College of Neuropsychopharmacology 34:74-89.

Martin-Merino E, Ruigomez A, Wallander MA, Johansson S, Garcia-Rodriguez LA (2010) Prevalence, incidence, morbidity and treatment patterns in a cohort of patients diagnosed with anxiety in UK primary care. Family practice 27:9-16.

Martina M, Royer S, Pare D (2001) Cell-type-specific GABA responses and chloride homeostasis in the cortex and amygdala. Journal of neurophysiology 86:2887-2895.

Mascagni F, McDonald AJ (2003) Immunohistochemical characterization of cholecystokinin containing neurons in the rat basolateral amygdala. Brain research 976:171-184.

Mattson MP (2008) Glutamate and neurotrophic factors in neuronal plasticity and disease. Annals of the New York Academy of Sciences 1144:97-112.

Matys T, Pawlak R, Matys E, Pavlides C, McEwen BS, Strickland S (2004) Tissue plasminogen activator promotes the effects of corticotropin-releasing factor on the amygdala and anxiety-like behavior. Proceedings of the National Academy of Sciences of the United States of America 101:16345-16350.

McDonald AJ (1982) Neurons of the lateral and basolateral amygdaloid nuclei: a Golgi study in the rat. The Journal of comparative neurology 212:293-312.

McDonald AJ (1985) Morphology of peptide-containing neurons in the rat basolateral amygdaloid nucleus. Brain research 338:186-191.

McDonald AJ (1992) Projection neurons of the basolateral amygdala: a correlative Golgi and retrograde tract tracing study. Brain research bulletin 28:179-185.

McDonald AJ (1998) Cortical pathways to the mammalian amygdala. Progress in neurobiology 55:257-332.

McDonald AJ, Mascagni F (2001) Colocalization of calcium-binding proteins and GABA in neurons of the rat basolateral amygdala. Neuroscience 105:681-693.

McDonald AJ, Mascagni F (2002) Immunohistochemical characterization of somatostatin containing interneurons in the rat basolateral amygdala. Brain research 943:237-244.

McDonald AJ, Pearson JC (1989) Coexistence of GABA and peptide immunoreactivity in non-pyramidal neurons of the basolateral amygdala. Neuroscience letters 100:53-58.

McEwen BS (1998) Protective and damaging effects of stress mediators. The New England journal of medicine 338:171-179.

McEwen BS (2001) Plasticity of the hippocampus: adaptation to chronic stress and allostatic load. Annals of the New York Academy of Sciences 933:265-277.

McEwen BS (2003) Mood disorders and allostatic load. Biological psychiatry 54:200-207.

McEwen BS (2006) Protective and damaging effects of stress mediators: central role of the brain. Dialogues in clinical neuroscience 8:367-381.

McEwen BS, Bowles NP, Gray JD, Hill MN, Hunter RG, Karatsoreos IN, Nasca C (2015a) Mechanisms of stress in the brain. Nature neuroscience 18:1353-1363.

McEwen BS, Gray J, Nasca C (2015b) Recognizing Resilience: Learning from the Effects of Stress on the Brain. Neurobiology of stress 1:1-11.

McEwen BS, Gray JD, Nasca C (2015c) 60 YEARS OF NEUROENDOCRINOLOGY: Redefining neuroendocrinology: stress, sex and cognitive and emotional regulation. The Journal of endocrinology 226:T67-83.

McEwen BS, Lasley EN (2002) The end of stress as we know it. Washington, D.C.: Joseph Henry Press.

McEwen BS, Nasca C, Gray JD (2015d) Stress Effects on Neuronal Structure: Hippocampus, Amygdala, and Prefrontal Cortex. Neuropsychopharmacology : official publication of the American College of Neuropsychopharmacology.

McEwen BS, Stellar E (1993) Stress and the individual. Mechanisms leading to disease. Archives of internal medicine 153:2093-2101.

McGaugh JL (2000) Memory--a century of consolidation. Science 287:248-251.

McGaugh JL (2002) Memory consolidation and the amygdala: a systems perspective. Trends in neurosciences 25:456.

McGuire J, Herman JP, Horn PS, Sallee FR, Sah R (2010) Enhanced fear recall and emotional arousal in rats recovering from chronic variable stress. Physiology & behavior 101:474-482.

McGuire JL, Larke LE, Sallee FR, Herman JP, Sah R (2011) Differential Regulation of Neuropeptide Y in the Amygdala and Prefrontal Cortex during Recovery from Chronic Variable Stress. Frontiers in behavioral neuroscience 5:54.

Meis S, Endres T, Lessmann V (2012) Postsynaptic BDNF signalling regulates long-term potentiation at thalamo-amygdala afferents. The Journal of physiology 590:193-208.

Merali Z, McIntosh J, Kent P, Michaud D, Anisman H (1998) Aversive and appetitive events evoke the release of corticotropin-releasing hormone and bombesin-like peptides at the central nucleus of the amygdala. The Journal of neuroscience : the official journal of the Society for Neuroscience 18:4758-4766.

Merlo Pich E, Lorang M, Yeganeh M, Rodriguez de Fonseca F, Raber J, Koob GF, Weiss F (1995) Increase of extracellular corticotropin-releasing factor-like immunoreactivity levels in the amygdala of awake rats during restraint stress and ethanol withdrawal as measured by microdialysis. The Journal of neuroscience : the official journal of the Society for Neuroscience 15:5439-5447.

Michel MC, Beck-Sickinger A, Cox H, Doods HN, Herzog H, Larhammar D, Quirion R, Schwartz T, Westfall T (1998) XVI. International Union of Pharmacology recommendations for the nomenclature of neuropeptide Y, peptide YY, and pancreatic polypeptide receptors. Pharmacological reviews 50:143-150.

Milad MR, Orr SP, Lasko NB, Chang Y, Rauch SL, Pitman RK (2008) Presence and acquired origin of reduced recall for fear extinction in PTSD: results of a twin study. Journal of psychiatric research 42:515-520.

Milani C, Katayama ML, de Lyra EC, Welsh J, Campos LT, Brentani MM, Maciel Mdo S, Roela RA, del Valle PR, Goes JC, Nonogaki S, Tamura RE, Folgueira MA (2013)

Transcriptional effects of 1,25 dihydroxyvitamin D(3) physiological and supra-physiological concentrations in breast cancer organotypic culture. BMC cancer 13:119.

Mineur YS, Taylor SR, Picciotto MR (2014) Calcineurin downregulation in the amygdala is sufficient to induce anxiety-like and depression-like behaviors in C57BL/6J male mice. Biological psychiatry 75:991-998.

Mirante O, Brandalise F, Bohacek J, Mansuy IM (2014) Distinct molecular components for thalamic- and cortical-dependent plasticity in the lateral amygdala. Frontiers in molecular neuroscience 7:62.

Mitra R, Ferguson D, Sapolsky RM (2009) SK2 potassium channel overexpression in basolateral amygdala reduces anxiety, stress-induced corticosterone secretion and dendritic arborization. Molecular psychiatry 14:847-855, 827.

Mitra R, Jadhav S, McEwen BS, Vyas A, Chattarji S (2005) Stress duration modulates the spatiotemporal patterns of spine formation in the basolateral amygdala. Proceedings of the National Academy of Sciences of the United States of America 102:9371-9376.

Mitrasinovic OM, Grattan A, Robinson CC, Lapustea NB, Poon C, Ryan H, Phong C, Murphy GM, Jr. (2005) Microglia overexpressing the macrophage colony-stimulating factor receptor are neuroprotective in a microglial-hippocampal organotypic coculture system. The Journal of neuroscience : the official journal of the Society for Neuroscience 25:4442-4451.

Molosh AI, Sajdyk TJ, Truitt WA, Zhu W, Oxford GS, Shekhar A (2013) NPY Y1 receptors differentially modulate GABAA and NMDA receptors via divergent signal-transduction pathways to reduce excitability of amygdala neurons. Neuropsychopharmacology : official publication of the American College of Neuropsychopharmacology 38:1352-1364.

Morales-Medina JC, Dominguez-Lopez S, Gobbi G, Beck-Sickinger AG, Quirion R (2012) The selective neuropeptide Y Y5 agonist [cPP(1-7),NPY(19-23),Ala31,Aib32,Gln34]hPP differently modulates emotional processes and body weight in the rat. Behavioural brain research 233:298-304.

Moreira CM, Masson S, Carvalho MC, Brandao ML (2007) Exploratory behaviour of rats in the elevated plus-maze is differentially sensitive to inactivation of the basolateral and central amygdaloid nuclei. Brain research bulletin 71:466-474.

Morgan CA, 3rd, Rasmusson AM, Winters B, Hauger RL, Morgan J, Hazlett G, Southwick S (2003) Trauma exposure rather than posttraumatic stress disorder is associated with reduced baseline plasma neuropeptide-Y levels. Biological psychiatry 54:1087-1091.

Morgan CA, 3rd, Wang S, Southwick SM, Rasmusson A, Hazlett G, Hauger RL, Charney DS (2000) Plasma neuropeptide-Y concentrations in humans exposed to military survival training. Biological psychiatry 47:902-909.

Morin LP (2013) Neuroanatomy of the extended circadian rhythm system. Experimental neurology 243:4-20.

Morys J, Berdel B, Kowianski P, Dziewiatkowski J (1998) The pattern of synaptophysin changes during the maturation of the amygdaloid body and hippocampal hilus in the rat. Folia neuropathologica / Association of Polish Neuropathologists and Medical Research Centre, Polish Academy of Sciences 36:15-23.

Munck A, Guyre PM, Holbrook NJ (1984) Physiological functions of glucocorticoids in stress and their relation to pharmacological actions. Endocrine reviews 5:25-44.

Murphy RC, Messer A (2001) Gene transfer methods for CNS organotypic cultures: a comparison of three nonviral methods. Molecular therapy : the journal of the American Society of Gene Therapy 3:113-121.

Nabavi S, Fox R, Proulx CD, Lin JY, Tsien RY, Malinow R (2014) Engineering a memory with LTD and LTP. Nature 511:348-352.

Nader K, Schafe GE, Le Doux JE (2000) Fear memories require protein synthesis in the amygdala for reconsolidation after retrieval. Nature 406:722-726.

Nakajima M, Inui A, Asakawa A, Momose K, Ueno N, Teranishi A, Baba S, Kasuga M (1998) Neuropeptide Y produces anxiety via Y2-type receptors. Peptides 19:359-363.

Nakayama AY, Harms MB, Luo L (2000) Small GTPases Rac and Rho in the maintenance of dendritic spines and branches in hippocampal pyramidal neurons. The Journal of neuroscience : the official journal of the Society for Neuroscience 20:5329-5338.

Namburi P, Beyeler A, Yorozu S, Calhoon GG, Halbert SA, Wichmann R, Holden SS, Mertens KL, Anahtar M, Felix-Ortiz AC, Wickersham IR, Gray JM, Tye KM (2015) A circuit mechanism for differentiating positive and negative associations. Nature 520:675-678.

Narvaez M, Millon C, Borroto-Escuela D, Flores-Burgess A, Santin L, Parrado C, Gago B, Puigcerver A, Fuxe K, Narvaez JA, Diaz-Cabiale Z (2015) Galanin receptor 2-neuropeptide Y Y1 receptor interactions in the amygdala lead to increased anxiolytic actions. Brain structure & function 220:2289-2301.

Nedelescu H, Kelso CM, Lazaro-Munoz G, Purpura M, Cain CK, Ledoux JE, Aoki C (2010) Endogenous GluR1-containing AMPA receptors translocate to asymmetric synapses in the lateral amygdala during the early phase of fear memory formation: an electron microscopic immunocytochemical study. The Journal of comparative neurology 518:4723-4739.

Neely MD, Schmidt DE, Deutch AY (2007) Cortical regulation of dopamine depletion-induced dendritic spine loss in striatal medium spiny neurons. Neuroscience 149:457-464.

Nestler EJ, Barrot M, DiLeone RJ, Eisch AJ, Gold SJ, Monteggia LM (2002) Neurobiology of depression. Neuron 34:13-25.

Nibuya M, Morinobu S, Duman RS (1995) Regulation of BDNF and trkB mRNA in rat brain by chronic electroconvulsive seizure and antidepressant drug treatments. The Journal of neuroscience : the official journal of the Society for Neuroscience 15:7539-7547.

Okamoto K, Ishikawa T, Abe R, Ishikawa D, Kobayashi C, Mizunuma M, Norimoto H, Matsuki N, Ikegaya Y (2014) Ex vivo cultured neuronal networks emit in vivo-like spontaneous activity. The journal of physiological sciences : JPS 64:421-431.

Olesen MV, Christiansen SH, Gotzsche CR, Holst B, Kokaia M, Woldbye DP (2012a) Y5 neuropeptide Y receptor overexpression in mice neither affects anxiety- and depression-like behaviours nor seizures but confers moderate hyperactivity. Neuropeptides 46:71-79.

Olesen MV, Christiansen SH, Gotzsche CR, Nikitidou L, Kokaia M, Woldbye DP (2012b) Neuropeptide Y Y1 receptor hippocampal overexpression via viral vectors is associated with modest anxiolytic-like and proconvulsant effects in mice. Journal of neuroscience research 90:498-507.

Osborne A, Hopes M, Wright P, Broadway DC, Sanderson J (2015) Human organotypic retinal cultures (HORCs) as a chronic experimental model for investigation of retinal ganglion cell degeneration. Experimental eye research 143:28-38.

Padival M, Quinette D, Rosenkranz JA (2013a) Effects of repeated stress on excitatory drive of basal amygdala neurons in vivo. Neuropsychopharmacology : official publication of the American College of Neuropsychopharmacology 38:1748-1762.

Padival MA, Blume SR, Rosenkranz JA (2013b) Repeated restraint stress exerts different impact on structure of neurons in the lateral and basal nuclei of the amygdala. Neuroscience 246:230-242.

Pape HC, Pare D (2010) Plastic synaptic networks of the amygdala for the acquisition, expression, and extinction of conditioned fear. Physiological reviews 90:419-463.

Pare D, Gaudreau H (1996) Projection cells and interneurons of the lateral and basolateral amygdala: distinct firing patterns and differential relation to theta and delta rhythms in conscious cats. The Journal of neuroscience : the official journal of the Society for Neuroscience 16:3334-3350.

Pare D, Quirk GJ, Ledoux JE (2004) New vistas on amygdala networks in conditioned fear. Journal of neurophysiology 92:1-9.

Park K, Lee S, Kang SJ, Choi S, Shin KS (2007) Hyperpolarization-activated currents control the excitability of principal neurons in the basolateral amygdala. Biochemical and biophysical research communications 361:718-724.

Parker MS, Lundell I, Parker SL (2002a) Internalization of pancreatic polypeptide Y4 receptors: correlation of receptor intake and affinity. European journal of pharmacology 452:279-287.

Parker SL, Parker MS, Lundell I, Balasubramaniam A, Buschauer A, Kane JK, Yalcin A, Berglund MM (2002b) Agonist internalization by cloned Y1 neuropeptide Y (NPY) receptor in Chinese hamster ovary cells shows strong preference for NPY, endosome-linked entry and fast receptor recycling. Regulatory peptides 107:49-62.

Pellow S, Chopin P, File SE, Briley M (1985) Validation of open:closed arm entries in an elevated plus-maze as a measure of anxiety in the rat. Journal of neuroscience methods 14:149-167.

Pena F (2010) Organotypic cultures as tool to test long-term effects of chemicals on the nervous system. Current medicinal chemistry 17:987-1001.

Phelps EA, Delgado MR, Nearing KI, LeDoux JE (2004) Extinction learning in humans: role of the amygdala and vmPFC. Neuron 43:897-905.

Phelps EA, LeDoux JE (2005) Contributions of the amygdala to emotion processing: from animal models to human behavior. Neuron 48:175-187.

Pitkanen A, Jolkkonen E, Kemppainen S (2000) Anatomic heterogeneity of the rat amygdaloid complex. Folia morphologica 59:1-23.

Poolos NP, Migliore M, Johnston D (2002) Pharmacological upregulation of h-channels reduces the excitability of pyramidal neuron dendrites. Nature neuroscience 5:767-774.

Porsolt RD, Bertin A, Jalfre M (1977) Behavioral despair in mice: a primary screening test for antidepressants. Archives internationales de pharmacodynamie et de therapie 229:327-336.

Primeaux SD, Wilson SP, Cusick MC, York DA, Wilson MA (2005) Effects of altered amygdalar neuropeptide Y expression on anxiety-related behaviors. Neuropsychopharmacology : official publication of the American College of Neuropsychopharmacology 30:1589-1597.

Qian J, Colmers WF, Saggau P (1997) Inhibition of synaptic transmission by neuropeptide Y in rat hippocampal area CA1: modulation of presynaptic Ca2+ entry. The Journal of neuroscience : the official journal of the Society for Neuroscience 17:8169-8177.

Qin S, Young CB, Duan X, Chen T, Supekar K, Menon V (2014) Amygdala subregional structure and intrinsic functional connectivity predicts individual differences in anxiety during early childhood. Biological psychiatry 75:892-900.

Quirk GJ, Armony JL, LeDoux JE (1997) Fear conditioning enhances different temporal components of tone-evoked spike trains in auditory cortex and lateral amygdala. Neuron 19:613-624.

Quirk GJ, Likhtik E, Pelletier JG, Pare D (2003) Stimulation of medial prefrontal cortex decreases the responsiveness of central amygdala output neurons. The Journal of neuroscience : the official journal of the Society for Neuroscience 23:8800-8807.

Quirk GJ, Repa C, LeDoux JE (1995) Fear conditioning enhances short-latency auditory responses of lateral amygdala neurons: parallel recordings in the freely behaving rat. Neuron 15:1029-1039.

Rainnie DG (1999) Serotonergic modulation of neurotransmission in the rat basolateral amygdala. Journal of neurophysiology 82:69-85.

Rainnie DG, Asprodini EK, Shinnick-Gallagher P (1991a) Excitatory transmission in the basolateral amygdala. Journal of neurophysiology 66:986-998.

Rainnie DG, Asprodini EK, Shinnick-Gallagher P (1991b) Inhibitory transmission in the basolateral amygdala. Journal of neurophysiology 66:999-1009.

Rainnie DG, Asprodini EK, Shinnick-Gallagher P (1993) Intracellular recordings from morphologically identified neurons of the basolateral amygdala. Journal of neurophysiology 69:1350-1362.

Rainnie DG, Bergeron R, Sajdyk TJ, Patil M, Gehlert DR, Shekhar A (2004) Corticotrophin releasing factor-induced synaptic plasticity in the amygdala translates stress into emotional disorders. The Journal of neuroscience : the official journal of the Society for Neuroscience 24:3471-3479.

Rainnie DG, Fernhout BJ, Shinnick-Gallagher P (1992) Differential actions of corticotropin releasing factor on basolateral and central amygdaloid neurones, in vitro. The Journal of pharmacology and experimental therapeutics 263:846-858.

Rasmusson AM, Hauger RL, Morgan CA, Bremner JD, Charney DS, Southwick SM (2000) Low baseline and yohimbine-stimulated plasma neuropeptide Y (NPY) levels in combat-related PTSD. Biological psychiatry 47:526-539.

Rattiner LM, Davis M, French CT, Ressler KJ (2004) Brain-derived neurotrophic factor and tyrosine kinase receptor B involvement in amygdala-dependent fear conditioning. The Journal of neuroscience : the official journal of the Society for Neuroscience 24:4796-4806.

Rattiner LM, Davis M, Ressler KJ (2005) Brain-derived neurotrophic factor in amygdala-dependent learning. The Neuroscientist : a review journal bringing neurobiology, neurology and psychiatry 11:323-333.

Rauch SL, Shin LM, Wright CI (2003) Neuroimaging studies of amygdala function in anxiety disorders. Annals of the New York Academy of Sciences 985:389-410.

Redmond L, Oh SR, Hicks C, Weinmaster G, Ghosh A (2000) Nuclear Notch1 signaling and the regulation of dendritic development. Nature neuroscience 3:30-40.

Redrobe JP, Dumont Y, Herzog H, Quirion R (2003) Neuropeptide Y (NPY) Y2 receptors mediate behaviour in two animal models of anxiety: evidence from Y2 receptor knockout mice. Behavioural brain research 141:251-255.

Reichmann F, Holzer P (2015) Neuropeptide Y: A stressful review. Neuropeptides.

Reinbold R (1954) [Organotypic differentiation of the eye of the chick embryo in vitro]. Comptes rendus des seances de la Societe de biologie et de ses filiales 148:1493-1495.

Repa JC, Muller J, Apergis J, Desrochers TM, Zhou Y, LeDoux JE (2001) Two different lateral amygdala cell populations contribute to the initiation and storage of memory. Nature neuroscience 4:724-731.

Riccio A, Li Y, Moon J, Kim KS, Smith KS, Rudolph U, Gapon S, Yao GL, Tsvetkov E, Rodig SJ, Van't Veer A, Meloni EG, Carlezon WA, Jr., Bolshakov VY, Clapham DE (2009) Essential role for TRPC5 in amygdala function and fear-related behavior. Cell 137:761-772.

Riccio A, Li Y, Tsvetkov E, Gapon S, Yao GL, Smith KS, Engin E, Rudolph U, Bolshakov VY, Clapham DE (2014) Decreased anxiety-like behavior and Galphaq/11-dependent responses in the amygdala of mice lacking TRPC4 channels. The Journal of neuroscience : the official journal of the Society for Neuroscience 34:3653-3667.

Ridoux V, Robert J, Perricaudet M, Mallet J, Le Gal La Salle G (1995) Adenovirus mediated gene transfer in organotypic brain slices. Neurobiology of disease 2:49-54.

Rivier C, Vale W (1983) Modulation of stress-induced ACTH release by corticotropin-releasing factor, catecholamines and vasopressin. Nature 305:325-327.

Robain O, Barbin G, Billette de Villemeur T, Jardin L, Jahchan T, Ben-Ari Y (1994) Development of mossy fiber synapses in hippocampal slice culture. Brain research Developmental brain research 80:244-250.

Rodrigues SM, Bauer EP, Farb CR, Schafe GE, LeDoux JE (2002) The group I metabotropic glutamate receptor mGluR5 is required for fear memory formation and long-term potentiation in the lateral amygdala. The Journal of neuroscience : the official journal of the Society for Neuroscience 22:5219-5229.

Rodrigues SM, Schafe GE, LeDoux JE (2004) Molecular mechanisms underlying emotional learning and memory in the lateral amygdala. Neuron 44:75-91.

Rogan MT, Staubli UV, LeDoux JE (1997) Fear conditioning induces associative long-term potentiation in the amygdala. Nature 390:604-607.

Roozendaal B, Brunson KL, Holloway BL, McGaugh JL, Baram TZ (2002) Involvement of stress-released corticotropin-releasing hormone in the basolateral amygdala in regulating memory consolidation. Proceedings of the National Academy of Sciences of the United States of America 99:13908-13913.

Roozendaal B, McEwen BS, Chattarji S (2009) Stress, memory and the amygdala. Nature reviews Neuroscience 10:423-433.

Rose M, Devine J (2014) Assessment of patient-reported symptoms of anxiety. Dialogues in clinical neuroscience 16:197-211.

Rosenkranz JA, Venheim ER, Padival M (2010) Chronic stress causes amygdala hyperexcitability in rodents. Biological psychiatry 67:1128-1136.

Ross WN, Nakamura T, Watanabe S, Larkum M, Lasser-Ross N (2005) Synaptically activated ca2+ release from internal stores in CNS neurons. Cellular and molecular neurobiology 25:283-295.

Rostkowski AB, Teppen TL, Peterson DA, Urban JH (2009) Cell-specific expression of neuropeptide Y Y1 receptor immunoreactivity in the rat basolateral amygdala. The Journal of comparative neurology 517:166-176.

Rowland AM, Richmond JE, Olsen JG, Hall DH, Bamber BA (2006) Presynaptic terminals independently regulate synaptic clustering and autophagy of GABAA receptors in Caenorhabditis elegans. The Journal of neuroscience : the official journal of the Society for Neuroscience 26:1711-1720.

Rumpel S, LeDoux J, Zador A, Malinow R (2005) Postsynaptic receptor trafficking underlying a form of associative learning. Science 308:83-88.

Russo SJ, Murrough JW, Han MH, Charney DS, Nestler EJ (2012) Neurobiology of resilience. Nature neuroscience 15:1475-1484.

Ryan SJ, Ehrlich DE, Jasnow AM, Daftary S, Madsen TE, Rainnie DG (2012) Spike-timing precision and neuronal synchrony are enhanced by an interaction between synaptic inhibition and membrane oscillations in the amygdala. PloS one 7:e35320.

Ryan SJ, Ehrlich DE, Rainnie DG (2014) Morphology and dendritic maturation of developing principal neurons in the rat basolateral amygdala. Brain structure & function.

Sah P, Faber ES, Lopez De Armentia M, Power J (2003) The amygdaloid complex: anatomy and physiology. Physiological reviews 83:803-834.

Sah R, Ekhator NN, Jefferson-Wilson L, Horn PS, Geracioti TD, Jr. (2014) Cerebrospinal fluid neuropeptide Y in combat veterans with and without posttraumatic stress disorder. Psychoneuroendocrinology 40:277-283.

Sah R, Ekhator NN, Strawn JR, Sallee FR, Baker DG, Horn PS, Geracioti TD, Jr. (2009) Low cerebrospinal fluid neuropeptide Y concentrations in posttraumatic stress disorder. Biological psychiatry 66:705-707.

Sah R, Geracioti TD (2013) Neuropeptide Y and posttraumatic stress disorder. Molecular psychiatry 18:646-655.

Sajdyk TJ, Fitz SD, Shekhar A (2006) The role of neuropeptide Y in the amygdala on corticotropin-releasing factor receptor-mediated behavioral stress responses in the rat. Stress 9:21-28.

Sajdyk TJ, Gehlert DR (2000) Astressin, a corticotropin releasing factor antagonist, reverses the anxiogenic effects of urocortin when administered into the basolateral amygdala. Brain research 877:226-234.

Sajdyk TJ, Johnson PL, Leitermann RJ, Fitz SD, Dietrich A, Morin M, Gehlert DR, Urban JH, Shekhar A (2008) Neuropeptide Y in the amygdala induces long-term resilience to stress-induced reductions in social responses but not hypothalamic-adrenal-pituitary axis activity or hyperthermia. The Journal of neuroscience : the official journal of the Society for Neuroscience 28:893-903.

Sajdyk TJ, Schober DA, Gehlert DR (2002a) Neuropeptide Y receptor subtypes in the basolateral nucleus of the amygdala modulate anxiogenic responses in rats. Neuropharmacology 43:1165-1172.

Sajdyk TJ, Schober DA, Gehlert DR, Shekhar A (1999a) Role of corticotropin-releasing factor and urocortin within the basolateral amygdala of rats in anxiety and panic responses. Behavioural brain research 100:207-215.

Sajdyk TJ, Schober DA, Smiley DL, Gehlert DR (2002b) Neuropeptide Y-Y2 receptors mediate anxiety in the amygdala. Pharmacology, biochemistry, and behavior 71:419-423.

Sajdyk TJ, Shekhar A (1997a) Excitatory amino acid receptor antagonists block the cardiovascular and anxiety responses elicited by gamma-aminobutyric acidA receptor blockade in the basolateral amygdala of rats. The Journal of pharmacology and experimental therapeutics 283:969-977.

Sajdyk TJ, Shekhar A (1997b) Excitatory amino acid receptors in the basolateral amygdala regulate anxiety responses in the social interaction test. Brain research 764:262-264.

Sajdyk TJ, Shekhar A, Gehlert DR (2004) Interactions between NPY and CRF in the amygdala to regulate emotionality. Neuropeptides 38:225-234.

Sajdyk TJ, Vandergriff MG, Gehlert DR (1999b) Amygdalar neuropeptide Y Y1 receptors mediate the anxiolytic-like actions of neuropeptide Y in the social interaction test. European journal of pharmacology 368:143-147.

Sanders SK, Shekhar A (1995) Regulation of anxiety by GABAA receptors in the rat amygdala. Pharmacology, biochemistry, and behavior 52:701-706.

Sandi C, Davies HA, Cordero MI, Rodriguez JJ, Popov VI, Stewart MG (2003) Rapid reversal of stress induced loss of synapses in CA3 of rat hippocampus following water maze training. The European journal of neuroscience 17:2447-2456.

Saveanu R, Etkin A, Duchemin AM, Goldstein-Piekarski A, Gyurak A, Debattista C, Schatzberg AF, Sood S, Day CV, Palmer DM, Rekshan WR, Gordon E, Rush AJ, Williams LM (2015) The international Study to Predict Optimized Treatment in Depression (iSPOT-D): outcomes from the acute phase of antidepressant treatment. Journal of psychiatric research 61:1-12.

Schafe GE, Atkins CM, Swank MW, Bauer EP, Sweatt JD, LeDoux JE (2000) Activation of ERK/MAP kinase in the amygdala is required for memory consolidation of pavlovian fear conditioning. The Journal of neuroscience : the official journal of the Society for Neuroscience 20:8177-8187.

Schafe GE, Nader K, Blair HT, LeDoux JE (2001) Memory consolidation of Pavlovian fear conditioning: a cellular and molecular perspective. Trends in neurosciences 24:540-546.

Schatzberg AF (2015a) Development of New Psychopharmacological Agents for Depression and Anxiety. The Psychiatric clinics of North America 38:379-393.

Schatzberg AF (2015b) Issues encountered in recent attempts to develop novel antidepressant agents. Annals of the New York Academy of Sciences 1345:67-73.

Schienle A, Ebner F, Schafer A (2011) Localized gray matter volume abnormalities in generalized anxiety disorder. European archives of psychiatry and clinical neuroscience 261:303-307.

Schoenbaum G, Setlow B, Saddoris MP, Gallagher M (2003) Encoding predicted outcome and acquired value in orbitofrontal cortex during cue sampling depends upon input from basolateral amygdala. Neuron 39:855-867.

Scott EK, Luo L (2001) How do dendrites take their shape? Nature neuroscience 4:359-365.

Seidah NG, Benjannet S, Pareek S, Chretien M, Murphy RA (1996) Cellular processing of the neurotrophin precursors of NT3 and BDNF by the mammalian proprotein convertases. FEBS letters 379:247-250.

Selye H (1946) The general adaptation syndrome and the diseases of adaptation. The Journal of clinical endocrinology and metabolism 6:117-230.

Selye H (1998) A syndrome produced by diverse nocuous agents. 1936. The Journal of neuropsychiatry and clinical neurosciences 10:230-231.

Sen S, Burmeister M, Ghosh D (2004) Meta-analysis of the association between a serotonin transporter promoter polymorphism (5-HTTLPR) and anxiety-related personality traits. American journal of medical genetics Part B, Neuropsychiatric genetics : the official publication of the International Society of Psychiatric Genetics 127B:85-89.

Serova LI, Tillinger A, Alaluf LG, Laukova M, Keegan K, Sabban EL (2013) Single intranasal neuropeptide Y infusion attenuates development of PTSD-like symptoms to traumatic stress in rats. Neuroscience 236:298-312.

Shekhar A, Sajdyk TJ, Gehlert DR, Rainnie DG (2003) The amygdala, panic disorder, and cardiovascular responses. Annals of the New York Academy of Sciences 985:308-325.

Shekhar A, Truitt W, Rainnie D, Sajdyk T (2005) Role of stress, corticotrophin releasing factor (CRF) and amygdala plasticity in chronic anxiety. Stress 8:209-219.

Shen W, Ganetzky B (2009) Autophagy promotes synapse development in Drosophila. The Journal of cell biology 187:71-79.

Sheriff S, Dautzenberg FM, Mulchahey JJ, Pisarska M, Hauger RL, Chance WT, Balasubramaniam A, Kasckow JW (2001) Interaction of neuropeptide Y and corticotropin-releasing factor signaling pathways in AR-5 amygdalar cells. Peptides 22:2083-2089.

Shin LM, Liberzon I (2010) The neurocircuitry of fear, stress, and anxiety disorders. Neuropsychopharmacology : official publication of the American College of Neuropsychopharmacology 35:169-191.

Shirayama Y, Chen AC, Nakagawa S, Russell DS, Duman RS (2002) Brain-derived neurotrophic factor produces antidepressant effects in behavioral models of depression. The Journal of neuroscience : the official journal of the Society for Neuroscience 22:3251-3261.

Silva AJ (2003) Molecular and cellular cognitive studies of the role of synaptic plasticity in memory. Journal of neurobiology 54:224-237.

Silveira MC, Sandner G, Graeff FG (1993) Induction of Fos immunoreactivity in the brain by exposure to the elevated plus-maze. Behavioural brain research 56:115-118.

Skrzypiec AE, Shah RS, Schiavon E, Baker E, Skene N, Pawlak R, Mucha M (2013) Stress-induced lipocalin-2 controls dendritic spine formation and neuronal activity in the amygdala. PloS one 8:e61046.

Smialowska M, Wieronska JM, Domin H, Zieba B (2007) The effect of intrahippocampal injection of group II and III metobotropic glutamate receptor agonists on anxiety; the role of neuropeptide Y. Neuropsychopharmacology : official publication of the American College of Neuropsychopharmacology 32:1242-1250.

Smith BN, Dudek FE (1996) Amino acid-mediated regulation of spontaneous synaptic activity patterns in the rat basolateral amygdala. Journal of neurophysiology 76:1958-1967.

Smith GW, Aubry JM, Dellu F, Contarino A, Bilezikjian LM, Gold LH, Chen R, Marchuk Y, Hauser C, Bentley CA, Sawchenko PE, Koob GF, Vale W, Lee KF (1998) Corticotropin releasing factor receptor 1-deficient mice display decreased anxiety,

impaired stress response, and aberrant neuroendocrine development. Neuron 20:1093-1102.

Smith MA, Makino S, Kvetnansky R, Post RM (1995) Stress and glucocorticoids affect the expression of brain-derived neurotrophic factor and neurotrophin-3 mRNAs in the hippocampus. The Journal of neuroscience : the official journal of the Society for Neuroscience 15:1768-1777.

Smith SM, Vale WW (2006) The role of the hypothalamic-pituitary-adrenal axis in neuroendocrine responses to stress. Dialogues in clinical neuroscience 8:383-395.

Sodickson DL, Bean BP (1996) GABAB receptor-activated inwardly rectifying potassium current in dissociated hippocampal CA3 neurons. The Journal of neuroscience : the official journal of the Society for Neuroscience 16:6374-6385.

Sorensen G, Lindberg C, Wortwein G, Bolwig TG, Woldbye DP (2004) Differential roles for neuropeptide Y Y1 and Y5 receptors in anxiety and sedation. Journal of neuroscience research 77:723-729.

Sosulina L, Schwesig G, Seifert G, Pape HC (2008) Neuropeptide Y activates a G-protein-coupled inwardly rectifying potassium current and dampens excitability in the lateral amygdala. Molecular and cellular neurosciences 39:491-498.

Spampanato J, Polepalli J, Sah P (2011) Interneurons in the basolateral amygdala. Neuropharmacology 60:765-773.

Spruston N, Johnston D (2008) Out of control in the dendrites. Nature neuroscience 11:733-734.

Stachniak TJ, Bourque CW (2006) Visually guided whole cell patch clamp of mouse supraoptic nucleus neurons in cultured and acute conditions. American journal of physiology Regulatory, integrative and comparative physiology 291:R68-76.

Stamatakis AM, Sparta DR, Jennings JH, McElligott ZA, Decot H, Stuber GD (2014) Amygdala and bed nucleus of the stria terminalis circuitry: Implications for addiction-related behaviors. Neuropharmacology 76 Pt B:320-328.

Stanic D, Mulder J, Watanabe M, Hokfelt T (2011) Characterization of NPY Y2 receptor protein expression in the mouse brain. II. Coexistence with NPY, the Y1 receptor, and other neurotransmitter-related molecules. The Journal of comparative neurology 519:1219-1257.

Stein DJ, Hollander E (2002) The American Psychiatric publishing textbook of anxiety disorders. Washington, DC: American Psychiatric Pub.

Sternson SM, Roth BL (2014) Chemogenetic tools to interrogate brain functions. Annual review of neuroscience 37:387-407.

Stoppini L, Buchs PA, Muller D (1991) A simple method for organotypic cultures of nervous tissue. Journal of neuroscience methods 37:173-182.

Stoppini L, Buchs PA, Muller D (1993) Lesion-induced neurite sprouting and synapse formation in hippocampal organotypic cultures. Neuroscience 57:985-994.

Sun N, Cassell MD (1993) Intrinsic GABAergic neurons in the rat central extended amygdala. The Journal of comparative neurology 330:381-404.

Sun QQ, Huguenard JR, Prince DA (2001) Neuropeptide Y receptors differentially modulate G-protein-activated inwardly rectifying K+ channels and high-voltage-activated Ca2+ channels in rat thalamic neurons. The Journal of physiology 531:67-79.

Suvrathan A, Bennur S, Ghosh S, Tomar A, Anilkumar S, Chattarji S (2014) Stress enhances fear by forming new synapses with greater capacity for long-term potentiation in the amygdala. Philosophical transactions of the Royal Society of London Series B, Biological sciences 369:20130151.

Swanson LW, Sawchenko PE, Rivier J, Vale WW (1983) Organization of ovine corticotropin-releasing factor immunoreactive cells and fibers in the rat brain: an immunohistochemical study. Neuroendocrinology 36:165-186.

Sweatt JD (2004) Mitogen-activated protein kinases in synaptic plasticity and memory. Current opinion in neurobiology 14:311-317.

Swerdlow NR, Geyer MA, Vale WW, Koob GF (1986) Corticotropin-releasing factor potentiates acoustic startle in rats: blockade by chlordiazepoxide. Psychopharmacology 88:147-152.

Taliaz D, Loya A, Gersner R, Haramati S, Chen A, Zangen A (2011) Resilience to chronic stress is mediated by hippocampal brain-derived neurotrophic factor. The Journal of neuroscience : the official journal of the Society for Neuroscience 31:4475-4483.

Tang G, Gudsnuk K, Kuo SH, Cotrina ML, Rosoklija G, Sosunov A, Sonders MS, Kanter E, Castagna C, Yamamoto A, Yue Z, Arancio O, Peterson BS, Champagne F, Dwork AJ, Goldman J, Sulzer D (2014) Loss of mTOR-dependent macroautophagy causes autistic-like synaptic pruning deficits. Neuron 83:1131-1143.

Tasan RO, Nguyen NK, Weger S, Sartori SB, Singewald N, Heilbronn R, Herzog H, Sperk G (2010) The central and basolateral amygdala are critical sites of neuropeptide Y/Y2 receptor-mediated regulation of anxiety and depression. The Journal of neuroscience : the official journal of the Society for Neuroscience 30:6282-6290.

Tasan RO, Verma D, Wood J, Lach G, Hormer B, de Lima TC, Herzog H, Sperk G (2015) The role of Neuropeptide Y in fear conditioning and extinction. Neuropeptides.

Tatemoto K, Carlquist M, Mutt V (1982) Neuropeptide Y--a novel brain peptide with structural similarities to peptide YY and pancreatic polypeptide. Nature 296:659-660.

Taylor AL (2012) What we talk about when we talk about capacitance measured with the voltage-clamp step method. Journal of computational neuroscience 32:167-175.

Thorsell A (2010) Brain neuropeptide Y and corticotropin-releasing hormone in mediating stress and anxiety. Experimental biology and medicine 235:1163-1167.

Thorsell A, Michalkiewicz M, Dumont Y, Quirion R, Caberlotto L, Rimondini R, Mathe AA, Heilig M (2000) Behavioral insensitivity to restraint stress, absent fear suppression of behavior and impaired spatial learning in transgenic rats with hippocampal neuropeptide Y overexpression. Proceedings of the National Academy of Sciences of the United States of America 97:12852-12857.

Tovote P, Fadok JP, Luthi A (2015) Neuronal circuits for fear and anxiety. Nature reviews Neuroscience 16:317-331.

Trent NL, Menard JL (2013) Lateral septal infusions of the neuropeptide Y Y2 receptor agonist, NPY(13-36) differentially affect different defensive behaviors in male, Long Evans rats. Physiology & behavior 110-111:20-29.

Tschenett A, Singewald N, Carli M, Balducci C, Salchner P, Vezzani A, Herzog H, Sperk G (2003) Reduced anxiety and improved stress coping ability in mice lacking NPY-Y2 receptors. The European journal of neuroscience 18:143-148.

Tye KM, Deisseroth K (2012) Optogenetic investigation of neural circuits underlying brain disease in animal models. Nature reviews Neuroscience 13:251-266.

Ugolini A, Sokal DM, Arban R, Large CH (2008) CRF1 receptor activation increases the response of neurons in the basolateral nucleus of the amygdala to afferent stimulation. Frontiers in behavioral neuroscience 2:2.

Ullrich C, Daschil N, Humpel C (2011) Organotypic vibrosections: novel whole sagittal brain cultures. Journal of neuroscience methods 201:131-141.

Ullrich C, Humpel C (2011) Mini-ruby is rapidly taken up by neurons and astrocytes in organotypic brain slices. Neurochemical research 36:1817-1823.

Verma D, Tasan RO, Herzog H, Sperk G (2012) NPY controls fear conditioning and fear extinction by combined action on Y(1) and Y(2) receptors. British journal of pharmacology 166:1461-1473.

Verma D, Wood J, Lach G, Mietzsch M, Weger S, Heilbronn R, Herzog H, Bonaventure P, Sperk G, Tasan RO (2015) NPY Y2 receptors in the central amygdala reduce cued but not contextual fear. Neuropharmacology 99:665-674.

Vouimba RM, Munoz C, Diamond DM (2006) Differential effects of predator stress and the antidepressant tianeptine on physiological plasticity in the hippocampus and basolateral amygdala. Stress 9:29-40.

Vouimba RM, Yaniv D, Diamond D, Richter-Levin G (2004) Effects of inescapable stress on LTP in the amygdala versus the dentate gyrus of freely behaving rats. The European journal of neuroscience 19:1887-1894.

Vyas A, Jadhav S, Chattarji S (2006) Prolonged behavioral stress enhances synaptic connectivity in the basolateral amygdala. Neuroscience 143:387-393.

Vyas A, Mitra R, Shankaranarayana Rao BS, Chattarji S (2002) Chronic stress induces contrasting patterns of dendritic remodeling in hippocampal and amygdaloid neurons. The Journal of neuroscience : the official journal of the Society for Neuroscience 22:6810-6818.

Vyas A, Pillai AG, Chattarji S (2004) Recovery after chronic stress fails to reverse amygdaloid neuronal hypertrophy and enhanced anxiety-like behavior. Neuroscience 128:667-673.

Walker DL, Toufexis DJ, Davis M (2003) Role of the bed nucleus of the stria terminalis versus the amygdala in fear, stress, and anxiety. European journal of pharmacology 463:199-216.

Walker MW, Wolinsky TD, Jubian V, Chandrasena G, Zhong H, Huang X, Miller S, Hegde LG, Marsteller DA, Marzabadi MR, Papp M, Overstreet DH, Gerald CP, Craig DA (2009) The novel neuropeptide Y Y5 receptor antagonist Lu AA33810 [N-[[trans-4-[(4,5-dihydro[1]benzothiepino[5,4-d]thiazol-2-yl)amino]cyclohexyl]me thyl]-methanesulfonamide] exerts anxiolytic- and antidepressant-like effects in rat models of stress sensitivity. The Journal of pharmacology and experimental therapeutics 328:900-911.

Wan CP, Lau BH (1995) Neuropeptide Y receptor subtypes. Life sciences 56:1055-1064.

Wang SJ (2005) Activation of neuropeptide Y Y1 receptors inhibits glutamate release through reduction of voltage-dependent Ca2+ entry in the rat cerebral cortex nerve terminals: suppression of this inhibitory effect by the protein kinase C-dependent facilitatory pathway. Neuroscience 134:987-1000.

Washburn MS, Moises HC (1992) Inhibitory responses of rat basolateral amygdaloid neurons recorded in vitro. Neuroscience 50:811-830.

Weisberg RB, Dyck I, Culpepper L, Keller MB (2007) Psychiatric treatment in primary care patients with anxiety disorders: a comparison of care received from primary care providers and psychiatrists. The American journal of psychiatry 164:276-282.

Weiskrantz L (1956) Behavioral changes associated with ablation of the amygdaloid complex in monkeys. Journal of comparative and physiological psychology 49:381-391.

Wessa M, Flor H (2007) Failure of extinction of fear responses in posttraumatic stress disorder: evidence from second-order conditioning. The American journal of psychiatry 164:1684-1692.

Wolak ML, DeJoseph MR, Cator AD, Mokashi AS, Brownfield MS, Urban JH (2003) Comparative distribution of neuropeptide Y Y1 and Y5 receptors in the rat brain by using immunohistochemistry. The Journal of comparative neurology 464:285-311.

Wolf MK (1970) Anatomy of cultured mouse cerebellum. II. Organotypic migration of granule cells demonstrated by silver impregnantion of normal and mutant cultures. The Journal of comparative neurology 140:281-298.

Wolf OT, Kuhlmann S, Buss C, Hellhammer DH, Kirschbaum C (2004) Cortisol and memory retrieval in humans: influence of emotional valence. Annals of the New York Academy of Sciences 1032:195-197.

Womble MD, Moises HC (1993) Hyperpolarization-activated currents in neurons of the rat basolateral amygdala. Journal of neurophysiology 70:2056-2065.

Woo NH, Teng HK, Siao CJ, Chiaruttini C, Pang PT, Milner TA, Hempstead BL, Lu B (2005) Activation of p75NTR by proBDNF facilitates hippocampal long-term depression. Nature neuroscience 8:1069-1077.

Wood GE, Young LT, Reagan LP, McEwen BS (2003) Acute and chronic restraint stress alter the incidence of social conflict in male rats. Hormones and behavior 43:205-213.

Woodruff AR, Sah P (2007) Inhibition and synchronization of basal amygdala principal neuron spiking by parvalbumin-positive interneurons. Journal of neurophysiology 98:2956-2961.

Yuste R (2011) Dendritic spines and distributed circuits. Neuron 71:772-781.

Yuste R, Bonhoeffer T (2001) Morphological changes in dendritic spines associated with long-term synaptic plasticity. Annual review of neuroscience 24:1071-1089.

Zambello E, Zanetti L, Hedou GF, Angelici O, Arban R, Tasan RO, Sperk G, Caberlotto L (2011) Neuropeptide Y-Y2 receptor knockout mice: influence of genetic background on anxiety-related behaviors. Neuroscience 176:420-430.

Zhou Z, Zhu G, Hariri AR, Enoch MA, Scott D, Sinha R, Virkkunen M, Mash DC, Lipsky RH, Hu XZ, Hodgkinson CA, Xu K, Buzas B, Yuan Q, Shen PH, Ferrell RE, Manuck SB, Brown SM, Hauger RL, Stohler CS, Zubieta JK, Goldman D (2008) Genetic variation in human NPY expression affects stress response and emotion. Nature 452:997-1001.

Zobel AW, Nickel T, Kunzel HE, Ackl N, Sonntag A, Ising M, Holsboer F (2000) Effects of the high-affinity corticotropin-releasing hormone receptor 1 antagonist R121919 in major depression: the first 20 patients treated. Journal of psychiatric research 34:171-181.

Zoladz PR, Park CR, Halonen JD, Salim S, Alzoubi KH, Srivareerat M, Fleshner M, Alkadhi KA, Diamond DM (2012) Differential expression of molecular markers of synaptic

plasticity in the hippocampus, prefrontal cortex, and amygdala in response to spatial learning, predator exposure, and stress-induced amnesia. Hippocampus 22:577-589.

Appendix I: Effects of the Y5-agonist in BLA OTCs and *in vivo.*

Figure AI.1

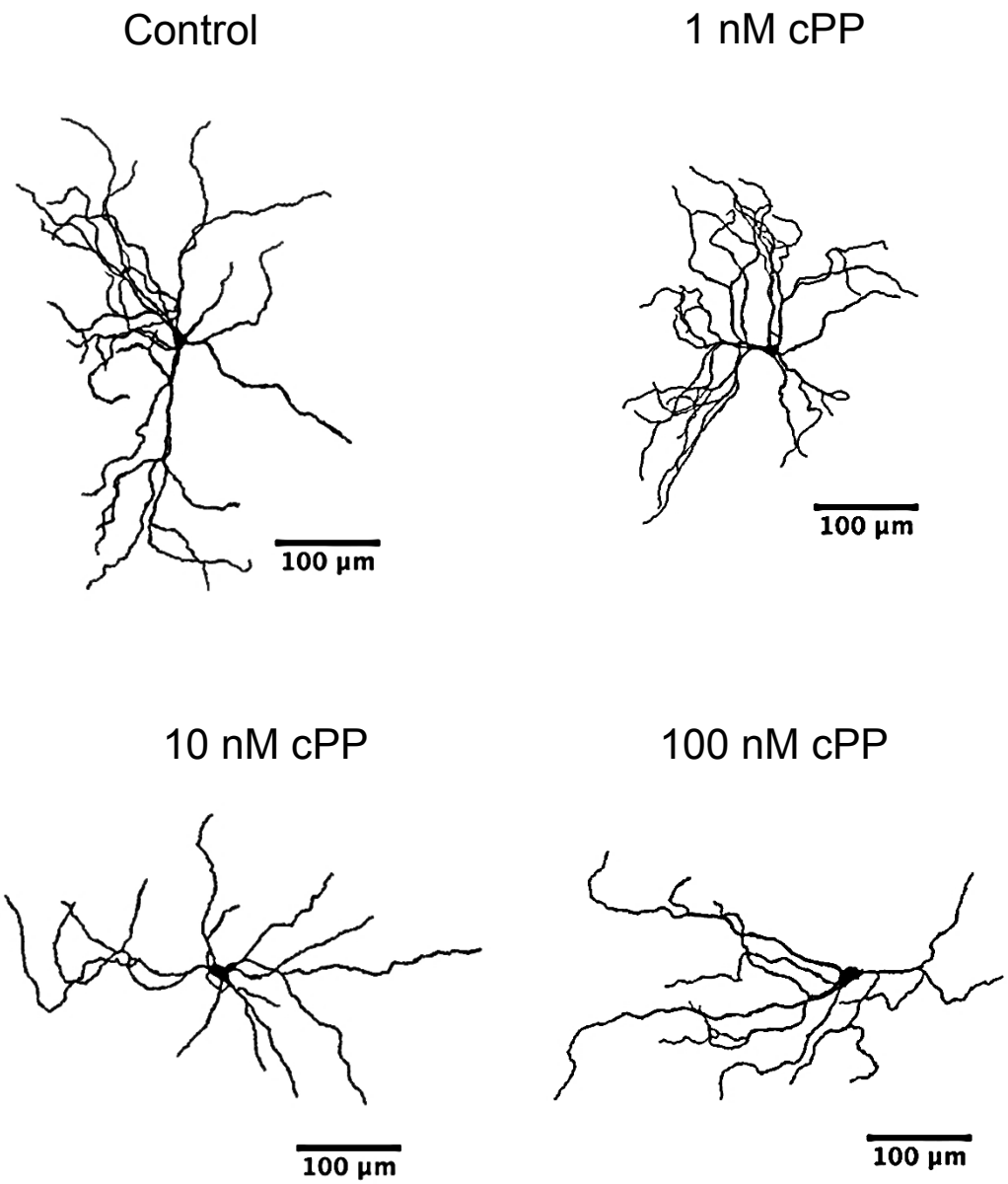

Figure AI.1 Representative reconstructed principal neurons in BLA OTCs following Y5-agonist (cPP) incubations.

Following electrophysiological recordings and filling of cells with neurobiotin, OTCs were fixed, stained and imaged. Reconstructions were made using the simple neurite tracer function in FIJI. Representative tracings of the total dendritic tree of principal neurons from 0, 1, 10 and 100 nM cPP treated BLA OTCs.

Figure AI.2

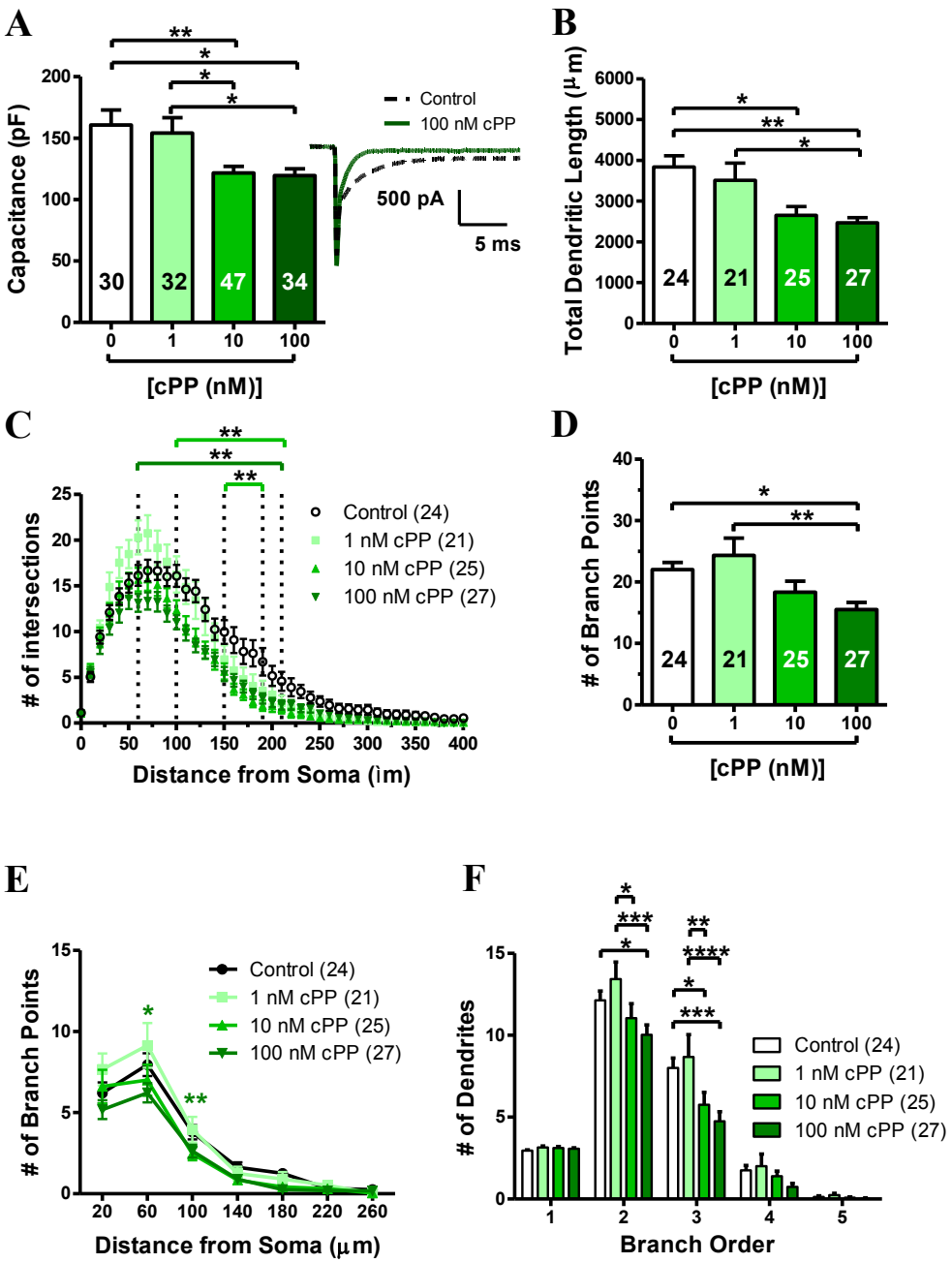
A
Capacitance (pF)
200
150
100
50
0
30
32
47
34
0
1
10
100
[cPP (nM)]
Control
100 nM cPP
500 pA
5 ms
B
Total Dendritic Length (μm)
6000
5000
4000
3000
2000
1000
0
24
21
25
27
0
1
10
100
[cPP (nM)]
C
# of intersections
25
20
15
10
5
0
0
50
100
150
200
250
300
350
400
Distance from Soma (im)
Control (24)
1 nM cPP (21)
10 nM cPP (25)
100 nM cPP (27)
D
# of Branch Points
40
30
20
10
0
24
21
25
27
0
1
10
100
[cPP (nM)]
E
# of Branch Points
15
10
5
0
20
60
100
140
180
220
260
Distance from Soma (μm)
Control (24)
1 nM cPP (21)
10 nM cPP (25)
100 nM cPP (27)
F
# of Dendrites
15
10
5
0
1
2
3
4
5
Branch Order
Control (24)
1 nM cPP (21)
10 nM cPP (25)
100 nM cPP (27)

Figure AI.2 Treatment with cPP results in hypotrophy of the dendritic arbor in BLA OTCs,

10 nM and 100 nM cPP incubations in BLA OTCs resulted in reductions of (A) cell capacitance, (B) total dendritic length, (C) number of intersections as a function of distance from the soma, and (D) branch points compared to controls and 1 nM cPP-treated principal neurons (*P<0.05, **P<0.01, one- and two-way ANOVA with Tukey's post hoc test). (A, right) Representative current traces of the capacitive transient following a -10 mV hyperpolarizing voltage step in control and 100 nM cPP neurons. Dendritic hypotrophy and branching was localized to proximal and intermediate regions along the dendritic tree (C and E). (F) Incubation with cPP resulted in diminished 2˚ and 3º dendrites compared to controls and 1 nM cPP incubated neurons (*P<0.05, **P<0.01, ***P<0.001, ****P<0.0001, two-way ANOVA with Tukey's *post hoc* test).

Figure AI.3

10 nM NPY +
30 nM CGP

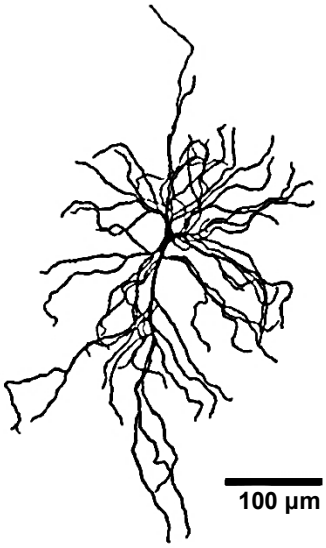

30 nM CGP

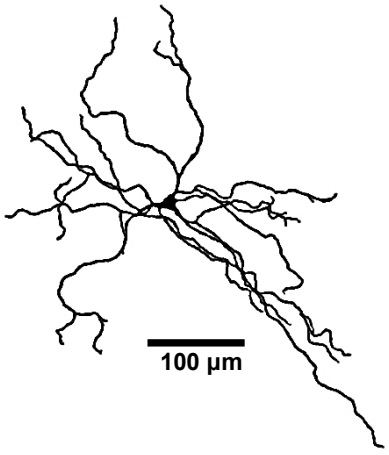

Figure AI.3 Representative reconstructed principal neurons in BLA OTCs following NPY + CGP and CGP alone.

Following electrophysiological recordings and filling of cells with neurobiotin, OTCs were fixed, stained and imaged. Reconstructions were made using the simple neurite tracer function in FIJI. Representative tracings of the total dendritic tree of principal neurons from 10 nM NPY + 30 nM CGP (NPY + CGP) and 30 nM CGP (CGP) alone treated BLA OTCs.

Figure AI.4

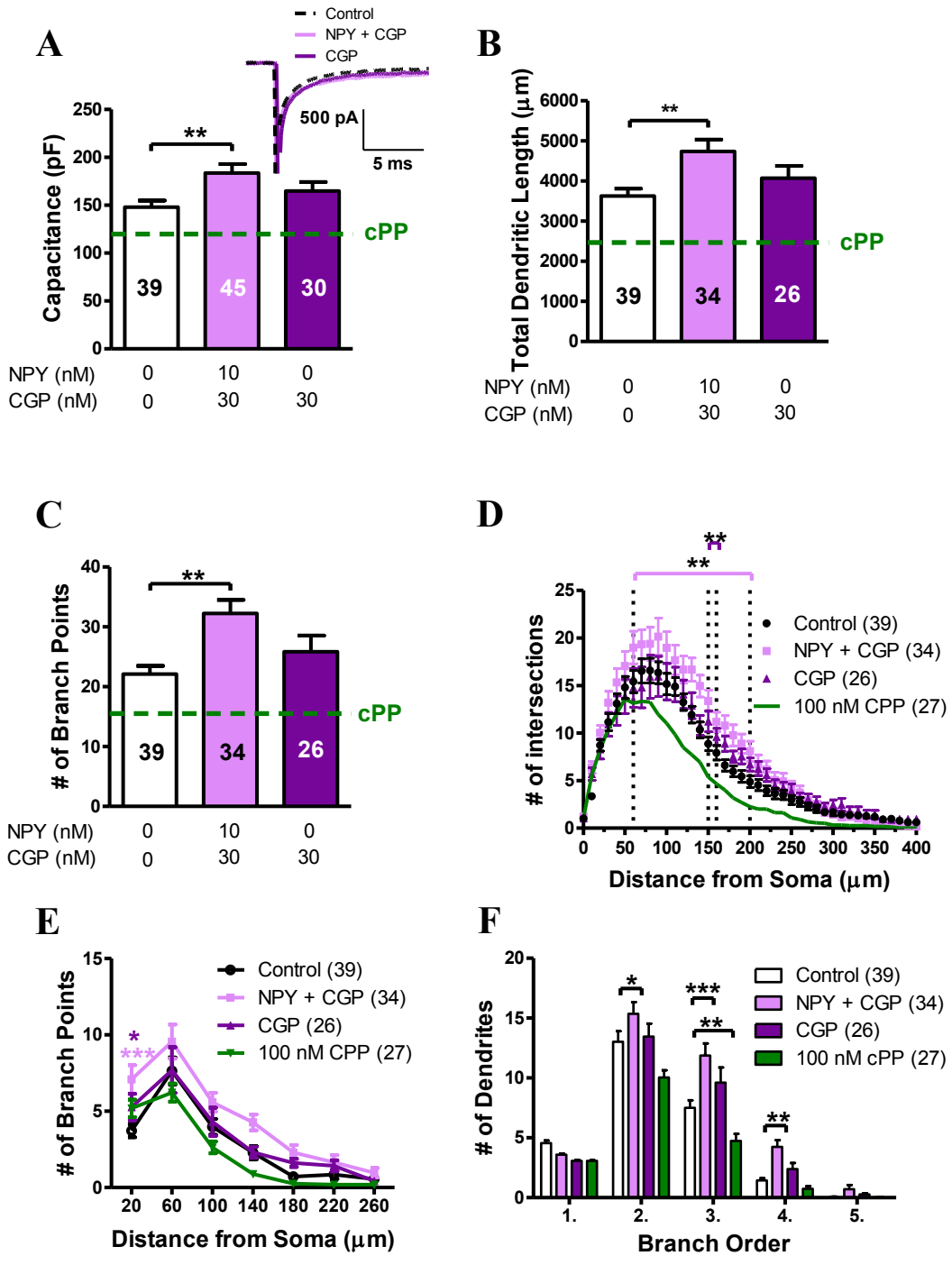
A
Control
NPY + CGP
CGP
500 pA
5 ms
Capacitance (pF)
**
cPP
39
45
30
NPY (nM) 0 10 0
CGP (nM) 0 30 30
B
Total Dendritic Length (µm)
**
cPP
39
34
26
NPY (nM) 0 10 0
CGP (nM) 0 30 30
C
# of Branch Points
**
cPP
39
34
26
NPY (nM) 0 10 0
CGP (nM) 0 30 30
D
# of intersections
**
**
Control (39)
NPY + CGP (34)
CGP (26)
100 nM CPP (27)
Distance from Soma (µm)
E
# of Branch Points
*
***
Control (39)
NPY + CGP (34)
CGP (26)
100 nM CPP (27)
Distance from Soma (µm)
F
# of Dendrites
*
***
**
**
Control (39)
NPY + CGP (34)
CGP (26)
100 nM cPP (27)
Branch Order

Figure AI.4 NPY + CGP incubations, but not CGP alone resulted in dendritic hypertrophy in BLA OTCs

NPY + CGP incubations resulted in increases of (A) cell capacitance, (B) total dendritic length, and (C) branch points (**P<0.01, one- and two-way ANOVA with Tukey's *post hoc* test). (D) Sholl analysis revealed the regions of dendritic hypertrophy were localized to proximal and intermediate regions along the dendritic tree (**P<0.01, two-way ANOVA with Tukey's *post hoc* test). (E-F) Increases in branching was localized to proximal regions of the dendritic tree, along with secondary, tertiary and quaternary dendrites (***P<0.001, one- and two-way ANOVA with Tukey's *post hoc* test). CGP alone, resulted in minor effects to the dendritic arbor (A-F). The number of analyzed cells is presented for each treatment in the figure legend or bar graph. For visual depiction, green points on graphs represent the effects of the Y5-agonist in BLA OTCs, but where not incorporated into statistical analysis.

Figure AI.5

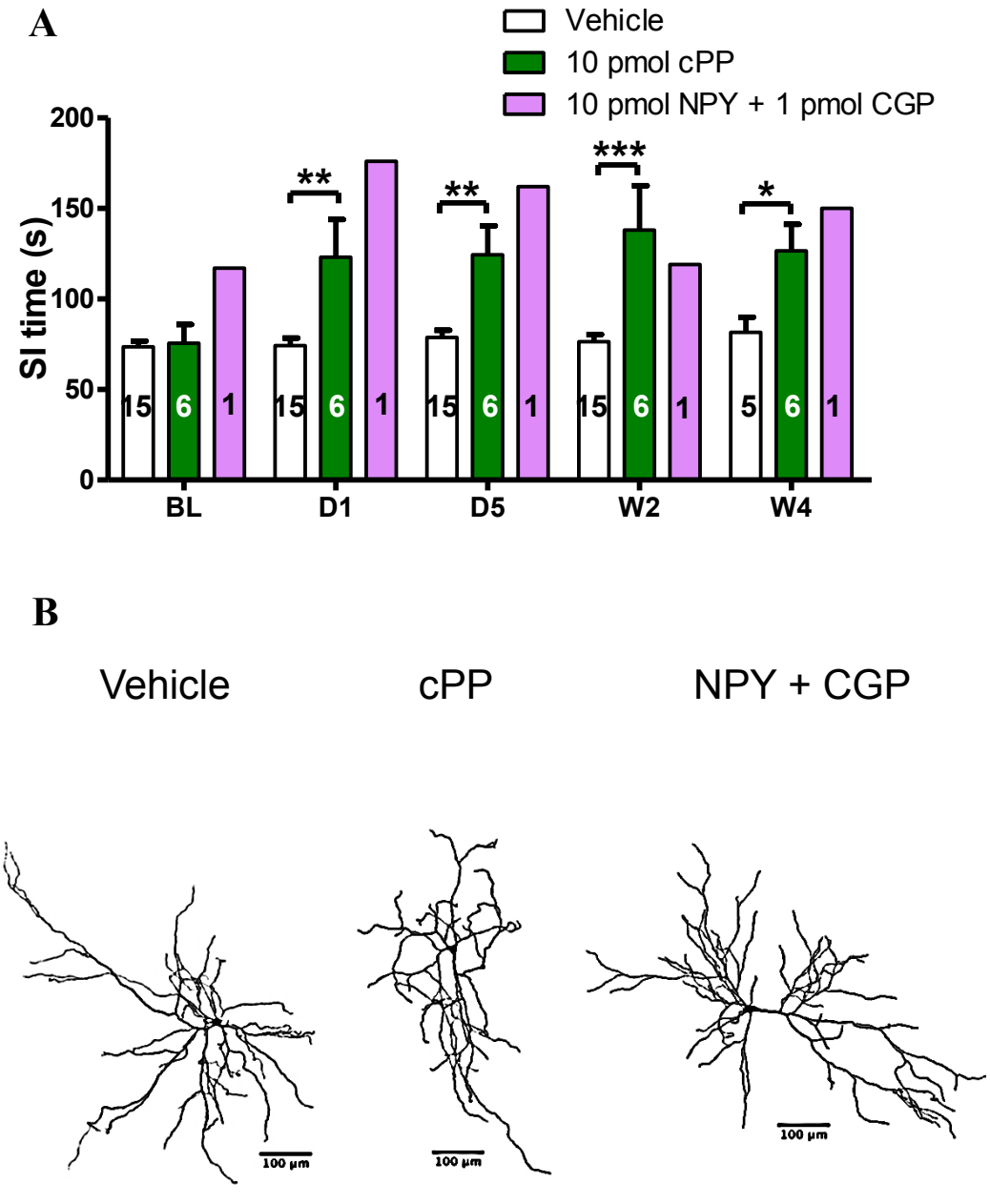
A
Vehicle
10 pmol cPP
10 pmol NPY + 1 pmol CGP
SI time (s)
200
150
100
50
0
**
**
***
*
15
6
1
15
6
1
15
6
1
15
6
1
5
6
1
BL
D1
D5
W2
W4
B
Vehicle
cPP
NPY + CGP
100 µm
100 µm
100 µm

Figure AI.5 Repeated injection of the Y5-agonist directly into the BLA *in vivo* results in an acute and persistent anxiolytic effect

(A) Social interaction (SI) was measured at baseline and at various time points after injection with PBS vehicle or 10 pmol cPP. At days 1 and 5, social interaction time significantly increased compared to vehicle treated animals (***P*<0.01, two-way ANOVA with Tukey's *post hoc* test). This effect persisted at later time points of 2 and 4 weeks, suggesting the Y5-receptor is mediating NPY-induced stress resilience (**P*<0.05, ****P*<0.001). Note only, one animal has been tested so for coinjections of cPP and CGP. (B) Representative reconstructions of principal neurons from *ex vivo* BLA slices following repeated injections of vehicle (left), cPP (middle) and NPY + CGP (right).

Figure AI.6

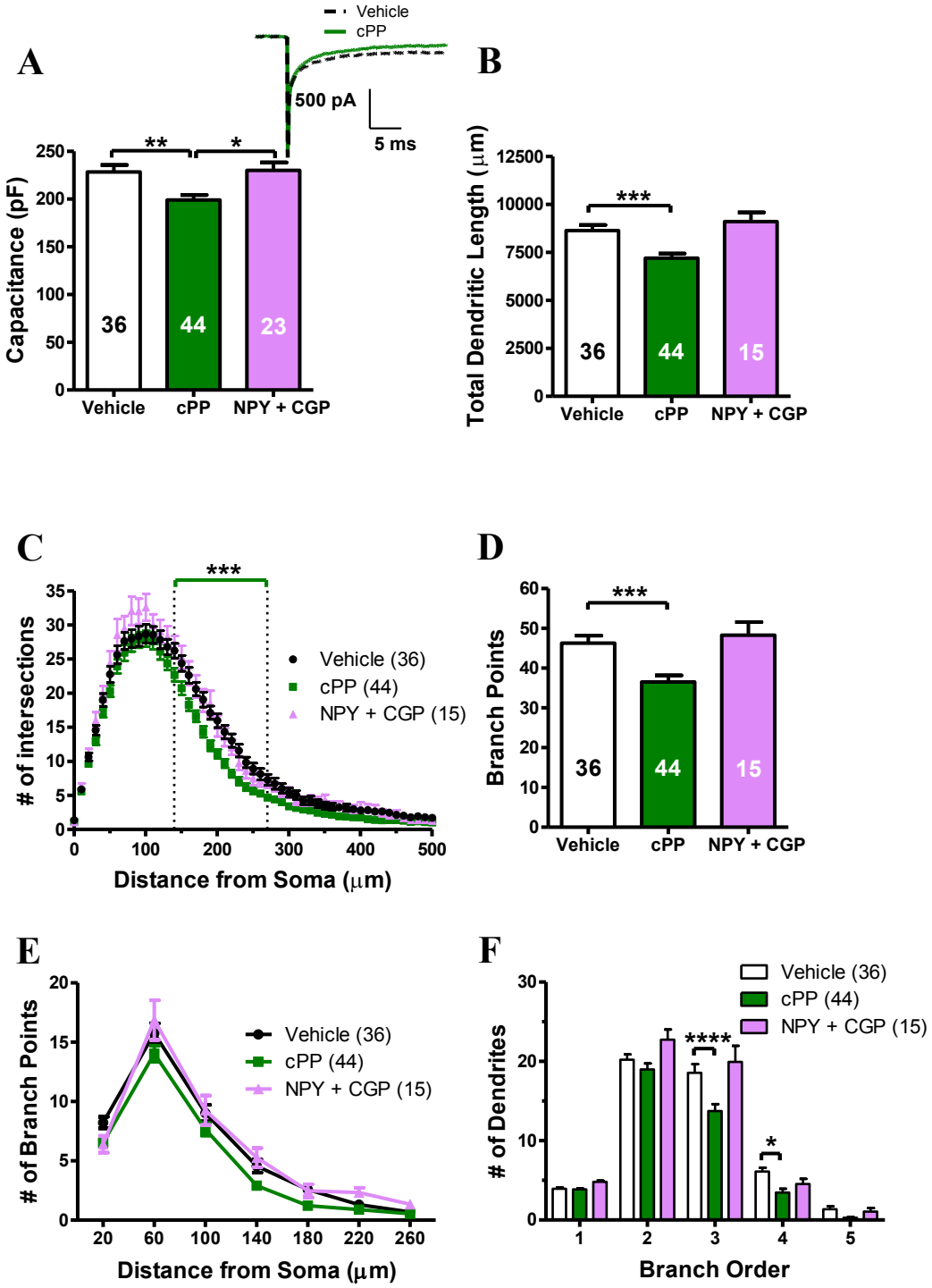
A
Vehicle
cPP
500 pA
5 ms
**
*
Capacitance (pF)
250
200
150
100
50
0
36
44
23
Vehicle
cPP
NPY + CGP
B
Total Dendritic Length (μm)
12500
10000
7500
5000
2500
0
***
36
44
15
Vehicle
cPP
NPY + CGP
C
***
# of intersections
35
30
25
20
15
10
5
0
0
100
200
300
400
500
Distance from Soma (μm)
Vehicle (36)
cPP (44)
NPY + CGP (15)
D
Branch Points
60
50
40
30
20
10
0
***
36
44
15
Vehicle
cPP
NPY + CGP
E
# of Branch Points
20
15
10
5
0
20
60
100
140
180
220
260
Distance from Soma (μm)
Vehicle (36)
cPP (44)
NPY + CGP (15)
F
# of Dendrites
30
20
10
0
****
*
1
2
3
4
5
Branch Order
Vehicle (36)
cPP (44)
NPY + CGP (15)

Figure AI.6 Repeated injection of cPP into the BLA *in vivo*, results in reductions in cell capacitance and dendritic hypotrophy in *ex vivo* brain slices.

(A) Capacitance measurements of principal neurons from *ex vivo* brain slices indicates that repeated injection of the Y5-agoinst reduces cell capacitance (left). (Right) Representative traces of the capacitive transients in vehicle and cPP treated principal neurons. Consistent with our findings in BLA OTCs, repeated injection of cPP did resulted in hypotrophy of BLA principal neurons. (B) Total dendritic length was reduced in cPP treated neurons compared to controls (***P<0.001, t-test). (C) Sholl analysis revealed the regions of increased number of intersections along the dendritic tree where remodeling occurred (***P<0.001, two-way and one-way ANOVA with Tukey's *post hoc* test). The dendritic retraction due to cPP appears to be positioned at more distal regions (intermediate only) compared to the effects of NPY. (D) Total branch points is reduced in principal neurons from the cPP treated animals compared to controls (***P<0.001, t-test). (E) Although all regions along the dendritic arbor where we analyzed changes in the number of branch points in neurons from cPP treated animals were reduced compared to vehicle injected animals, post hoc analysis revealed no single point that was significantly reduced compared to controls (P>0.05, two-way and one-way ANOVA with Tukey's *post hoc* test). (F) Repeated injection of cPP reduced the number of dendrites on 2º and 3º branch orders compared to controls (*P<0.05, ****P<0.0001, two-way and one-way ANOVA with Tukey's *post hoc* test). Although we included results for the repeated injections of NPY + CGP, no statistical analysis can be made, as there is only data from animal at this point. The number of analyzed cells is presented for each treatment in the figure legend or bar graph.

Appendix II: Importance of recognition loops B and D in the activation of human 5-HT3 receptors by 5-HT and meta-chlorophenylbiguanide.

Introduction

The 5-HT_3 receptor (5-HT_3R) is a member of the Cys-loop family of ligand-gated ion channels, and, like the archetypal member of the family, the nicotinic acetylcholine receptor (nAChR), it is cation selective. The $GABA_A$ and strychnine sensitive glycine receptors represent the anion selective receptors of the family. Five genes have been associated with the 5-HT_3R and are designated A–E, but only two receptor subtypes have been significantly characterized: the homomeric 5-HT_3A and the heteromeric 5-HT_3AB receptors. The 5-HT_3R exhibits pentameric pseudosymmetry and fits into a cylinder with a diameter of 8 nm and a long axis of 11 nm, perpendicular to the cell membrane (Boess et al., 1995). The subunits exhibit around 20% homology to those of the nAChR from *Torpedo marmorata*, the structure of which has been resolved to 4Å using cryo-electron microscopy (Unwin, 2005). This receptor family exhibits three domains: an extracellular domain (ECD), a transmembrane domain (TMD) and an intracellular domain (ICD). The ECD forms a 3 nm diameter ion vestibule and is responsible for agonist recognition. The TMD contains four helices from each subunit, the second, TM2, forms the lining of the ion pore that gates ion flow. The ICD is incompletely resolved but exhibits a single membrane associated (MA) helix, which has been shown to restrict channel conductance of the homomeric 5-HT_3AR (Kelley et al., 2003).

Agonist recognition within this receptor family appears to be delineated by six non-contiguous loops at the subunit interfaces, three, A–C, associated with the principal subunit and three, D–F with the complementary subunit. Much of the information about the importance of individual amino acids within these loops of this particular member of the family has been accrued from mutagenic studies carried out on the homomeric 5-HT_3AR (see Barnes et al., 2009 and Lummis, 2012 for amplification), although it is the heteromeric 5-

HT_3AB receptor that exhibits characteristics which more closely reflect those of neuronal receptors (Fletcher and Barnes, 1998 and Davies et al., 1999). There is little evidence for the differentiation of the two receptor subtypes by competitive antagonists (Brady et al., 2001) although it has recently been reported that this can be achieved by a novel antagonist, exhibiting higher affinity for the homomer than the heteromer (Thompson et al., 2012). The two receptor subtypes exhibit distinct concentration–response curves to the natural agonist in human where the presence of the B subunit increases the relative efficacy of mCPBG and 1-phenylbiguanide (1-PBG) compared to the natural agonist 5-HT (Dubin et al., 1999), compatible with the view that agonist activation in the homomeric and heteromeric receptors is distinct.

In this study we have explored further the distinct receptor activation characteristics of two agonists, 5-HT and mCPBG, focusing on selected amino acids from recognition loops B and D, found to be important in agonist activation of the homomeric receptor by 5-HT. Loop B of the A subunit contains a tryptophan residue which forms an important cation-π interaction with the aliphatic amine of the natural agonist 5-HT in the homomeric receptor (Beene et al., 2002), while the aligned position of the B subunit is occupied by isoleucine, which is unable to support such an interaction. Comparison of the D loop between the A and B subunits shows that they contain a distinct triplet of amino acids, of particular interest as this loop appears to be important in activation, but not recognition, in nAChR (Akk, 2002). We have replaced these residues in the A subunit by those found in homologous positions of the human B subunit; the converse experiments have also been carried out in which residues in the B subunit have been replaced by those in the homologous positions of the A subunit. The A subunit mutants have been expressed alone or together with the wild type (wt) B

subunit; the B subunit mutants have been expressed with the wt A subunits. Expression was carried out in *Xenopus* oocytes and the receptors functionally characterized using two-electrode voltage clamp.

Experimental procedures

Materials

All drugs were purchased from Sigma–Aldrich (St. Louis, MO, USA) and were made as stock solutions (3–10 mM) in sterile water or frog Ringer's buffer (110 mM NaCl, 2 mM KCl, 1.8 mM $CaCl_2$ and 5 mM HEPES, pH 7.4). mCPBG was heated and then sonicated to make 3 mM solutions. Restriction enzymes and cRNA transcript preparation materials were purchased from Invitrogen (Burlington, ON, Canada), Promega (Madison, WI, USA), or New England Biolabs (Pickering, ON, Canada). *Pfu* Turbo DNA polymerase, for site directed mutagenesis was purchased from Stratagene (La Jolla, CA, USA). Custom primers were prepared by IDT (Coralville, IA, USA).

Site-directed mutagenesis

Mutagenesis was performed as previously described (Derry et al., 2004). Briefly, the QuickChange protocol (Stratagene, La Jolla, CA) was used to introduce the B loop I176W and separately the D loop triplet QEV-85, 86, 87-RQY into the wild-type human 5-HT3B subunit cDNA sequence. The homologous mutations for the 5-HT3A subunit B loop W178I, and the D loop RQY-87, 88, 89-QEV were also constructed. The individual subunit cDNA sequences, 5-HT3A (accession number P40698) and 5-HT3B (accession number O95264), had been previously subcloned into pcDNA3.1(+) (Invitrogen, San Diego, CA) and these plasmids were used as templates in polymerase chain reaction-mediated (PCR) mutagenesis protocols. The

mutants were screened by restriction endonuclease digestion and all mutations were confirmed by DNA sequencing. *In vitro* transcription of cRNA was performed using standard protocols (Invitrogen).

Expression of receptors in Xenopus oocytes

Stage V–VI *Xenopus laevis* oocytes were isolated and prepared as previously described (Smith et al., 2004). Oocytes were microinjected with 50 nL total of 1 μg/μL wild-type or mutant 5-HT3A and mutant or wild-type 5-HT3B subunit cRNA in a 1:1 ratio. Injected oocytes were incubated in ND96 buffer (96 mM NaCl, 1.8 mM $CaCl_2$, 2 mM KCl and 1 mM $MgCl_2$ and 5 mM HEPES, pH 7.4 with NaOH) containing 50 μg/mL gentamicin (GIBCO, Grand Island, NY, USA) in 96-well plates at 14 °C for 2–7 days prior to functional analysis.

Fluorescent visualization of 5-HT3B subunit mutants in Xenopus oocytes

Five days after mRNA injection, oocytes were fixed in Z-fix for 15 min at 4 °C. Oocytes were rinsed with PBS containing 50 mM NH_4Cl then blocked for 30 min with 2% bovine serum albumin (BSA) in PBS. Rabbit anti-5-HT3B (Sigma–Aldrich Canada, Oakville, Canada Cat.AV35186) directed to the N-terminal region of the protein was diluted in blocking buffer and applied to oocytes overnight. Oocytes were washed in PBS for 30 min, followed by incubation for 1 h with a chicken anti-rabbit Alexa 488 secondary antibody (Molecular probes, Eugene, OR) diluted in blocking buffer. Oocytes were rinsed in PBS for 30 min and imaged with a 20× objective on a spinning disk confocal microscope (Perkin Elmer UltraView ERS6) using GFP laser (488 nm). The acquisition was performed with a Hamamatsu digital camera (C9100-50 EM CCD) and analysed with Volocity 5.5.1 software.

Electrophysiological recordings

Oocytes were continuously bathed in frog Ringer's buffer by gravity flow (~5 mL/min) in a custom-made recording chamber. Agonist-induced currents were measured by standard two-electrode voltage clamp techniques using a GeneClamp 500B amplifier (Axon Instruments Inc., Foster City, CA, USA) at a holding potential of −60 mV. Electrodes were filled with 3 M KCl and had a resistance between 0.3 and 1.5 MΩ in Frog Ringer's solution. Oocytes were only used for experiments when current responses were stable (±10%) between successive applications of agonist. All stock solutions of drugs were diluted in perfusion (frog Ringer's) buffer.

To measure the effects of 5-HT and mCPBG, the agonist was applied via gravity perfusion for 10–30 s. This was followed by an 8–12 min washout to ensure complete recovery from desensitization.

Data analysis

Concentration–effect curves for agonist activation were analysed by non-linear regression techniques using GraphPad Prism 5.00 software (San Diego, CA, USA) and the following equation:

$$I = \frac{I_{\max} * [L]^{nH}}{EC_{50}^{nH} + [L]^{nH}}$$

where I is the amplitude of agonist-evoked current for a given concentration [L], I_{max} is the maximum amplitude of current, EC_{50} is the agonist concentration that evokes half maximal receptor activation, and nH is the Hill coefficient. EC_{50}, which is log normally distributed, together with nH data were analysed by one-way ANOVA and levels of significance were

determined by Tukey post-test for multiple comparisons (GraphPad Prism 5.00, San Diego, CA, USA). Residual plots were created simultaneously to confirm no systematic deviation of data from the line of best fit, which would be expected if desensitization was compromising measurement of currents at higher agonist concentrations (Supplementary Fig. 1).

Relative efficacy was determined for mCPBG using the equation:

$$\%\ \text{Relative Efficacy} = \frac{I_{\text{max m-CPBG}}}{I_{\text{max 5-HT}}} * 100$$

where $I_{\text{max mCPBG}}$ is the maximum current produced by a saturating concentration of mCPBG and $I_{\text{max5-HT}}$ is the maximum current produced by a saturating concentration of 5-HT. The I_{max} for each agonist was determined on the same oocyte for each of the individual receptor subtypes to provide a measure of relative efficacy. In order to make appropriate use of the matched pair comparisons carried out in this work, the I_{max} value for each agonist in a single oocyte was converted to its logarithmic equivalent and the matched pair comparisons were carried out on these values (Motulsky, 2003). The 95% confidence intervals on these differences were anti-logged for display in Table 3.

Results

The 5-HT3B subunit mutants are trafficked to the cell membrane of the oocytes

Co-injection of *Xenopus* oocytes with mRNA for both the wt 5-HT3A and mutant 5-HT3B subunits results in the cell surface expression of the mutant proteins. Since the 5-HT3A subunit can express as homomeric receptors, in order to establish that the 5-HT3B subunit was expressing, immunofluorescence was employed. Fig. 1 shows the fluorescent images for both the triple D loop mutant (centre panel) and the B loop mutant (right panel) five days after

oocyte injection. The left panel, which shows no fluorescence, was injected with only the wt 5-HT3A subunit mRNA and demonstrates the specificity of the antibody staining of only the 5-HT3B subunit after exposure to Alexa 488 labelled secondary antibodies. Non-injected oocytes or those which had not been exposed to the primary antibody failed to exhibit fluorescence (data not shown).

Comparison of the wt homomer and heteromer with the B loop mutants: 5-HT$_3$A(W178I), 5-HT$_3$A(W178I)B and 5-HT$_3$AB(I176W)

The concentration dependence of 5-HT activation on the wt 5-HT$_3$A and 5-HT$_3$AB receptors was compared with that produced by the heteromeric receptors in which the 5-HT3A or 5-HT3B subunit carried the W178I or I176W mutation, respectively, and the data is shown in Table 1. The EC_{50} of the human wt homomeric receptor (1.78 μM) is significantly lower than that found for the wt heteromeric receptor (8.71 μM) while the Hill coefficient is significantly higher (2.67 vs 1.10, respectively). The homomeric receptor bearing the W178I mutation in loop B has a much higher EC_{50} (77.6 μM) than that exhibited by the wt receptor, however the Hill coefficient is not different at 2.32. Likewise, when this mutation to the 5-HT3A subunit is expressed with the wt 5-HT3B subunit, the EC_{50} for 5-HT is also much higher than wt at 165.9 μM. This Hill slope is also not different from the wt heteromeric receptor at 1.57. The heteromeric receptor carrying the I176W mutation in the 5-HT3B subunit exhibits an EC_{50} between those of the two wt comparators (3.98 μM), and is significantly different from neither. While the Hill coefficient is significantly smaller than that obtained for the wt homomer (0.84), it does not differ from that of the wt heteromeric receptor.

Similar studies were carried out on these receptors with the agonist mCPBG (Table 2). At the wt homomeric receptor, mCPBG has an EC_{50} value of 1.51 μM and a Hill coefficient of 2.08. 5-HT and mCPBG elicit approximately the same amplitude of maximum current from matched oocytes and since we are not comparing any other agonists, we will consider both 5-HT and mCPBG full agonists at the wt homomeric receptor. The heteromeric receptor has an EC_{50} for mCPBG of 1.02 μM and a Hill coefficient of 1.88, neither of which differ significantly from the homomer. However, the maximum current evoked by mCPBG is 1.56 times the maximum current evoked by 5-HT (Table 3). At the heteromeric receptor, 5-HT behaves as a partial agonist compared with mCPBG.

The potency of mCPBG is significantly lower for receptors bearing the loop B mutation in the 5-HT3A subunit compared with the wt homomer and wt heteromer. The 5-HT_3A(W178I) homomeric mutant receptor has an EC_{50} for mCPBG of 22.9 μM, while the 5-HT_3A(W178I)B heteromeric mutant receptor has an EC_{50} of 28.84 μM. In contrast, this B loop mutation in the 5-HT3B subunit results in a much smaller change in the EC_{50} of this heteromeric receptor mutant for mCPBG (2.04 μM), although this remains significant. None of these B loop mutations affected the Hill coefficient of the mCPBG concentration–response curves. However, the maximum current elicited by mCPBG was greatly reduced when this mutation was expressed in the 5-HT3A subunit of both the homomeric and heteromeric receptor, compared with the maximum current evoked by 5-HT on the same oocyte, as well as oocytes expressing wt receptors (Table 3). mCPBG has become a weak partial agonist at both the homomeric and heteromeric receptors bearing this B loop mutation in the 5-HT3A subunit. In the receptor bearing this mutation in the B subunit, 5-HT_3AB(I176W), 5-HT remains a partial agonist with respect to mCPBG, as is the case with the wt heteromer.

The B loop mutation W178I to the 5-HT3A subunit markedly increases the EC_{50} for agonists 5-HT and mCPBG in both the homomeric and heteromeric receptors carrying his mutation, it also profoundly reduces the efficacy of mCPBG. The impact of the homologous B loop mutation, I176W, in the 5-HT3B subunit has limited impact on the EC_{50} of either agonist and does not compromise their relative efficacies found in the wt heteromeric receptors.

Comparison of the wt homomer and heteromer with the D loop mutants

Three sequential amino acid residues of the D loop in the 5-HT3A subunit, RQY, are distinct from the aligned residues of the 5-HT3B subunit, QEV. These residues in the 5-HT3A subunit were replaced with those of the 5-HT3B subunit and expressed as homomeric and heteromeric receptors, in the latter case with the wt 5-HT3B subunit. In both cases, the potency for 5-HT was decreased by this triple mutation in the D loop: the EC_{50} values were 54.9 μM for the mutant homomeric receptor and 169.8 μM for the mutant heteromeric receptor. In neither case was there a significant impact on the Hill coefficient of the mutants compared to the wt receptor. This triple mutation in the A subunit resulted in a decrease in the mCPBG EC_{50} in the homomeric receptor (0.34 μM) together with a significant increase in the Hill slope (2.88) compared to the wt homomer, but the mutation did not significantly affect the EC_{50} (1.23 μM) or the Hill slope (1.24) of the heteromeric receptor. The major consequence of this triplet mutation of the 5-HT3A subunit was a dramatic decrease in the maximum current elicited by 5-HT activation, an effect that did not occur on activation with mCPBG: the natural agonist became a very weak partial agonist (Table 3).

The equivalent triplet mutation in the 5-HT3B subunit, in which the sequential amino acids QEV of the D loop are changed to the aligned amino acids of the 5-HT3A subunit,

RQY, results in an EC_{50} for 5-HT (1.74 μM) numerically similar to that of the wt homomer, and the Hill coefficient of this mutant (2.19) is not statistically distinct from the homomer. Therefore, introducing these three amino acid residues from the D loop of the 5-HT3A subunit into the 5-HT3B subunit result in the 5-HT_3AB(RQY) receptors displaying similar 5-HT concentration–response characteristics to the wt homomeric receptor. The concentration–response curve for mCPBG does not differentiate clearly between the wt homomer and heteromer and the triplet mutant 5-HT_3AB(RQY) does not differ significantly from the homomeric receptor. Surprisingly, both agonists exhibit essentially the same Imax values at this mutant, a characteristic which again mimics that found at the wt homomer.

Discussion

Studies with the mouse wt homomer have shown that a cation-π interaction forms an important recognition element between the aliphatic amine of 5-HT and W178 of the B loop (Beene et al., 2002). The –OH of this agonist is constrained by a hydrogen bond with E124 of the A loop (Price et al., 2008), correcting an earlier suggestion, prior to the emergence of structural models, that E124 interacted with the aliphatic amine of 5-HT (Boess et al., 1997). Recent studies from Miles et al. (2012) have probed this interaction further using mutant cycle analysis with both natural and unnatural amino acids, demonstrating that D119, just five residues N-terminal to E124, forms two hydrogen bonds with the backbone –NHs of B-loop residues W178 and L179. It is argued that these hydrogen bonds are responsible for the relative positioning of the B and A loops and further that they are tightly coupled to the cation-π and E124 hydrogen bond with the natural agonist, suggesting that they operate as a functional unit. The study also identifies functional differences between the agonists 5-HT and mCPBG at these residues: the mutation E124Q, or loss of the hydrogen bond from either

W178 or L179 to E124 increases the EC_{50} for 5-HT activation but converts mCPBG to an antagonist, although its efficacy can be rescued by re-establishment of the hydrogen bond between D119 and L179. In the mutant D119N both agonists retain their efficacy but exhibit marked increases in their EC_{50}s. It is also clear from this study that the interaction of mCPBG with W178 is not supported by a cation-π interaction, neither is it possible for this agonist to form a H-bond with E124. While the positioning of mCPBG in this recognition domain remains ill-defined, its activity is clearly sensitive to the relative orientation of the A and B loops (Miles et al., 2012).

The studies reported here were carried out with human homologues of the mouse receptor. The W178I mutation, expressed alone as a homomer, exhibits characteristics very similar to those rehearsed above, mCPBG efficacy is compromised, although it retains very weak partial agonist activity, while the efficacy of 5-HT remains unchanged and the concentration response curves for both agonists are shifted to the right. Loss of the cation-π interaction of the natural agonist does not appear to impact on its ability to gate the channel but could reasonably be expected to increase the EC_{50} for activation. The mutation, W178I, must so compromise the steric environment of the recognition domain to eliminate the sensitive steric interactions required by mCPBG to cause significant channel activation, as suggested by Miles et al. (2012). The homologous mutation, I176W, in the 5-HT3B subunit does not modify activation by either agonist in the heteromer carrying this mutation. However, the A subunit mutant, W178I, when expressed with the wt 5-HT3B subunit, exhibits essentially the same characteristics as those observed in the mutant homomer: the efficacy of 5-HT remains intact while that of mCPBG is seriously compromised, although the concentration–response curve of both agonists is shifted to the right. The impact of these

mutations in the B loop of 5-HT3A subunit in both the homomer and the heteromer is consistent with the 5-HT3A subunit as the principal subunit of the interface responsible for receptor activation.

The D loop of the 5-HT_3A receptor has been significantly less well characterized but there is clear evidence that both W85 and R87 interact with granisetron indicating that these residues face the binding pocket. Using a double mutant cycle analysis it has been proposed that W85 interacts with the tropane moiety of this competitive antagonist while the indazole ring interacts with R87 (Yan and White, 2005). This has been supported by recent studies in which the acetylcholine binding protein from *Lymnaea stagnalis* has been mutated to mimic the recognition domain of the 5-HT_3A receptor, subsequently being used to show that the indazole of granisetron and R87 form a cation-π complex (Kesters et al., 2013). Studies with the mouse nAChR have suggested that the D loop is involved in gating, but not recognition (Akk, 2002), while in the neuronal α4β2 receptor it has been proposed that residues on the D and E loops are integral to the partial agonist activity of varenicline, used to facilitate smoking cessation (Billen et al., 2012). This compound suffers from significant emetic side effects, that may find explanation in its 80% efficacy at the human 5-HT_3AR (Lummis et al., 2011). The structural studies of Kesters et al. (2013), are consistent with the presence of hydrophobic interactions between 5-HT and residues of the E loop, while the aminoethyl group exhibits van der Waals interactions with W85 of the D loop, although as the authors indicate, the conclusions are limited to the isolated recognition domain and may not reflect the interactions within the complete native protein.

Mutation RQY-QEV, in the D loop of the 5-HT3A subunit, results in a profound loss of 5-HT efficacy in the homomeric receptor bearing this mutation, together with a 31-fold

increase in the EC_{50} but no significant change in the Hill coefficient. Interestingly this mutation also results in a significant increase in the Hill coefficient for activation by mCPBG together with a five-fold decrease in the EC_{50}, perhaps associated with a gating interaction of E88 which faces away from the binding site. Expression of this mutant A subunit with the wt B subunit again results in a marked reduction in the efficacy of the natural agonist together with an increase in the EC_{50}, although there is no impact on either the EC_{50} or Hill coefficient of activation by mCPBG. This profound effect on 5-HT efficacy as a consequence of the triplet mutation RQY-QEV in the D loop of the 5-HT3A subunit suggests that this subunit may be required for efficient 5-HT mediated gating of the heteromeric receptor: vicinal A subunits acting as both the principal and complimentary subunits. This has previously been suggested as a consequence of the observation that double Cys mutations within the C and F loops of the A subunit, and their subsequent cross linking blocked receptor activation, which was reinstated only subsequent to Cys–Cys bond reduction with dithiothreitol (Thompson et al., 2011).

The homologous mutation of the B subunit, QEV-RQY, when expressed with the wt A subunit, has little impact on the interaction of mCPBG with the expressed receptor but surprisingly, there is a five-fold decrease in the EC_{50} of the natural agonist 5-HT together with a doubling of the Hill coefficient for this agonist. Indeed, the agonist concentration response curve cannot be differentiated from that of the wt homomeric receptor (Fig. 2 and Table 1). The fluorescence studies examining the expression of the B subunit in this construct provide unequivocal evidence for the presence of the B subunit. The parsimonious explanation for these triplet mutations in the D loop is that RQY is integral to activation by the natural agonist, multiple such interfaces being present in the wt homomer of which three appear to be

necessary to provide full activation (Corradi et al., 2009), while in the wt heteromer only a single site is perhaps required to support the reduced Hill coefficient. It is tempting to argue that the replacement of the 5-HT3A subunit signature, RQY, with the aligned 5-HT3B loop signature, QEV, is sufficient to seriously compromise the ability of the natural agonist to gate receptors harbouring this element, whether expressed as homomer or a heteromer. The introduction of the 5-HT3B subunit mutation, QEV-RQY, is able to rescue this gating activity of 5-HT in the heteromer, suggesting that an additional interface expressing the 5-HT_3A receptor RQY signature, albeit on a 5-HT3B subunit background, in the heteromeric receptor may be sufficient to provide the increased Hill coefficient for 5-HT and the normalization of its efficacy with respect to mCPBG.

Conclusions

In summary, exchanging B and D loop signatures of the 5-HT3A and 5-HT3B subunits differentiate the gating capacities of the two agonists, mCPBG and 5-HT. The disruption produced mutation W178I in the 5-HT3A can be accommodated by the natural agonist but not by mCPBG, the molecular interactions of which are less well defined at this sub-site. The D loop RQY-QEV mutation in the 5-HT3A subunit results in a marked decrease in potency and efficacy of the natural agonist, and when expressed alone increases the Hill coefficient of mCPBG and shifts the concentration response curve to the left, which does not occur in the heteromer with the wt 5-HT3B subunit as a partner. Exchange of the D loop signatures in the 5-HT3B subunit produces a most surprising result when expressed with the wt 5-HT3A subunit, the concentration response curve for the natural agonist is not significantly different from that of the wt homomeric receptor, and the efficacy of both agonists is equalized. The ability of 5-HT to gate the homomeric or heteromeric receptor appears to rely on the D loop

triplet RQY of the complementary face. Detailed gating studies will be required to explore this further.

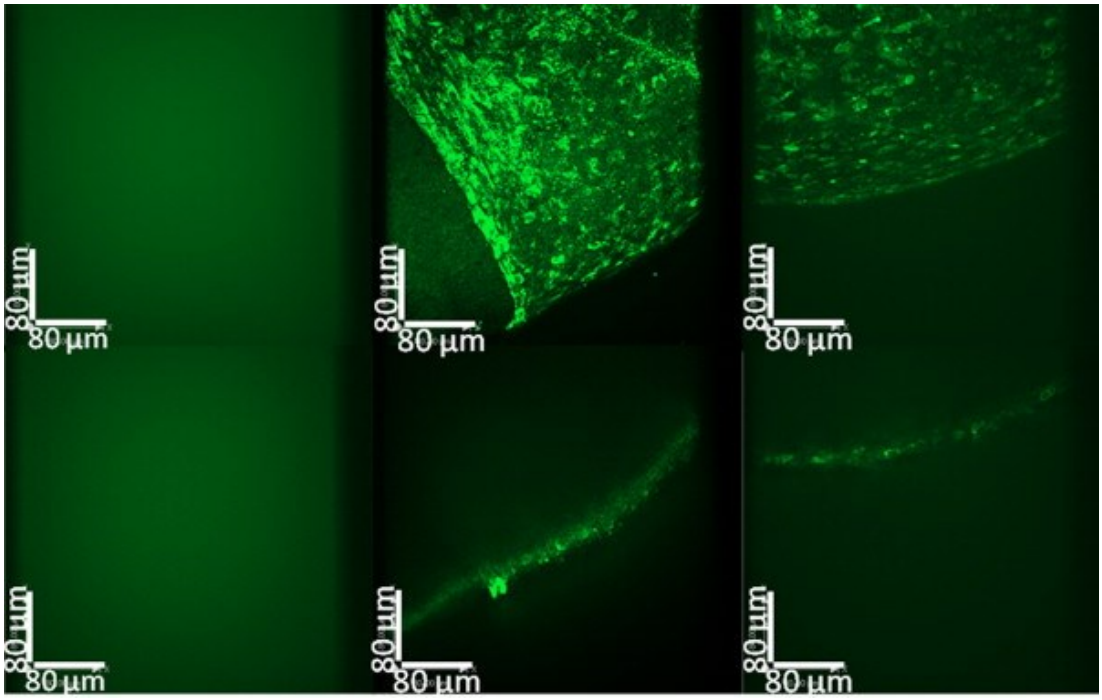

Figure AII.1: The 5-HT3B mutant subunits are trafficked to the membrane surface of the oocyte.

Indirect confocal micrographs of Xenopus oocytes injected with mRNA for the 5-HT3A subunit alone (left panels), 5-HT3AB(RQY) (middle panels) and 5-HT3AB(I176W) (right panels) at 5 days post injection. A rabbit antibody to the N-terminal region of the 3B subunit was used which does not recognize the 3A subunit (left panels). Chicken anti-rabbit Alexa-488 was used as the secondary antibody. The extended focus is shown in the top panels and slices of 2.5 µM through the X–Y axis are shown in the bottom panels. This depicts 3B subunit plasma membrane localization (middle and right panels). Scale bar represents 80 µm.

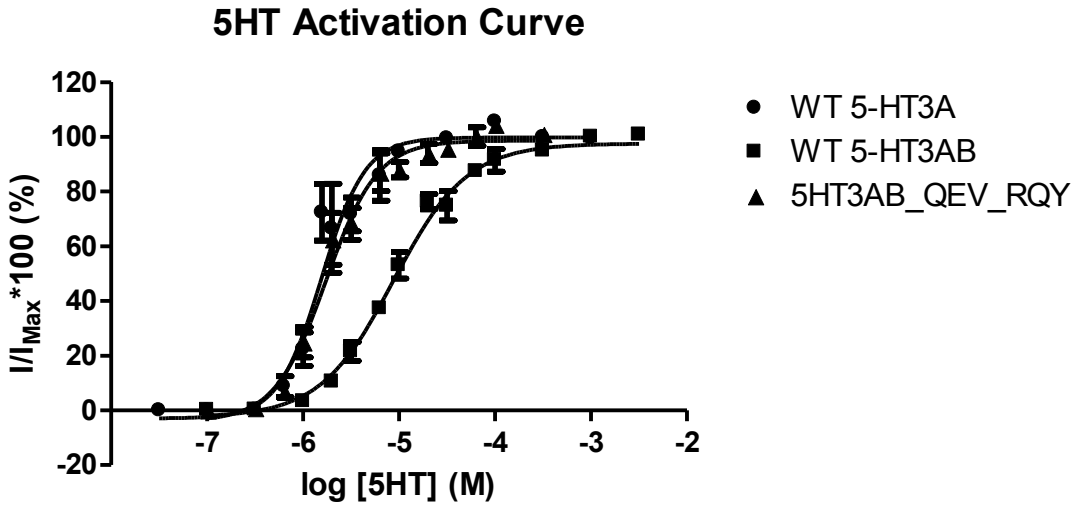

Figure AII.2: The effects of the mutation 5-HT3AB(RQY) on agonist activation by 5-HT. Concentration–response curves for 5-HT activation of wt 5-HT3A, wt 5-HT3AB and the mutant 5-HT3AB(RQY). Data were pooled from 7 (5-HT3A), 6 (5-HT3AB) and 5 (5-HT3AB(RQY)) independent experiments using different batches of oocytes. Average parameters obtained from the fitting of independent curves are shown in Table 1.

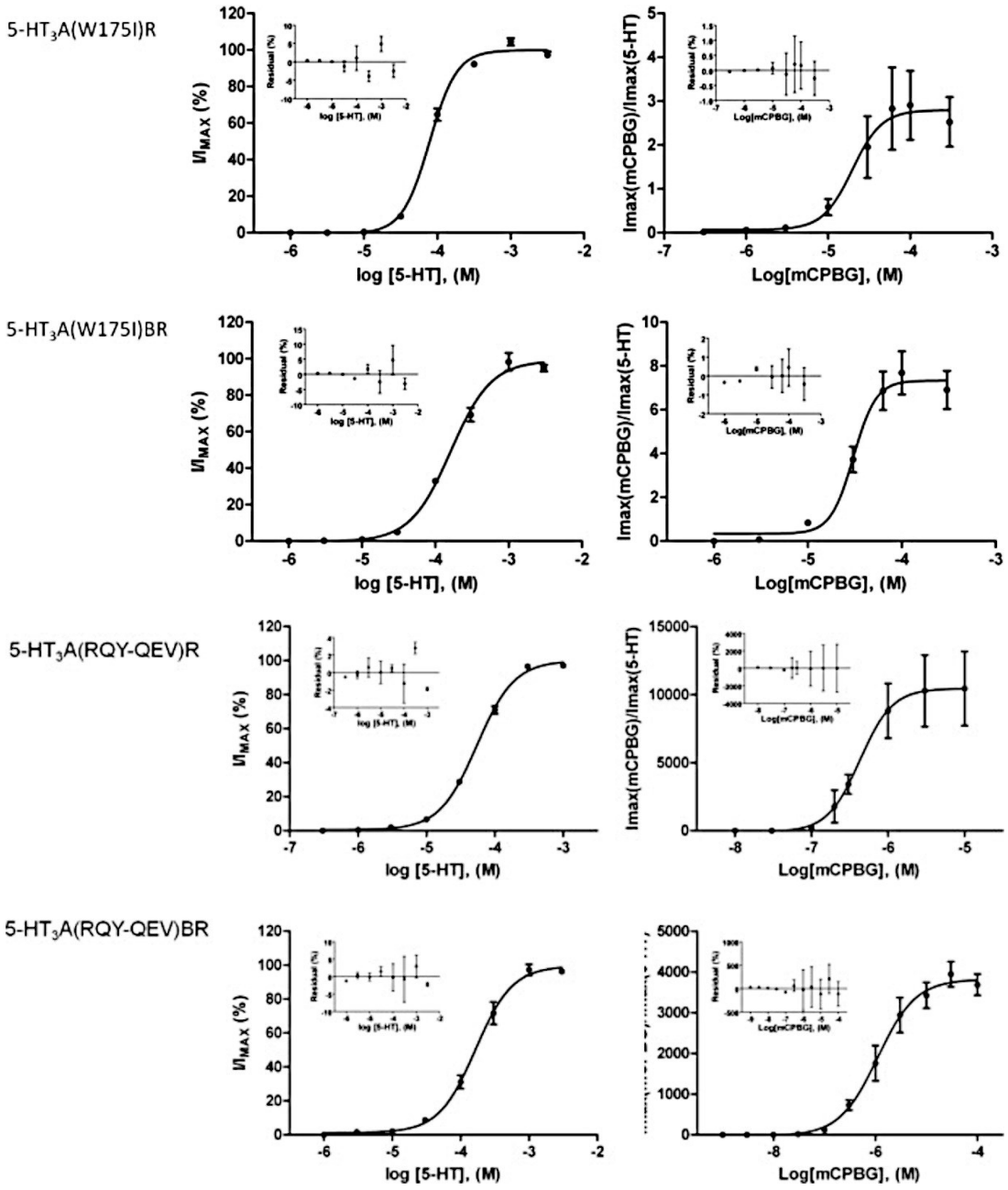

Supplementary Figure A.II.1:

Concentration–response curves for agonist activation by both 5-HT (on the left) and mCPBG (on the right) of the named mutant receptors. The calculated residuals plots are inset. In no case was there any evidence of a relationship between agonist concentration and deviation of the experimental data from the fitted curves, as described in the Methods.

Table AII.1: 5-HT Activation

Receptor	$logEC_{50}$ ± SEM, M	EC_{50} (μM) (95% CI)	n_H ± SEM	n
A	-5.75 ± 0.06$^{\#\#}$	1.78 (1.62-1.95)	2.67 ± 0.27$^{\#\#}$	7
A(W178I) Loop B(+)	-4.11 ± 0.03***$^{\#\#\#}$	77.6 (72.4-83.2)	2.32 ± 0.10	3
A(RQY-QEV) Loop D(-)	-4.26 ± 0.02***$^{\#\#\#}$	54.9 (52.5-57.5)	1.59 ± 0.04	3
AB	-5.06 ± 0.07***	8.71 (7.59-10.0)	1.10 ± 0.11***	6
A(W178I)B Loop B(+)	-3.78 ± 0.04***$^{\#\#\#}$	166 (151-182)	1.57 ± 0.15	4
A(RQY-QEV)B Loop D(-)	-3.77 ± 0.06***$^{\#\#\#}$	170 (144-200)	1.65 ± 0.16	3
AB(I176W) Loop B(+)	-5.40 ± 0.13*	3.98 (2.95-5.37)	0.84 ± 0.05***	4
AB(QEV-RQY) Loop D(-)	-5.76 ± 0.09$^{\#\#\#}$	1.74 (1.45-2.09	2.19 ± 0.50	5

*p<0.05, **p<0.01, ***p<0.001 significantly different from wt homomeric receptor

#p<0.05, ##p<0.01, ###p<0.001 significantly different from wt heteromeric receptor

Table AII.2: mCPBG Activation

Receptor	$logEC_{50}$ ± SEM, M	EC_{50} (μM) (95% CI)	n_H±SEM	N
A	-5.82 ± 0.10	1.51 (1.17-1.95)	2.08 ± 0.40	3
A(W178I) Loop B (+)	-4.64 ± 0.07*** ###	22.91 (19.50-26.92)	2.30 ± 0.25	4
A(RQY-QEV) Loop D (-)	-6.47± 0.13*** ###	0.34 (0.25-0.46)	2.88 ± 0.18#	4
AB	-5.99 ± 0.04	1.02 (0.93-1.12)	1.88 ± 0.22	4
A(W178I)B Loop B(+)	-4.54 ±0.03*** ###	28.84 (26.92-30.90)	2.50 ± 0.20	4
A(RQY(-QEV)B Loop D(-)	-5.90 ± 0.15	1.23 (0.85-1.86)	1.24 ± 0.22	3
AB(I176W) Loop B(+)	-5.69 ± 0.06	2.04 (1.78-2.34)	1.35 ± 0.11	4
AB(QEV-RQY) Loop D(-)	-5.62 ± 0.08	2.40 (1.95-2.95)	1.42 ± 0.06	3

*p<0.05, **p<0.01, ***p<0.001 significantly different from wt homomeric receptor

#p<0.05, ##p<0.01, ###p<0.001 significantly different from wt heteromeric receptor

Table AII.3: Comparison of maximum currents evoked by 5-HT and mCPBG in matched oocytes

Receptor	Max 5-HT evoked I ± SEM (nA)	Max mCPBG evoked I ± SEM (nA)	Max I mCPBG/Max I 5-HT x 100 (%) 95% CI	N
A	2825 ± 803	2688 ± 779	95.1 110 – 99	4
A(W178I) Loop B(+)	4808 ± 724	155 ± 54	2.6 7.1 – 0.9	4
A(RQY-QEV) Loop D(-)	99 ± 47	7210 ± 1493	9760 24900 - 3800	4
AB	1678 ± 94	2642 ± 229	156 196 - 125	3
A(W178I)B Loop B(+)	1746 ± 644	150 ± 72	6.8 9.9 – 4.6	4
A(RQY-QEV)B Loop D(-)	44 ± 37	1926 ± 1672	4100 5445 - 3083	3
AB(I176W) Loop B(+)	645 ± 310	1392 ± 553	245 351 - 171	4
AB(QEV-RQY) Loop D(-)	2991 ± 1038	3220 ± 1099	108 113 - 104	3

References

Akk, G., 2002. Contributions of the non-alpha subunit residues (loop D) to agonist binding and channel gating in the muscle nicotinic acetylcholine receptor. J. Physiol. 544, 695-705.

Barnes, N.M., Hales, T.G., Lummis, S.C.R., Peters, J.A. 2009. The 5-HT_3 Receptor - the relationship between structure and function. 2008. Neuropharmacology 56, 273-84

Beene, D.L., Brandt, G.S., Zhong, W., Zacharias, N.M., Lester, H.A., Dougherty,D.A., 2002. Cation-pi Interactions in ligand recognition by serotonergic (5-HT3A) and nicotinic acetylcholine receptors: The anomalous binding properties of nicotine. Biochemistry 41, 10262-10269.

Billen, B., Spurny, R., Brams, M., van Elk, R., Valera-Kummer, S., Yakel, J.L., Voets, T., Bertrand, D., Smit, A.B., Ulens, C. 2012. Molecular actions of smoking cessation drugs at α4β2 nicotinic receptors defined in crystal structures of a homologous binding protein. Proc Natl Acad Sci USA 109, 9173-9178.

Boess, F.G., Beroukhim, R., Martin, I.L., 1995. Ultrastructure of the 5-hydroxytryptamine3 receptor. J. Neurochem. 64, 1401-1405.

Boess, F.G., Steward, L.J., Steele, J.A., Liu, D., Reid, J., Glencorse, T.A., Martin, I.L., 1997. Analysis of the ligand binding site of the 5-HT_3 receptor suing site directed mutagenesis: importance of glutamate 106. Neuropharmacology 36, 637-647.

Brady, C.A., Stanford, I.M., Ali, I., Lin, L., Williams, J.M., Dubin, A.E., Hope, A.G., Barnes, N.M., 2001. Pharmacological comparison of human homomeric 5-HT_3A receptors versus heteromeric 5-HT_3AB receptors. Neuropharmacology 41, 282-284.

Corradi, J., Gumilar, F., Bouzat, C., 2009. Single-channel kinetic analysis for activation and desensitization of homomeric 5-HT3A recptors. Biophys. J. 97, 1335-1345.

Davies, P.A., Pistis, M., Hanna, M.C., Peters, J.A., Lambert, J.J., Hales, T.G.,Kirkness, E.F., 1999. The 5-HT3B subunit is a major determinant of serotonin receptor function. Nature 397, 359-363

Derry, J.M., Dunn, S.M., Davies, M., 2004. Identification of a residue in the gamma-aminobutyric acid type A receptor alpha subunit that differentially affects diazepam-sensitive and -insensitive benzodiazepine site binding. J Neurochem. 88, 1431-8.

Dubin, A.E., Huvar, R., D'Andrea, M.R., Pyati, J., Zhu, J.Y., Joy, K.C. Wilson, S.J., Galindo, J.E., Glass, C.A., Luo, L., Jackson, M.R., Lovenberg, T.W., Erlander, M.G., 1999. The Pharmacological and Functional Characteristics of the

Serotonin 5-HT_3A Receptor Are Specifically Modified by a 5-HT3BReceptor Subunit. J. Biol. Chem. 274, 30799-30810..

Fletcher, S., Barnes, N.M., 1998. Desperately seeking subunits: are native 5-HT3 receptors really homomeric complexes? Trends Pharmacol. Sci. 19, 212-215.

Kelley, S.P., Dunlop, J.I., Kirkness, E.F., Lambert, J.J., Peters, J.A., 2003. A cytoplasmic region determines single-channel conductance in 5-HT3 receptors. Nature 424, 321-324.

Kesters, D., Thompson, A.J., Brams, M., van Elke, R., Spurny, R., Geitmann, M., Villalgordo, J.M., Guskov, A., Danielson, U.H., Lummis, S.C.R., Smit, A.B., Ulens, C.. 2013. Structural basis of ligand recognition in 5-HT_3 receptors. EMBO Reports 14, 49-56.

Lummis, S.C.R., 2012. 5HT_3 receptors. J. Biol. Chem. 287, 40239-40245.

Lummis, S.C.R., Thompson, A.J., Bencherif, M., Lester, H.A., 2011. Varenicline is a potent agonist of the human 5-nydroxytryptamine$_3$ receptor. J Pharmacol exp Therap. 339, 125-131.

Miles, T.F., Bower, K.S., Lester, H.A., Doughery, D.A., 2012. A coupled array of noncovalent interactions impacts the function of the 5HT3A serotonin receptor in an agonist specific way. ACS Chem Neurosci. 3, 753-760.

Motulsky, H.J. 2003. Prism 4 statistics guide – Statistical guide for laboratory and clinical researchers. GraphPad Software Inc, San Diego, CA www.graphpad.com pp51-53

Price, K.L., Bower, K.S., Thompson, A.J., Lester, H.A., Dougherty, D.A., Lummis, S.C.R., 2008. A Hydrogen Bond in Loop A Is Critical for the Binding and Function of the 5-HT_3 Receptor. Biochemistry 47, 6370-6377.

Smith, K.M., Ng, A.M., Yao, S.Y. et al. 2004. Electrophysiological characterization of a recombinant human Na+-coupled nucleotide transporter (hCNT1) produced in Xenopus oocytes. J. Physiol. 58, 807–823.

Thompson, A.J., Price, K.L., Lummis, S.C.R., 2011. Cysteine modification reveals which subunits form the ligand binding site in human heteromeric 5-HT_3AB receptors. J. Physiol. 589, 4243-4257.

Thompson, A.J., Verheij, M., De Esch, I., Lummis, S.C.R., 2012.VUF10166, a novel compound with differing activities at 5-HT_3A and 5-HT_3AB receptors. J Pharmacol exp Ther 341, 350-359.

Unwin, N., 2005. Refined structure of the nicotinic acetylcholine receptor at 4Å resolution. J. Mol. Biol. 346, 967-89.

Yan, D., White, M.M., 2005. Spatial orientation of the antagonist granisetron in the ligand-binding site of the 5-HT_3 receptor. Mol. Pharmacol. 68, 365-371.